Aix Marseille Université

Thèse de Doctorat

ED352 Physique et Sciences de la Matière

Centre Interdisciplinaire de Nanoscience de Marseille (CINaM)/AMU-CNRS, UMR 7325

Thèse présentée pour obtenir le grade universitaire de docteur

Discipline : Biophysique

Emmanuelle BENARD

Adhésion des Lymphocytes T sur des substrats innovants : influence du nano-regroupement des ligands.

T cell adhesion on engineered substrates: influence of ligand nano-clustering.

Soutenue le 15/12/2017 devant le jury :

Composition du Jury:

Claire	Hivroz	Institut Curie	Rapporteur
Olivier	Thoumine	Institut Interdisciplinaire de neuro-science	Rapporteur
Alice	Nicolas	Laboratoire des Technologies de la microélectronique	Membre de jury
Ralf	Richter	School of Biomedical Sciences	Membre de jury
Laurent	Limozin	LAI	Membre de jury
Jacques	Nunes	CRCM	Membre de jury
Kheya	Sengupta	CINaM	Directrice de thèse

Abstract

The interface between an Antigen Presenting Cell (APC) and a T-lymphocyte (T cell), sometimes called a synapse, plays a key role in sensitivity and precision of antigen recognition by T-cells. The importance of clustering of T cell receptors (TCR) is well established. In addition, it has recently been shown that the antigens, in the form of peptide Major Histocompatibility Complex (pMHC) recognized by TCR, are present on the membrane of APCs as defined submicronic clusters. The aim of this work is to study how such clustering of ligands influences T-cell membrane and actin organization.

To achieve this, we developed a novel hybrid system, where a synthetic substrate mimics the APC-membrane. The substrate consist of an array of sub-micrometric protein dots (diameter: 800±100 nm; spacing: 2μm), surrounded by a fluid supported lipid bilayer (SLB), which is optionally functionalized. The dots and the SLB are alternatively functionalized with molecules of anti-CD3 (targeting the TCR-complex), or ICAM-1 (ligand for the T-cell integrin LFA-1), or with a co-receptor molecule (B7 against CD28).

In T cells adhered to these substrates, local parameters like organization of TCR, zeta-chain-associated protein kinase 70 (ZAP-70, one of the first molecules to be recruited to the TCR complex on activation), the actin distribution and membrane topography (measured using Reflection Interface Contrast Microscopy - RICM and Total Internal Reflection Fluorescence Microscopy - TIRFM) are impacted by ligand clustering. Colocalization of microclusters of both TCR and ZAP-70 with anti-CD3 dots is seen. The presence of ICAM-1 on the SLB does not appreciably perturb this organization, whereas B7 may have a slight impact. On ICAM-1 dots, as expected, the TCR is not organized in micro-clusters.

The membrane of the adhering T cells exhibit a characteristic topography (revealed in RICM), when adhesive ligands (either ICAM-1 or anti-CD3) are present only in the dots but not on the SLB. Based on marking of glycocalyx molecules, we believe that the presence of the polymers of the glycocalyx prevent intimate contact between the membrane and the substrate outside the adhesive dots. In the presence of ligands on the SLB, the membrane adheres also to the SLB, either crushing or expulsing the polymers. Interestingly, the presence of an artificial polymer like polyethylene glycol on the SLB enhances the membrane topographical patterning, pointing to the repulsive role of membrane polymers in defining the topography of the synaptic interface. Global parameters like cell area (quantified from RICM images) depend on the nature (ICAM-1 or anti-CD3) of the ligands present. On substrates with anti-CD3 (no ICAM), the cell area is the same on clustered and homogeneously distributed ligands as long as the average ligand density remains the same. However in presence of ligands of LFA1, the global parameters are influenced by clustering or not of the TCR ligands. Specifically, the cell

area is significantly increased when the same amount of anti-CD3 is clustered, rather than homogeneous.

Classically, the actin distribution in T cells adhering to a SLB functionalized with both ICAM-1 and anti-CD3, is in the form of a peripheral ring. However, on substrates patterned with dots of either ICAM-1 or anti-CD3 (no SLB functionalization), the actin is in form of colocalized dots. When in addition, the SLB is functionalized with the complementary ligand, the actin distribution becomes either homogeneous or peripheral. Dynamic imaging hints that TCR organizes the actin at early time and LFA-1 at late time, thus pointing to the crucial but different role of both in adhesion of T cells.

Résumé

L'interface entre une cellule de présentation d'antigène (CPA) et un lymphocyte T (LT), parfois appelée synapse, joue un rôle clé dans la sensibilité et la précision de la reconnaissance d'antigène par les LT. L'importance du regroupement des récepteurs des lymphocytes T (RTC) est bien établie. De plus, il a récemment été démontré que les antigènes sous la forme de peptide associés au Complexe Majeur d'Histocompatibilité (pMHC) et reconnu par TCR, sont présents sur la membrane des CPA sous forme de clusters submicroniques. Le but de ce travail est d'étudier comment un tel groupe de ligands influence l'organisation de la membrane et de l'actine des LT.

Pour ce faire, nous avons développé un nouveau substrat synthétique imitant la membrane de la CPA. Le substrat consiste en un ensemble d'ilots protéiques sous-micrométriques (diamètre: 800 ± 100 nm, espacement: $2~\mu$m), entouré d'une bicouche lipidique supportée fluide (SLB), qui est facultativement fonctionnalisée. Les ilots et la SLB sont alternativement fonctionnalisés avec des molécules d'anti-CD3 (ciblant le complexe du RTC), ou avec ICAM-1 (ligand pour l'intégrine de LT : LFA-1), ou avec un corécepteur B7 (ligand pour CD28).

Pour les LT adhérent à ces substrats, des paramètres locaux comme l'organisation du TCR, de la protéine kinase ZAP-70 (une des premières molécules à être recruter sur le complexe TCR lors de l'activation), la distribution de l'actine et la topographie de la membrane (mesurée à l'aide de la Microscopie par contraste d'interférence - RICM et de la Microscopie de fluorescence à réflexion interne totale - TIRFM) sont influencées par le regroupement du ligand du RCT. La co-localisation des micro-clusters de RCT et ZAP-70 avec les ilots d'anti-CD3 est observée. La présence d'ICAM-1 sur la SLB ne perturbe pas cette organisation, alors que la présence de B7 peut avoir un léger impact. Sur les ilots d'ICAM-1, comme prévu, le RTC n'est pas organisé en micro-clusters.

La membrane des LT adhérent au substrat présente une topographie caractéristique lorsque les ligands adhésifs (comme ICAM-1 ou anti-CD3) sont présents que dans les ilots mais pas sur la SLB. Grace au marquage des molécules du glycocalyx, nous pensons que c'est la présence des polymères du glycocalyx qui empêche un contact étroit entre la membrane et le substrat en dehors des ilots adhésifs. En présence de ligands sur la SLB, la membrane adhère également sur SLB, soit en écrasant ou en expulsant les polymères. De manière intéressante, la présence d'un polymère artificiel comme le polyéthylène glycol sur la SLB promeut la structure topographique de la membrane, ce qui montre le rôle répulsif des polymères membranaires dans la détermination de la topographie de l'interface synaptique. Les paramètres globaux comme l'aire d'adhésion cellulaire dépendent de la nature (ICAM-1 ou anti-CD3) des ligands présents. Sur les substrats avec qu'anti-CD3, l'aire d'adhésion est la même lorsque les ligands sont

groupés ou distribués de façon homogène tant que la densité moyenne du ligand reste la même. Cependant, en présence d'ICAM-1, les paramètres globaux sont influencés par le regroupement ou non des ligands du RCT. En effet, l'aire d'adhésion augmente de manière significative lorsque la même quantité d'anti-CD3 est sous forme d'ilots plutôt qu'homogène.

Généralement, la distribution de l'actine dans les LT adhérent à une SLB fonctionnalisé avec ICAM-1 et anti-CD3, se présente sous la forme d'un anneau périphérique. Cependant, sur des substrats présentant des ilots d'ICAM-1 ou d'anti-CD3 (sans fonctionnalisation de la SLB), l'actine est sous forme d'ilots co-localisés. De plus lorsque la SLB est fonctionnalisé avec le ligand complémentaire, la distribution d'actine devient homogène ou périphérique. L'imagerie dynamique indique que le RCT organise l'actine au début et que le LFA-1 l'organise à la fin du processus, soulignant ainsi le rôle crucial mais différent de ces deux molécules lors de l'adhésion des LT.

Remerciements

Ces 3 années de thèse ont été une source de savoirs scientifiques mais pas que, en effet ça m'a permis de mûrir humainement. Cette aventure m'a énormément appris sur moi-même. Ceci a été possible grâce à toutes les personnes que j'ai pu côtoyer durant cette période. C'est le moment pour moi de les remercier (en espérant n'oublier personne).

Je tiens tout d'abord à remercier ma directrice de thèse, Kheya Sengupta qui m'a beaucoup appris, soutenue et grâce à qui je pense sortir de cette expérience avec plus de confiance en moi. Elle m'a fait confiance pour ce projet et je lui en suis très reconnaissante.

J'aimerais aussi remercier tous les collaborateurs qui ont participé à la réussite de cette thèse : Laurent Limozin, du Laboratoire d'Adhésion et d'Inflammation, pour ses conseils et son aide matérielle, Igor Ozerov et Frédéric Bedu de la plateforme PLANETE pour leur travail en salle blanche et leur aide dans la fabrication des substrats et aussi Jacques Nunes du CRCM et Guillaume Voisin du CIML pour leur collaboration et pour m'avoir fourni en protéines et cellules pour mes expériences.

Je tiens a remercier aussi les membres du jury :Dr C. Hivroz, Dr O. Thoumine, Dr A. Nicolas, Dr R. Richter, Dr L.Limozin et Dr J. Nunes pour leur intérêt dans mon travail. Un grand merci aux personnels administratifs et plus particulièrement à Elodie qui m'a facilité les différentes tâches administratives et Bruno qui été toujours là en cas de problèmes informatiques.

J'aimerais aussi remercier mes collègues: Pierre Dillard qui a eu la gentillesse et surtout la patience de répondre à toutes les questions scientifiques et autres, et d'animer les pauses cafés, Fuwei PI pour avoir pris le temps de me transmettre ses connaissances, et aussi Astrid, Ranime, Scott, Arif, Cécile, Sébastien, Arnaud, Aya, Etienne, Anne et Manue avec qui j'ai pu discuter et partager des moments intéressants

Je tiens aussi à remercier spécialement mon père et ma sœur jumelle à qui je me suis plains de temps en temps de ma thèse mais qui m'ont toujours soutenue même éloignés à 8 810 km. C'est grâce à eux que j'ai réussi à faire tout ce chemin.

Contents

List of Figures

List of Tables

Nomenclature

APC Antigen-Presenting Cells

APTES (3-AminoPropyl)-TriEthoxySilane

BMCL Block Copolymer Micelles nanoLithography

BSA Bovine serum albumin

CAMs Cell Adhesion Molecules

ECM Extra Cellular Matrix

ICAM-1 InterCellular Adhesion Molecule-1

IS Immune Synapse

ITAM Immunoreceptor Tyrosine-based Activation Motif

LAT Linker for Activation of T-cells

LB/LS Langmuir Blodgett / Langmuir Schaefer

LFA-1 Lymphocyte function-associated antigen 1

MHC Major Histocompatibility Complex

NaV Neutravidin

PBS Phosphate Buffered Saline

PEG Polyethylene glycol

pMHC peptide associate to MHC complex

PRR Pattern Recognition Receptors

RICM Reflection Interface Contrast Microscopy

SLB Supported Lipid Bilayer

SMAC Supramolecular Activation Complex

T-Cell T lymphocytes cell

TCR T-Cell Receptor

TIRFM Total Internal Reflection Fluorescence Microscopy

VS Vesicles spreading

ZAP-70 Zeta-chain-associated protein kinase 70

Chapter 1

Introduction

Contents

This chapter summarizes the background, state of art and motivations for the work reported in this thesis, and sets out the basic structure of the document. After presenting text-book knowledge of the immune system pertinent for this thesis [1, 2, 3], more specific recent knowledge on biophysics of T cells is presented and set in a general cell biology context. Finally the outline of the thesis is introduced.

1.1 Basics of immune system

Our ability to avoid infections is based on our adaptive immune system and, at the beginning of the pathogen exposition, our innate immune system.

Innate immunity: On evolutionary terms, innate immunity was the first to appear; It is developed during organism Evolution and it is always present in different forms in every organism [3]. The innate immunity, also known as the non-specific immune system [4], is our first line of defense against pathogens. It consists of defense mechanisms present from birth and is genetically inherited. It has a fast but limited and non-specific recognition capacity for microorganisms, nevertheless it prevents the majority of infections at an early stage. Moreover it does not confer long-lasting or protective immunity to the host [5]. The response can be humoral (release of chemicals into a body fluid) or cellular (direct intervention by specialized cells like neutrophils, macrophages and natural killer cells etc).

Adaptive immunity: The adaptive immunity, also known as the specific immunity or the acquired immune system, is found only in vertebrates. It is called "adaptive" because the specificity to pathogens is acquired during the lifetime of the host. Indeed, a large directory of very diversified immunoreceptors is created after an initial response to a specific pathogen thus allowing a quicker recognition and enhanced response during a new encounter with the same pathogen. This immunity is composed of specialized cells like T and B lymphocytes. B lymphocytes produce antibodies (known as humoral immunity). Antibodies are large proteins which identify and neutralize foreign objects. Each antibody produced recognizes an unique antigen, and neutralizes specific pathogens [3]. T lymphocytes (or T-cells) play a key role in the adaptive immunity. They differ from other lymphocytes by the presence on the cell surface of a specialized receptor T-Cell Receptor (TCR). Their most important function is to identify foreign antigenic peptides and form the basis for cell mediated response.

These two immunities are different on several points (activation, mode of action, molecules involved) but are indispensable in order to have an effective immune system. Indeed, pathogen surviving the innate immunity activate Antigen-Presenting Cells (APC) (like dentritic cells) via antigen threshold levels and specific signals. APCs ingest and present pathogen antigenic peptides on their surface, then the lymphocytes of the adaptive immune system recognize these peptides and induce a immune response. Once the lymphocytes are activated they are able to activate other cell types which then allow the destruction of infected cells or cancer cells.

To ensure good health, the quantity of immune cells (like T-cells) needs to be controlled. On one hand if the quantity is too high immune cells can react against the host inducing autoimmune diseases like diabetes or lupus; On the other hand if this quantity is too weak, the immune system will not be able to stop any infections. The last situation

is observed during HIV infection where the level of T-cells drops allowing the apparition of several diseases and eventually leading to death.

1.1.1   Antigen Presenting cell
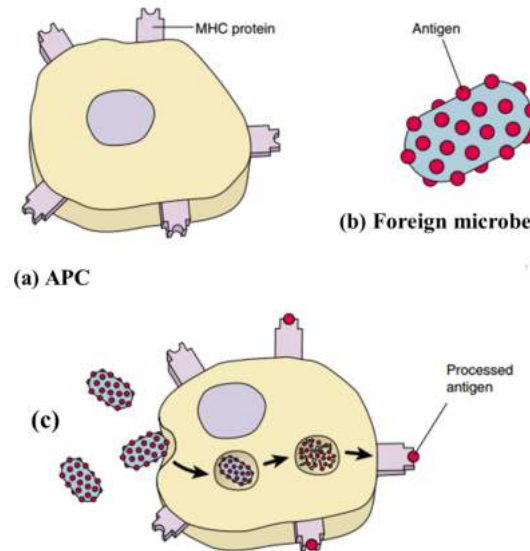
Figure 1.1: **Antigenic peptides presented by APC on MHC.**(a) Presence of MHC at the surface of an APC. (b) Foreign microbe presenting antigens on its surface. (c) After capture of an antigen, the APC presents the antigen in the form of a peptide associated to the MHC to the lymphocytes. Adapted from [6].

As the name suggests, Antigen Presenting Cells (APC) are capable of presenting an antigen from a pathogen to lymphocytes. There are various types of APCs: monocytes, macrophages, B lymphocytes but also dendritic cells. These cells are found in the tissues and have a size between 10 and 15 μm. APCs have two main functions: the capture of antigens (via phagocytosis) and the presentation of the antigen in the form of a peptide to the lymphocytes. In the infected tissue, immature APCs recognize characteristic molecular patterns of pathogens via the Pattern Recognition Receptors (PRR). This recognition induces the activation of the APC and initiates the capture of the antigen. The APCs are then activate and migrate to the secondary lymphoid organs to present this antigen to the lymphocytes. This presentation is made via the Major Histocompatibility Complex (MHC) which binds the antigenic peptide forming the peptide MHC complex (pMHC).This pMHC will be recognized by the appropriate T-cells which will induce an immune response. In order to optimize the interaction with the T lymphocyte, APCs have molecules of co-stimulation on their surface such as CD80, CD86 and CD40 as well as adhesion molecules such as ICAM (IntraCelular Adhesion Molecule).
Proteins on the surface of the APCs
Different proteins are presented on the surface of APCs to allow efficient interaction with T cells leading to their activation.

First, there are **MHC molecules** carrying the antigenic peptide which will be recognized by T-cells. Two types of MHC can be presented on APCs membrane. There is
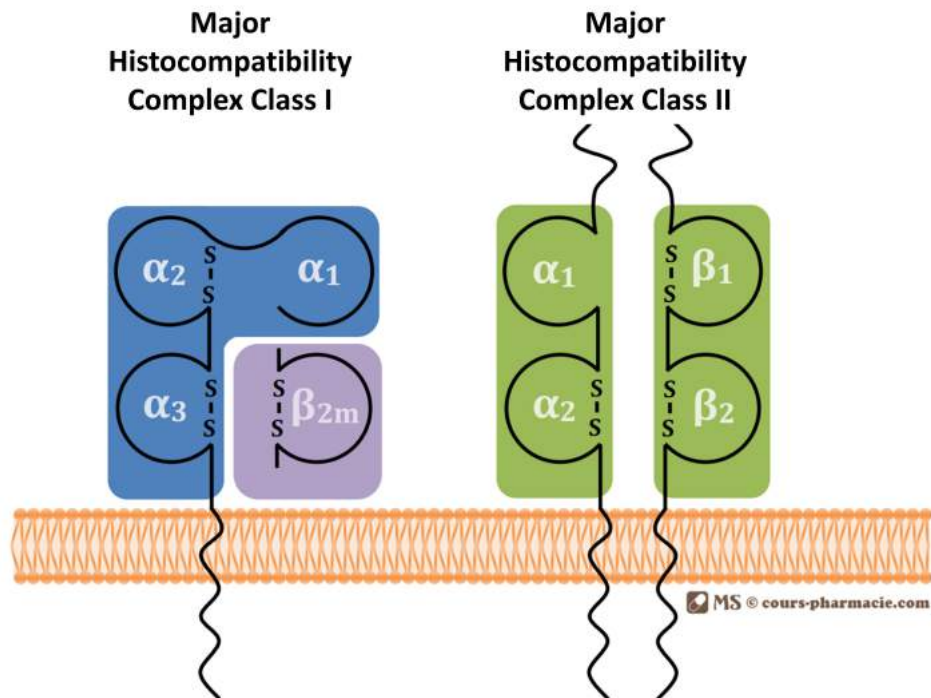
Figure 1.2: **Schematic structure of MHC class I and II.** MHC class I, composed of an α chain and a $\beta2$ microbulin chain, present peptides from endogenous antigen and is capable of activating the CD8$^+$ T-cell. MHC class II composed of two α and β chains, present peptides from exogenous antigen and is capable of activating the CD4$^+$ T-cell. Adapted from [7]
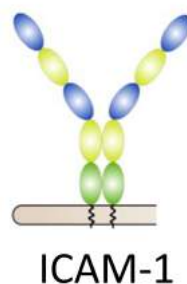
Figure 1.3: **Schematic structure of ICAM-1.** ICAM-1 is a highly glycosylated molecule that belongs to the immunoglobulin superfamily. It is composed of 5 extracellular domains which can interact with other adhesion molecules, one transmembrane domain and an intracytoplasmic tail which can interact with the cytoskeleton. Adapted from [8]

MHC class I which is express on all nucleated cells and MHC class II which is normally expressed on professional APC like dentritic cells, macrophages or B cells. MHC class I will activate CD8$^+$ T-cells and MHC class II will activate CD4$^+$ T-cells. The type of the MHC is determined by the origin of the pathogen, antigenic peptides from intra-

cellular pathogens will be presented by MHC class II whereas antigenic peptides from extracellular pathogens will be presented by MHC class I (Figure1.2). Prior to contact with a pathogen, low level of MHC is expressed, but after pathogen exposition, APCs become active and this level increases. This will allow T-cell interaction and activation. Moreover this activation up-regulates expression of co-stimulatory molecules like B7-2 which will interact with CD28 on T-cells.

B7-2 provides an important co-stimulatory signal binding CD28 on T-cells allowing a complete activation of the T-cells [9].

On APCs, there is an adhesion molecule called **ICAM-1** which permits the strengthening of the adhesion between T-cells and APCs during the antigen recognition phase [10]. ICAM-1 or CD54 is a highly glycosylated molecule that belongs to the immunoglobulin superfamily. It is composed of 5 extracellular domains which can interact with other adhesion molecules (Figure1.3), one transmembrane domain and an intracytoplasmic tail which can interact with the cytoskeleton . ICAM-1 binds to the integrin Lymphocyte Function-associated Antigen 1 (LFA-1) present on the surface of T-cells. Diffusivity of the molecules and viscoelasticity of APC are suspected to be important for T-cell/APC interaction.

Studies have shown that according to the types of cells and the experimental conditions, the lateral diffusion of the MHC class II can vary from 1.10^{-5} to 32.10^{-2} μm^2/sec [11].

Using a single-cell rheometer, viscoelasticity was measured on different APCs and it was shown that their rigidity varies according their nature and the stimuli they received [12].

Also it has been shown that on APCs, pMHCs are presented in the form of clusters with a diameter between 200-300 nm. These clusters are observed before the interaction with T-cells [13].

These findings point out the need to take into account mechanical properties and ligand organization in the form of clusters during the T-cell/APC study.

1.1.2   T-lymphocyte

T-lymphocytes (or T-cells) are responsible for the specific cellular immune response and play an important role in the immune system. Their development begins in the bone marrow and their maturation takes place in the thymus. They are found in the blood but also in the lymphoid organs and their size is about 10 μm. T-cells are activated by interacting with an APC exhibiting a pMHC. The global structure of T lymphocytes is constant and several types of proteins are embedded in the plasma membrane. Each T-cells differ from the other immune cells by having a distinct T-Cell Receptor (TCR) which reacts with different ligands: either MHC class I or MHC class II on APC surface. They have also specific clusters of differentiation like CD3, CD4 (for T-cells helper) or CD8 (for T-cells cytotoxic). Moreover T-cells express other proteins such as integrins, immunoglobulins, selectins, cytokine receptors and some other CDs (CD28 and C45 for example).

T-cell membrane proteins
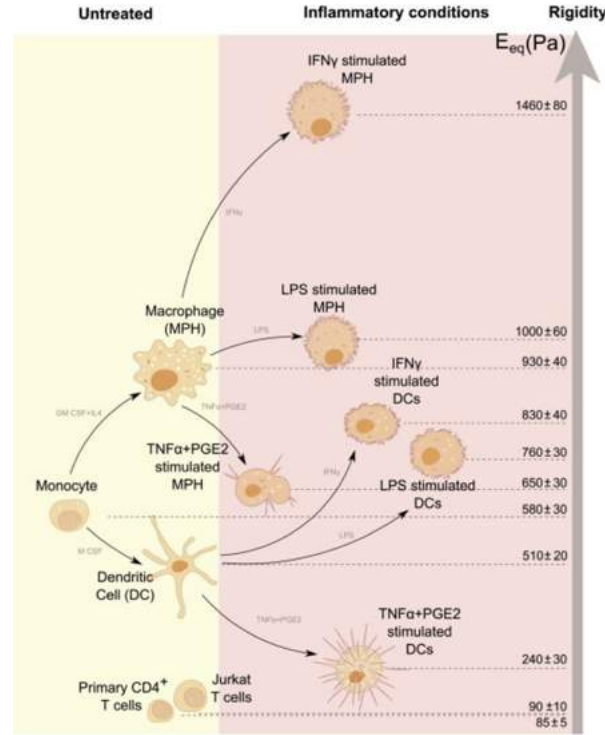
Figure 1.4: **Summary of elasticity values for different immune cells.** Adapted from [12]

TCR is expressed on the surface of T-cells. It recognizes specifically antigenic fragments bound to MHC (pMHC). The TCR is in the form of a heterodimere complex in which we find the α and β (or $\gamma\delta$) chains associated by a disulfide bond.

Due to the absence of an intracytoplasmic domain enabling signal transduction, the TCR is always associated with a group of molecules: **the CD3 complex**. This multimeric complex is composed of the γ, ε, δ and ζ which have one or more ITAM (Immunoreceptor Tyrosine-based Activation Motif) domains enabling them to initiate the transduction signal (Figure1.6A). ITAM motif presents tyrosines which can be phosphorylated by kinases when the signal transmission occurs in order to activate the T-cell. It should be noted that some antibodies directed against CD3 can also induce cell activation [14].

Since the affinity of the TCR for the pMHC complex is low, there exists a co-receptor present on the lymphocyte allowing it to be reinforced, that is the role of the **co-receptors CD4 or CD8**.

CD8 is a hetero-dimeric membrane protein and is expressed by T-cells CD8$^+$. It allows to recognize antigenic peptides presented by MHC class I.

CD4 is a monomeric protein which presents four immunoglobulin-like domains. It is expressed by CD4$^+$ T-cells and allows to recognize antigenic peptides presented by MHC class II (Figure1.6B). These co-receptors reinforce T-cell-APC interaction and signal transduction by recruiting the LcK kinase which can phosphorylate the tyrosines of the ITAMs of the CD3 chains and thus initiate the intracellular signal [15, 16].
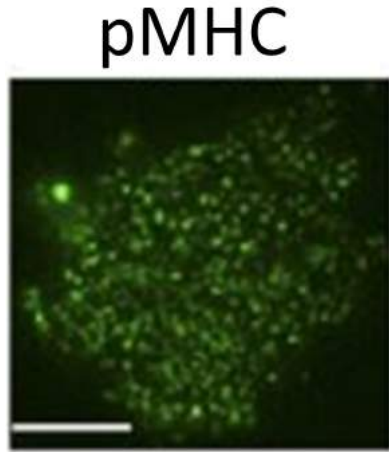
pMHC

Figure 1.5: **Expression of pMHC microclusters on a APC.**Adapted from [13]
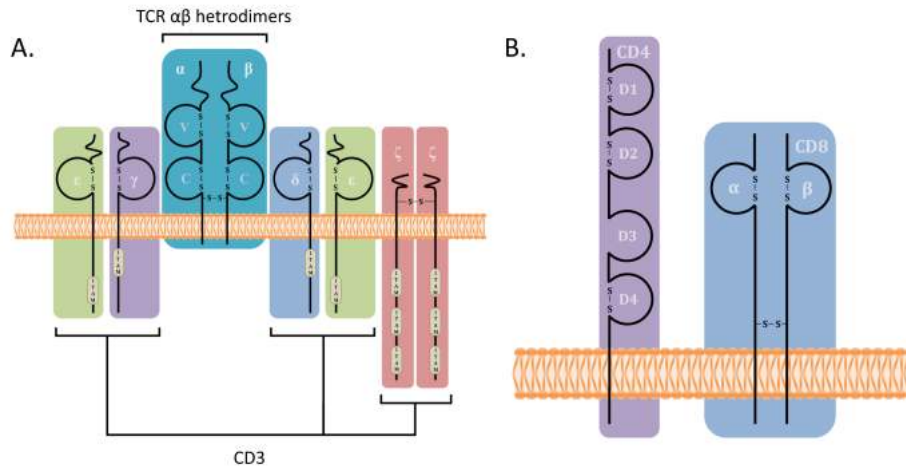
Figure 1.6: **Schematic structure of TCR, CD3, CD4 and CD8.**Orange structure represents the cell membrane. A. The structure of the TCR-CD3 complex is composed of an $\alpha\beta$ heterodimer for the TCR associated with the 6 chains of the CD3: γ,ζ, two ε and two δ. B. Structures of the CD4 and CD8 are presented. The CD4 consists in a monomer of four immunoglobulin domains and the CD8 consists in a heterodimer of $\alpha\beta$ chains. Adapted from [1]

In order to fully activate, the lymphocyte needs a co-stimulation signal delivered by the APCs. For this, there is the CD40L molecule present on the lymphocyte which interacts with CD40 on the surface of the APCs allowing the over expression of other co-stimulatory ligands on the APC as CD80 and CD86 which both interact with **CD28** present on the lymphocyte [17].

On T-cells membrane there are polysacharides collectively called **glycocalyx**. The glycocalyx is a negatively-charged layer which allows to control and mediate adhesion [18, 19, 20, 21, 22], by creating a controllable repulsive barrier[23][24].

These molecules have an important but different role in the process of T-cell activation. The following section will describe the different steps leading to the activation of
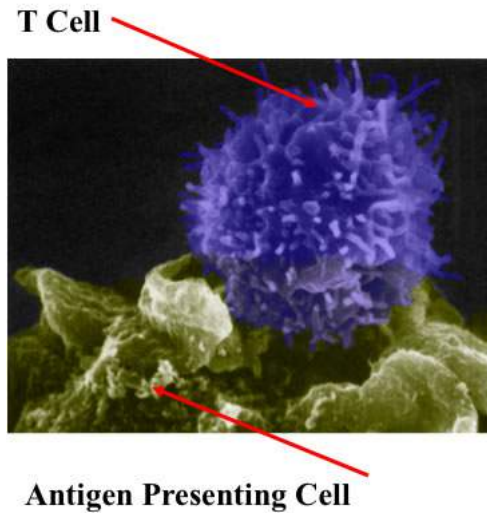
Figure 1.7: **Interaction between T-cell and an APC.** Electronic photography of an interaction between a T-cell (in blue) and a dentritic cell (in green). From [25]

T-cells.

1.2 T-cell/APC interactions

The encounter between a T-cell and an APC occurs most frequently in the lymph node. In vitro studies of this interaction have been done first using 2D and then 3D culture systems (Figure 1.7). Based on these, the T-cell/APC interaction can be divided in three steps :
- Contact with APC and antigenic peptide recognition
- T-cells-APC adhesion
- T-cell detachment and migration.

1.2.1 Contact, recognition and T cell activation

In order to trigger an activation of the T-cell, the TCR has to bind to an agonist peptide loaded on a MHC molecule on APC. This encounter happens generally in the lymph nodes for naive T-cells. Many lymphocytes come into contact with mature APC in order to find a specific peptide present on MHC. It is through the release of chemokines by the APC (CXCL12) which polarizes and makes the lymphocyte migrate towards the APC. This polarization allows an enrichment in LFA-1 and TCR at the front of the lymphocyte. This binding requires the membrane of the two interacting cells to be close to each other (around 13 nm) and is mediated via the binding LFA-1/ICAM-1. Affinity measurements revealed a weak affinity of the TCR for the peptide loaded on the pMHC with a K_D comprised between 10^{-7} and 10^{-4} M [26, 27]. The half-life of the association of the TCR/pMHC is very short (measured to be a few second or less) [26, 28, 29]. Moreover, the T-cells/APC binding is specific and sensitive as it has been shown that only four agonist peptides are required to achieve a completely activation of the T-cell

[30] and only one pMHC/TCR complex is sufficient to trigger a calcic response [31].
If the TCR is unable to bind the pMHC complex with good affinity, the lymphocyte
detaches from the APC to look for another with a more specific antigenic peptide. Once
the correct pMHC is found, TCR molecules will initiate the activation signal and the
transition to the next step [32].

1.2.1.1 Models of T cell activation

In a resting T-cell, TCR is randomly phosphorylated by Lck and dephosphorylated by
the phosphatase CD45 [33]. Then after pMHC/TCR recognition, a signaling pathway
is initiated. This will lead to a signaling cascade involving first the kinase Lck. This
kinase will phosphorylate the ITAM motifs of CD3 chains. This phosphorylation will
then allow the recruitment and the activation of the ZAP-70 kinase. Downstream events
will then occur like the phosphorylation of the adaptive protein LAT and SLP-76. These
events will lead to the activation of transcription factors. Then CD28 will bind to its
ligand (CD80 and CD86) allowing a co-stimulatory signal leading to the production of
interleukin 2. Finally, the last signal necessary for complete activation involves cytokines
produced by APCs. The main cytokines produced are interleukins 1, 2, 6, 10, 15.

This signaling machinery leading to the TCR activation is understood in quite details
(see Figure 1.8. However, the first steps of activation remain unclear with many specu-
lations [34]. Different models have been proposed: aggregation models, conformational
change models and segregation or redistribution models. The latter is based on the
segregation/redistribution of the proteins membrane following TCR engagement. This
reorganization will lead to the exclusion of the phosphatase CD45 from the TCR-CD3
complex allowing the phosphorylation of the ITAM motifs by Lck [33]. For this model,
there is formation of microclusters without CD45 allowing a local enrichment of TCR-
CD3 complex and kinases (Figure 1.9A). Another model proposed a segregation of the
CD45 due to the steric hindrance imposed by the close apposition of the T-cell/APC
membrane. Studies have also demonstrated that this segregation can be a consequence
of a enrichement of lipid rafts that enrich Lck but exclude CD45 [35, 36](Figure 1.9B.
There is mounting experimental evidence in favor of the segregation model [37], but in
reality, element from other models may probably also be valid.

1.2.2 T-cells APC adhesion, detachment and migration

Cell adhesion is the process by which cells interact and attach to an other surface (sub-
strate or cell) by making interactions. This interaction is made through proteins called
Cell Adhesion Molecules (CAMs) which include integrins, selectins, cadherins etc [39].
Through these proteins, complexes anchoring the cell cytoskeleton to the Extra Cellular
Matrix (ECM) via integrins can be formed, and called Focal adhesion. In fact focal adhe-
sion is formed by integrin clusters which will assemble F-actin cytoskeleton and generate
tension leading to cell spreading (Figure 1.10)[40, 41]. Also presence of polysacharides
at the cell surface controls and mediates adhesion[19].

This process is important for T-cells because in order to scan the APC membrane
surface it needs to adhere on it. Indeed, one of the first step after pMHC recognition is
T-cells adhesion. This will allow to interact and attach to the APC surface to scan the
pMHC. T-cells-APC adhesion can be divided in three phases [42]:
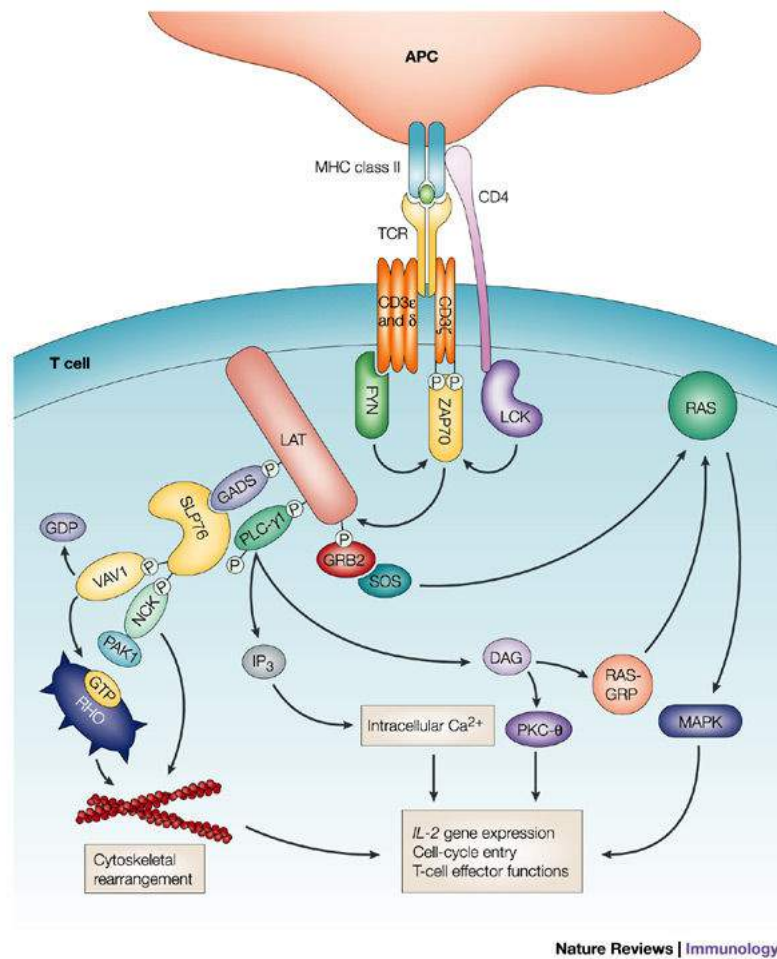
Figure 1.8: **Proximal signaling complexes and downstream responses induced by TCR ligation.** Following TCR ligation, tyrosine kinases Lck is activated, resulting in phosphorylation of CD3 and activation of ZAP-70. Activated ZAP-70 phosphorylated LAT and SLP76. Tyrosine-phosphorylated LAT then recruits several SH2-domain-containing proteins, including growth factor receptor-bound protein 2 (GRB2), GRB2-related adaptor protein (GADS) and phospholipase C-γ1 (PLC-γ1). Through its constitutive association with GADS, SLP76 is also recruited to LAT following TCR stimulation. Activation of PLC-γ1 results in the hydrolysis of phosphatidylinositol 4,5-bisphosphate to inositol 3,4,5-triphosphate (IP3) and diacylglycerol (DAG). IP3 production leads to increases of intracellular free Ca2+concentration, whereas DAG can activate both protein kinase C-θ (PKC-θ) and RAS guanyl nucleotide-releasing protein (RASGRP). Phosphorylated LAT also recruits the SH2 domain of GRB2, and therefore, the GRB2-associated RAS guanosine nucleotide-exchange factor (GEF), son-of-sevenless (SOS), thereby providing an additional possible mechanism of RAS activation through LAT. Tyrosine-phosphorylated SLP76 also associates with the RHO-family GEF, VAV1, and the adaptor protein, NCK. A trimolecular complex between SLP76, VAV1 and NCK-associated p21-activated kinase 1 (PAK1) has been proposed as a potential mechanism for SLP76 regulation of actin cytoskeletal rearrangements following TCR stimulation. APC, antigen-presenting cell; IL-2, interleukin-2; MAPK, mitogen-activated protein kinase. Adapted from [38].

32

Figure 1.9: **Mechanisms of TCR triggering by segregation.** Adapted from [34].

- a phase of transitory contacts
- a phase of stable contacts
- and again a phase of transitory contacts.

The stable contact required a "Stop signal" which is initiate by the TCR/pMHC binding and completed by the LFA-1/ICAM-1 binding [43]. This stop signal will allow to stop the T-cell in order to scan the APC surface. During this phase the formation of the so-called Immune Synapse (IS) occurs. This IS leads to the formation of Supramolecular Activation Complex (SMAC) at the T-cell-APC interface[44] . The details of the IS will be described in section 1.3.

The last phase corresponds to the detachment of the T-cell from the APC and the migration of the T-cell. The mechanisms involved in these steps are :
- the internalization and degradation of the TCR [45] and of the adhesion molecules[46],
- the increase of the expression and of the recruitment of inhibitory receptors such as CTLA-4,
- and the induction of the expression of cytokines and their receptors [47].

1.3   T-cell/APC interface: the Immunological Synapse

Interaction between APCs and T-cells is critical to the outcome of the adaptive immune response. This interaction was studied using a number of strategies as described below. T-cell/APC interaction happens at the interface between the two cells. The phrase "Immunological synapse" (IS) was first used by Norcross in 1984 [48] to describe the specific interaction between a T-lymphocyte and an APC by analogy to the neural synapse. Nowadays this model has evolved and is highly debated among the scientific community. This IS is highly dynamic allowing T-cells to interact with several APCs before choosing the one with the specific pMHC [49].

1.3.1   Experimental approaches

In-vivo experiments were done using the two photon confocal microscopy technique. In this case, the dynamics of the interaction can be observed directly on the lymph nodes [50, 51, 52]. Another method consists to study the interaction T-cell/APC *in-vitro*. This method allows to look at the molecule distribution between two cells but also to quantify the signaling (release of interleukine, cytokine, calcium.. etc) which occurs during the
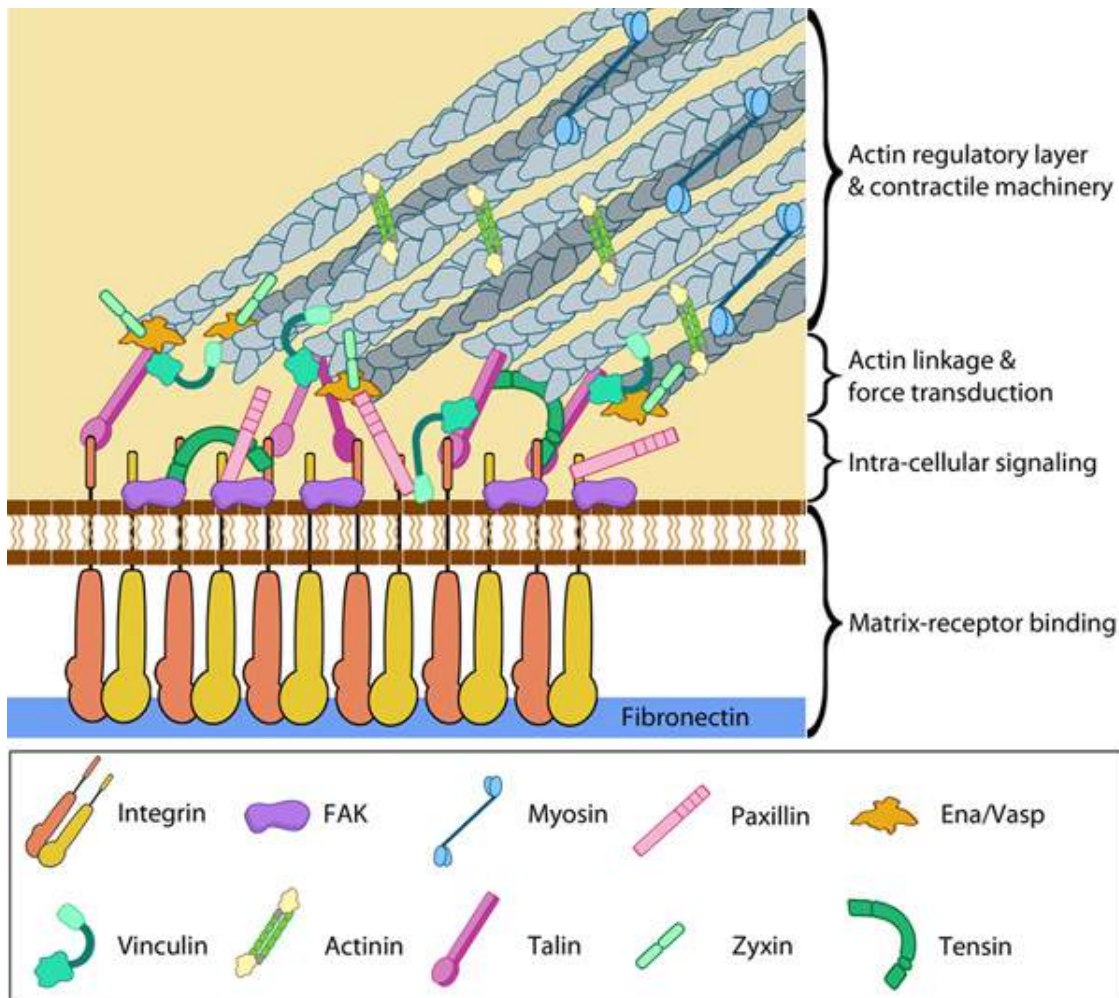
Figure 1.10: Schematic representation of a focal adhesion. A mature focal adhesion contains hundreds of proteins that are grouped based on their contribution to four basic processes: receptor/matrix binding, linkage to actin cytoskeleton, intracellular signal transduction and actin polymerization. Both actin polymerization and acto-myosin contractile machinery generate forces that affect mechanosensitive proteins in the actin linking module, the receptor module (e.g. integrins), the signaling module and the actin polymerization module. The combined activity of the mechanosensitive components forms the mechanoresponsive network. From [40, 41]
.
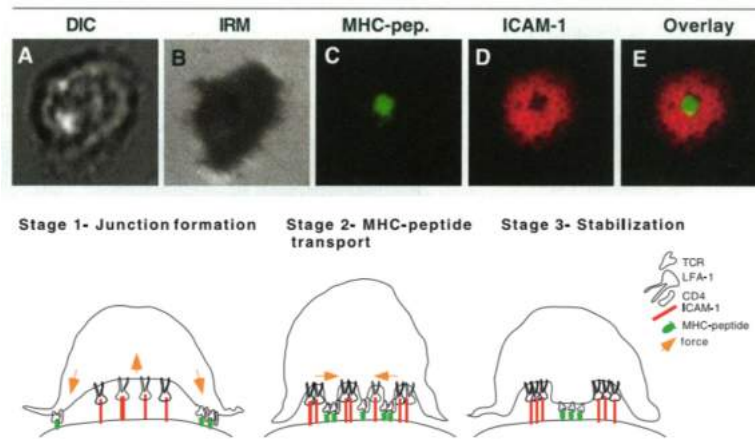
Figure 1.11: **Immunological synapse formation.** (A) Bright-field image. (B) IRM image. (C) Fluorescent image of pMHC. (D) Fluorescent image of ICAM-1. (E) Overlay of pMHC and ICAM-1. Bottom : Model for immunological synapse formation with receptor reorganization. Side view of T cell forming an immunological synapse with an APC [44].

.

interaction [53]. T-cells and APCs can originate from a host (from secondary lymphoid organs like lymph node and spleen of immunized or infected host) or cell lines. However, in order to understand how the organization of receptors and signaling molecules at the cell-cell interface could have an impact on lymphocyte activity, experiments *in-vitro* using artificial APCs were used. They allows a good control of the composition of the APCs surface as well as high resolution imaging.

One approach is to use a mimetic system by replacing the APC by a Supported Lipid Bilayer (SLB) on which ICAM-1 molecules and pMHC complex are grafted allowing a free diffusion on the surface (see Figure 1.11) [44]. This synthetic substrate where the ligands are mobile allows the formation of an functional immunological synapse. This result demonstrated that the formation of this synapse was done by reorganization of receptors at the T-cell-APC interface and thus that ligand mobility has an impact on IS formation and T-cell activation. This conclusion was confirmed by Hsu et al. where they studied the impact of the ligand mobility on IS formation and T-cell activation [54]. To do so, they changed the lipids composition mixture in order to vary the diffusion coefficient of the SLB and thus the ligands mobility. Moreover on this substrate, TCR ligand is anti-CD3 molecules grafted on SLB. Anti-CD3 can activate TCR as well as pMHC. They conclude that a higher ligand mobility favored a full T-cell activation(Figure 1.12).

1.3.2 Structure of the immunological synapse

The synapse is formed at the interface between two cells, and is therefore mediated through the cell membrane. The cell membrane (also called as plasma membrane) is a major actor in adhesion of cells as it forms a barrier between the inside of the cell and the outer environment. The membrane is generally composed of double-chained phospholipids, cholesterol, glycolipids and proteins arranged as a fluid bilayer (Figure1.13).
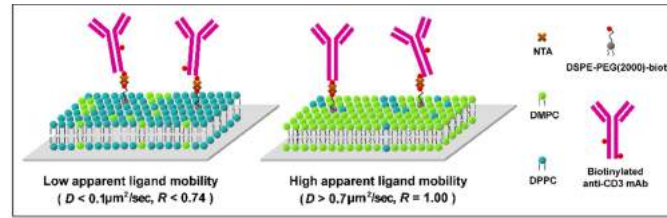
Figure 1.12: **Schematic illustration of self-assembled supported lipid bilayers containing a mixture of DMPC, DPPC, and 2% DSPE-PEG2000-biotin. Biotinylated anti-CD3 monoclonal antibody was anchored to bilayer surfaces via neutravidin (NTA)** Adapted from [54].
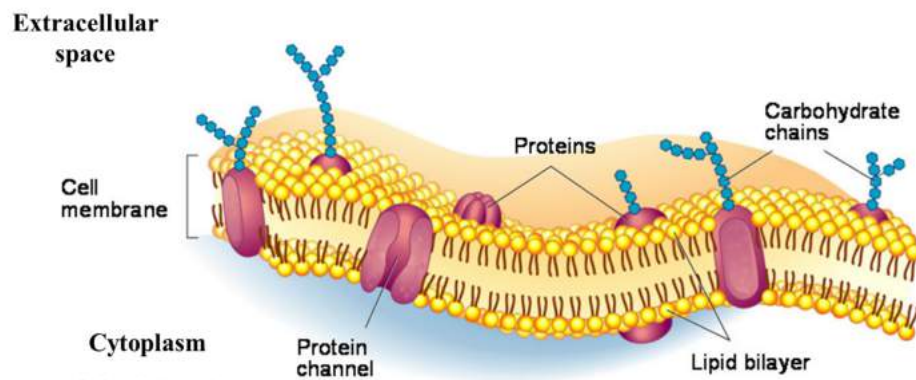
Figure 1.13: **Fluid mosaic model of the plasma membrane.** Adapted from [58]

The thickness of a lipid bilayer is around 4-5 nm. The most important properties of lipid bilayers, which makes lipids the ideal choice for the material of the cell membrane, are flexibility, softness, fluidity and semi-permeability. The diffusion constant of the lipids in the membrane is around $1\mu m^2$/sec and for the proteins the fluidity was measured to be around 0.01-$0.1\mu m^2$/sec.

The IS has been observed in different forms [55] but here we will focus our study on the traditional monocentric "Bull's eye" characterized by concentric rings enriched of different molecules called Supramolecular Activation Cluster (SMAC). [56, 53] (Figure 1.14). The first observation of these concentric rings was done by Monks et al. in 1998 by looking at the interaction between a T-cell and a B-cell in the presence of antigens [57]. As shown on Figure 1.14, the central zone (designed as cSMAC) is enriched in signaling molecules like the TCR on T-cell surface which will interact with pMHC on APC. Then in the peripheral zone (designed as pSMAC), there are molecules like the co-receptors CD4 or CD8 or LFA-1 which will stabilize the interaction by binding to the pMHC or ICAM-1. The last ring (designed as dSMAC) is enriched in large proteins such as CD45 and CD18.

This concentric structure as been shown to achieve a complete activation of the T-cell by facilitating the engagement of different transmembrane molecules and the recruitment of signaling molecules in the same time and restricted place[44].
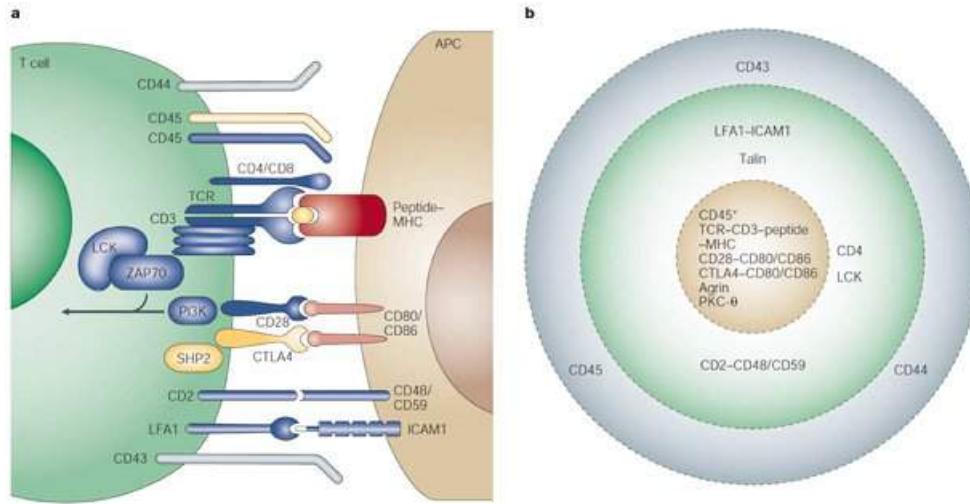
Figure 1.14: **Representative schema of Immunological Synapse molecular organization.** (a) Profile view showing important ligands and signaling molecules involved during the interaction. Activating/co-stimulatory molecules are blue, the stimulatory pMHC molecule is shown in red. (b) Face view showing the characteristic "Bull's eye" organization. The different SMAC are represented: the cSMAC in yellow, the pSMAC in green and the dSMAC in gray. From [53].

Any pathologies affecting these crucial T-cell/APC interaction step can have an impact on the immune system activation and regulation. This phenomenon of adhesion is crucial for T-lymphocytes because it permits their activation and therefore the activation of the whole adaptive immune system. Pathologies affecting this step such as some T-cell lymphoma [59] have an important impact on the immune system regulation and activation that allow the elimination of the pathogen via cell-mediated response or via an antibody response.

1.3.3 Dynamics at immunological synapse

There is a link between the dynamics of cell adhesion and membrane coupled actin based cytoskeleton reorganization. The cytoskeleton is a dynamic network with multiple functions such as maintenance of the cell shape, mechanical resistance to deformation and more [60]. Cytoskeleton is constituted of three components: microtubules, intermediate filaments and the actin fibers. Actin fibers (or microfilaments) are the thinnest filaments and are linear polymers of G-actin subunits. Actin is able to generate force when the growing end of the filament pushes against the cell membrane. In order to generate contractile forces, a molecular motor called Myosin is attached to the actin and moves along the filaments. Actin was shown to be implicated in T-cell mobility in a Ca^{2+} dependent manner, demonstrating the importance of its recruitment when T-cells are activated [61]. Additionally, the actin cytoskeleton (precisely F-actin) is dynamic and plays an important role during the formation of the IS. Indeed, proteins clusters are drive by the actin centripetal flow in order to form the SMAC. In a mature synapse, actin is
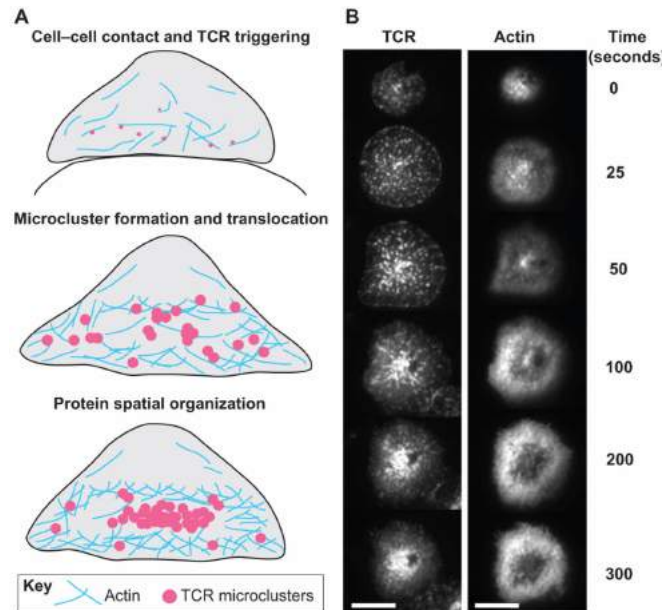
Figure 1.15: **Actin dynamics during T cell activation.** A: After T cell triggering, the actin cytoskeleton promotes cell polarization, maintains cell–cell contact and facilitates TCR signaling across the plasma membrane. Actin acts as a scaffold for the clustering of proteins, drives their centripetal translocation and spatially organizes the microclusters to different domains to form the immunological synapse. In a mature immunological synapse, actin is depleted from the central area where TCR microclusters accumulate. B: Transport of TCR microclusters and actin retrograde flow are temporally coordinated during T cell activation. In a T cell triggered by a stimulatory supported lipid bilayer, the TCRs and actin are imaged simultaneously by using total internal reflection fluorescence microscopy (TIRFM). Scale bar: 5μm. Adapted from [62].

depleted from the center where TCR microclusters accumulate (Figure 1.15) [62]. Actin dynamics at the IS is characterized by polymerization in the lamellipodium, centripetal flow, and filament disassembly in the central region.

Dynamic studies have shown that the cSMAC structure is actually the result of the fusion of TCRs microclusters which migrated toward the center of the cell in an actin dependent manner[63, 64]. Moreover ICAM-1 ligand was also shown to form micro-clusters at the interface between a T-cell and an activating surface [65]. The TCR associated protein like the kinase ZAP-70 were also shown to form micro-clusters which co-localized with the TCR's [66] (Figure 1.16). Recently this co-localization was confirmed using single-molecule localization microscopy showing that only dense clusters of TCR-CD3 complexes were phosphorylated and associated with downstream proteins, like ZAP-70 and the adaptor linker for activation of T-cells (Lat) [67].

TCR/pMHC recognition induces an actin and microtubule cytoskeleton rearrangement which leads to the movement of the different microclusters toward the center of the IS (Figure 1.17). This rearrangement is induced by the ERM proteins (Ezrin, Radixin, Moesin) which make a link between membrane component and actin cytoskeleton. More-
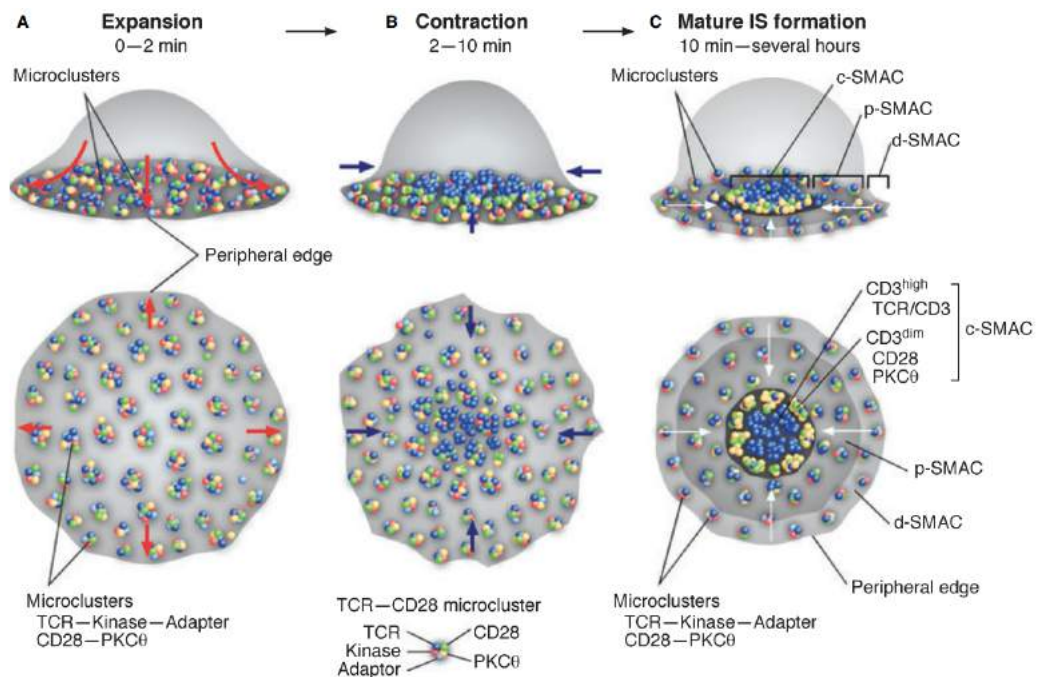
Figure 1.16: **Dynamics of microclusters during the immunological Synapse.** Formation of the IS in a T-cell allowed to spread on lipid bilayer containg pMHC, ICAM-1 and CD80. Microclusters are formed as soon as the cell begins to spread and are directed to the center where they fuse together. New microclusters are continuously formed at the periphery and directed towards the center of the cell. From [64].
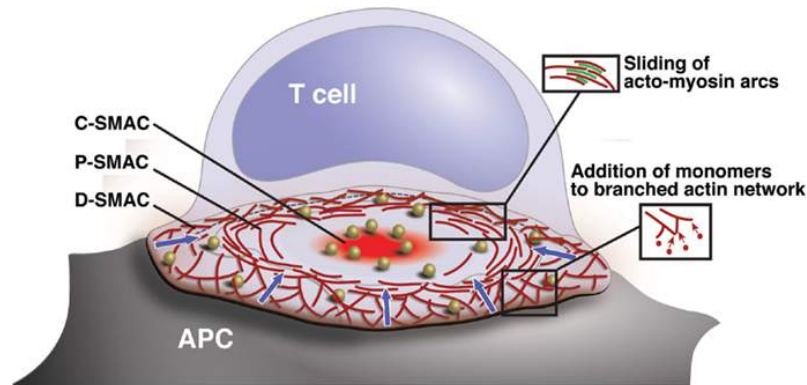
Figure 1.17: **Actin organization at the interface T-cells/APC.** Microclusters of signaling molecules including TCR form and are transported toward the center (golden balls) via a centripetal flow of the actin network (blue arrows). From [72].

over the actin cytoskeleton polarization is required during this process. This is done with polarity regulator like Dlg1 ([68, 69]). Together these two types of proteins will ensure the microtubules organization at the IS [70, 71].

Any pathologies affecting these crucial T-cell/APC interaction steps can have an impact on the immune system activation and regulation. For example, T-cells infected by HIV-1 will have a deregulation of the cytoskeleton organization leading to a defective IS with reduced TCR clustering [71]. This phenomenon of adhesion is crucial for the T-lymphocytes because it permits their activation and therefore the activation of the whole adaptive immune system. Pathologies affecting this step such as some T-cell lymphoma [59] have an important impact on the immune system regulation and activation that allow the elimination of the pathogen via cell-mediated response or via an antibody response.

1.4 T-Cell mechanics and micro-environment sensing

It is well established that cell have a mechanosensitivity toward their environment. They are not only sensitive to the surface chemistry but also to the cell environment mechanical properties like rigidity as well as the spatial organization and the topography. In this section we present basics of cell mechanics and micro/nano environment sensing and put it in the context of T-cells.

1.4.1 Cell mechanics

It was shown that the stiffness of the environment is an important factor to maintain cell integrity and cells can apply forces and in turn react to the resistance offered by their environment [73, 74, 75, 76, 77, 78]. Using hard surface such as glass does not fully represent the soft physiological environment of cells. Therefore, in order to better mimic this environment, soft substrates become an interesting tools [79, 80, 81].

However contradictory results can be found about behavior on soft substrates ac-

cording T-cells origin. For example, naive mouse T-cells are more activated on stiffer substrates made with polyacrylamide gels [82] whereas human T-cells on silicon rubber (PDMS) show the opposite [83]. Recently in our group further study was done using Jurkat T-cell and PDMS substrates with an elasticity ranging from 3kPa to 2MPa. These experiments have shown that T-cells have a larger cell spreading area on soft substrates. Moreover a recent study showed that T-cells apply more force on harder surfaces. Moreover, soft patterned substrates were also fabricated showing that only the TCR distribution is sensitive to this soft topography [84].
Additionally, stiffness have been shown to affect human primary CD4$^+$ T-cell functions, which adapt their responses accordingly [85].

Moreover, another property of the T-cell environment to take into account during cell study is the mobility of the ligands. By using a fluid supported lipid bilayer functionalized with mobile ligand (for example anti-CD3 as TCR ligand) this property has been demonstrated to be important. Indeed it has been shown that cell spreading area as well as actin organization are influenced by the ligand mobility (Figure 1.18) [86].

1.4.2 Micro/nano-environment sensing

Cells are now known to be sensitive to their micro and nano-environement. Both chemical [87, 88] and topographical [89] structures were studied.

Early in 1997 Chen et al. presented the importance of the adhesion spot size for cell life and growth. Indeed, it was shown that by decreasing the size of adhesive patches cells could switch from growth to apoptosis. Moreover, they showed also that cells can vary their shape while maintaining the total cell-ECM area constant by decreasing the size and spacing between the focal adhesion points (Figure1.19)[90]. Following this study, it became clear that localization of focal adhesion points can be controlled by patterning patches of adhesive proteins [91]. Micro-patterning, of either bio-chemical or topographical origin, is now a standard technique in different domains of biology and biophysics [92, 93, 94].

After these discoveries, strategies of large scale patterning at the nano-scale were performed. The technique called Block Copolymer Micelles nanoLithography (BCML) is based on the fabrication of patterns of gold particles on glass slides. Each nano-dot can be functionalized with a single molecule, for example adhesion receptors and the distance between each dot can be precisely control [95, 96]. Using this technique, further studies have shown that there is a spacing limit (50-70 nm) beyond which cells do not recognize single ligands as clusters. In fact nano-gold particles were functionalized with RGD peptides, and if the spacing between the dots is superior to 70 nm, the cell adhesion and spreading is affected by reducing the formation of focal adhesions and actin stress fibers. And in a other hand, if the spacing between the dots is inferior to 60 nm, it will allow an effective adhesion[88]. These micro-nano fabrication techniques became a tool to mimic the cell environment for cell adhesion study, allowing to easily be able to change the topography and biochemistry of the synthetic ECM.
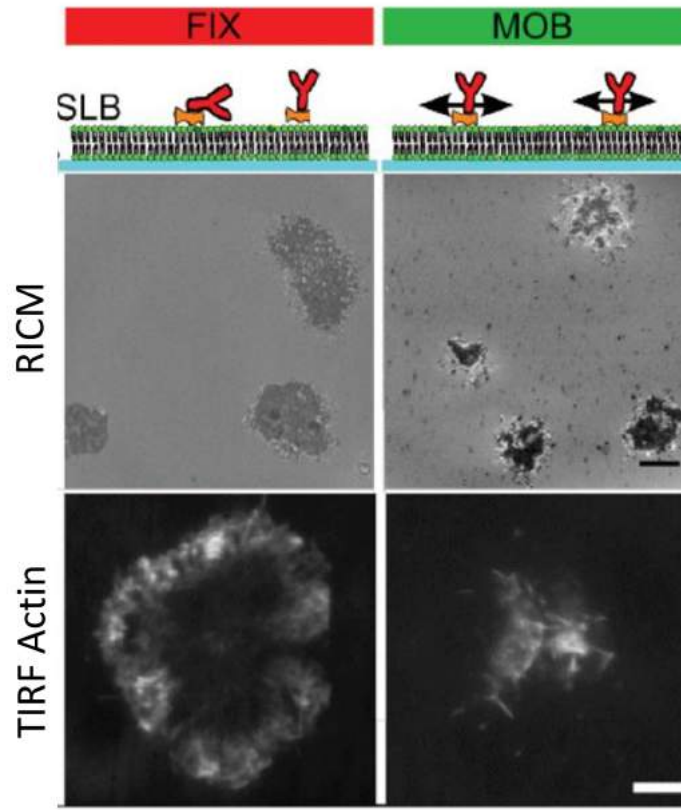
Figure 1.18: **Ligand mobility determines the T-cell spread area and actin distribution** Row 1: Scheme of the functionalization of the substrates with mono-biotin fluorescent Anti-CD3 coupled via Neutravidin. Fix: immobilized Anti-CD3 on Supported Lipid Bilayer (SLB). Mob: mobile Anti-CD3 on SLB. Row 2: RICM images of Jurkat T cells after 15 min engagement on substrates. Row 4: TIRF images after labelling actin with Rhodamine Phalloidin. Scale bars: 5 μm. Adapted from [86].
.
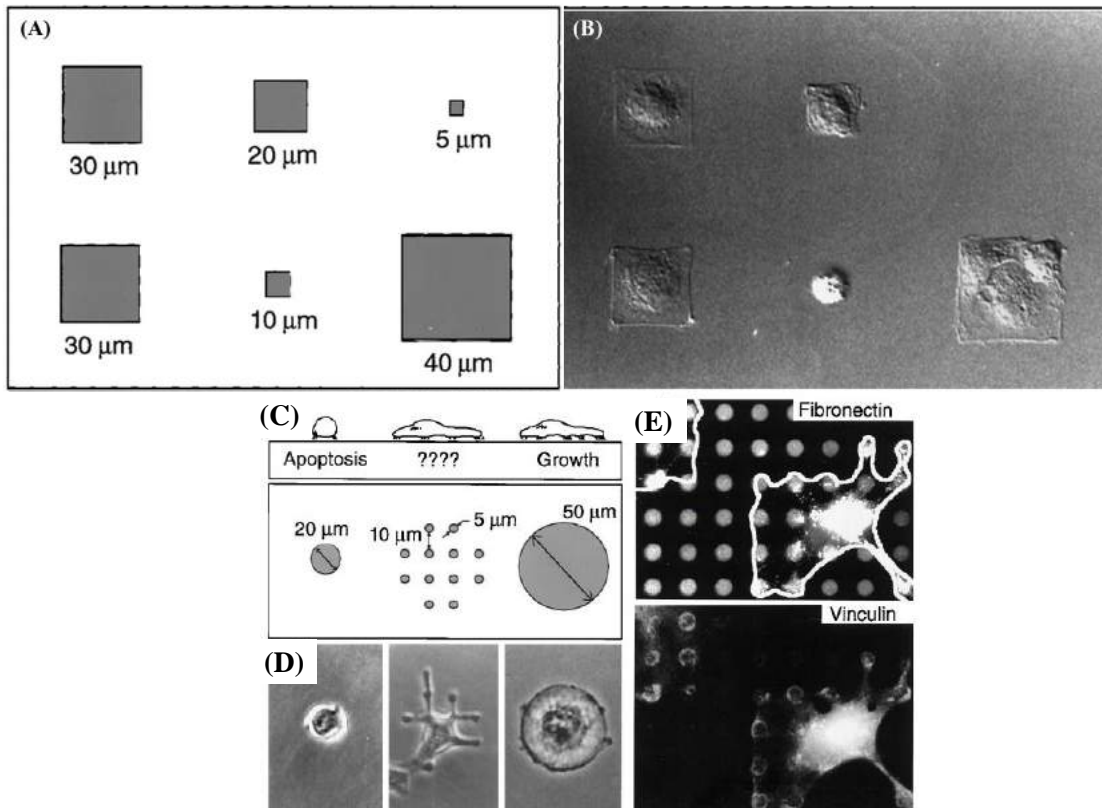
Figure 1.19: **Effect of ligands geometry on cell adhesion and growth** (A) Different squares size of adhesive islands coated with fribronectin. (B) Final shapes of enthodelial cells adhering to the adhesive islands. Cells adapt their shape and adhesion area according to the adhesive island. (C) Substrates used to explore the shape variation of the cell independently of the cell-ECM contact area. (D) Phase contrast images of cell spreading on the patterns shown in (C). (D) Immunofluorescence staining of fibronectin or vinculin for cell spreading on (C). Adapted from [90].
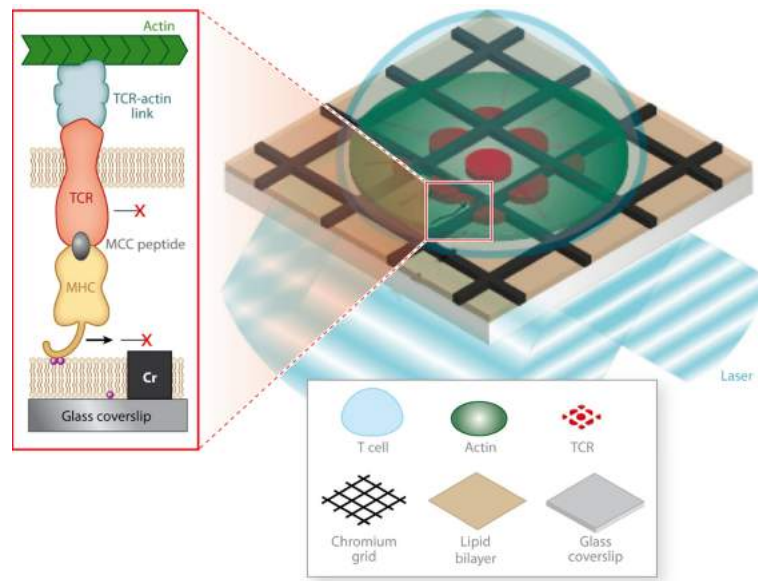
Figure 1.20: **Schematic of a hybrid live-cell-supported membrane junction.** pMHC, ICAM1, and possibly other molecules such as CD80 can be incorporated into a supported membrane where they are free to diffuse laterally and engage their cognate receptors on the live T cell. Structures, at nanometer-scale, may be fabricated onto the underlying substrate to corral and guide the motion of these supported membrane molecules. Then, through specific receptor-ligand interactions, molecules within the living T cell become subject to the same physical constraint. From [65].

.

1.4.2.1 SLB micro-patterned

Motivated by the different molecular organizations through which the immunological synapse undergoes before being mature, studies aimed to understand how the organization of receptors and signaling molecules at the cell-cell interface could have an impact on the activity of lymphocytes. In this perspective Groves et al. have demonstrated, by confining TCR ligands within a micrometer perimeter using a barrier in the bilayer (Figure 1.20), that receptors reorganization via actin toward the center is important on T-cell signaling [65].

1.4.2.2 Immobilized micro-pattern

Irvine et al [97] have studied T-cells activation on fixed substrates composed of antibodies directed against the CD3 molecule of the TCR complex (anti-CD3) surrounded by the adhesion molecule ICAM-1. They used photolithography in order to immobilize the anti-CD3 into different organizations. They have thus been able to create different patterns which mimic the molecular organization found at the APC surface during the formation of the immunological synapse, such as, for example, the presentation of the TCR ligands in the form of microclusters or the characteristic motif of the synapse, with the TCR ligands in the center surrounded by adhesion molecules (Figure 1.21). They found that T-cells can be fully activated when focal spots of TCR ligand are in the center of the

interacting surface. Later Kam et al.[98] have shown that T-cells were able to produce IL-2 when anti-CD3 dots are surrounded by CD28 (co-stimulating molecule that binds to CD80/86) whereas when both are co-localized they did not. These studies emphasized the importance of the organization of the ligands on the formation of the immunological synapse and the activation of the LT.

1.4.2.3   Immobilized nano-patterned

In order to study the roles of the substrate's physical properties and the presentation of nanoscale ligands on adhesion and T cell activation, new substrates were developed. For these it is necessary to precisely control the characteristics of the substrate. With this idea, Spatz and his team developed a substrate composed of a nanoscale protein pattern whose size, molecular density and distribution were controlled. This nano-pattern is obtained by a nanolithography technique (block copolymer micellar nanolithography BCML) which allows gold nanoparticles to be disposed on glass in an organized manner on which the proteins of interest are directly immobilized [99, 100, 101]. Although this substrate confirms the existence of a relationship between molecular density, ligand organization and cell adhesion and activation, it does not allow the observation of the molecular organization at the T-cell-APC interface due to its incompatibility with the Total Internal Reflection Fluorescence Microscopy (TIRF) microscopy.

1.4.2.4   Immobilized submicro-patterned

To overcome this compatibility issue, and in order to be able to look at the molecular organization at the T-cell-APC interface a technique based on nanosphere lithography was developped in our team [102]. With this technique, the spacing between ligand is well controlled by the diameter of the beads. Moreover, the absence of metal on this substrate facilitates imaging with sensitive surface microscopy technique like TIRF-M or RICM. T-cell studies on this kind of substrate have shown that local cell membrane adhesion, membrane topography and distribution of the T-cell receptors (TCRs) and the kinase ZAP-70, are influenced by dot-geometry, whereas the cell spreading area is determined by the overall average density of the ligands rather than specific characteristics of the dots (Figure 1.23) [103].

1.5   Surface patterning techniques

Micro/nano fabrication techniques were first developed for the fabrication of integrated circuits but their application have emerged in other fields like biology, biotechnology, biomedical and engineering [104]. In cell biology, this technique is used to further study cellular process like cell adhesion, spreading, motility, proliferation and also cell interaction with their environment [105]. A patterned surface can be achieved by two types of approaches either **top-down** or **bottom-up** [106]. The **top-down** approach consist of creating micro/nano scale structures from a larger dimension (e.g Photolithography) and the **bottom-up** approach consist to assemble small structure to form a bigger one (e.g molecular self-assembly).
This section will describe the main techniques used to fabricate micro/nano patterned surface.
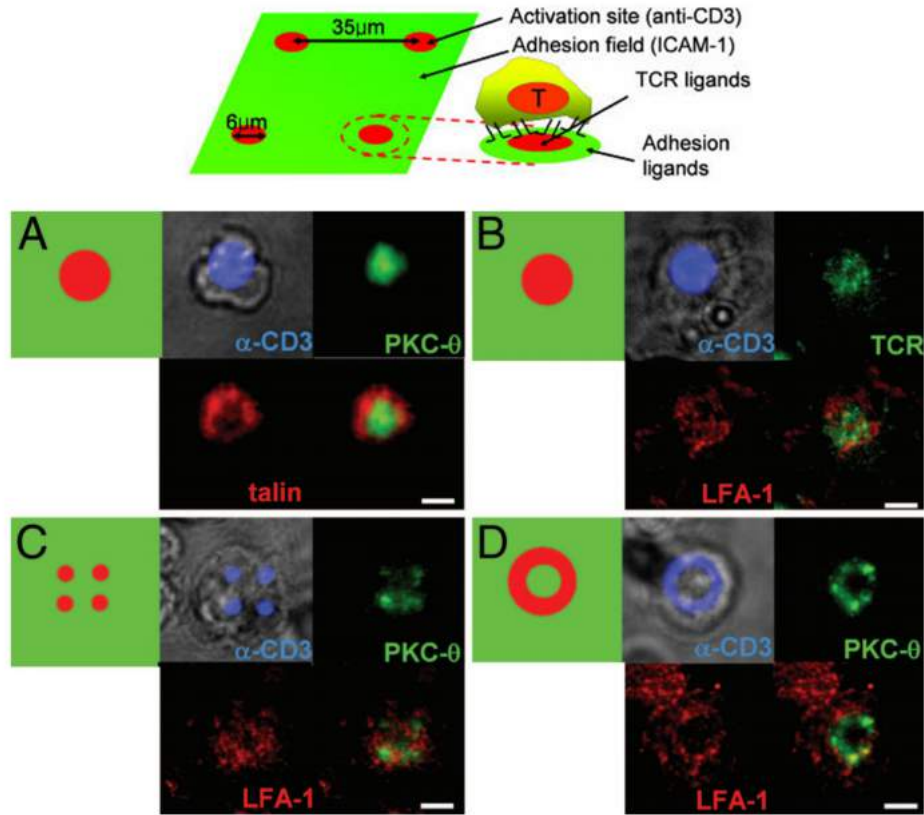
Figure 1.21: **Synapse array patterns template T cell surface receptor and intracellular signaling molecule accumulation at the cell-surface contact site.** Top: Schematic of immunological synapse array surface pattern. In each panel there is a schematic of the anti-CD3/ICAM-1 substrate pattern and representative immunofluorescence images at the cell-substrate contact plane. A. and B. Immunostaining of PKC-θ (green) and talin (red) (A) or TCR and LFA-1 on focal anti-CD3 patterns (B) (C) and (D). Immunostaining of PKC-θ (green) and LFA-1(red) on multifocal patterns (each anti-CD3 spot 2 μm in diameter) (C). or annular anti-CD3 patterns (D). (Scale bars: 5 μm.) From [97].

.

Figure 1.22: **Nano-patterned antigen arrays mimicking APC surface during T-cell activation.** Substrates are biofunctionalized with pMHC molecules following a spatial arrangement, local density, and orientation that are presumed to have a major impact on T cell activation. From [99].

.

1.5.1 Photolitography

To pattern surfaces with the lithography technique, two approaches is possible: either the substrate is coated with a positive photoresist or a negative one. The surface is then exposed to UV light through a mask with the desired pattern. In the case of a positive photoresist, the area exposed to the UV light will depolymerize and be chemically removed during the development step. And in the case of a negative photoresist, the area exposed to the UV light will polymerize and remain during the development process (Figure1.24). The remaining pattern can be used as a mask (for deposition or etching techniques) or as mold to shape polymers such as PDMS.

The advantages of this technique are :
- the reproducibility
- the high resolution of the pattern
and the drawbacks are :
- the need of clean room facilities which may not be easily accessible
- the incompatibility with chemical functionalities and delicate ligands which will be denatured or deactivated
- the fact that it is usable only on flat substrates.

1.5.2 Contact Printing

Micro-contact printing was developed by the Whitesides group in 1993 [109]. It consists of transferring molecules from a elastomeric stamp which is micro/nano structured to another surface. To do so, an elastomeric stamp (obtained using a mold fabricated by lithography) is coated with a layer of molecules of interest which are then transfered to another surface by contact [110, 111] (Figure 1.25). The non-coated regions can also be functionalized with another molecule [97]. In order to successfully transfer the molecules, the substrate needs to have a more attractive interaction for the molecules than the stamp. Also the resolution can be improved (i.e feature of 50 nm) by increasing the stiffness of the stamp [112].

47
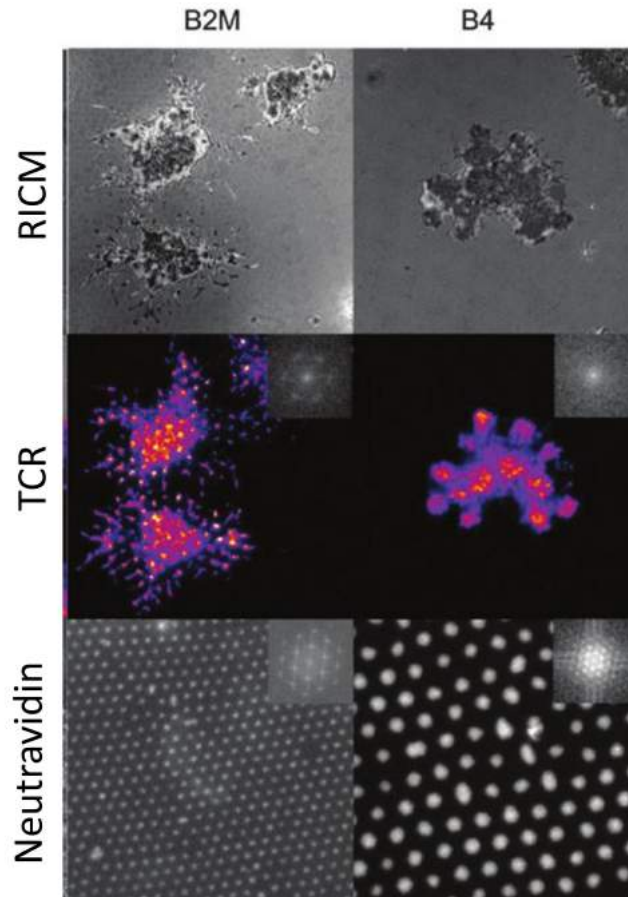
Figure 1.23: **Distribution of TCR on submicro-patterned substrates** Row 1: RICM images of Jurkat cells allowed to interact with dots. B2M: dot pitch of 2μm with dot size= 640±30 nm. B4: dot pitch of 4μm with dot size= 1600±100 nm. Row 2: TIRF images of TCRs clusters. On B2M, the TCR clusters are clearly visible and are usually well localized on the site of the underlying antibody dots as evidenced by FFT (Fast Fourier Transform)in the inset. On B4, the TCR clusters are usually localized on the dots but a closer inspection shows that each dot often recruits several clusters. Insets show FFT which reflects the ordering (or not) of the TCR clusters. Scale bar 5 μm. On Row 3: Underlaying TCR ligand dots. Adapted From[103]
.
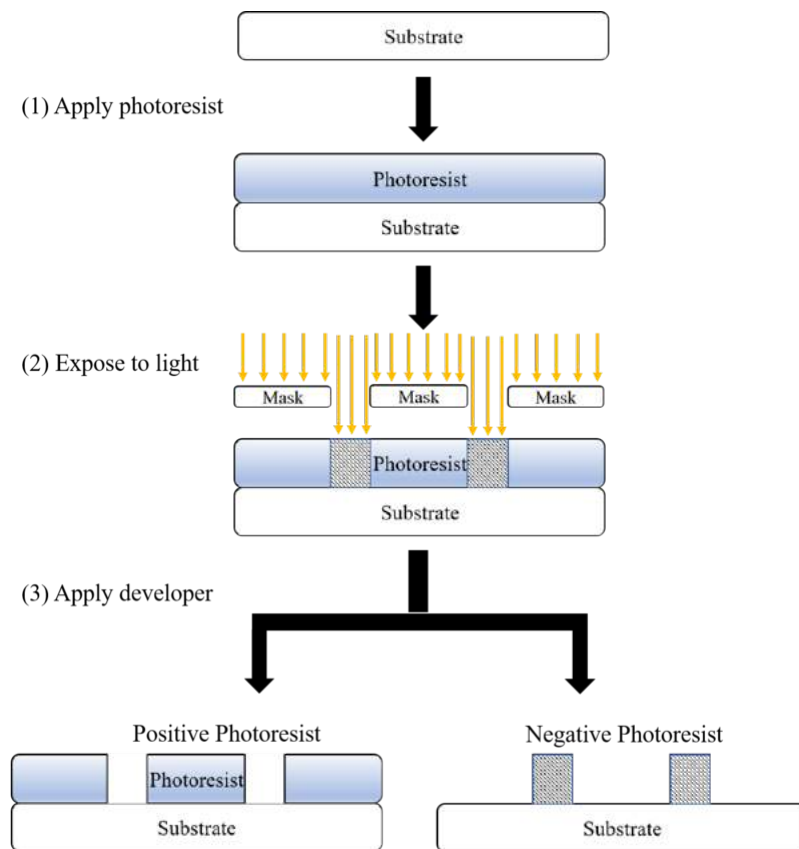
Figure 1.24: **Photolithography using positive or negative photoresist** Adapted From[107]

.
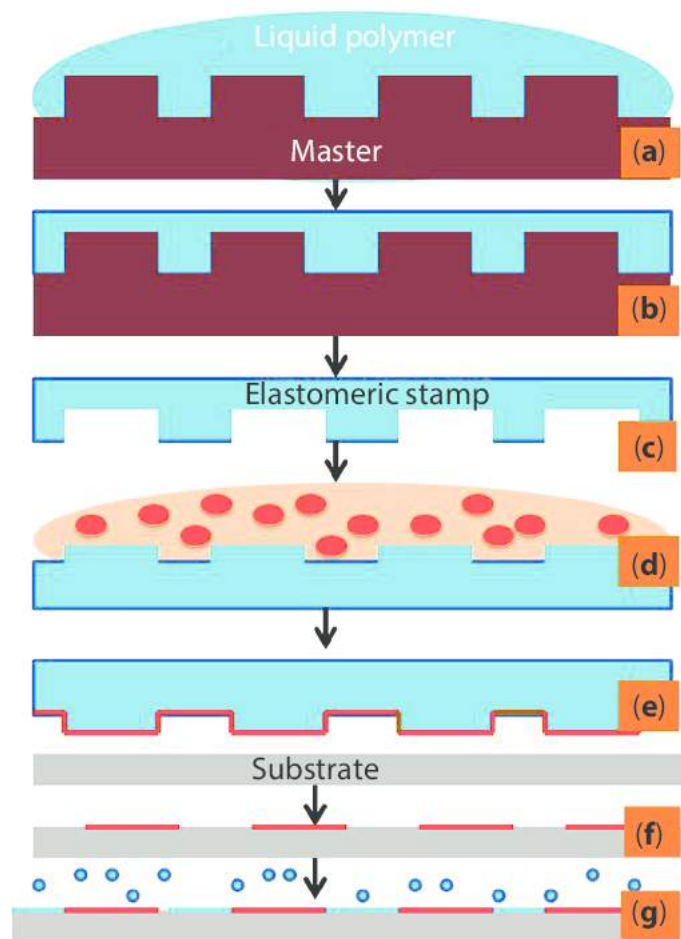
Figure 1.25: **Schematic representation of the micro-contact printing technique** (a) Liquid polymer is cast on the structured master surface. (b) Cure of the stamp (c) The elastomeric stamp after curing, (d) the stamp is inked with the solution containing the bio molecules to be printed. (e) Transfer of molecules by printing onto the substrate. (f) Removal of the stamp. (g) depicts the surface being overflown with the passivating molecular solution. Adapted From[108]

.
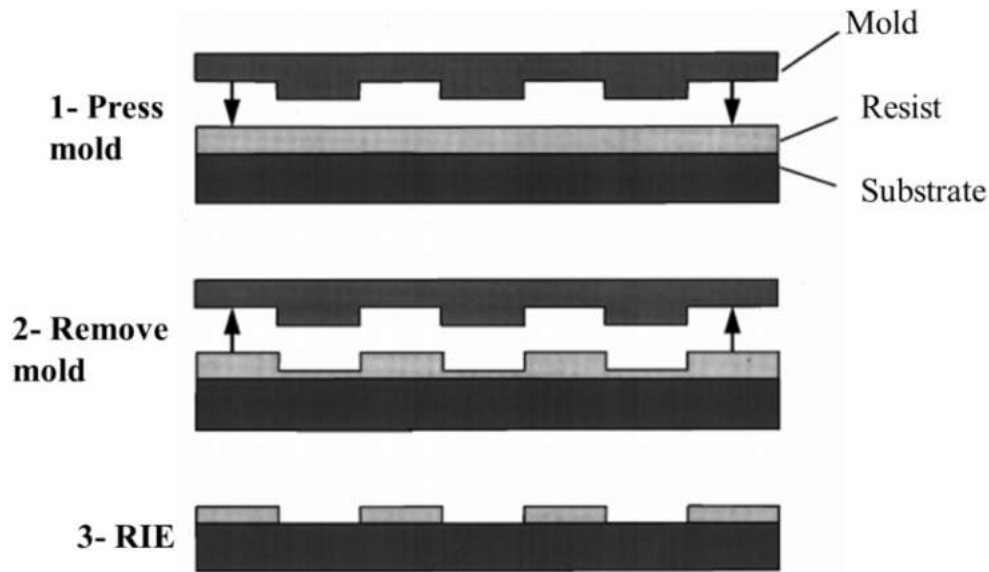
Figure 1.26: **Schematic representation of the Nanoimprint Lithography technique** Adapted From[113]

.

The advantages of this technique are :
- the simple fabrication process
- the fact that it is easy to use
- the capacity of patterning large areas on various materials
and the drawbacks are :
- the possibility to denature the protein if they stay dry too long before the printing.

1.5.3   Nanoimprint Lithography

Nanoimprint Lithography (NIL) consists of mechanically deforming the imprint resist. The imprint is usually a resist which can be cured by heat or UV light[114]. To do so, a hard mold is pressed on a thin layer of resist, then after removing this mold a pattern resist topography is created on the resist. The final step consists of removing the residual resist present on the compressed area with a etching process like reactive ion etching (RIE) (Figure 1.26). Three types of NIL exist: either thermoplastic, photo or electrochemical methods. The thermoplastic-NIL consists of using a thermoplastic polymer then pressing the mold and heating up above the glass transition temperature of the polymer, in order soften the polymer film. The photo-NIL consists of using a photo curable liquid resist and a transparent mold. When the mold and the substrate are pressed together, the resit is exposed to UV light and becomes solid. The residual resist present on the compressed area can be removed by RIE. The electrochemical-NIL consists of using a conductive mold and applying a high voltage when the mold and the substrate are pressed together in order to pattern the surface by electrochemical etching.

The final imprint resist can be use as a substrate with 3D topography [115] or as stamp for contact printing [116]. However, the quality of the obtained pattern is uncertain due
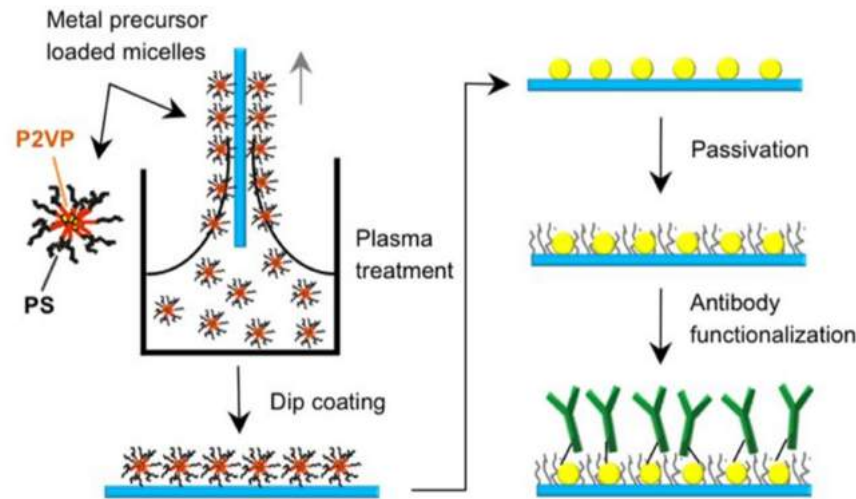
Figure 1.27: **Schematic representation of the Block Copolymer Micelles Nano-lithography technique.** A scheme of stimulatory nanoarray fabrication process including substrate nanopatterning by BCML, passivation, and biofunctionalization. Adapted from[100]

.

to a lack of control during the transfer step.

1.5.4   Block Copolymer Micelles Nanolithography

Block Copolymer Micelles Nanolithography or BCML is a simple technique to fabricate nano-scale structure over large areas [117]. This technique is based on the tendency of block copolymers to self assemble into uniform monomicellar form with ordered domains at the nanoscale. A block copolymer is composed of polymer chains attached by a covalent bond in which a metal nano-particle is embedded. By spin coating or dipping into the micelles solution, the micelles will form a uniform hexagonally close-packed pattern on the surface. Then, the solvent is evaporated and after a plasma treatment the polymer shell is removed leaving the metal nanoparticle pattern (Figure1.27). In general the metallic nanoparticle arrays obtained is with gold. The distance between each particle can be changed by changing the molecular weight of the block copolymer[95]. Also, the particle size can be independently changed by combining BCML with electroless deposition [118]. This technique is used in cell biology for example study the impact of clustering and density ligand on cell adhesion and activation (Figure 1.28) [99, 100, 101].

The advantages of this technique are :
- the versatility technique
- the fact that it is easy to use
- the capacity of nano-patterning large area on various materials
and the drawbacks are :
- the use of metallic particles which are incompatible with high sensitive surface microscopy technique like TIRF and RICM which are essential in cell biology.
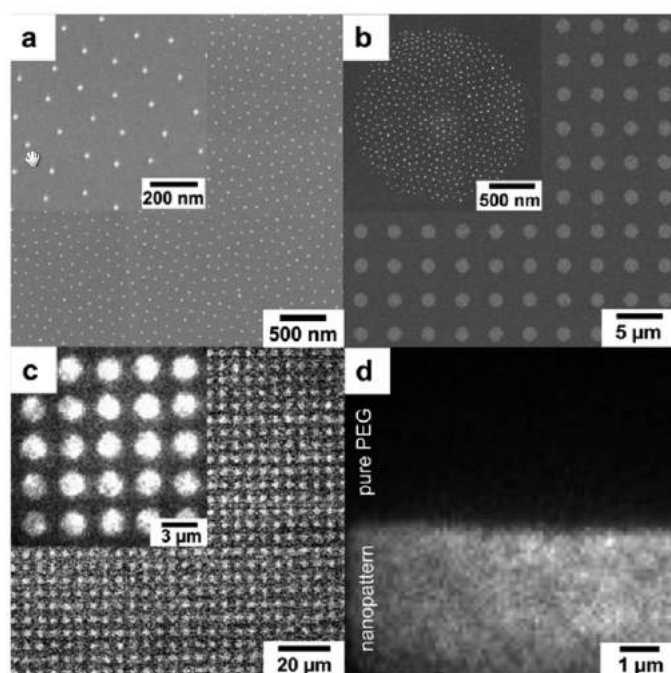
Figure 1.28: **Scanning electron microscopy image of Au pattern obtained with BCML technique.** Scanning electron microscopy of (a) an extensive continuous Au nanopattern and (b) a micronanopattern; (c) fluorescent microscopy image of pMHC labeled with a fluorescent Atto-655 dye and specifically immobilized on a micro-nanopattern; (d) fluorescent microscopy image of the border between a functionalized Au-patterned and a nonpatterned area; fluorescently labeled pMHC only binds to the area with embedded Au particles (bottom bright side). From[99]

.
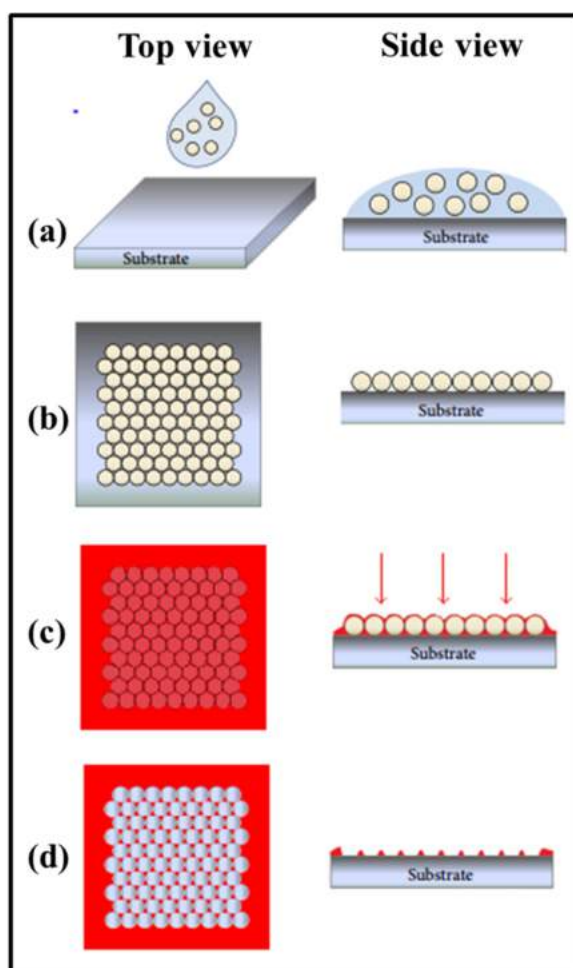
Figure 1.29: **Schematic representation of the Nanosphere Lithography technique** (a) Cleaning of the substrate and deposition of the colloidal suspension. (b) Self assembly of the colloidal suspension on the substrate. (c) Deposition of the material of interest. (d) Removal of the spheres. Adapted from[119]

.

1.5.5   Nanosphere lithography

Nanosphere lithography (NSL) or natural lithography or colloidal lithography was reported in the first place by Fisher and Zingsheim in 1981. It consisted of using a suspension of colloidal sphere to form an ordered monolayer on glass, which was used as a lithographic mask for preparation of platinum nanostructures. Following this work, new approaches were developed to improve the quality of this technique. This technique allows a regular and homogeneous patterned distribution of nanoparticles. To do so, a suspension of colloidal spheres (e.g polystyrene or silica) is deposited on substrate (e.g glass), then after drying, the material (e.g polymers and proteins) is deposited through the holes of the ordered mask. Finally when the spheres are removed an array of ordered nanodots on the surface of the substrate is formed (Figure 1.29).

This nano-scale technique can be compatible with TIRF and RICM however, the

size and the inter-spacing is dependently determined by the nanosphere diameter, which means that the dot size can not be independently changed which is an important requirement for cell study. Different strategies have been tried to overcome this issue [120, 121] but without any conclusive outcome. In our group, a new NSL approach was developed by creating nano-dots whose size can be changed independently of the spacing [102]. This technique was used during this thesis to fabricate nano-patterned substrates and will be explained in more detail in section 3.1.

1.6   Thesis outline

This thesis work is the continuation of the work begun previously in the team to understand the impact of the organization and/or mobility of the ligands found on the surface of APC on the T-cell behavior[102, 103].

Following these observations which have shown that the mobility and the presentation of ligands have an influence on cell behavior, the aim of this thesis was to combine these two elements (mobile ligands and presentation in the form of nano-patch) in a single substrate and to study its impact on cellular behavior. This substrate mimics the surface of the APCs in a better way through an antigenic presentation in the form of controlled clusters integrated within a fluid lipid bilayer that may or may not be functionalized with proteins. Moreover the substrate is compatible with various microscopic techniques including Total Internal Reflection Fluorescence Microscopy (TIRF-M) and Reflection Interference Contrast Microscopy (RICM).

The chapters of this thesis can be broadly divided into two categories: a technical part about the fabrication and characterization of the patterned substrates (*Chapters 2 and 3*) and an experimental part on cellular studies using these patterned substrates (*Chapters 4 and 5*). Finally, a concluding chapter that presents an overview, recalling key results in the context of the state of art and discusses possible explanations and consequences of the presented experimental results.

Chapter 2

Materials and Methods

Contents

In this chapter, I will present the proteins, lipids and other chemicals as well as cells used in this thesis. Standard methods and techniques are also detailed here. Specific techniques and protocols developed for this thesis will be presented in the next chapter.

2.1 Slides and chambers

2.1.1 Glass slides

The majority of experiments were conducted using the following glass slides:
- Glass coverslides (Thickness = 170 microns, Assistant, Karl Hecht KG, Germany, 24 x 24 mm) for open chambers.
A second type of slides was used for a limited number of experiments involving supported lipid bilayers prepared using vesicle spreading (VS) (see 3.3.4) :
- Round glass coverslides (Thickness = 0.17 ± 0.05 mm, 40 mm coverslides) for FCS2 chambers.

Two different cleaning procedures were used in order to prepare the glass coverslides: either with a mild surfactant solution for majority of cases (called procedure 1 see Appendix A.1) or based on a long incubation in piranha acidic solution specifically for VS (called procedure 2 see Appendix A.2)

2.1.2 Chambers

Two types of chamber were used for substrates deposition :

- Round open home-made chambers used with square coverslides for bilayer made using Langmuir-Blodgett/Langmuir-Schaefer technique or using vesicles spreading technique (Figure 2.1).

- Flow chambers Focht Chamber System 2 (FCS2 ®,Bioptechs, USA) used with round coverslides for bilayer made using vesicles spreading technique.
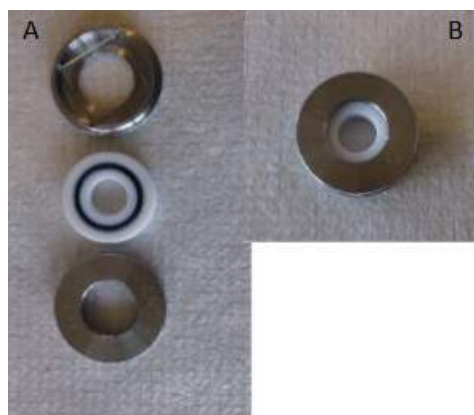
Figure 2.1: **Chambers** A:Home-made open chamber unmounted, from top to bottom; Lower part with spacing to fit the coverslide; Teflon ring with a rubber gasket; Upper part; B: Home-made open chamber mounted.

2.2 Principle of metal sputtering

The nano-fabrication platform of CINaM (Clean room of class 1000) was used for two distinct steps in pattern fabrication : metal sputtering and E-Beam lithography.

The process of sputtering is based on the bombardment of a metal target by gas ion (most of the time Argon) under high vacuum. An exchange between the ions and the metal atoms can occur due to collisions, and the released atoms are guided to the sample. To do so, a voltage is applied between the two electrodes : the cathode where the metal target is fixed and the anode where the sample is placed, which will create a discharge. The Argon ions (Ar^+) created will be accelerated on the target and acquire more energy that is released during the impact with the target, provoking the ejection of the metal atoms which are then deposited on the sample. In our case, in order to enhance the ionization of the target by the Ar^+, we add a magnet to the cathode, which will traps the atoms around the target and increases the sputtering (Figure 2.2).
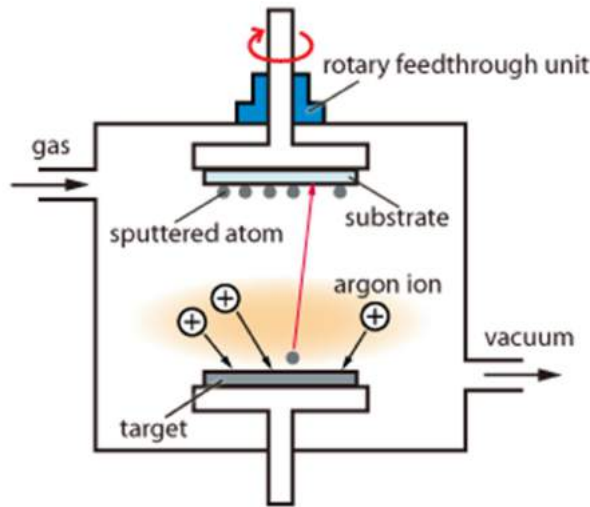
Figure 2.2: **Principle of sputtering.** Argon atoms bombard the target which induces release of metal atoms which are deposited on the substrate. And then the atoms reach the sample .Source image [122].

2.3 Substrate functionalization

The clean glass slides were either functionalized homogeneously (usually with proteins) for control experiments or were first nano-patterned (see protocol in Chapter 3) and then functionalized. In either case, the steps are identical and are explain bellow.

2.3.1 Organo-silane based Functionalization

3-aminopropyltriethoxysilane (APTES) (Sigma-Aldrich, France) was used in order to render the glass slides hydrophobic, and to encourage protein absorbtion (Figure 2.3). APTES covered slides served as basis for further functionalization as described in Chapter 3.
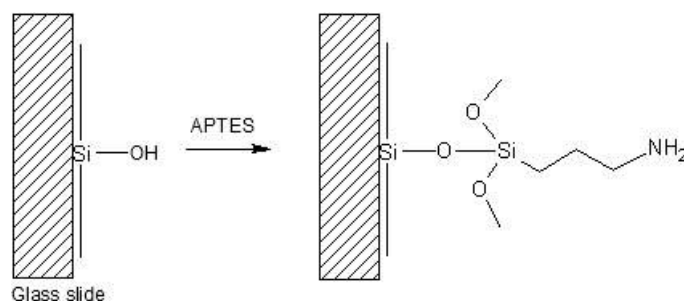
Figure 2.3: **Functionalization of glass slides using APTES.** Adapted from [123].

2.3.2 Lipids bilayer based Functionalization

Lipid bilayers were either used as passivating layer to discourage cell adhesion to bare glass or were themselves functionalized.

Lipids were received either dried or already solubilized in chloroform. Dry lipids were dissolved with clean chloroform (99.9%, Sigma, France) before use. The lipids were then mixed to the desired concentration (typically 1 mg/ml) and composition (see below). The lipids solution were kept protected from light at -20° C under argon atmosphere and sealed with Teflon tapes for no longer than 1 week for the working solution and 6 weeks for the stock solution. Before their use, the lipids solution was warmed up to room temperature to ensure the absence of condensation when opening of the bottle.

2.3.2.1 Lipids

The following lipids were used (see Figure 2.4 for their structure):

1- DOPC (1,2-dioleoyl-sn-glycero-3-phosphocholine (Avanti Polar Lipids, USA)) was used as the main ingredient for the SLBs. Often, one or more of the following lipids were used in addition :

2- NTA: 1,2-dioleoyl-sn-glycero-3-[(N-(5-amino-1-carboxypentyl)iminodiacetic acid)succinyl] (nickel salt) (Avanti Polar Lipids, USA) typically used with a 5% ratio. This lipid presents a Ni-NTA-Tag permitting the fixation of protein with a His-tag tail.

3-Cap-biot: 1,2-dipalmitoyl-sn-glycero-3-phosphoethanolamine-N-(cap biotinyl) (sodium salt) (Avanti Polar Lipids, USA) typically used with a 2'% ratio. This lipid presents a biotin-Tag permitting the fixation of protein from the avidin family.

4- PEG2000 PE : 1,2-dioleoyl-sn-glycero-3-phosphoethanolamine-N-[methoxy(polyethylene glycol)-2000] (ammonium salt) used with 2% ratio. This lipids presents a PEG-Tag permitting to add an repulsif effect on the bilayer and to mimic the glycocalyx of the cell membrane.

5- C-12 bodipy (Life technologies, USA) is a fluorescent fatty acid analogue that has been used for fluidity measurements of the lipid bilayer.

6- Dansyl PE :1,2-dioleoyl-sn-glycero-3-phosphoethanolamine-N-(5-dimethylamino-1-naphthalenesulfonyl) (ammonium salt) (Avanti Polar Lipids, USA) has been used for fluidity measurements of the lipid bilayer.
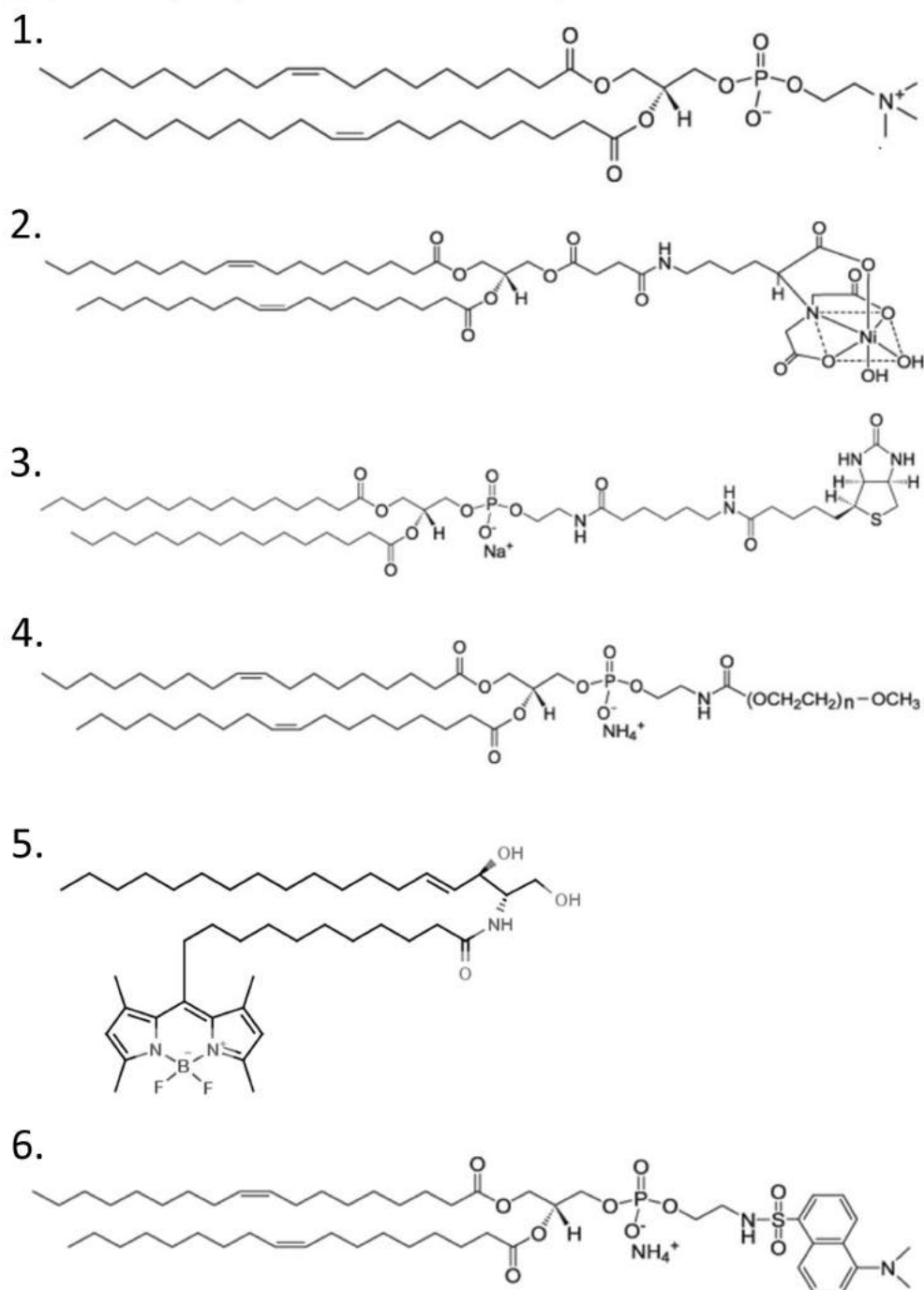
Figure 2.4: **Lipids structure.** 1. DOPC:1,2-dioleoyl-sn-glycero-3-phosphocholine; 2. NTA:1,2-dioleoyl-sn-glycero-3-[(N-(5-amino-1-carboxypentyl)iminodiacetic acid)succinyl] (nickel salt); 3. Cap-biot:1,2-dipalmitoyl-sn-glycero-3-phosphoethanolamine-N-(cap biotinyl) (sodium salt); 4. PEG2000PE:1,2-dioleoyl-sn-glycero-3-phosphoethanolamine-N-[methoxy(polyethylene glycol)-2000] (ammonium salt); 5. C-12 bodipy; 6. Dansyl PE:1,2-dioleoyl-sn-glycero-3-phosphoethanolamine-N-(5-dimethylamino-1-naphthalenesulfonyl) (ammonium salt)
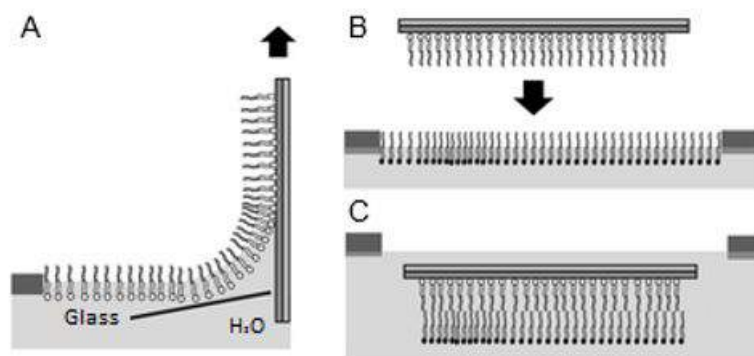
Figure 2.5: **Lipid bilayer formation using Langmuir-Blodgett/Schaefer technique** A. Langmuir-Blodgett first layer deposition; B-C Langmuir-Schaefer second layer deposition. Adapted from [125].

2.3.2.2 Supported Lipid Bilayers

Langmuir-Blodgett/Langmuir-Schaefer technique
For most experiments SLBs were made using Langmuir-Blodgett/Langmuir-Schaefer (LB/LS) technique.

Since lipids are amphiphilic molecules, a film of lipids is formed at the water-air interface: the head is immersed in water and the tail is repelled and oriented perpendicularly to the water surface. This organization is in form of a monolayer. A method which use this property to produce easily a monolayer of lipids molecules was developed by Vincent Schaefer and Katharine Burr Blodgett.The LB/LS is a technique using this phenomena in order to produce lipid bilayers. The first layer is deposited on a glass slide using Langmuir-Blodgett technique (see Figure 2.5 A) and the second is deposited on top of the first one using Langmuir-Schaefer technique ([124]) (see Figure 2.5 B-C)

The apparatus

Here a commercial Langmuir trough (NIMA) with size 30X10 cm was used to make SLB. The balance was placed in the room whith a definite temperature of (23° C). Chambers, glass slides and Teflon elements used for this procedure were cleaned using cleaning procedure 1 (see Appendix A.1). The LB/LS technique requires a specific device which is called a film balance which is composed of four main elements (Figure 2.6):
- The teflon enclosure (Figure 2.6 A.1) which is completely filled with ultra-pure water and in which the lipids will be dispersed.
- The Wilhelmy plate (Figure 2.6 A.2) which is a thin plate (made from filter paper in our case) that is used to measure interfacial tension at an air–liquid interface. In this method, the plate is oriented perpendicular to the interface, and the force exerted on it is measured [126]. The plate is attached to a microbalance and wetted by a partial immersion into the ultra-pure water. The force exerted on the plate due to wetting is
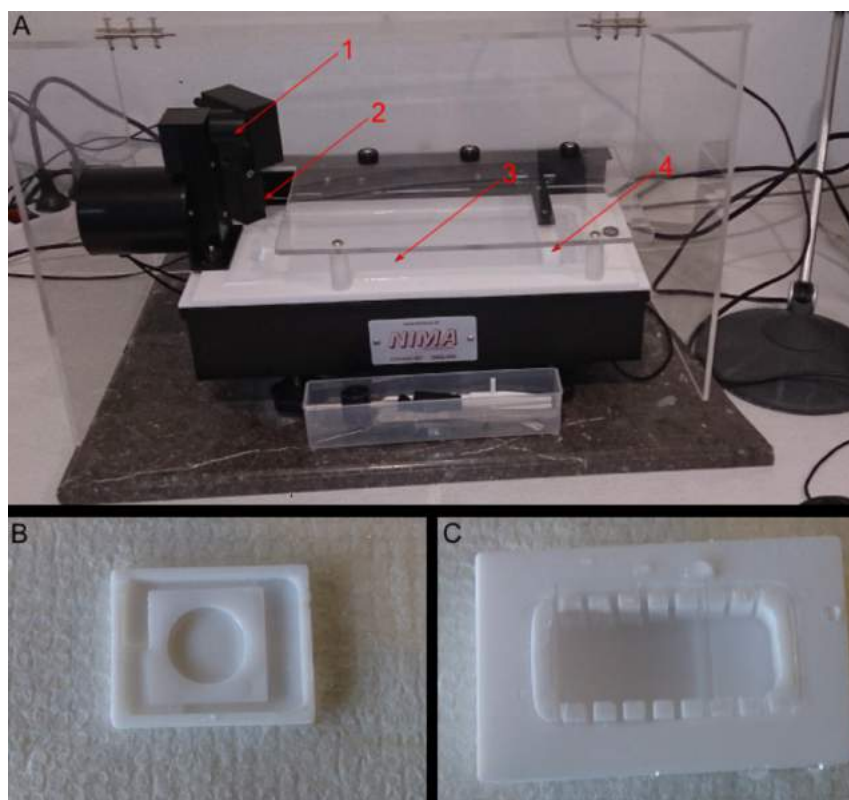
Figure 2.6:   **Materials for Supported Lipid Bilayer deposition with LB/LS technique** A. Film balance: 1.Dipper, 2.Pressure sensor, 3.Teflon enclosure, 4.Teflon barrier, B.Teflon insert tray, C.Teflon Holder. Graphic re-used from [86].

measured and used to calculate the surface tension using the Wilhelmy equation [127]:

$$\gamma = \frac{F}{l.cos\theta}. \tag{2.1}$$

where l is the wetted perimeter of the Wilhelmy plate and θ is the contact angle between the liquid phase and the plate. In our case, we assumed that the plate is totally wetted and θ is constant. The wetted perimeter is the perimeter of the entire plate which is constant. In our experiment, we were only interested in variations of the surface tension which explains why the surface tension measured was set to 0 prior to the experiment.

- The mobile teflon barrier (Figure 2.6 A.4) is used to compress the lipid film by reducing the area of the enclosure. It is motorized and controlled by the software to ensure the maintenance of the desired compression pressure.

- The motorized dipper (Figure 2.6 A.3) that permits to immerse and extract the glass slide from the pit in the teflon enclosure. The film balance was controlled by a software developed by the provider.

Film Balance cleaning procedure

In order to ensure the formation of homogeneous and fluid bilayers, the material used required a very high level of cleanliness of the material used (see Appendix A).

First layer deposition with Langmuir-Blodgett

The teflon tray (see Figure 2.6 B) was placed in the teflon enclosure (see Figure 2.6 A.3) of the film balance which was then filled with ultrapure water (at room temperature). The pressure measured by the film balance was set to 0 mN/m using the software control panel. A typical amount of 30 μL of a 1 mg/mL lipid solution was deposited carefully, close to the water surface, using a 10 μL syringe (previously cleaned with pure chloroform) in the teflon enclosure. The teflon barrier was then displaced with a speed of 80 cm/min, in order compress the lipid layer to the desired pressure (usually 27 mN/m). Using the motorized clamp, glass slides were dipped into the teflon enclosure then raised up with a speed of 15 mm/min, thus depositing the first lipid layer. During all this procedure a feedback loop on the teflon barrier permitted to keep the pressure constant.

Second layer deposition with Langmuir-Schaefer

The glass slides carrying the lipid monolayer was gently placed parallel to the water surface above the teflon tray inserted previously. Then the glass slide was pushed down with tweezers such that it is immersed in the water. The teflon tray containing the glass slide was then transferred into a glass crystallizer full of water. The bilayer coated glass slide was transferred into the round open chamber while working under water. After deposition, the bilayer was rinsed gently by adding and removing 500 μL of PBS into the chamber 10 times.

2.3.2.3 Supported Lipid Bilayer by vesicles spreading

Vesicles spreading was used for some experiments. This method aims to produce lipid bilayer with nano-vesicles (100 nm of diameter in our case), which when they come burst in contact with the glass slide (Adapted from [128]). Upon bursting, they fuse to form a homogeneous patch of bilayer which may span the whole slide.

2.3.2.3.1 Cleaning procedure

The appartus was cleaned with ethanol and ultrapure water. After several use, two additional wash in ultrapure water using a ultrasonic bath were performed to ensure complete cleanliness. The glass slides were cleaned using procedure 1 or 2 (see appendix A).

2.3.2.3.2   Liposome preparation

A lipid solution was prepared as described previously (see 2.3.2.1). 300 μL of this solution was transferred into a clean glass bottle. The chloroform was evaporated under argon flow. Afterwards, in order to evapore completly the chloroform, the bottle was placed in a glass desiccator connected to a membrane pump at maximum power for 12 hours at room temperature. The lipids were then hydrated using 300 μL of ultrapure water, vortexed several times, and placed at 4°C during one hour. The lipid vesicles were produced using an extruder (AVESTIN, Germany) which was previsouly rinsed extensively using ethanol and ultrapure water to minimize the risk of lipid contamination. The lipid solution was extruded 20 times through a polycarbonate membrane with pore size of 100 nm. The choice of membrane pore size defines the final vesicle diameter.

2.3.2.3.3   Bilayer formation in FCS2 chamber

A droplet (25 μL) of the extruded lipid solution was deposited at the centre of the microaqueduct glass slides. Then a 40 mm clean glass slide was put on top of it separated from the lower glass by a gasket. The FCS2 was then closed using the metal lower part, by ensuring to remain as horizontal as possible to prevent any movement of the lipid droplet. The bilayer was allowed to form during 30 min at room temperature then washed gently with 3 mL of pure water (in order to burst all the remaining vesicles by osmotic pressure), and finally washed with 10 mL of PBS.

2.3.2.3.4   Bilayer formation in Open chamber

This protocol was adapted from [129]. In this technique the SLB was formed by direct spreading of vesicles on glass slides.
The vesicles were prepared as previously described (see 2.3.2.3.2). For these procedure the glass slides were cleaned using procedure 1 or 2 (see Appendix A)and mounted in a open chamber.The protocol was the following :

- 200μl of 1mg/ml of vesicles were deposited in the chamber on the glass slide.
- The Chamber was placed at 37°C during 2.5 hours. The chamber was covered by a glass slide.
- 125μl of Buffer A (250mM NaCl, 20 mM TRIS, ph 7.3) was added to increased the osmolarity of the media. Then the chamber was incubated during 1 hour at 37°C.
- The sample was rinsed carefully 10 times with Buffer B (150 mM NaCl, 20 mM TRIS, ph 7.3)

2.3.3   Bilayer blocking step

In order to prevent unspecific adsorption of proteins on the lipid bilayer, a blocking step is required. To do so, 100 μg/mL of BSA ([128]) was incubated during 30 min at room

temperature. The bilayer was rinsed gently by adding and removing 500 μL of PBS into the round chamber 10 times or by wash with 10 ml of PBS into the FCS2 chamber.

2.3.4 Proteins

To create the protein nano-dots arrays, different layers of various proteins were deposited on glass. The stock solution of protein was prepared as indicated by supplier. The stock was stored at either -20°C or -4°C as required. The solution for use from the stock at -4°C, and was used directly or stored in the refrigerator for maximum of two days. Phosphate buffer saline (pH = 7.4; osmolarity = 300 mOsm) (PBS, Sigma Aldrich, France) was dissolved in deionized water to a concentration of 1X, and used to store and wash all proteins.

2.3.4.1 Bovine Serum Albumin

Bovine serum albumine (BSA) and its derivative molecules are often the first layer on glass and in this thesis different modified BSA were used :

- Un-conjugated BSA (Sigma Aldrich, France) to passivated the SLB or as a blocker before the labeling of the cells. ([128])

- BSA coupled to biotin (BSA-Biotin) (Sigma Aldrich, France) for further functionalization with biotin binding protein. Biotin is a relatively small molecule (244.3 Daltons), that can be conjugated to many proteins (such as BSA) without significantly altering their biological activity. The highly specific interactions of biotin with biotin-binding proteins make it a useful tool in assay systems designed to detect and target biological analytes.

- BSA coupled to Nitrilotriacetic acid (BSA-NTA) for further functionalization with His-tag binding protein. BSA molecules were grafted with a Nitrilotriacetic acid (NTA) molecules and nickel. They were used as linkers to bind His-tag proteins on the glass substrate. The coupling between NTA and the His-Tag protein was achieved through the ability of His to bind nickel.The amine coupling protocol was the following :

  – NTA (Sigma-Aldrich, France)was mixed with 1-Ethy-3-(3-dimethylaminopropyl)carbodiimide (EDC, Sigma-Aldrich, France) and N-Hydroxysuccinimide (NHS,Sigma-Aldrich, France) for 20 minutes at room temperature while preventing the tube's exposure to light. This step allowed the activation of the NTA molecule.
  – BSA was added to the mix to activate NTA (BSA and NTA were at the same molar ratio)
  – The tube was then mixed for 2 hour at room temperature while preventing exposure to light
  – The reaction was stoped with ethanolamine (Sigma-Aldrich, France) and dialysis was made against PBS using Amicon Ultra-0,5 ml (cut off 30kDa,Merck, France)
  – Nickel was added to the mix. The nickel is bound by chelation using NTA.

The solution could be keept at 4°C during one month.

2.3.4.2 Neutravidin

For our studies, we chose to use neutravidin as a biotin binging protein. We use fluorescent neutravidin in order to be able to see the dots and quantify the density of the proteins in the dots. Three forms of neutravidin were employed:

- Un-conjugated neutrAvidin (NaV no-fluo, ThermoFisher scientific, France).

- NeutrAvidin, Fluorescein isothiocyanate conjugated (NaV-FITC, Sigma Aldrich, France)

- Neutravidin, Dylight650 conjugated (NaV, Life technology, France)

2.3.4.3 Anti-CD3

Anti-CD3 (α-CD3)(Multi-biotinylated anti-CD3, mouse anti-human Clone (UCHT1 Beckman Coulter, France) is a monoclonal antibody that binds to the CD3 molecules on the surface of T-Cells. Biotinylated anti-CD3 was used in order to bind to the neutravidin via the biotin, and to further target the TCR complex.

2.3.4.4 Intercellular Adhesion Molecule 1 (ICAM-1)

ICAM-1 is a glycoprotein which binds to the integrin LFA-1 present on T-cells. To be able to graft this molecule either on the SLB or in the nano-dots array, we used a version tagged with 6 histidine groups : ICAM-1 His-Tag (ICAM1 Recombinant Human Protein, hIgG1-Fc.His Tag, ThermoFisher) which could bind to the Ni-NTA lipids or to BSA-NTA.

2.3.4.5 B7

B7-2 or CD86 is a transmembrane co-stimulation protein which binds CD28 on T-cell membrane ([17]). This commercial molecule (which was a gift from Nunes.J) is tagged with 6 histidine groups and was grafted on the Ni-NTA lipids via its His-Tag.

2.4 Cells

2.4.1 Lymphocytes lines

2.4.1.1 Jurkat E6

Jurkat T cells (Clone E6-1, ATCC) will be referred to in the following chapters as wild-type T-cells. The Jurkat cell line was established from the peripheral blood of a 14 year old boy with leukemia ([130]). As this cell line is stable and give reproductive results Jurkat E6 represent a good T-cell model for *in-vitro* experiment.

2.4.1.2 LifeAct-GFP Jurkat E6

In order to study live cell imaging of the actin dynamic of T-cell during their interaction with the substrate Jurkat T cells were modified. The cells were transfected with a plasmid expressing actin coupled to a fluorescent protein(GFP). First the plasmid was obtained in

HEK 293T cells by co-transfecting the lentiviral plasmids (pLenti.PGK.LifeAct-GFP.W) with plasmid for packaging(psPAX2) and envelope (pMD2.G) . Then Jurkat E6 were transduced by spinoculation .The transfection were in the frame work of collaboration with L. LIMOZIN (Laboratoire d'Adhesion et d'Inflammation-LAI) by Martine Biarnes-Pelicot (protocol adapted from [131]). The expression of LifeAct-GFP were checked by flow cytometry.

2.4.1.3   Cell Culture

Cells were cultured in complete RPMI 1640 medium (Life Technologies, France) containing red phenol and L-glutamine supplemented with 1 % glutamax (Life Technologies, France) and 10% FCS (Life Technologies, France). This medium were prepared every two months and filtered through 0.22 μm pore filter and stored at 4 °C).

Cells lines were received frozen from ATCC and kept in a freezer at -80 °C until use. Cells were cultured using the following protocol:

- 1 mL of cells was brought to room temperature.

- The cells were thawed until a small piece of ice remains.

- 10 mL of complete RPMI medium was added gently to the cells which were then transfered into a flask.

- The culture was kept during 24 hours in an incubator at 37 °C under a 5 % CO2 atmosphere before use.

Cells were split 3 times a week to obtained a density of 0.3 millions of cells per mL using the following protocol:

- A volume of culture containing about 0.3 million cells was taken

- It was centrifuged during 4 min at 1100 rpm

- The supernatant was aspirated and the pellet was resuspended in 10mL of complete RPMI 1640 medium.

The cell culture was maintained during 2 months and then replaced by a fresh one. Every month the culture was scanned for mycoplasm presence using MycoSEQ ®kit (Life Technologies, USA). Concerning the characterization of the cells line, two tests were previously realized([86]) :

- A proliferation test following the concentration of cells in a flask during 10 days with a starting concentration of 0.1 millions cells per mL. The proliferation trend seems not to be affected

- A quantification over culture duration of the number of anti-CD3 receptor to ensure that cells keep their biological activity over the considered period. Using fluorescent Anti-CD3 (Anti-CD3 APC, Life technologies, France), cells were screened for CD3 presence using flow cytometry (Calibur, BD, USA) after 6 passages (3 weeks) and 20 passages (9 weeks). Results show a decrease of 6% of CD3+ cells (from 96% to 90%) between this two dates. This result explains why the culture was not maintained more than 9 weeks in order to be sure that over 90% of the cells are CD3+.

2.4.2   Primary cells

Two different type of primary T-cell were used : T-cell from mouse and from human.

2.4.2.1   Mouse T-cell

Mouse T-cells were kindly gifted by Guillaume VOISINNE (CIML). The cells were extract from the pooled lymph nodes and spleens of wild-type B6 mice. Then, CD4+ were purified using Dynabeads Untouched Mouse CD4+ T Cell Kit (Life Technologies, CA, USA) with a purity of 95%. In order to expand, purified CD4+ were incubate in complete RPMI with plate-bound anti-CD3 (145-2C11, 5 ug/ml, from Exbio) and soluble anti-CD28 (3751; 1 ug/ml, from Exbio) for 48h . After this, CD4+ T-cells were harvested and grown in the presence of IL-2 (510 U/ml) in complete RPMI for an other 48 h. Cells were then resuspended in complete RPMI prior use.

2.4.2.2   Human T-Cell

Human T-cells were obtained in the context of collaboration with L.LIMOZIN (LAI) and were isolated in LAI by Adeline QUERDRAY and Martine BIARNES. This were obtained from peripheral blood of healthy donor.

The Peripheral Blood Mononuclear Cell (PBMC), containing lymphocytes, was isolated from all blood with density gradient solution using Lymphocyte Separation Medium (Eurobio, Les Ulis, France). Then in order to isolate CD4+ T-Cell, negative selection was done using a cocktail of bead coated antibodies (kit CD4+, Miltenyi Biotec, France) [132].

2.4.3   Flow cytometry

Flow cytometry (Calibur, BD) was perform on Jurkat cell and Primary human T-cell to compare the expression level of CD3 and LFA-1. It was done with Martine BIARNES (LAI). For CD3 , the antibody anti-CD3 APC (Life technologies) was used. For LFA-1 two kind of antibodies were used : anti-CD11a, clone Hi111 (BD) or anti-CD11a, clone G43-25B (BD) both labelled with FITC. Results show higher expression level of CD3 on Jurkat T cell than on Primary T cell. But for LFA-1 (with both antibodies), the expression level is higher on Primary T cell than Jurkat T cell.

2.4.4   Cell preparation

Prior the experiments the cells were washed in order to remove the cell culture medium by using the following :

- 1 ml of the culture (containing about 0.6 millions of cells) was centrifuged during 4 minutes at 1100 rpm.

- 950 μl of the supernatant was remove carefully.

- The pellet was re-suspend in 950 μl of observation medium : composed with PBS+0.1% of BSA (which was previously incubate at 37°C for at least 15 minutes).

The choice of the observation medium was based on its refractive index close to water, on the no intrinsic fluorescence and on the limited interactions with the substrates.

2.4.5 Cell engagement on substrates

After the washing step and before the engagement on the substrates cells were maintained at 37°C for 10 minutes for a complete recovery.

For experiments,the cells were gently introduced in the observation chamber in order to have around 0.3 million of cells (in our case 200 μl of cells in 200μl observation medium). They were allowed to sediment and adhere for 30 minutes at 37 °C under a 5 % CO2 atmosphere.

2.4.5.1 Cell fixation

To fix the adhering cells, paraformaldehyde (PFA) (Merck, France) at 37°C with a final concentration of 2% was used during 15 minutes. To do so, add 400 μl of PFA 4% in the sample. The PFA need to be introduce very gently in order to prevent the risk of detachment of the cells. Then the substrate was washed carefully 10 times with PBS.

2.4.5.2 Live cell observation

For live imaging precautions were done to minimize the risk of phototoxicity and photobleaching of the fluorophore caused by a long illumination of the cells to light. Therefore low power (10%) and high exposure time (300ms) were chosen. The cell can also be fixed after their use to further analysis.

2.4.5.3 Blocking step

After fixation, a blocking step was realized to prevent any non-specific adhesion of the markers. To do so 5 mg/ml of BSA was incubated for overnight at 4°C (or at least 4 hours at room temperature). To do so, remove 400 μl and put 400μl of BSA at 10mg/ml. Then the substrate was washed 10 times with PBS.

2.4.5.4 Cell labeling

Prior cell labeling, a step of permeabilization of the membrane was done by incubating 0.1% of Triton X-100 (Sigma, France) for 10 minutes at room temperature. Then the sample was rinsed 10 times with PBS.

Labeling of actin

The actin was marked by using a fluorescent phalloidin. Differents fluorophores were used :
- Rhodamine-phalloidin (dissolved in DMSO, Sigma-Aldrich, France)
- Alexa Fluor 488 -phalloidin (dissolved in methanol, ThermoFischer, France)
- Alexa Fluor 647- phalloidin (dissolved in methanol, ThermoFischer, France)

Each of them were used at 20 μg/ml in PBS and incubated during 30 minutes at room temperature. The the sample was washed 10 times with PBS.

Labeling of TCR

To mark the TCR cells were incubated with 5 μg/ml of FITC fluorescent Anti-Vβ8 TCR during 30 minutes at room temperature. Then the sample was washed 10 times with PBS.

Labeling of ZAP-70

To mark the kinaze ZAP-70 20μl of Alexa Fluor 647 Mouse Anti-ZAP70 (PY319)/Syk (PY352) (BD bioscience) was incubated in 400 μl of PBS during 30 minutes at room temperature.Then the sample was washed 10 times with PBS.

Labeling of LFA-1

To label LFA-1 proteins, 20μl of FITC Mouse Anti-Human CD11a (Clone G43-25B) (BD bioscience) was incubated 400 μl of PBS during 30 minutes at room temperature.Then the sample was washed 10 times with PBS.

Labeling of CD45

To label CD45 protein of T-cells , 5μl of Alexa Fluor 532 CD45 Monoclonal ANtibody (HI30) (eBioscience) was incubated 400 μl of PBS during 30 minutes at room temperature.Then the sample was washed 10 times with PBS.

2.5   Microscopic observation

2.5.1   Epifluorescence

2.5.1.1   Principle

Fluorescence microscopy uses the property of fluorophores to emit light when they are excited by light. When a high intensity excitation light reach the sample (Figure 2.7(1)) and excite the fluorophore, the excited fluorophore emit a lower energy light (Figure 2.7(3)) which will be collect and detect by an camera. The fluorescence process is due to a transition of electrons, from a excited state (S_1) to a ground state (S_0)by an emission of radiation. And these is during these transition that, the fluorophore emit the fluorescence light.

2.5.1.2   Materials and settings

The fluorescent microscope is composed of (Figure 2.8):
    - A mercury lamp that emits a hight intensity light with a broad spectrum.
    - An excitation filter what select the desired wavelength.
    - A beam splitter that reflect the excitation light in order that the light arrive perpendicularly to the sample.
    - An objective that focus the excitation light into the sample and collect the emitted fluorescent light of the sample.
    - An emission filter that select the desired emitted wavelength.
    - A CCD camera connect to a computer screen that detect the fluorescence imaging.

In our experiments, epi-fluorescence images were performed using an inverted optical microscope (Axio Observer, Zeiss,Germany) equipped with an EM-CCD camera (iXon, Andor, NorthIreland) . Acquisition was performed using Andor IQ software. Excitation was done using a metal Halide lamp XCite 120 (Excelitas Technologies, USA). Epi-fluorescence images were taken using a high magnification oil immersion objectives
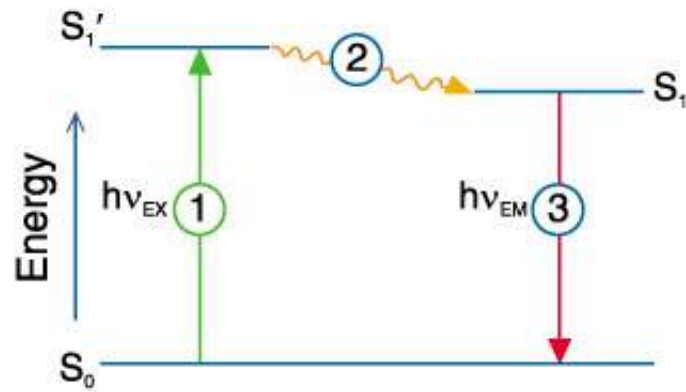
Figure 2.7: **Jablonski diagram describing the fluorescence process.**1: Excitation of the fluorophore with light. 2.Excitation state of the fluorophore. 3. Emission of fluorescence by the fluorophore.Adapted from [133].
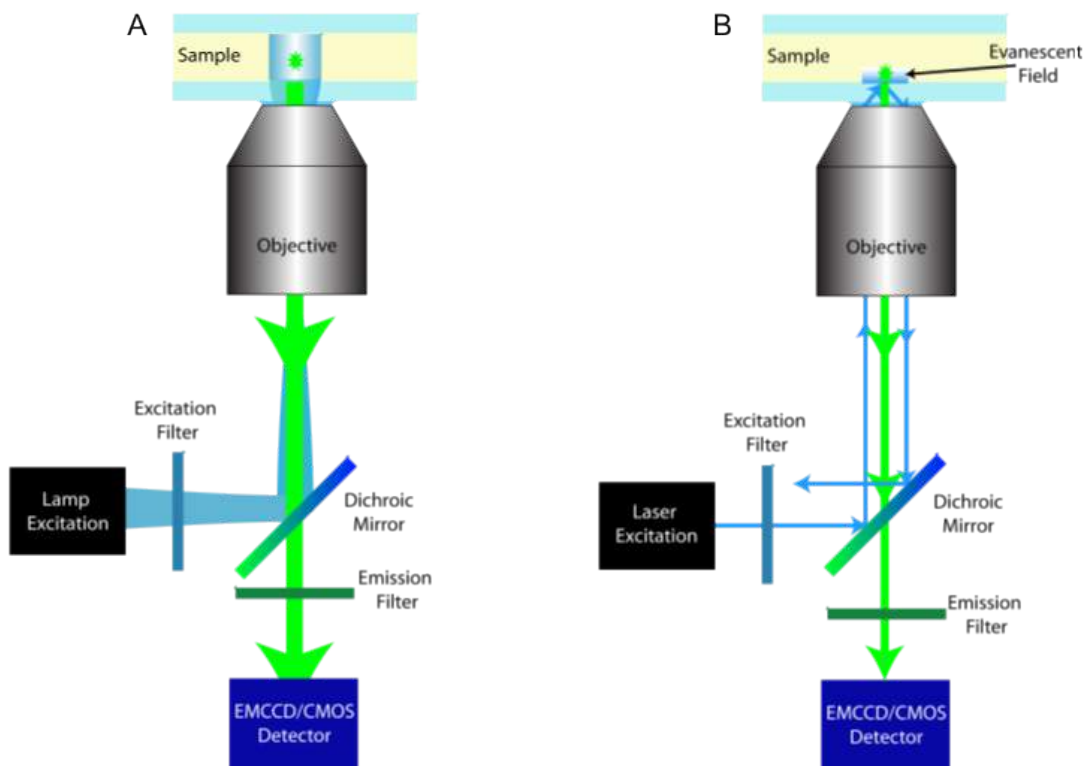
Figure 2.8: **Light path in an Epifluorescence and TIRF microscope**A. Epifluorescence microscope. B.TIRF microscope. Adapted from [134]

(100X; N.A 1.4 or 100X; N.A 1.45, Zeiss Germany). Cubes were selected to perform epifluorescence in the following exciting wavelength: 365, 488, 514 and 647 nm. Epifluorescence images were taken using one of the following objectives :

- a custom 100 x 1.46 NA oil antiflex objective (Zeiss),

- a 100 x 1.4 NA oil apochromat objective (Zeiss)

- a 63 x 1.25 NA oil antiflex objective (Zeiss).

The cubes used according to the fluorophores are summarized in table 2.1 (For the settings see appendix B)

With the 100x objective, the pixel size correspond to 0.08μm and with the 63x objective, the pixel size correspond to 0.125μm.

Fluorophores	Filter set	Excitation (nm)	Beam Splitter (nm)	Emission (nm)
Dansyl	2	365	395	420
Alexa 532	17	485±20	510	515-565
FITC and Alexa 488	17	485±20	510	515-565
	44	475±40	500	530±
Bodipy	45	560±40	585	630±75
Texas Red	45	560±40	585	630±75
	76	561	578	608
Rhodomine	76	561	578	608
Alexa 647 and Dyelight 647	77	642	659	688

Table 2.1: **Filter cubes from Zeiss used for fluorescent imaging.**

2.5.2 Total Internal Reflection Microscopy (TIRF)

2.5.2.1 Principle

This microscopic technique permits the observation of fluorescents molecules only in a region very near of the surface ($\leq$100 nm) (see Figure 2.9). These property is due to the production of evanescent waves at the interface between two media with different refractive index. These production is caused by the phenomenon of Total Internal Reflection (TIR). When a light pass trough a sample, one part is refracted and the other part is reflected. But at a certain angle of incidence (called critic angle) all the light is reflected. TIR can only be observed if the light pass through a media with higher refractive index (from glass n=1.52) to a media with a lower refractive index (to aqueous medium, n=1.33). The critical angle (θ_c) of incident light, at which total internal reflection occurs, can be determined by Snell's law :

$$\theta_c = \sin^{-1}\left(\frac{n_2}{n_1}\right)$$

The evanescent wave then propagates parallel to the surface with an intensity I that decays exponentially (the penetration of the light wave is small) with perpendicular
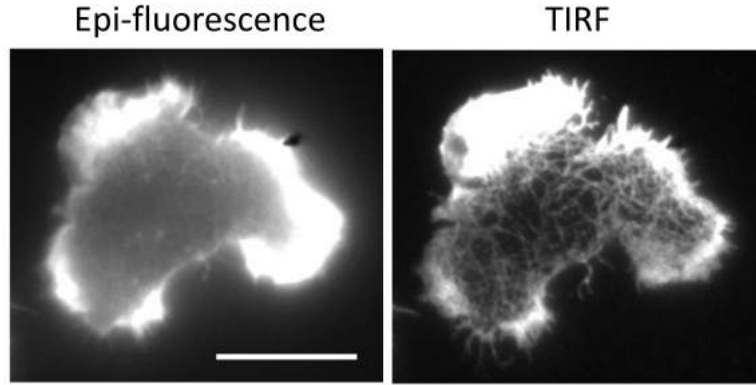
Figure 2.9: **Difference between epi-fluorescence and TIRF images**. On epi-fluorescence fluorescence within the all cell is collected, whereas with TIRF-M technique only fluorescence at the interface is collected allowing to observe precise structure like actin filaments. Scale bar: 10μm.

distance z from the interface.Therefore, a fluorophore that is closer to the interface is excited more strongly than a fluorophore that is further from the interface (Figure 2.8B and 2.10). The intensity of the evanescent field at any position z is described by :

$$I = I_0 e^{\left(\frac{-z}{d}\right)}$$

where I_0 is the intensity of the evanescent field at z=0; and d, is the depth of the evanescent field. In typical case, d is equal to 200 nm.
The main advantage of this microscopic technique is the fast recording of high definition images of features close to surface, without interference of light from the depth of the sample.
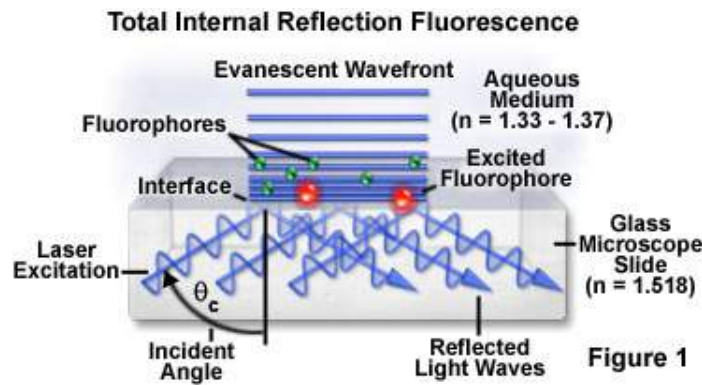
Figure 2.10: **Induction of evanescent waves**. A laser beam oriented with a critical angle (θ_c) generated a localised electromagnetic field and excite the fluorophore only at the interface.Adapted from [135]

Fluorophores	Exposure time (milisec)	Electronic gain	Pre-Amp gain	Angle (°)	Laser power (%)
Dyelight 647	100	10	10	60.8	12
Alexa 647	100	10	62	61	10
FITC and Alexa 488	200	10	10	57	13
Texas Red	200	10	10	55	10
Rhodomine	200	10	10	52	10

Table 2.2: **Settings for TIRF imaging**Note that these settings are microscope/camera specific.

2.5.2.2   Materials and settings

Most of the TIRF images were performed using an inverted microscope Axio ObserverZ1 (Zeiss) equipped with an Laser Tirf III system, an EM-CCD camera (iXon) and three lasers with wavelength appropriate to the fluorophore used (488nm, 639nm and 561nm). Acquisition was performed using Zen. Cubes were selected to perform TIRF in the following wavelength: 488, 514 and 642 nm. TIRF images were taken either using a custom 100 x 1.46 NA oil antiflex objective (Zeiss) either a 100 x 1.45 NA oil objective (Zeiss). The cubes used according to the fluorophores are summarized in table 2.1. The settings were summarized in table 2.2

2.5.3   Reflection Interference Contrast Microscopy (RICM)

2.5.3.1   Principle
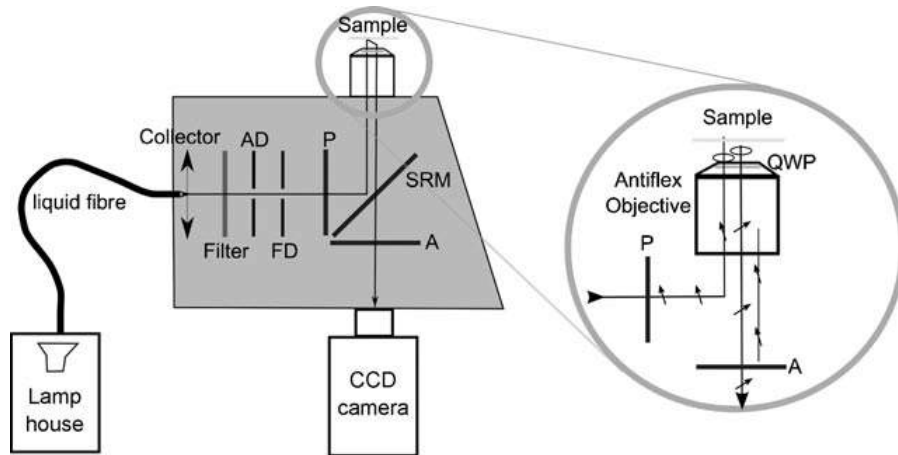
Figure 2.11: **Set-up and optical path for RICM.** AD: aperture diaphragm;FD: field diaphragm; QWP: quarter-wave plate; SRM: semi-reflecting mirror; P: polarizer; A: analyzer. The circular zoom illustrates the polarization of light with the antiflex method. From [136].

RICM is an interferometric technique to determine the vertical distance and the
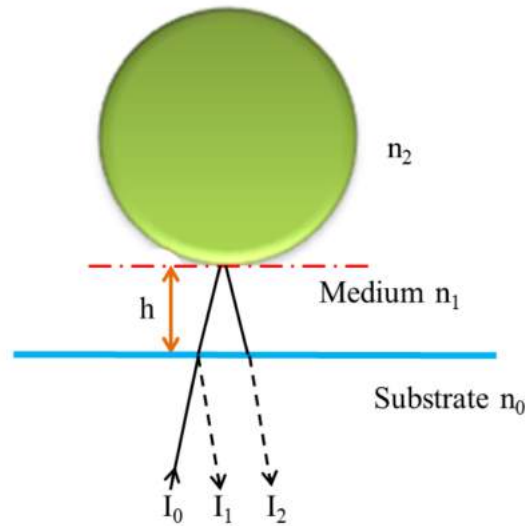
Figure 2.12: **Schematic representation of RICM principle.** I_0: incident light; I_1 et I_2: reflected light; h: distance between the interacting surface; n_0,n_1,n_2: refractive indexes. Image from [[137]]
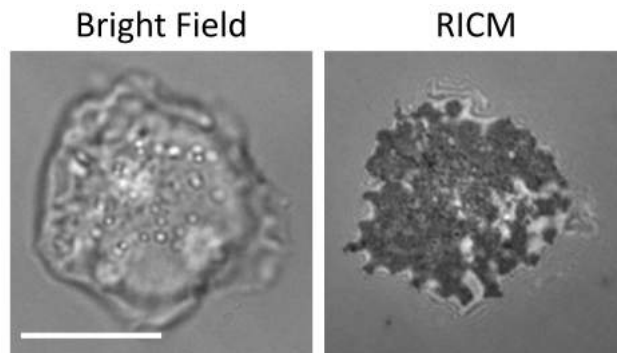
Figure 2.13: **Difference between bright field image and RICM image.** On bright field image the adhesion features is not visible whereas on RICM the membrane adhesion as well as the topography is observed. Scale bar: 10μm.

contact area between two surfaces.

Adam Curtis was the first to apply this technique in order to study the interaction of cells with a glass substrate under water by using an optical microscope [138]. He named this technique "interference reflection microscopy" (IRM). Later a related technique called "Reflection Interference Contrast Microscopy" (RICM) was developed in the 1980's by Sackman and co-workers [139] and showed that between a planar transparent substrates (like glass slide) and optically controlled objects (like model membrane) the distance at the interface can be measured with very high accuracy not possible for alls (Figure 2.12). These discovery make RICM a powerful technique to study inter-surface interactions and in particular cell adhesion[136]. Moreover, RICM uses a simple set up as it can be implemented on a standard inverted microscope and does not need a fluorescent sample.

As presented in Figure 2.13, the advantage of RICM technique compare to Bright-field, is the possibility to observe the membrane adhesion and topography at the interface cell-substrate.

2.5.3.2   Materials and settings

For our experiments, the set up was the same as the epi-fluorescence set-up (see 2.11). a pre-filters (green: 436±17nm and blue: 546nm±11nm) and a cube composed of two polarizer perpendicularly oriented and a dichroic mirror were added. Objectives used were custom 100 x 1.46 NA oil antiflex and 63 x 1.25 NA oil antiflex. The settings used were the following :

   - Exposure time : 140 ms or 300 ms
   - Diaphragm aperture : 11 %

For dynamic imaging a frame rate of 5 image/s was applied .

2.6   Techniques for substrates characterization

All analysis were performed using Fiji (ImageJ)[140] and Igor Pro WaveMetrics (http://www.wavemetrics.con

2.6.1   SLB fluidity measurement

The fluidity of the SLB was measured using the continuous photobleaching technique (CPB) [141]. In our implementation, this technique consists in observing, in epifluorescence, the fluorescent SLB through a partially closed diaphragm, with an continuous exposure. Throughout this process, the fluorophores are irreversibly bleached. Therefore, if the SLB is fluid , which mean that the lipids are able to diffuse within the SLB, they can enter and exit the observation area. This situation induces at the edge of the observation area, a luminous ring (due to non-bleached fluorescent lipids entering the field via diffusion) and a dark area in the center (due to the continuous photobleaching of the fluorescent lipids during the observation) .

It is possible to establish the equations corresponding to the fluorescence intensity as a function of the position and the time. This will allow to obtain the bleaching rate of the fluorophore (B) and the diffusion constant (D).

First the bleaching rate of the fluorophore (B), is determined by measuring the time evolution of the fluorescence intensity I(t) in a box of $1.5\mu m^2$ placed in the center of the field (see Figure2.14) and fitted using the following model :

$$I(t) = I_0 e^{-Bt} + I_{B_g} \tag{2.2}$$

where I_0, B and I_{B_g} are fitting parameters.

Then, the fluorescence intensity along 12 radial profiles perpendicular to the edge of the diaphragm is measured (see Figure2.14) and fitted by the following equation:

$$I(x) = I_0 e^{-x\sqrt{B/D}} + I_{B_g} \tag{2.3}$$

where by knowing B, the diffusion constant (D) can be extracted [124].
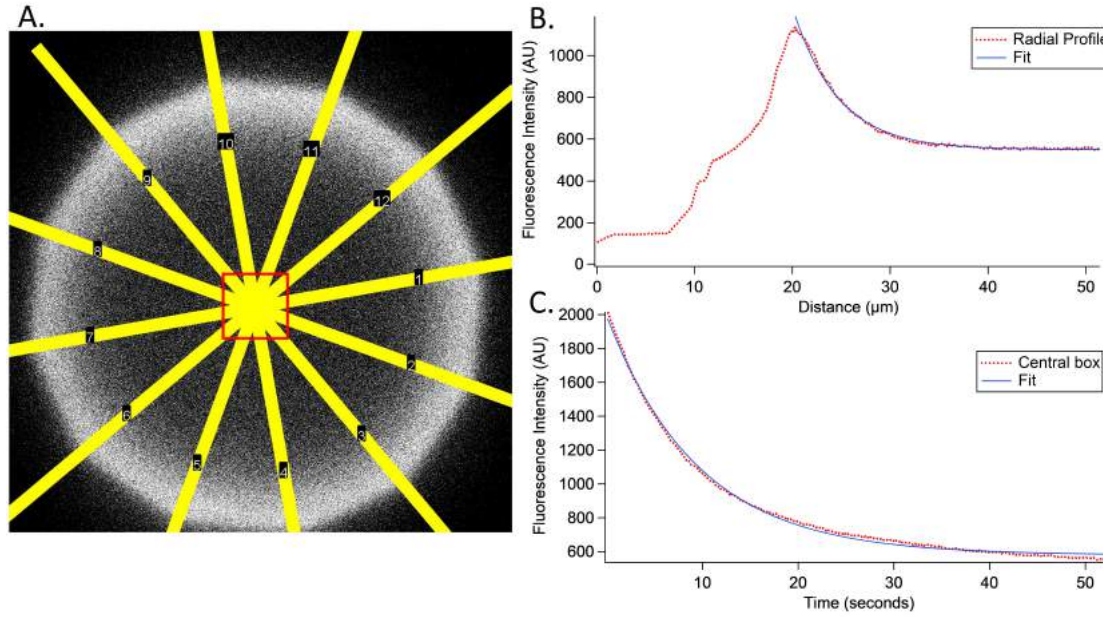
Figure 2.14: **Lateral molecular diffusion measured by Continuous Photo-Bleaching** A- Average image of the time-lapse film taken on a DOPC bilayer supplemented with 1% of Bodipy lipids made with LB/LS technique. Yellow lines represent the radial profiles that will be averaged and plotted over the radius. The red square represents the area where the fluorescence intensity will be measured along the film. This results will be plotted over time. B. Average profile line. D extracted equal 2,20μm²/sec. C. Intensity decay over time measured in the red square.B extracted equal 0.10 sec^{-1}.

.

2.6.2   Dots characterization

Proteins dots are characterized in terms of diameter size and fluorescence intensity. The spacing between each dots is set by the diameter of the beads used. The fluorescence intensity is an important parameter as it is proportional to the protein density. Intensity will be analyzed inside the dots (referred as I_{max}), outside the dots (referred as I_{min}) and on all the substrate (referred as I_{avg})

2.6.2.1   Manual analysis

To measure the size of the nano-dots array, an intensity profile along a line drawn through several fluorescent dots in the field is represented (Figure 2.15). From this profile, several parameters can be extract :

- The distance between two protein dots (d) : it's estimated from the distance between two peaks in the profile.

- The diameter of the protein dots ($\emptyset$) : it's estimated from the Full Width at Half-Maximum (FWHM) of the peaks.

- The intensity inside (I_{max}) and outside (I_{min}) of the protein dots. It's estimated from respectively the value of the intensity of the peak for each dot and from the value of the intensity around each each dot.
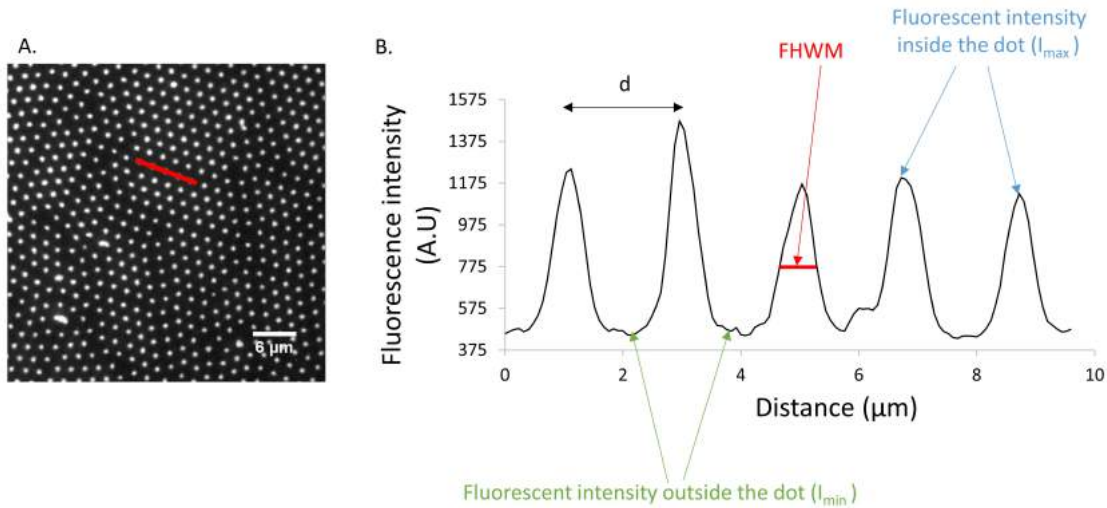
Figure 2.15: **Manual characterization of the protein nano-dots.** A-Epi-fluorescence image of the protein nano-dots arrays reveals by fluorescent neutravidin. B. Intensity profile of the line drawn in A; FHWM: Full width at half maximum; d: distance between the dots

.

2.6.2.2 Automatized analysis

A macro was created in order to more easily analyze a larger quantity of dots. For each field of fluorescent nano-dot array, each dot was segmented and a median dot was constructed. The parameters are automatically extract from this median dot as the same manner as with manual analysis (see 2.6.2.1 and Figure 2.16).

The data for dot size measurements were obtained from the FWHM extract from the analysis (see 2.6.2.1 and Figure 2.15 and 2.16).

2.6.3 Protein density quantification

Protein density is obtained from fluorescence images of NaV. Density inside and outside the dots as well as density on all the substrate is calculated from the respective fluorescence intensities I_{max}, I_{min} and I_{avg}. In order to convert fluorescence intensity value of NaV to a estimate density, a calibration was done. For this a special substrate with very low surface density of fluorescent molecules was prepared by following this protocol :

- Glass slides were cleaned using procedure 1 (see Appendix A.1)
- Biotin-BSA was incubated at 25μg/ml during 30 minutes.
- Rinsing 10 times with PBS
- NaV fluorescently labeled was incubated at 0.2 μg/ml during 30 minutes
- Rinsing 10 times with PBS

The surfaces were imaged with the standard microscope and camera setting as above. 5 boxes of 52 μm^2 were drawn per field for each four fields. The number of fluorescent dots, assumed to correspond to single molecules, was counted in each of these boxes. The average intensity in each box was measured and corrected by background value. The number
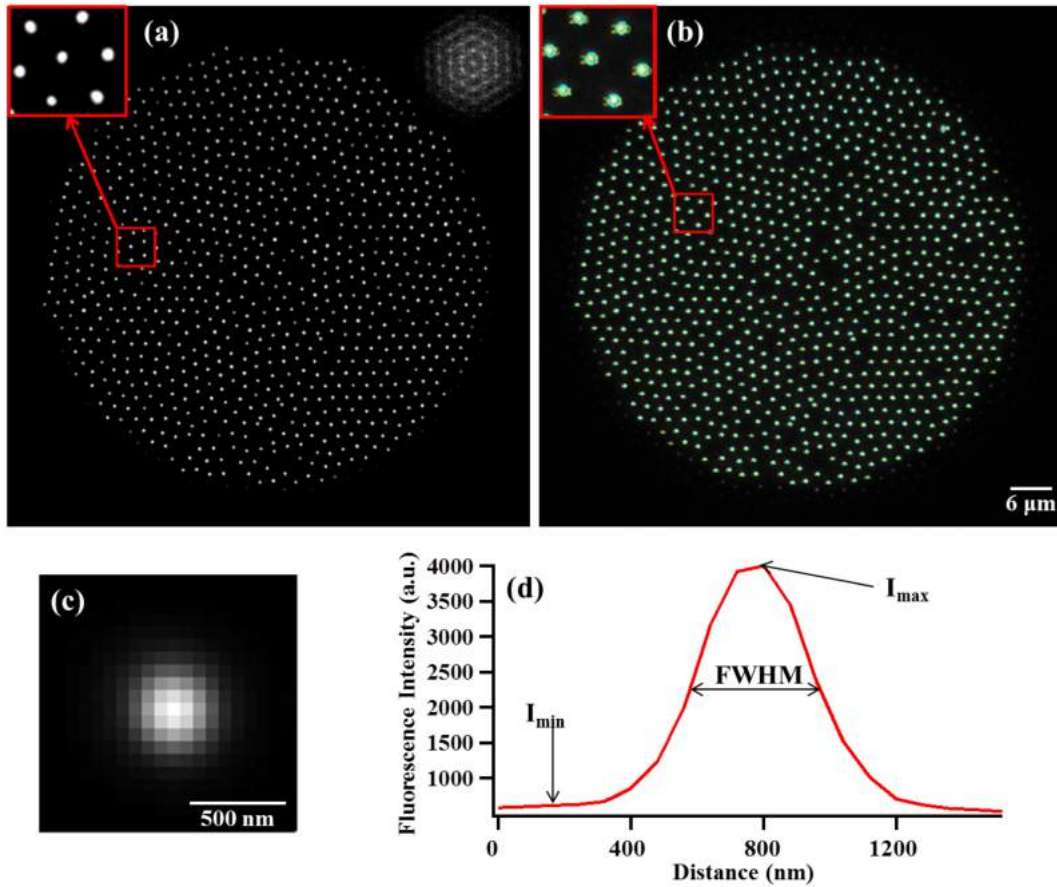
Figure 2.16: **Segmentation of the dots and construction of the median dot for quantification of the dot characteristics.** A-Epi-fluorescence image of the protein nano-dots arrays reveals by fluorescent neutravidin with a zoom on a hexagonal unit. B-Green ROIs segmenting the dots obtained by automated intensity thresholding. C-The median dot obtained for the field. D- Radial intensity profile of the median dot, showing the FHWM and the maximum and minimum intensity (I_{max} and I_{min}) Images from [137].

.

of fluorescent molecules/μm² was calculated, by assuming that fluorescent dots correspond to one molecule. Then for a corresponding intensity value, the density is known. Therefore, by comparison of the emitted light intensity of experimental substrates, the density of NaV can be determined. For NaV-Dyelight (see 2.17 for example), the number of fluorescent molecules corresponds to an average of 0.3 molecules/μm² (Figure 2.17B). This give a conversion factor of 2.2 molecules/μm² for 1000 Arbitrary Units of Intensity.

Before analyzing the epi-fluorescent images, some corrections were done in order to remove the heterogeneity of the luminosity. This correction was achieved by making a median image of the epi-fluorescence image stack which was then used to divide each image of the stack. The corrected stack was then multiplied by the mean intensity value
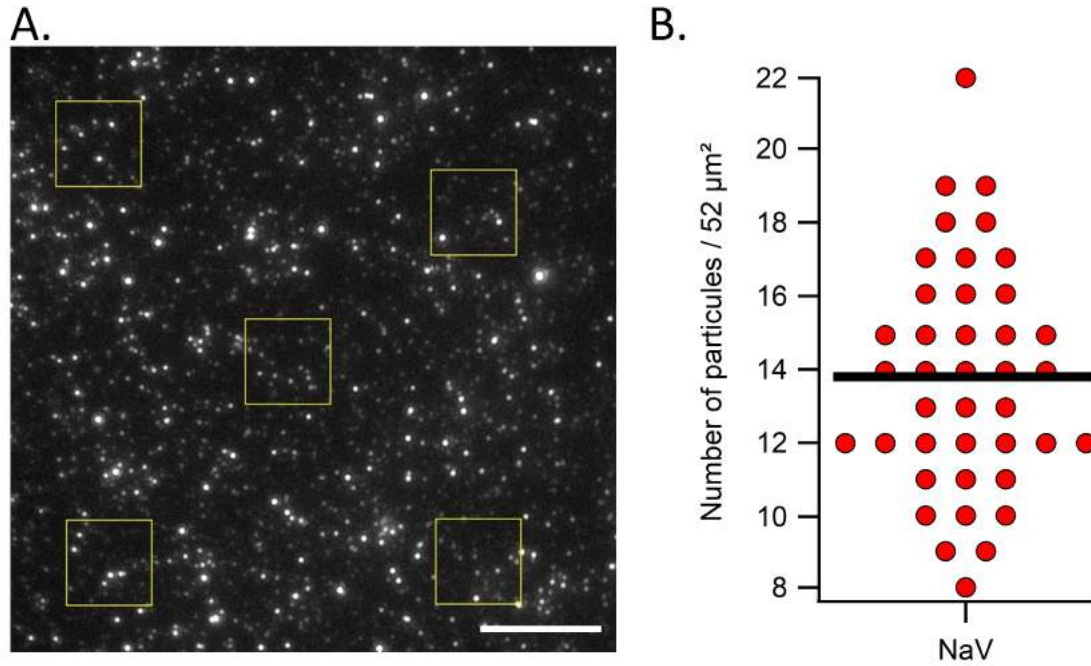
Figure 2.17: **From relative to absolute surface density of Neutravidin.** A:Epifluorescence image of spare NaV molecules. Intense dots are assumed to be single molecules. 5 boxes of 52 μm^2 are drawn as shown. The number of molecules per box as well as the average intensity per box are determined and compared. B: Data of one sample. Each point corresponds to one box, with 5 boxes in 4 fields. Scale bare: 10 μm.

of the median image. Controls were done to ensure that this correction did not affect the density measurements. As shown in Figure 2.18, the corrections allowed the illumination to become uniform without significantly changing the measurements, however standard deviation were significantly reduced. The standard deviation of the initial image was ±15 molecules/μm^2 for the density average and was ±3 for the corrected image.

2.7 Images analysis

In this section, will be described the different methods use to analyses the cell behavior.

2.7.1 Static description

2.7.1.1 Adhesion area

Cell adhesion area was analyzed based on RICM images of cells adhered during 30 minutes on different surfaces, and using image J/Fiji macro. The principle of the macro is the following:

first a spatial variance filter was applied with a radius of 8 or 4 pixels followed by a color threshold. Results obtained with a spatial variance filter of 8 and 4 pixels were

A.

B.

C.
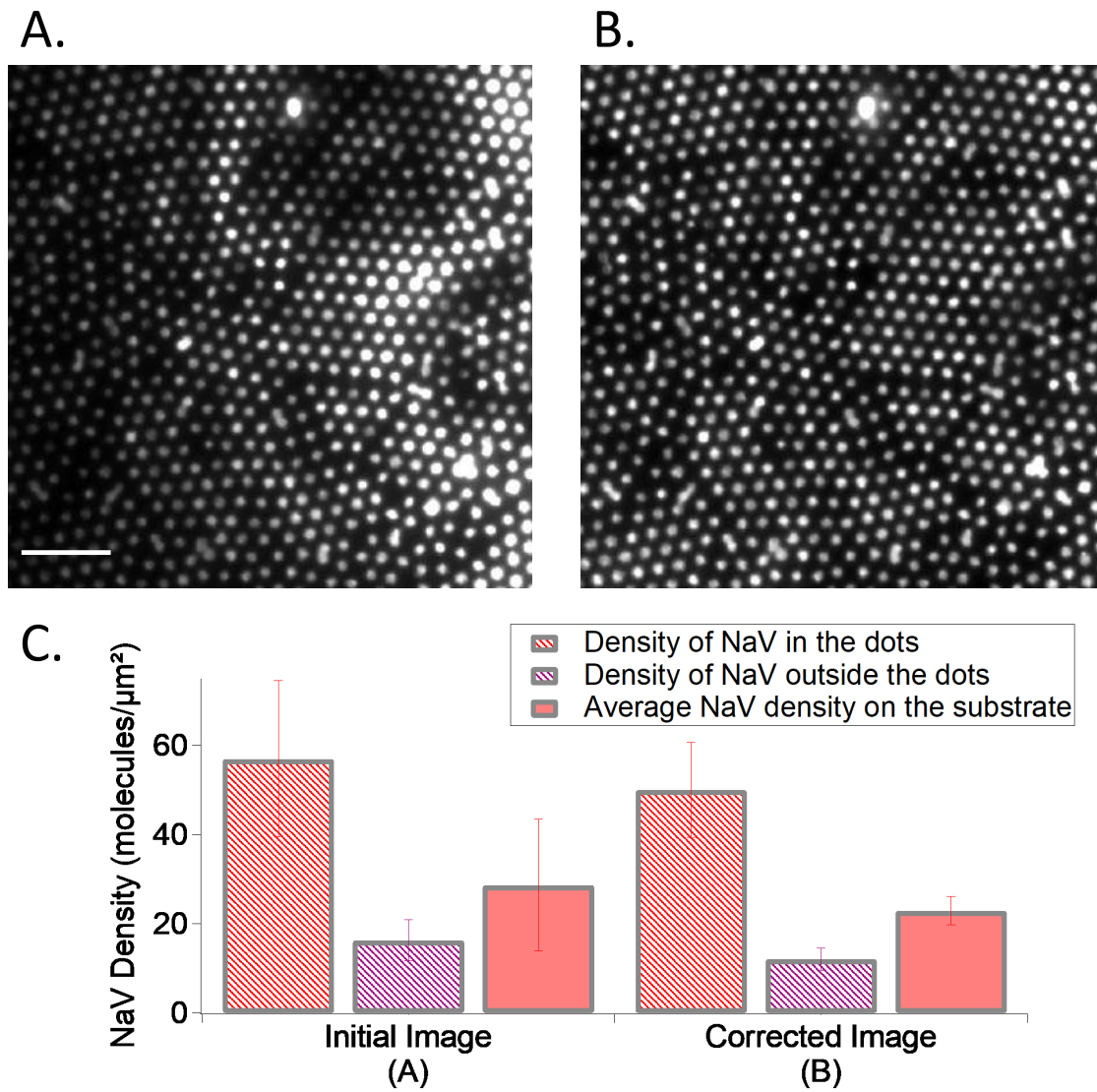
Figure 2.18: **Correction of the heterogeneous illumination of an epi-fluorescent image of a nano-dot array.** A: Initial epi-fluorescence image of the nano-dot array labeled with NaV dyelight650. Circular fringes can be observed on the top-right of the image. B: Epi-fluorescence image after corrections. The fringes disappear and the fluorescence is more homogeneous. Scale bar:10μm. C: NaV density extracted from images (A) and (B). Error bars represent standard deviation measurements.

similar, with a more accurate contour of the cell when they are patterned (Figure 2.19). Then the function "Particle analysis" of ImageJ was applied to identify the edge of the cell. Then the measure command was executed on the ROI determined with the following outputs : area (in pixel), coordinates of the center and the shape descriptors (including the circularity). The data were processed in Igor Pro. The adhesion area was
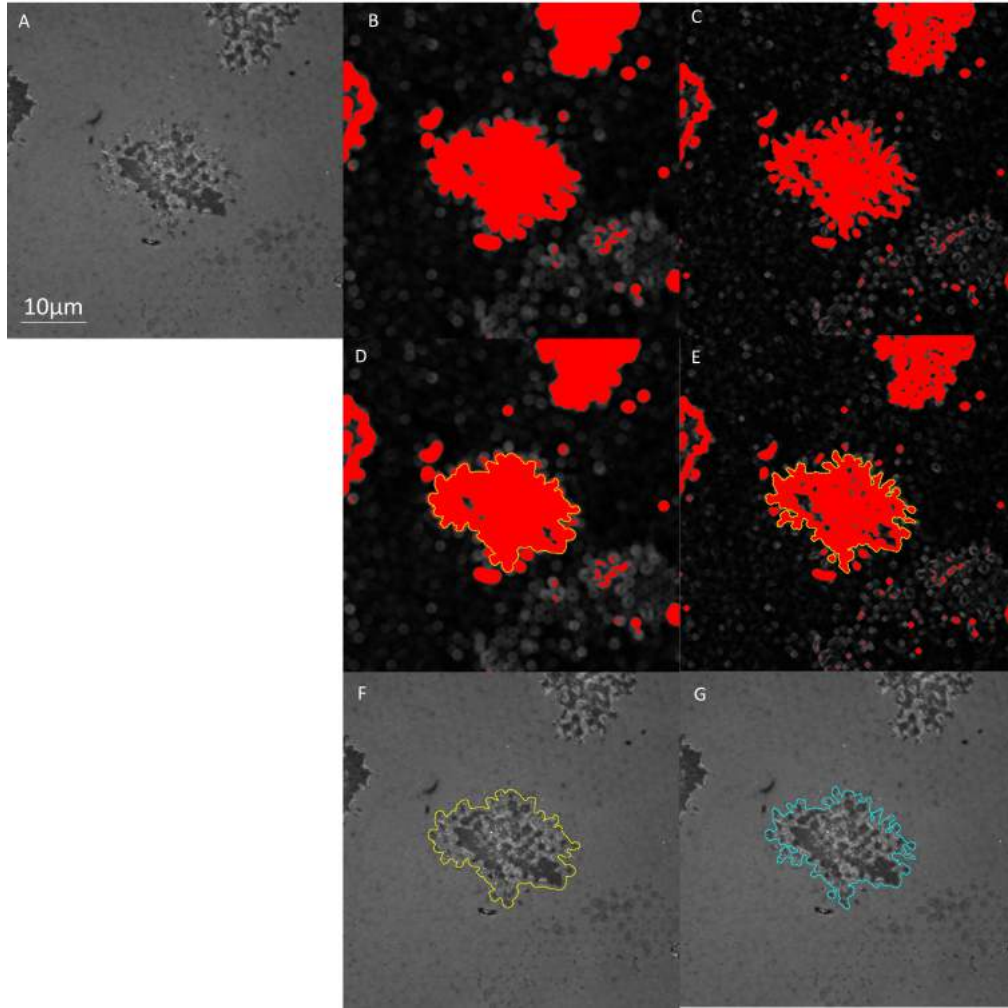
Figure 2.19: **Steps require in order to calculate area of the adhered cells.** A-Raw RICM image from which the cell-substrate contact region will be segmented. B-Thresholding image with a pixel spatial variance filter of 8 pixels, representing 0,8 μm. C-Thresholding image with a pixel spatial variance filter of 4 pixels, representing 0,4 μm . D-E: Detection of the edge odf the cell using Particle analysis macro in ImageJ. F-G: Superposition of the cell boundary from D-E on the initial RICM image A. Scale bar : 10 μm

.

converted to μm^2.

2.7.1.2   Actin distribution

In order to determine the organization of the actin (centralized or homogeneous or peripheral), fluorescence intensity in the center (I_{Center}) and in the rest ($\mathrm{I}_{restCell}$)of the cell is measured and then the distribution parameter was calculated using :

$$p = \frac{I_{Center}}{I_{RestCell}} \tag{2.4}$$

To do so, a macro in-housse written in ImageJ was used which does the following :

- From a RICM image, ROI corresponding to the edge of the cell is determined using 2.7.1.1) - This ROI is reported on the fluorescent image of the actin - A circle of 1.2μm was traced, centered on the intensity center of mass inside the ROI - The mean fluorescence intensity of this circle and in the rest of the cell is measured and the ratio calculated.

So, if p=1, the actin is homogeneously distributed, if p < 1, the actin is peripherally distributed and if p>1, the actin is centrally distributed.

2.7.1.3   Protein clustering
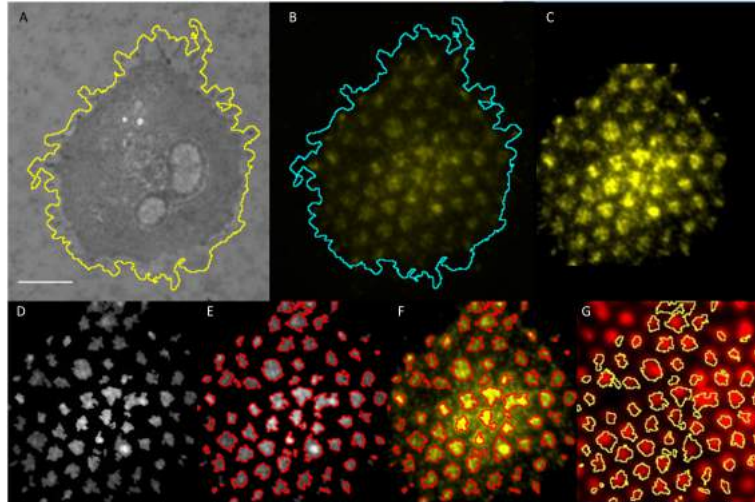
Figure 2.20: **Steps involved in the image analysis for protein clustering.** A: Raw RICM image from which the cell-substrate contact region is segmented. B: Raw fluorescent image of TCR (labelled with anti-vβ8) of superposed with the segmented edge from A. C: Segmented Fluorescent image on which the algorithm will be applied. D: Segmented clusters detected by the thresholding. E: ROIs of each clusters from D. F: Superposition of the cluster ROIs and the raw fluorescent image. G: Superposition of the clusters ROIs and the underlaying nano-dots array of anti-CD3. Scale bar: 10 μm.

Analysis of the protein clustering on the T-cell surface was done using the following principle : First, the fluorescent images of TCR or ZAP70 were prepared in ImageJ by segmenting the cells using the corresponding RICM images (detect from 2.7.1.1). Then a thresholding algorithm was used to segment the clusters. This algorithm was kindly provided be Dr.Rajat Varma. The algorithm uses an initial intensity thresholding using the mean intensity under the cell but outside the clusters. Then different parameters were defined :

84

- an upper cutoff for cluster size (typically 10 pixels , corresponding to 1 μm)
- a step value for convergence (here 0.05)
- a step value to determine how much to trim each cluster (here 0.8)

All the parameters were kept constant across samples, except the initial intensity threshold, which was set approximately to the background intensity (excluding TCR clusters) within the cell under consideration. The algorithm outputs the size of the clusters, the number of clusters per cell, and the average intensity in each cluster. These informations were used to constructed the size histograms. The clusters density was calculated by dividing the number of clusters in a cell by the area of the cell which was determined from segmentation of RICM image. The average cluster intensity was normalized by the average intensity under the cell to compensate for possible differences in the level of immunostaining [103, 142].. A co-localization between the proteins clusters and the nano-dot array can be determinate by overlapping the ROIs of the segmented clusters on the nano-dot array image (Figure 2.20).

2.7.2 Dynamic description

2.7.2.1 Adhesion kinetics

In order to study the dynamic of the cell on substrates, adhesion area analysis were done on each slides of the record (see section 2.7.1.1). Then the area measurements were plotted versus time.

2.7.2.2 Actin dynamics

In order to study the dynamic of the action re-organization on substrates, actin distribution analysis were done on each slide of the record (see section 2.7.1.2). Then the parameter measurements were plotted versus time.

2.8 Statistical analysis

Statistical tests were done using Student-T test. Table 2.3 show the statistical significance according the p-value (p). Note that on graphs with bar charts or scatter dot plots, absence of stats means "not significant".

p-value (p)	statistical significance	Representation
$\leq$0.05	Non-significant	no stars or NS
0.01$\leq$ p $\leq$ 0.05	Low significance	*
0.001$\leq$ p $\leq$ 0.01	Medium significance	**
p $\leq$ 0.001	High significance	***

Table 2.3: **Description of the statistical significance according the p-value.**

Chapter 3

Patterning Technique

Contents

In this chapter, a step by step description of the patterning technique is presented. It consists of creating a protein nano-dot array in a fluid supported lipid bilayer. Briefly, a primary mask is created either by self-assembly or by E-beam lithography on which a layer of aluminum is deposited. A secondary mask is revealed by removing the primary mask. Then a template consisting of tagged BSA is created by deposition through this secondary mask. And finally the SLB is deposited (Figure 8.1).Different combination of proteins and lipids were used and this chapter will described these different substrates used in this thesis.
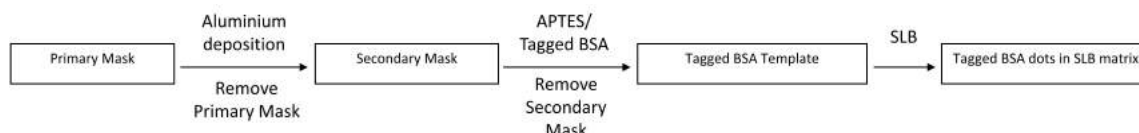
Figure 3.1: **General scheme of the patterning technique.**

3.1   Preparation of masks by Nano-sphere lithography

The main technique used during my thesis to create the nano-dots array used colloidal beads self-assembly for creating the primary mask.

3.1.1   Preparation of colloidal bead mask

Self-assembly of colloidal beads was used to create the primary mask (Figure 8.1). Silica colloidal bead (micro-spheres) of 2μm of diameter was used (Corpuscular). The concentration of the beads suspension need to be optimized in order to avoid multilayer of beads during the deposition. Moreover in order to have an optimal mask, size standard beads was used. The beads suspension was washed with the following protocol:

- The beads suspension was centrifuged at 2000 rpm for 4 minutes to clear the supernatant

- The supernatant were removed and discarded from the tube

- The beads were resuspended in water and vortexed to re-disperse

- These steps were repeated 6 times

- The beads were cleaned and were then ready to be used.

The protocol for the bead deposition is the following (see Figure 3.3):

- A glass platform is placed with an edge angle of 4°

- A glass-slides (24 X 24 mm)cleaned using protocol 1 (see Appendix A.1) are placed on the platform with an angle of 13°. The hydrophilicity of the slide needs to be sufficiently high to allow a good spreading of the liquid suspension

- 80 to 100 μL of the bead-suspension was deposited drop by drop on the cover slide

Figure 3.2: **Sheme of the nano-sphere lithography.** A: Glass slide with colloidal beads mask (note that for simplicity, a square pattern is shown. In reality the lattice is hexagonal); B: Aluminum is deposited by sputtering; C: The beads are removed by sonication, lifting off the aluminum deposited on top. In the end is left a thin layer of aluminum with empty holes.

- The suspension was allowed to spread under gravity from the top of the glass slide. This step facilitate uniform spreading and avoids the formation of multilayers or clusters of beads

- The liquid was evaporated at room temperature, while maintaining the slide with an angle of 4°. This decrease of angle creates a back flow of the suspension which carries some beads and fills the defects formed during spreading.

After complete evaporation, a large area covering most of the slide of a very ordered array of beads is generated. The distance between beads (center to center) corresponds to the diameter of the beads used. Figure 3.4 shows a good bead-mask visualized with optical microscopy. The beads mask can be kept in a clean box in ambient conditions for up to 2 days.
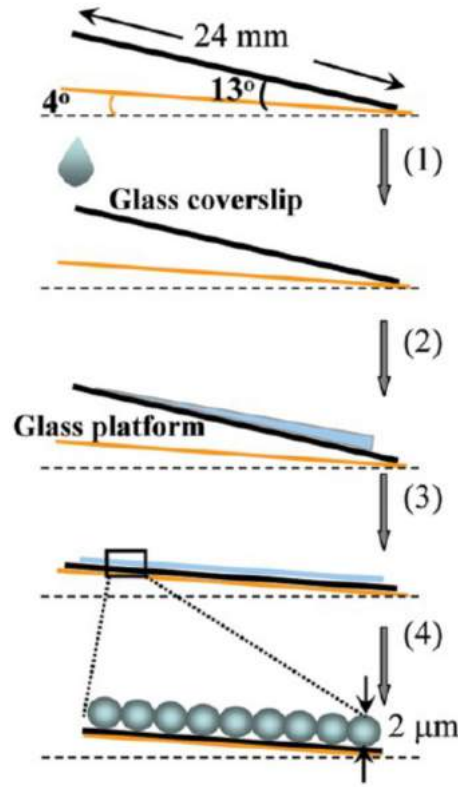
Figure 3.3: **Steps for colloidal bead self-assembly on glass substrate.**(1):A glass slide is set at a controlled angle. (2)-(3): A drop of the bead-suspension is spread on the glass slide until it attends the bottom of the slide.(4): The edge angle of the glass slide is decreased. [102].

3.1.2 Aluminum layer by sputtering

The aluminum deposition uses radio frequency (RF) magnetron sputtering technique which allows a controlled deposition of a thin homogeneous layer of aluminum (principle describe previously in section 2.2).

3.1.2.1 Material and setting

For the deposition, the samples were placed at a distance of 105 mm onto a rotating table. A target with Aluminum with 1% silicon (Kurt J. Lesker Company, purity 99,99%) was used.

The protocol and settings for the deposition were the following :

- A turbo-molecular pump was use to achieve a pressure of 2.6×10^{-4} Pa in the deposition chamber.

- Argon pure atmosphere (5N, 99.999%) was introduce with a flux of 10 s.c.c.m at a pressure of 0.8 Pa (6.6 mTorr)

Figure 3.4: **Optical microscopy (bright field transmission) image of 2μm silica colloidal beads mask on glass substrate.**Inset displays the Fourier transform of the image showing the ordering of the lattice. Objective X100, Scale bare: 10μm.

- After switching on the RF, a sputter for 2 minutes was done with the shutter closed in order to remove eventual gas impurities from the target

- The shutter was opened. The samples can be stored up to at least one month in clean hermetically sealed box either before or after removal of the beads. The deposition was done for 60 min corresponding to an aluminum thickness of 200 nm.

- The beads are removed by ultrasonication in ultra-pure water during 10 seconds. At this step the glass slide is an aluminum layer with empty nano-hole array. This forms the secondary mask (see 8.1). As expected, the distance between the holes corresponds to the size of one beads used for forming the mask. Previous work in the lab [143] showed that the size of holes depends on the thickness of the deposited aluminum layer. In this thesis, only one set of conditions was used : 2 μm beads and 200 nm aluminum thickness.

3.2 Preparation of masks by Electron-beam lithography

We developed an alternative way to create the patterned substrate, by electron-beam lithography (e-beam lithography). The advantage of this technique is the reproducibility

and the resolution of the pattern (20 nm is expected). See Figure 8.3 for the general scheme of the protocol of e-beam lithography, which will be detailed in this section.
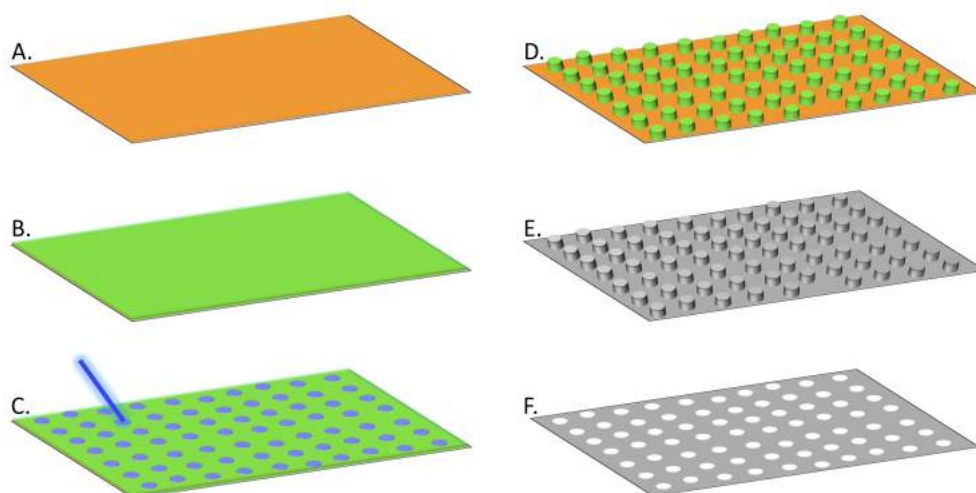
Figure 3.5: **Scheme of the E-beam patterning protocol.**A: Glass slide coated with a bonging layer. B: An electro negative resist is spin-coated onto the glass-slide. C: The pattern is drawn by exposing the resist to the E-beam. D: After development, only the exposed resist is left, leaving an array of resist pillars. E. Aluminum is deposed by evaporation. F. The resist is dissolved, lifting off the aluminum deposited on top. In the end is left a thin layer of aluminum with an array of empty holes.

In e-beam lithography, a beam of electrons is used in order to create the desired pattern. To do so, an electron-sensitive film (resist) is deposited on the surface . This resist can be positive or negative. In the case of a positive resist, the electrons depolymerize the resist and therefore the exposed resist can be removed after development. Conversely for a negative resist, the electrons polymerize the resist and therefore the exposed resist stays in place after the development (Figure 3.6). After patterning the substrate with E-beam through the resist, the latter is immersed in a solvent to remove the non-polymerized part. This reveals the primary mask in form of pillars of resist (Figure 8.1). In this technique, aluminum is deposited by evaporation. Vapor particles of aluminum are created by heating the metal in vacuum. Then the particles condense and deposed directly in the form of a thin layer on the substrate. Finally, the pillars of resit is dissolved in order to reveal the secondary mask (Figure 8.1).

3.2.1   Materials and settings

Before the e-beam lithography, the glass-slides were cleaned using the following protocol:

- Glass-slide was sonicated in acetone during 15 minutes

- After drying, glass-slide was sonicated in isopropanol during 15 minutes
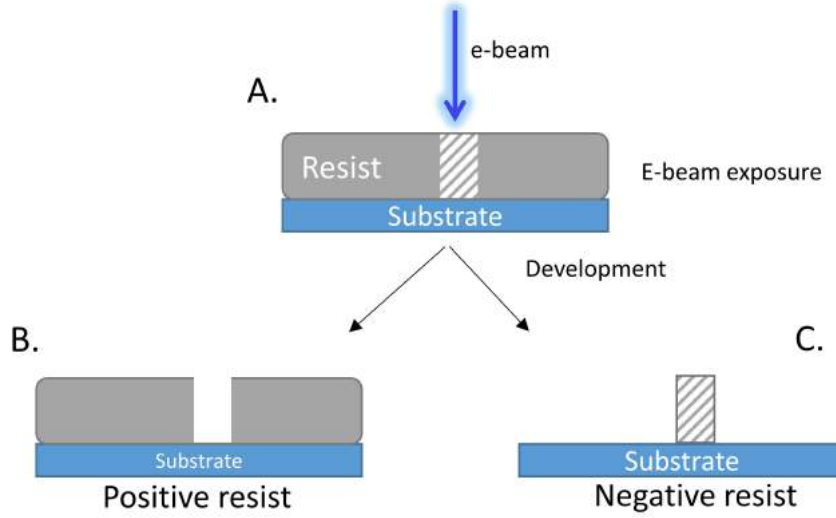
Figure 3.6: **Positive and negative resist in E-beam** A: Exposition of the resist to the E-beam. The desired design is drawn on the resist using the E-beam as a pen. The hatched portion corresponds to the exposed region. B: With a positive resist, after development, the exposed region is removed by the solvent. C: With a negative resist, after development, the exposed region remains.

- After cleaning with ultra-pure water and drying, the glass-slide was cleaned with oxygen plasma at 150°C during 10 minutes.

In order to enhance the grafting of the resist, bonding layer was deposited on the glass-slide (AR 300-80, AllRESIST). In our case, the resist used is negative (ARN 7520-18, AllRESIST), which means that after development, the resist exposed will remain (see Figure 3.6). Before spin-coating the resist, a layer of conductor resist was deposited (ARPCSX, AllRESIST). The E-beam lithography was done with a electronic microscope (Pionner,Raith). The pattern drawn is hexagonal as the pattern obtained with the beads (Figure 3.4). We decided to test different type of pattern by changing the pitch and the size of the dots while getting close to the same percentage of covering by the dots obtained with the nano-sphere lithography which correspond to 11% (zone C and D) (see Figure 8.1). This percentage of the surface covered by the dots (S_{dot}) can indeed be determined by the following equation :

$$S_{dot} = \frac{A_d}{A_T} 100 = \left(\frac{\frac{\pi}{8} d^2}{\frac{\sqrt{3}}{4} p^2} \right) 100 \qquad (3.1)$$

where A_d represent the area of a dot and A_T represent the area of the equilateral triangle with a lenght of p, with d= dot diameter and p= pitch . The different pattern obtained are shown in Figure 8.4
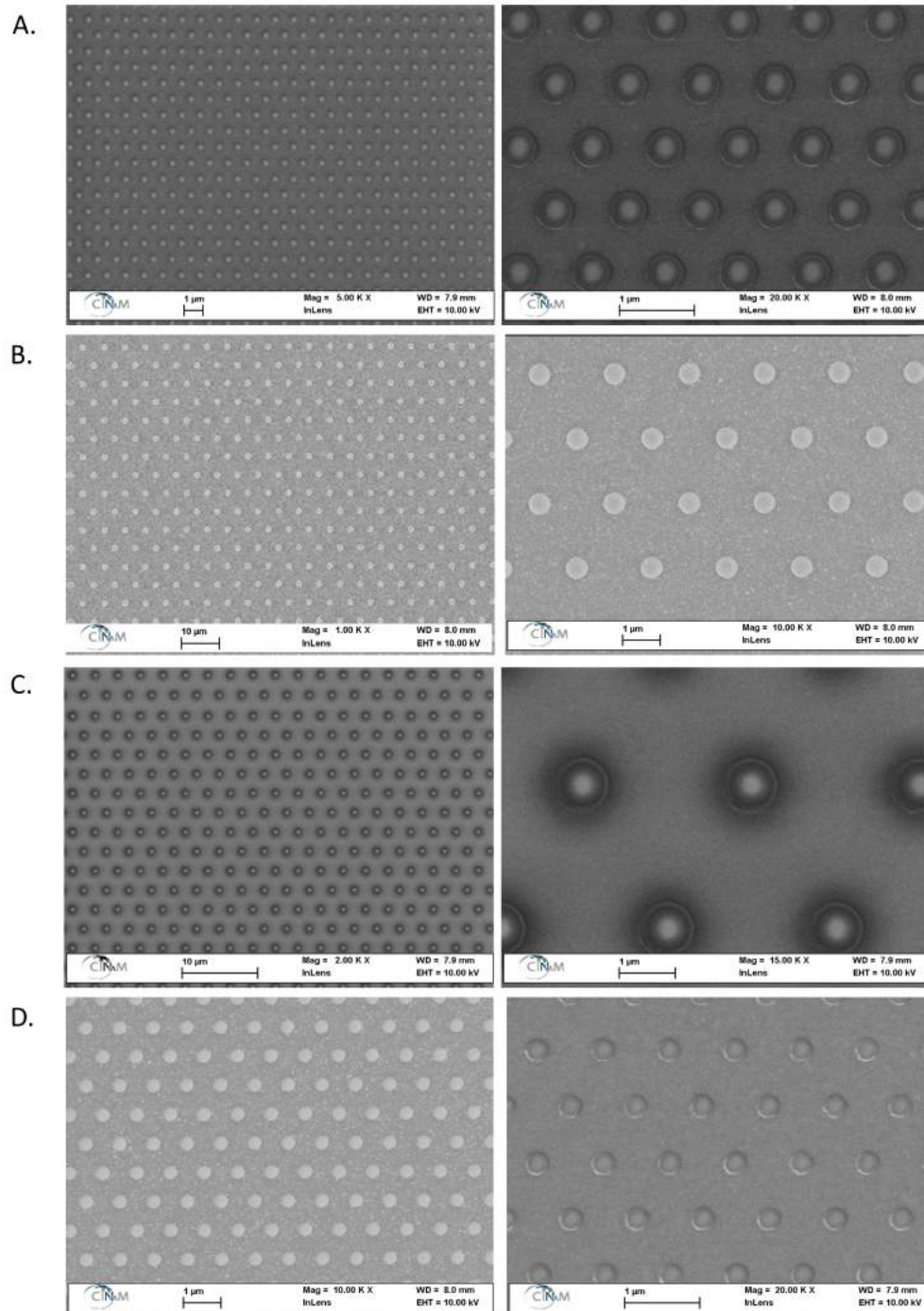
Figure 3.7: **Scanning electron microscopy images of the different pattern (holes in aluminum)realized with E-beam technique described in table 8.1.** A: Zone A with a pitch of 1μm and dots size of 500 nm; B: Zone B with a pitch of 2μm and dots size of 500 nm; C: Zone C with a pitch of 3μm and dots size of 1000 nm; D: Zone D with a pitch of $0{,}9\mu$m and dots size of 300 nm.

Zone	Pitch (μm)	Dots size (nm)	S_{dot} (%)
A	1	500	23
B	2	500	6
C	3	1000	10
D	0,9	300	10

Table 3.1: **Description of different patterns drawn with e-beam lithography.**

3.3 Preparation of protein template

Prior to the preparation of the protein template, the beads were removed by ultra-sonication in ultra-pure water for 10 seconds, then dried with nitrogen. At this stage, the slide is covered with aluminum containing holes exposing the underlying glass.

To make the protein nano-dot array, first, proteins were grafted to surface based on a silane adsorption, then the aluminum is removed (Figure 8.5 A-D). Then the supported lipids bilayers is deposited (Figure 8.5 E). Figure 8.6 shows the different proteins composition and organization on the different substrates used in this thesis. Note that the molecule scale is not respected, the molecule size and geometry is presented in Figure 8.10.
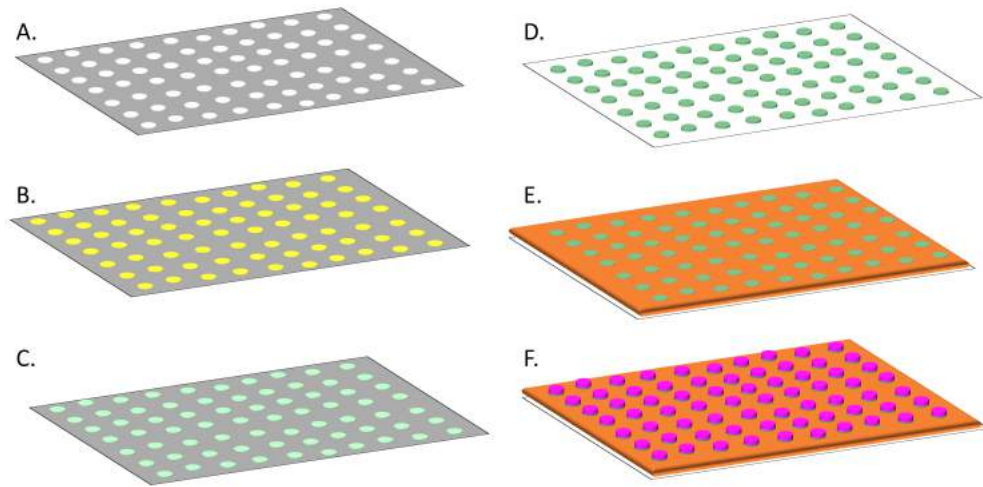
Figure 3.8: **General scheme of functionalization of the pattern substrate**. A: Glass-slide with thin layer of aluminum with empty holes. B: Deposition of layer af APTES. C: Functionalization with the first layers of proteins in the dots (BSA-Biotin or BSA-NTA). D: Removal of aluminum layer leaving only the nano-protein dots. E: Deposition of lipid bilayer which go around the dots. F: Final step of functionalization of the dots typically with either NaV+anti-CD3 or ICAM-1-histag. The lipids bilayer can also be functionalized.
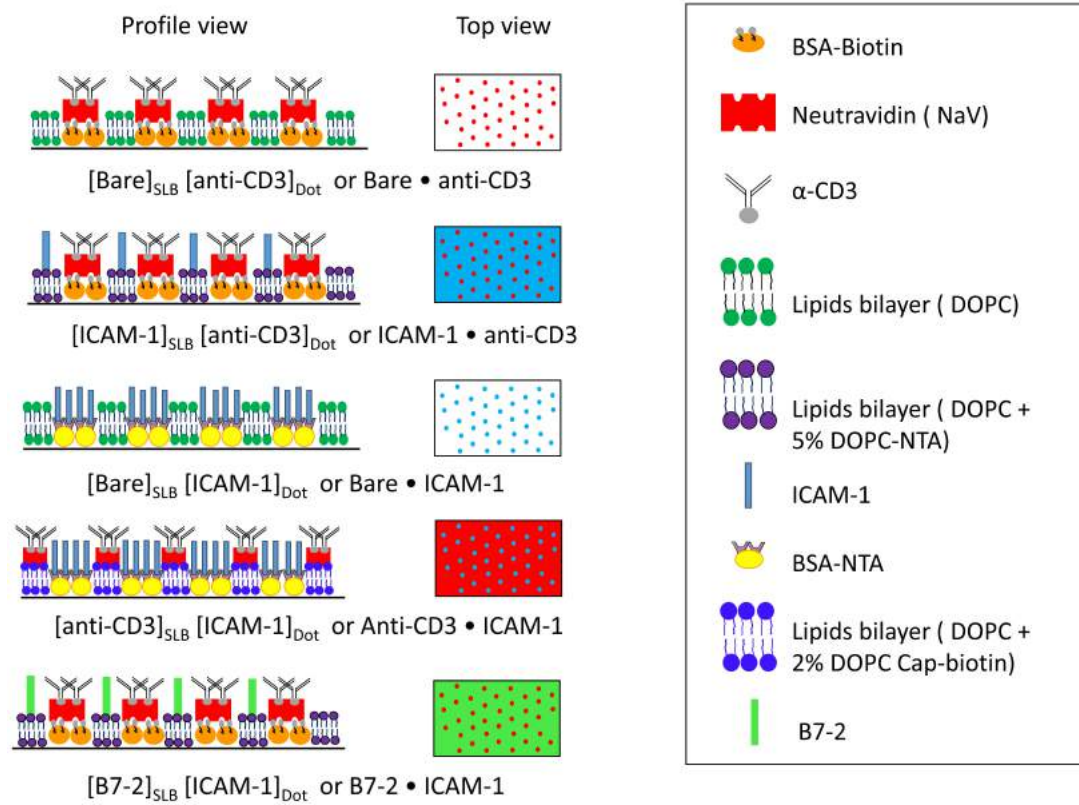
Figure 3.9: **Schematic of the protein composition and organization for patterned substrates**. Schematic representation of the different substrates used during this thesis. Substrates are composed of either biotinylated anti-CD3 dots or His-Tagged ICAM-1 dots surrounded by either a non-functionalized SLB or a SLB functionalized with ICAM-1, B7-2 or anti-CD3. A profile view and top view is represented. Note that the scale for the proteins is not respected.

3.3.1 APTES and Biotin-BSA/ NTA-BSA

In order to graft the proteins, an APTES deposition was done. The protocol used is the following:

- Cleaned glass slides (obtained using Procedure 1-see Appendix A.1) were disposed on a ceramic grid in a glass desiccator

- In a Petri dish under the ceramic grid, 0.5 mL of APTES was deposited

- The desiccator was then connected to a membrane pump at maximum power (8 mbar) during 30 minutes

- After closing the valve, the desiccator was heat for one hour at 50°C

- The glass slides were transferred to another clean desiccator for storage for no longer than 48 hours

Then proteins were grafted using the following protocol:

- An APTES functionalized glass slide was mounted into the open chambers and rinsed 5 times with PBS

- 25 μg/mL of BSA biotin or BSA-NTA was deposited during 30 minutes at room temperature

- The sample was rinsed 10 times with PB

At this stage the tagged BSA template is obtained, consisting of nano-dots of protein on glass (Figure 8.1 and 8.5).

3.3.2 Aluminium removal

The layer of aluminum was remove with PBS + Sodium hydroxide (NaOH), pH $\geq$ 11 (if it was BSA-Biotin in the dots) or with PBS+10% Phosphatidic acid 1M (if it was BSA-NTA in the dots). The substrate was incubate in this solution for at least 4 hours until complete dissolution at room temperature. The success of the lift-off was checked by RICM (see Figure 3.10 for example good and bad lift-off).
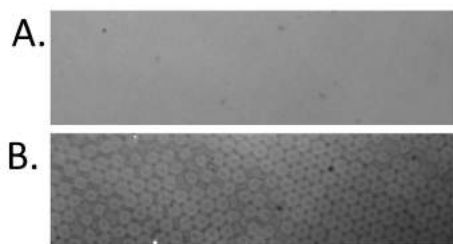
Figure 3.10: **RICM images of the surface after removing aluminum with PBS-NaOH** A: Complete dissolution of the aluminum. The RICM image is clear. B: Incomplete dissolution of aluminum. The RICM image shows non uniform image.

3.3.3 Supported Lipids Bilayer by Langmuir-Blodgett technique

The lipid bilayers were deposited by Langmuir-Blodgett technique in the majority of cases,(see section 2.3.2.2).The SLB gets deposited only around the nano-dots and not on them (as represented schematically in Figure 8.5E). For each substrates, the fluidity of the lipids was verified and measured by continuous bleaching (as described in section 2.6.1), where a halo is visible only if the lipids are diffusing (see Figure 3.11. Only fluid SLBs were accepted for cell experiments reported in the next chapter.

In Figure 3.12 I present a selection of SLBs, either patterned or not, functionalized or not, over the period of this work. As can be seen, the diffusion constant (D) does not appreciably vary from year to year and does not depend on the substrate type. D seen to vary between 4 μm²/sec and 6 μm²/sec for both homogeneous and patterned SLBs, with D being slightly lower for the patterned case. The mean diffusion constant(D) are 4.2 $\pm$0.3 μm²/sec and 5.4 $\pm$1.5 μm²/sec for respectively SLB surrounding nano-dots arrays of proteins and homogeneous SLB.
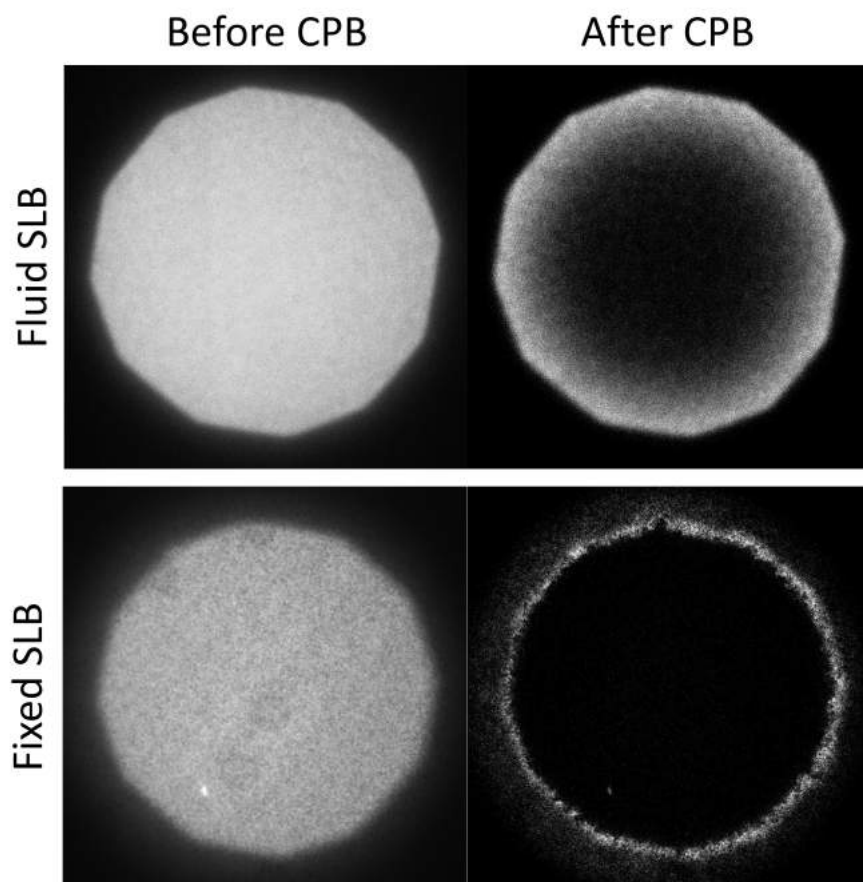
Figure 3.11: **Comparison between fluid and fixed SLB**. SLB fluidity was measured by CPB. After 50 sec of constant illumination a halo is visible if the lipids are diffusing (top raw). In the case of fixed SLB, the illuminated area is completely bleach (bottom row).

3.3.4 Supported Lipids Bilayer by vesicles spreading techniques

Other technique using small unilamellar vesicles spreading (VS) was performed to make bilayers on glass-surface (see section 2.3.2.3). Previous work from the lab [86] had shown that for homogeneous SLB, the fluidity of the bilayer is high with VS and therefore the diffusion of proteins grafted on top. The deposition was done either in open chamber or in FCS2 chamber (see section 2.3.2.3). The results obtained showed mixed results. Indeed using FCS2 chamber, the percentage of success to obtained homogeneous fluid lipid bilayers was around 60% and using open chamber the percentage decrease to 50%. But with both chambers, the percentage of success to obtained fluid lipid bilayers on glass with nano-proteins arrays dropped to 20% . Also the diffusion constant of these SLB (3,5±0,8 μm²/sec) was not higher than with Langmuir-Blodgett technique as was hopped.
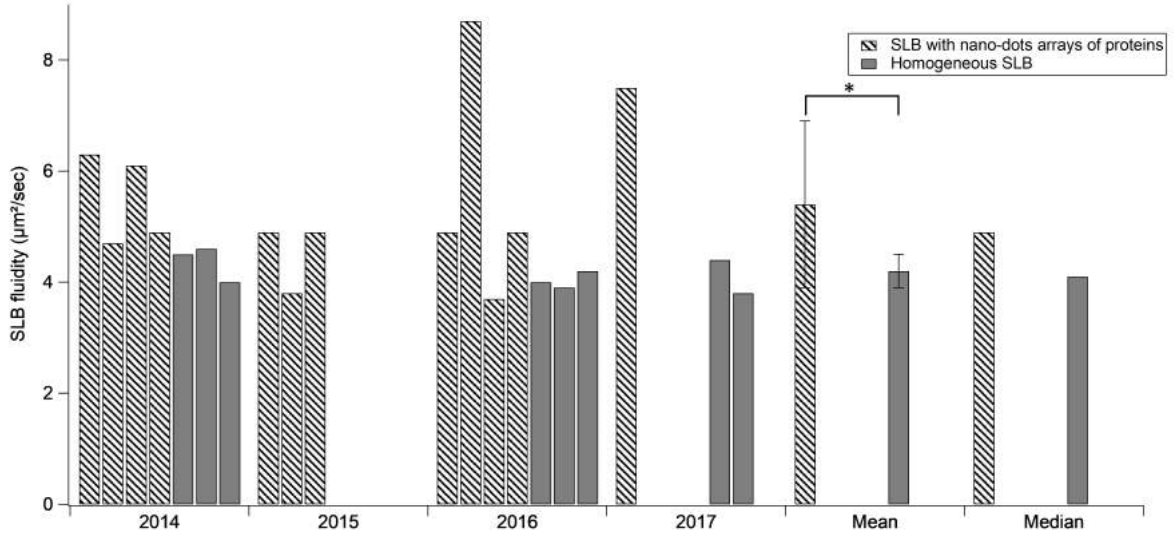
Figure 3.12: **Diffusion constant of SLB over experiments and between homogeneous and SLB with nano-dots arrays**. Fluorescent SLB diffusion was measured using CPB technique (see section 2.6.1). One bar correspond to one experiment done with DOPC lipid + 0,1% of fluorescent lipids. Error bars represent standard deviation measurements.

3.4 Protein Functionalization

Many different combination of dot and SLB functionalization were used in this thesis. The dots were functionalized with anti-CD3,ICAM-1 or with non activating molecules like BSA-biotin or an isotype control. The SLB was either left bare or was functionalized with anti-CD3, ICAM-1 or B7-2 or it contained PEG. The substrates are subsequently named after these functionalizations as summarized in table 8.2.

The name are given as $[SLB]_{SLB}$ $[Dot]_{Dot}$ or SLB • Dot. For example, a substrate with anti-CD3 dots in bare SLB is called $[Bare]_{SLB}$ $[anti\text{-}CD3]_{Dot}$ or, Bare • anti-CD3. In the following, the specific protocol for each type of functionalization is described.

3.4.1 Functionalization of the nano-dots

3.4.1.1 Dot: NaV and α-CD3

Starting with BSA-biotin template, functionalization of the dots with α-CD3 was done using the following protocol:

- Neutravidin diluted in PBS to the desired concentration (typically 2 μg/ml) was incubated during 30 min

- The sample was rinsed 10 times with PBS

- Biotinylated α-CD3 diluted in PBS to the desired concentration (typically 2μg/ml) was incubated during 30 min

- The sample was rinsed 10 times with PBS.

3.4.1.2   Dot: ICAM-1

Starting with BSA-NTA template, functionalization of the dots with ICAM-1 was done using the following protocol:

- ICAM-1 diluted in PBS to the desired concentration (typically 5 μg/ml) was incubated during 30 min

- The sample was rinsed 10 times with PBS.

3.4.1.3   Dot: Control

A non-specific antibody in the dots was used as a negative control. To do so, functionalization of the dots with anti-rat IgG2b isotype control, starting with BSA-Biotin template, was done using the following protocol:

- Anti-rat IgG2b isotype control diluted in PBS to the desired concentration (typically 5 μg/ml) was incubated during 30 min

- The sample was rinsed 10 times with PBS.

An other negative control was obtained by stopping the dot functionalization at the stage of BSA-Biotin.

3.4.2   Functionalization of the SLB

After deposition of the SLB, a blocking step was made with 100μg/ml of BSA in order to prevent the non-specific adsorption of the proteins used to further functionalize the nano-dot arrays (see section2.3.3). The bilayer need to be functionnalized immediately after preparation. Indeed, it as been shown that the fluidity of the bilayer drop dramatically several hours after the BSA incubation ([86]). Protein functionalization of the dots is done after SLB deposition. Due to non-specific adsorption, the proteins may also be deposited on the bilayer despite its passivation. Therefore, SLB may contain non-negligible amounts of the proteins used to functionalize the dots.
DOPC lipids are used as a major components of lipids matrix. Different lipids are added to create different lipids compositions as need. The functionalization of the SLB was done at the same time as the functionalization of the dots. The protein contents of the SLB and the dots will be characterized in the next chapter.
After functionalization of the SLB the substrate was used immediately for cell experiments.

3.4.2.1   Non-functionalized SLB

Non-functionalized SLB corresponds to SLB composed of only DOPC. Due to the non-specific adsorption, different types of SLB can be created:

Neg1: The non-functionalized SLB was exposed to NaV and α-CD3.

Neg2: The non-functionalized SLB was exposed to ICAM-1.

NB: For future use, the SLB Neg1 and Neg2 will be referred as "Bare" on patterned substrates (see Table 8.2). It's should be kept in mind that "Bare" SLB may contain non-negligible amounts of the proteins used to functionalize the dots.

3.4.2.2 Functionalization of SLBs with anti-CD3

To functionalize the SLB with anti-CD3, lipid solution containing DOPC + 2 % of cap-biotinylated lipids was used to form the SLB (see section 2.3.2.1). Then the bilayer was functionalized with Neutravidin and anti-CD3 using the protocol previously describe for the dots (see section 3.4.1.1).

3.4.2.3 Functionalization of SLBs with ICAM-1

To functionalize SLBs with ICAM-1, lipid solution containing DOPC + 5% of NTA-lipids was used (see section 2.3.2.1). Then bilayer was functionalized with ICAM-1 at a concentration of 5μg/ml during 30 min at room temperature. The sample was then rinsed 10 times with PBS.

3.4.2.4 Functionalization SLB with B7

To functionalize the SLBs with B7-2, lipid solution containing DOPC + 5% of NTA-lipids was used (see section 2.3.2.1). Then bilayer was functionalized with B7-2 at a concentration of 5μg/ml during 30 min at room temperature. The sample was then rinsed 10 times with PBS.

3.4.2.5 SLB with PEG

SLB can be functionalized with PEG in addition to other molecules, to do so, 2% of PEG lipids was add to the lipids solution used to make the SLB.

3.5   Homogeneous controls

In addition to patterned substrates, homogeneous controls were made. These controls mimic the composition of either the dots (Dots controls) or the SLB (SLB controls). Moreover in order to compare the impact of protein clustering, homogeneous substrates on which the density was controlled in order to have the same protein density as on patterned substrates were done (Homogeneous substrates) . This section will describe how these controls were prepared.

3.5.1   Dots controls

These controls present the same protein conditions as in the dots. As three types proteins were used on the dots, 3 controls were made :

- Homogeneous α-CD3 on glass (named as POS anti-CD3)

- Homogeneous ICAM-1 on glass (named ad POS ICAM-1)

- Homogeneous anti-rat IgG2b isotype control (named as POS isotype control)

To obtain these homogeneous substrates, bare glass were functionalized using the following protocol :

- APTES deposition was performed as describe previously (see section 3.3.1)

- 25μg/ml of BSA-biotin or BSA-NTA was deposited during 30 minutes at room temperature

- The sample was rinsed 10 times with PBS

- Protein of interest (α-CD3 or ICAM-1 or anti-rat IgG2b isotype control) was incubated in the same condition as for the dots functionalization (see section 3.4.1).

- The sample was rinsed 10 times with PBS.

3.5.2   SLB controls

During the functionalization of the protein dots for patterned substrates, the SLB is in contact with proteins used to functionalized the dots. And due to non-specific adsorption, some of these proteins stay on the SLB and change the property of the SLB. In order to know the impact on cells, SLB controls were made in the same conditions as for patterned substrate which means that they were incubate with the different proteins used to functionalized the dots. These controls present the same protein conditions as on the SLB by taking into account the non-specific adsorption that occurred during the functionalization of the associated dots (this controls are named as Homogeneous SLB control type 1).

- Non-functionalized SLB exposed to anti-CD3

This substrate is a SLB control for patterned substrate with anti-CD3 in the dots surrounded by a bare SLB. This control was done with SLB containing pure DOPC. After deposition, the bilayer was incubated with neutravidin and anti-CD3 in the same condition as if it was on the patterned substrate (see section 3.4.1.1).

- SLB functionalized with ICAM-1 exposed to anti-CD3

This substrate is a SLB control for patterned substrate with anti-CD3 in the dots surrounded by SLB functionalized with ICAM-1. This SLB was fabricate using solution of DOPC + 5% of NTA-lipids and functionalized with ICAM-1 as describe in section 3.4.2.3. After fabrication, the bilayer was also incubated in neutravidin and anti-CD3 in the same condition as if it was on the patterned substrate(see section 3.4.1.1).

- SLB functionalized with B7-2 exposed to anti-CD3

This substrate is a SLB control for patterned substrate with anti-CD3 in the dots surrounded by SLB functionalized with B7-2. This SLB was fabricate using solution of

DOPC + 5% of NTA-lipids and functionalized with B7-2 as describe in section 3.4.2.4. After fabrication, the bilayer was also incubated in neutravidin and anti-CD3 in the same condition as if it was on the patterned substrate(see section 3.4.1.1).

- Non-functionalized SLB exposed to ICAM-1

This substrate is a SLB control for patterned substrate with ICAM-1 in the dots surrounded by a bare SLB. This SLB was made using pure solution of DOPC. But after fabrication, the bilayer was also incubated with ICAM-1 in the same condition as if it was on the patterned substrate(see section 3.4.1.2)

- SLB functionalized with anti-CD3 exposed to ICAM-1

This substrate is a SLB control for patterned substrate with ICAM-1 in the dots surrounded by SLB functionalized with anti-CD3. This SLB was made using solution of DOPC+ 2 % of cap-biotinylated lipid and functionalized with anti-CD3. But after fabrication, the bilayer was also incubated with ICAM-1 in the same condition as if it was on the patterned substrate(see section 3.4.1.2).

3.5.3   Homogeneous controls

In order to study the impact clustering of proteins, homogeneous SLB controls were done with the same proteins density as on patterned substrates. The lipids solution was modified to achieved the same level of adsorption and therefore the same quantity of proteins as on patterned substrates but in this cases homogeneously distributed (called Homogeneous controls type 2).

- SLB non functionalized and anti-CD3

This substrate (called SLB Neg1+anti-CD3) is a SLB control for patterned substrate with anti-CD3 in the dots surrounded by a bare SLB. This SLB was made using solution of DOPC+0,1% of cap-biotinylated lipid. The bilayer was then functionalized with neutravidin and anti-CD3 as for pattern substrate (see section 3.4.1.1).

- SLB functionalized with ICAM-1 and anti-CD3

This substrate (called SLB ICAM-1+anti-CD3) is a SLB control for patterned substrate with anti-CD3 in the dots surrounded by SLB functionalized with ICAM-1. This SLB was made using solution of DOPC + 5% of NTA-lipids+ 0,1% of cap-biotinylated lipid and functionalized with ICAM-1. After fabrication, the bilayer was also functionalized with neutravidin and anti-CD3 in the same condition as if it was on the patterned substrate(see section 3.4.1.1).

- SLB non functionalized and ICAM-1

This substrate (called SLB Neg2+ICAM-1) is a SLB control for patterned substrate with ICAM-1 in the dots surrounded by a bare SLB. This SLB was made using solution of DOPC+0,1% of NTA-lipids. The bilayer was then functionalized with ICAM-1 in the same condition as if it was on the patterned substrate(see section 3.4.1.2)

- SLB functionalized with anti-CD3 and ICAM-1

This substrate (called SLB anti-CD3+ICAM-1) is a SLB control for patterned substrate with ICAM-1 in the dots surrounded by SLB functionalized with anti-CD3. This SLB was made using solution of DOPC+ 2 % of cap-biotinylated + 0,1% of NTA-lipids and functionalized with anti-CD3. After fabrication, the bilayer was also functionalized with ICAM-1 in the same condition as if it was on the patterned substrate(see section 3.4.1.2)

N°	Description		Name	Short Name
	SLB	**Dot**	**[SLB]**$_{SLB}$ **[Dot]**$_{Dot}$	**SLB • Dot**
	Patterned Substrates			
1	Neg1	α-CD3	[Bare]$_{SLB}$ [αCD3]$_{Dot}$	Bare • αCD3
2	ICAM-1	α-CD3	[ICAM-1]$_{SLB}$ [αCD3]$_{Dot}$	ICAM-1 • αCD3
3	B7-2	α-CD3	[B7-2]$_{SLB}$ [αCD3]$_{Dot}$	B7-2 • αCD3
4	Neg1+PEG	α-CD3	[Bare+PEG]$_{SLB}$ [αCD3]$_{Dot}$	BarePEG • αCD3
5	ICAM-1+PEG	α-CD3	[ICAM-1+PEG]$_{SLB}$ [αCD3]$_{Dot}$	ICAM-1+PEG • αCD3
6	Neg2	ICAM-1	[Bare]$_{SLB}$ [ICAM-1]$_{Dot}$	Bare • ICAM-1
7	α-CD3	ICAM-1	[α-CD3]$_{SLB}$ [ICAM-1]$_{Dot}$	α-CD3 • ICAM-1
8	Neg1	BSA-Biotin	[Bare]$_{SLB}$ [BSA-Biotin]$_{Dot}$	Bare • BSA-Biotin
9	Neg1	anti-rat IgG2b isotype control	[Bare]$_{SLB}$ [anti-rat IgG2b isotype control]$_{Dot}$	Bare • non-specific
	Dot controls			
10	α-CD3		[αCD3]$_{Dot}$	POS α-CD3
11	ICAM-1		[ICAM-1]$_{Dot}$	POS ICAM-1
12	anti-rat IgG2b isotype control		[non-specific]$_{Dot}$	POS non-specific
	Homogeneous SLB controls type 1			
13	Neg1		[Neg1]$_{SLB}$	SLB Neg1
14	Neg1+PEG		[Neg1+PEG]$_{SLB}$	SLB Neg1+PEG
15	ICAM-1		[ICAM-1]$_{SLB}$	SLB ICAM-1
16	ICAM-1 +PEG		[ICAM-1+PEG]$_{SLB}$	SLB ICAM-1+PEG
17	B7-2		[B7-2]$_{SLB}$	SLB B7-2 1
18	Neg2		[Neg2]$_{SLB}$	SLB Neg2
19	α-CD3		[α-CD3]$_{SLB}$	SLB α-CD3
	Homogeneous SLB controls type 2			
20	Neg1+ α-CD3		[Neg1+α-CD3]$_{SLB}$	SLB Neg1+ α-CD3
21	ICAM-1+ α-CD3		[ICAM-1+ α-CD3]$_{SLB}$	SLB ICAM-1+ α-CD3
22	Neg2+ICAM-1		[Neg2+ICAM-1]$_{SLB}$	SLB Neg2+ICAM-1
23	α-CD3+ICAM-1		[α-CD3+ICAM-1]$_{SLB}$	SLB α-CD3+ICAM-1

Table 3.2: **Description of substrates, their names and short names.**

Chapter 4

Characterization of substrates

Contents

In this chapter, I will report the characterization of patterned substrates which were fabricated using protocols described in Chapter 3.

Patterned substrates used in this thesis can be separated in two kinds, either with nano-dots of anti-CD3 or with nano-dots of ICAM-1. In both cases, the nano-dot arrays were surrounded by different types of fluid lipid bilayers. In addition, several control substrates were also made, either with homogeneous SLB or with proteins homogeneously grafted directly on glass. These substrates were characterized in terms of SLB fluidity, protein nano-dot size and protein density inside and outside the dots. Homogeneous substrates were characterized in terms of protein density and fluidity of the SLB.

The fluidity of the bilayer is an important parameter as this may define the fluidity of the proteins grafted on top.

In this chapter, each type of characterization is presented in the form of bar charts where the colors correspond to nature of the dot proteins: red for anti-CD3 and blue for ICAM-1. Color codes for all substrates are explained in appendix D.

4.1   Patterned substrates

As described in Chapter 3, anti-CD3 dots were created from templates of BSA-Biotin which were subsequently functionalized successively with NaV and anti-CD3. In the vast majority of cases, the NaV was fluorescently labeled and served as a means of quantification of protein density.

4.1.1   Anti-CD3 dots in non-functionalized SLB

$[\text{Bare}]_{SLB}$ $[\alpha\text{CD3}]_{Dot}$ or Bare • αCD3 substrate is composed of anti-CD3 nano-dots surrounded by a non-functionalized bilayer. This substrate was extensively used to standardize fabrication protocol as well as for cell studies. As such, it can be considered as the standard substrate.

4.1.1.1   Characterization of SLB fluidity

For this substrate, the DOPC bilayer was supplemented with fluorescent lipids in order to visualize the quality of the deposited SLB and to measure the diffusion constant (D) using the Continuous Photo-Bleaching(CPB) technique. As shown in Figure 4.1, the SLB was deposited around the dots. The fluidity measured with the CPB technique (Figure 4.2 for example) gave a diffusion constant of $5.6\pm1.8\mu$m²/sec (Figure 4.3). The fluidity of the SLB was relatively constant over experiments.

4.1.1.2   Characterization of protein dot size

Protein dot size is determined by the thickness of the aluminum layer deposited during sputtering [143]. We chose to keep this deposition parameter constant. Fluorescent patterns were fabricated using the protocol described in Chapter 3. Figure 8.7 shows an epi-fluorescence image of the obtained NaV pattern. The dot sizes were characterized using this type of epi-fluorescence images. To do so, for each field of fluorescent nano-dot array, each dot was segmented and a median dot was constructed. The dot size was then measured using the Full Width Half-Maximum (FWHM) (see section 2.6.2). Since
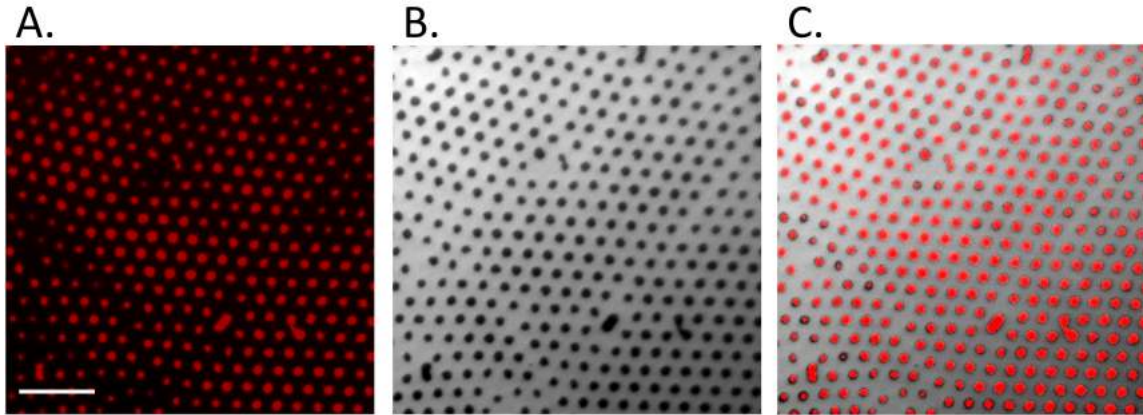
Figure 4.1: **NaV dots surrounded by a fluid SLB.** A: Epi-fluorescent image of nano-dot arrays of NaV labeled with Dyelight650. B: Epi-fluorescent image of DOPC bilayer supplemented with 1% of fluorescent lipids deposited as a SLB with LB/LS technique surrounding the NaV dots. C: Composite image of (A) and (B) showing the good complementary of the SLB and the protein dots. Scale bare = 10μm.
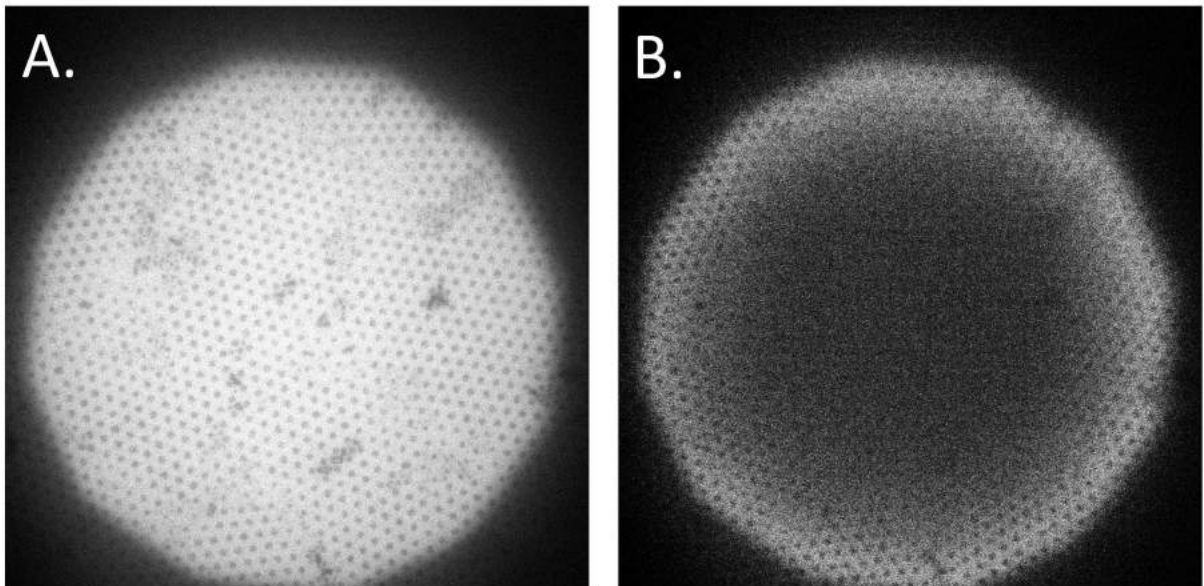
Figure 4.2: **Lateral molecular diffusion measurement by Continuous Photo-Bleaching on patterned substrate.** A: DOPC bilayer supplemented with 1% of fluorescent lipids before Photo-Bleaching. B: The bilayer after 50 seconds of continuous photo-leaching. Here the diffusion coefficient was measured to 5 μm^2/sec (with B=0.13 seconds^{-1} (see section 2.6.1)).

the fabrication technique is complicated and conditions slightly differed over the years (mainly beads type and clean room conditions), we first check the dot size reproducibility over the years of this thesis. As shown on Figure 4.5 the technique of nano-sphere lithography induced a reproducible dot size over all experiments, with an obtained mean
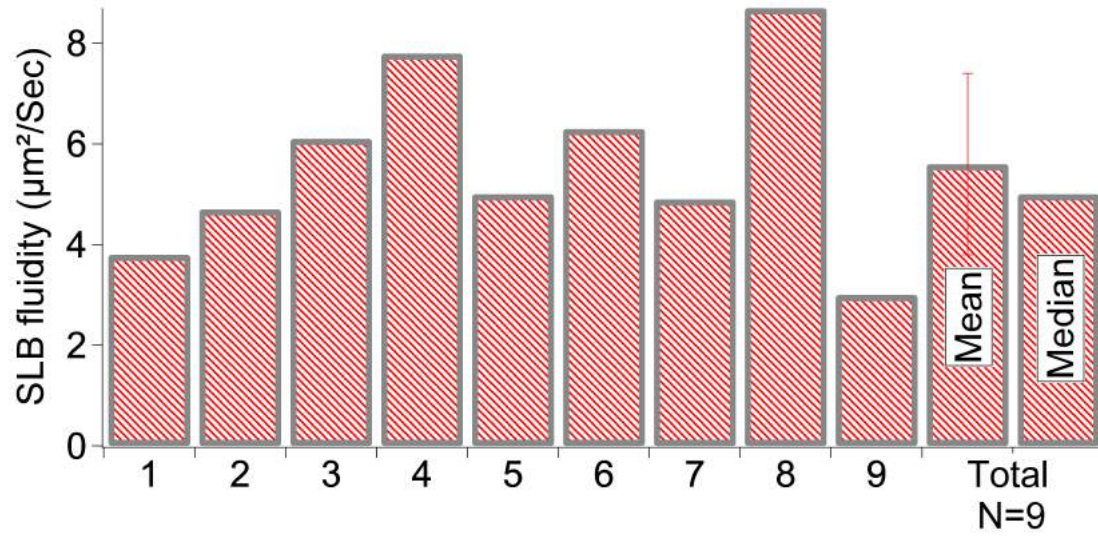
Figure 4.3: **Diffusion constant of Bare-SLB surrounding nano-dot arrays of anti-CD3**. Bars from 1 to 9 correspond to experiments done with DOPC lipid + 0,1% of fluorescent lipids. The mean diffusion constant was $5.6\pm1.8\mu m^2$/sec with the error bar representing the standard deviation (N=9).

size of 780$\pm$120 nm.
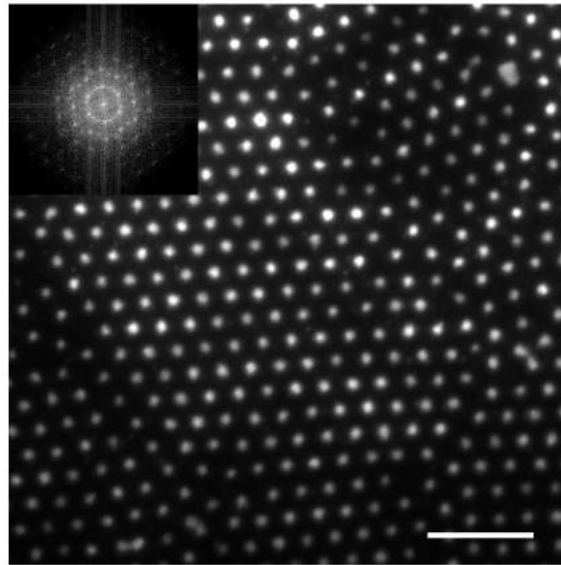
Figure 4.4: **Epi-fluorescence image of NaV nano-dot array.** Fluorescent NaV dots formed an uniform array with an hexagonal lattice. Inset displays Fourier transform showing the ordering of the lattice. Scale bar $=10\mu$m.

(a) Protein dot size obtained during the first year

(b) Protein dot size obtained during the second year

(c) Protein dot size obtained during the third year

(d) Overal protein dot size
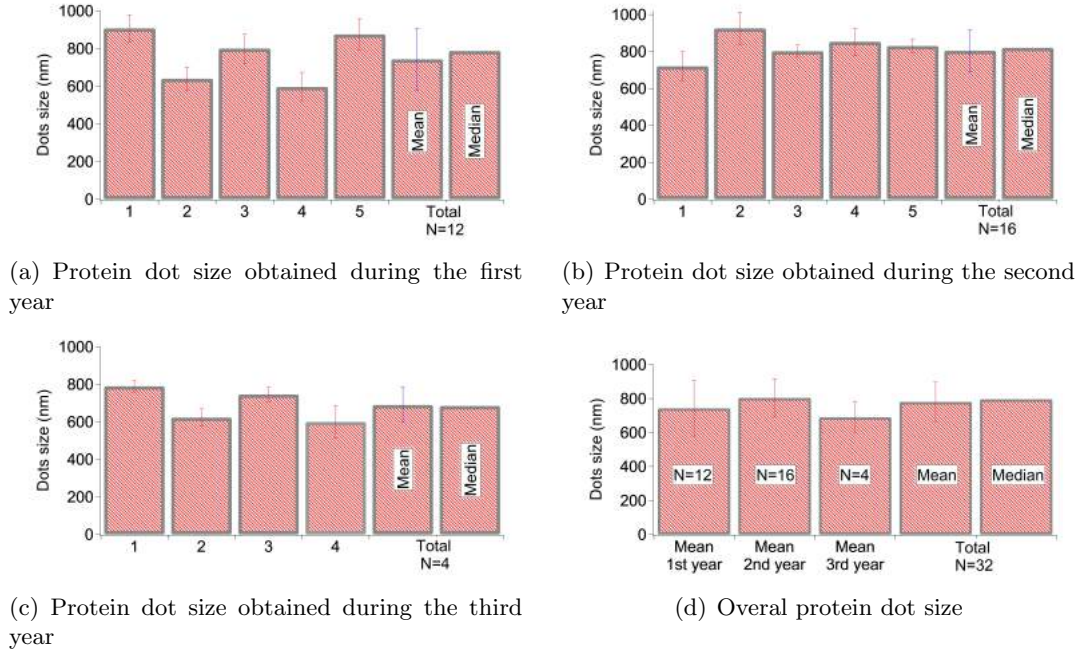
Figure 4.5: **Protein dot size measured from Full Width Half-Maximum from epi-fluorescent images.** The mean protein dot size equals 780±120 nm. Error bars represent standard deviations.

4.1.1.3 Characterization of fluorescence intensity

Epi-fluorescent images were also used to extract the fluorescence intensity inside and outside the dots. The fluorescence intensity is expected to be proportional to the amount of NaV (and therefore anti-CD3). Different fluorophores and microscopy parameters were used during this thesis, and each condition was therefore analyzed separately.

Figure 4.6 shows that the fluorescence intensity does not vary within experiments and an important difference of intensity is observed between the fluorescence inside and outside the dots. This difference can be quantified by calculating a ratio. The ratio is defined by the followed equation :

$$I_{Ratio} = \frac{I_{in}}{I_{out}} \tag{4.1}$$

with I_{in} representing the peak of the intensity profile for each median dot and I_{out} the baseline around each profile (see Figure 2.16). Figure 4.7 shows that the ratio equals 5±2 for all substrates analyzed (N=21). As the SLB covers the whole area outside the dots, this ratio tells us that there is 5 times more fluorescence in the protein dots than on the SLB. The fluorescence being proportional to the protein density, this also indicates the protein ratio between the dots and the SLB. This result confirms an enough passivation of the SLB and validates the substrate. If this ratio is close to 1, meaning that the proteins were deposited equally on the dots and SLB, the substrate is then consider as homogeneous and is thus not validated. We also show that the type of fluorophore used

does not change this ratio.

The same ratio can be done using the protein density, in this case the protein ratio it will be refer as ρ_{Ratio}.
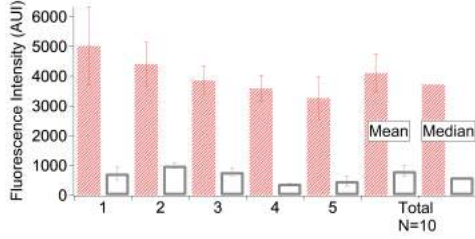
(a) Fluorescence intensity of NaV-fluorescein during the first year
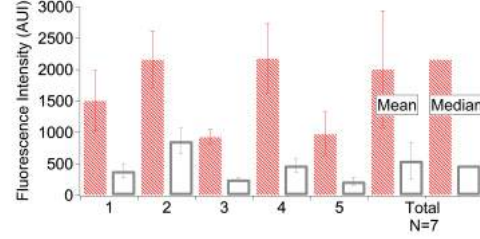
(b) Fluorescence intensity of NaV during the second year
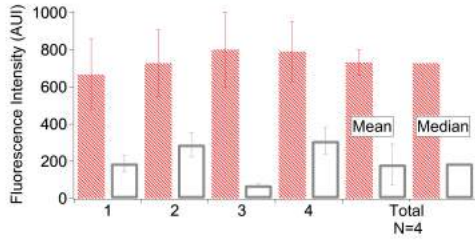
(c) Fluorescence intensity of NaV during the third year
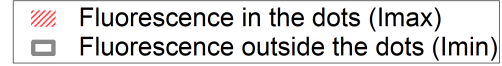
(d) Fluorescence intensity of NaV during the third year

Figure 4.6: **Fluorescence intensity of Nav inside and outside the dots**Error bars represent standard deviation.

4.1.1.4   Characterization of NaV density

From the intensity measurements, it is possible to quantify the NaV density inside and outside the dots, and also the average density of NaV presented by the substrate to the cell. To do so, the fluorescence intensity is converted in protein density via the conversion factor determined during the calibration (see section 2.6.3). As NaV is used as a linker to attach anti-CD3 to the surface, the NaV density measurement is a indirect way to measure the anti-CD3 density present on the substrate.

The Figure 4.8 shows that the protein density varies between experiments with a standard deviation of $\pm$ 23, $\pm$ 8 and $\pm$ 15 molecules/μm^2 for protein density respectively inside the dots, outside the dots and on all the substrate for 12 analyzed experiments. The highest variation observed is inside the dots and can be explain by the APTES deposition which can be a source of heterogeneity coming from the deposition itself. But as shown previously, the inside/outside protein ratio remains fairly stable between experiments.

4.1.2   Anti-CD3 dots in SLB functionalized with ICAM-1

This substrate, which is referred to as [ICAM-1]$_{SLB}$ [αCD3]$_{Dot}$ or ICAM-1 $\bullet$ αCD3, is composed of nano-dots of anti-CD3 surrounded by a bilayer functionalized with ICAM-1.

(a) Protein ratio for substrates done in first year with NaV-fluorescein

(b) Protein ratio for substrates done in second year with NaV

(c) Protein ratio for substrates done in third year with NaV

(d) Total
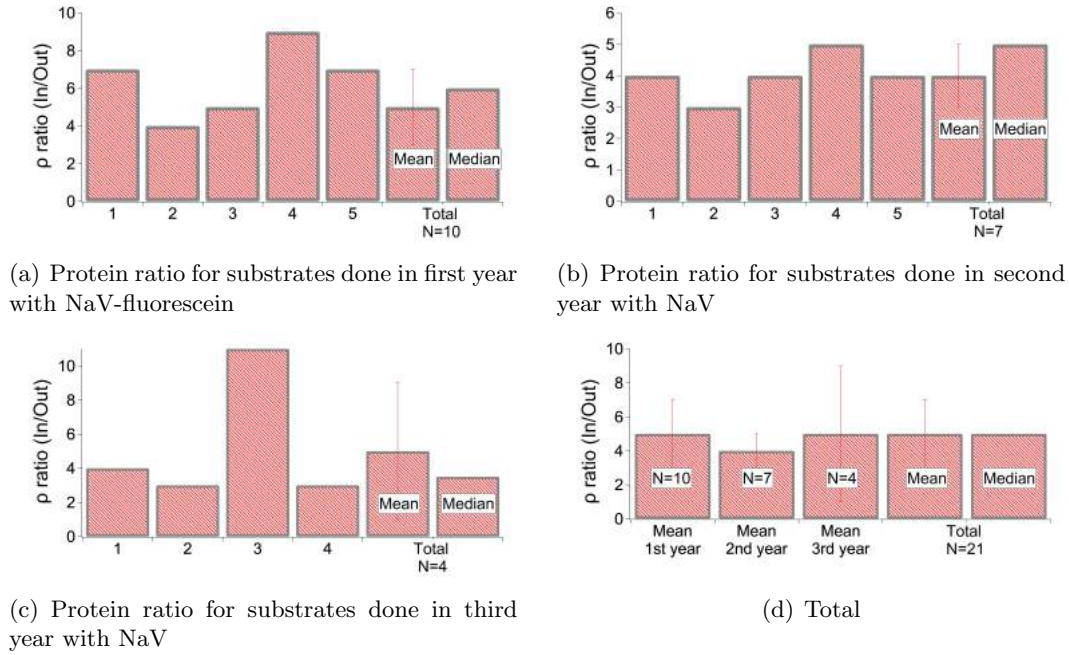
Figure 4.7: **Protein ratio between inside and outside the nano-dot array on substrates with nano-dot array surrounded by bare SLB.**

The ICAM-1 protein was grafted on the bilayer via a NTA-histidine binding.

4.1.2.1 Characterization of SLB fluidity

As shown on Figure 4.9(a), the lipid composition of the SLB does not affect its fluidity. The diffusion constant was measured at 5.7 ± 1.8 μm^2, which is very close to the diffusion constant observed for the substrate $[\text{Bare}]_{SLB}$ $[\alpha\text{CD3}]_{Dot}$.

4.1.2.2 Characterization of a protein grafted on NTA lipids

ICAM-1 was not available in fluorescent form, therefore its characterization is indirect. Fluorescent antibody against ICAM-1 was first used to reveal ICAM-1 and study the fluidity, but because of it non-specific adsorption and the fact that the addition of a layer of protein on the SLB reduce the fluidity, this indirect observation was not successful. So a direct fluidity measurement was done through a fluorescent hist-tagged protein. First the specific adsorption of hisTag proteins on the NTA bilayer was checked by measuring the fluorescence intensity of YFP-hisTag before and after an elution with imidazole. Imidazole is considered as a strong competitor of the NTA-hisTag binding. In case of specific adsorption, all the hisTag proteins will detach from the NTA molecule. In our case, we obtained 95% of elution which confirms the specific adsorption of hisTag proteins on the NTA-bilayer. This specificity allowed for a good control of the quantity of proteins grafted on the SLB.
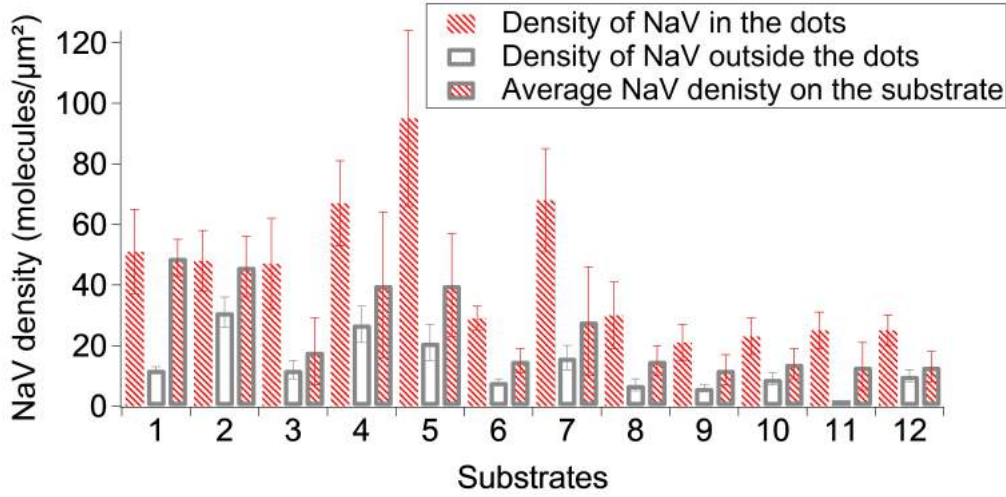
(a) Variation of NaV density between experiments
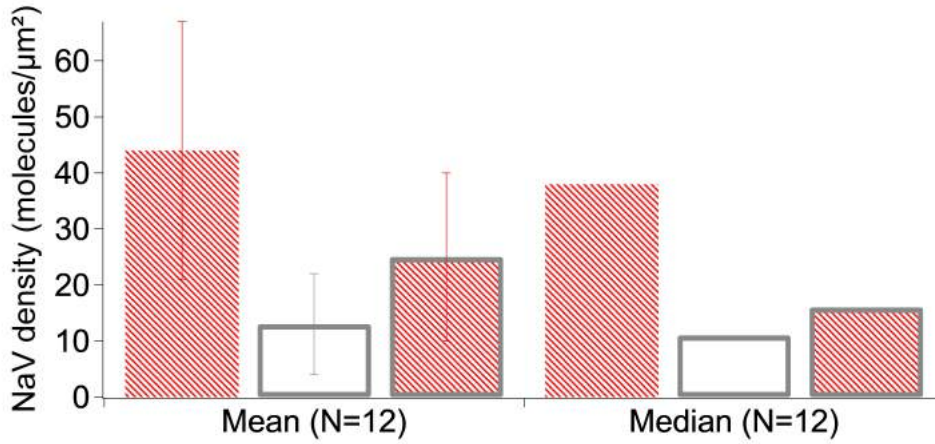
(b) Overall NaV density

Figure 4.8: **Quantification of NaV density on substrate [Bare]$_{SLB}$ [αCD3]$_{Dot}$.** Error bars represent standard deviation measurements.

Next the fluidity of the NTA-coupled protein was checked.

To get an idea whether a protein connected to NTA tagged lipids can be able to diffuse, YFP-hisTag proteins were used. In order to better observe the CPB effect, the measurements of YFP-hisTag bleaching were effectuated on homogeneous SLB substrates. Figure 4.10 shows an example of the lateral diffusion of the protein observed during CPB. The YFP-hisTag protein can diffuse at 1.1μm^2/sec, so we assumed that the ICAM-1 hisTag protein grafted on the SLB would have the same capacity of diffusing even on patterned substrate.

(a) Diffusion constant of SLB ICAM-1 surrounding nano-dot arrays of anti-CD3.

(b) Protein dot size measured from FWHM. For 1-5: Error bars represent standart deviations inside the sample. For Total: Error bars represent standart deviations for all the substrates

(c) Quantification of NaV density. Error bars represent standart deviations for all the substrates

(d) Protein ratio between inside and outside the nano-dot arrays. Error bars represent standart deviations for all the substrates

Figure 4.9: **Characterization of [ICAM-1]$_{SLB}$ [αCD3]$_{Dot}$ substrates.** Error bars represent standard deviations.

4.1.2.3   Characterization of protein dot size

Analyses of the dot size showed no differences between Bare SLB and SLB ICAM-1 with a mean NaV dot size equal to 690$\pm$130 nm.(Figure 4.9(b)). Meaning that the addition of a protein on the SLB does not affect the deposition of the SLB, which remains outside the dots.

4.1.2.4   Characterization of NaV density and density ratio

The quantification of NaV on [ICAM-1]$_{SLB}$ [αCD3]$_{Dot}$ substrates showed a surprising decrease in terms of density compared to [Bare]$_{SLB}$ [αCD3]$_{Dot}$ (Figure 4.9 (c)). The protein density ratio remained the same (Figure 4.9(d)). ICAM-1 density was estimated using YFP-hisTag for calibration. On this substrate, the ICAM-1 density was estimated to be around 100 molecules/μm^2.

4.1.3   Other patterned substrates with anti-CD3 dots in SLB

This part details the characterization of all other patterned substrates composed with nano-dots of anti-CD3 surrounded by a fonctionalized SLB. Specifically [B7-2]$_{SLB}$ [αCD3]$_{Dot}$ which has B7-2 grafted on the SLB, [BarePEG]$_{SLB}$ [αCD3]$_{Dot}$ which has Bare SLB supplemented with PEG molecules, [ICAM-1+PEG]$_{SLB}$ [αCD3]$_{Dot}$ which is supplemented with PEG and has also ICAM-1 grafted on top. This part also characterizes a control
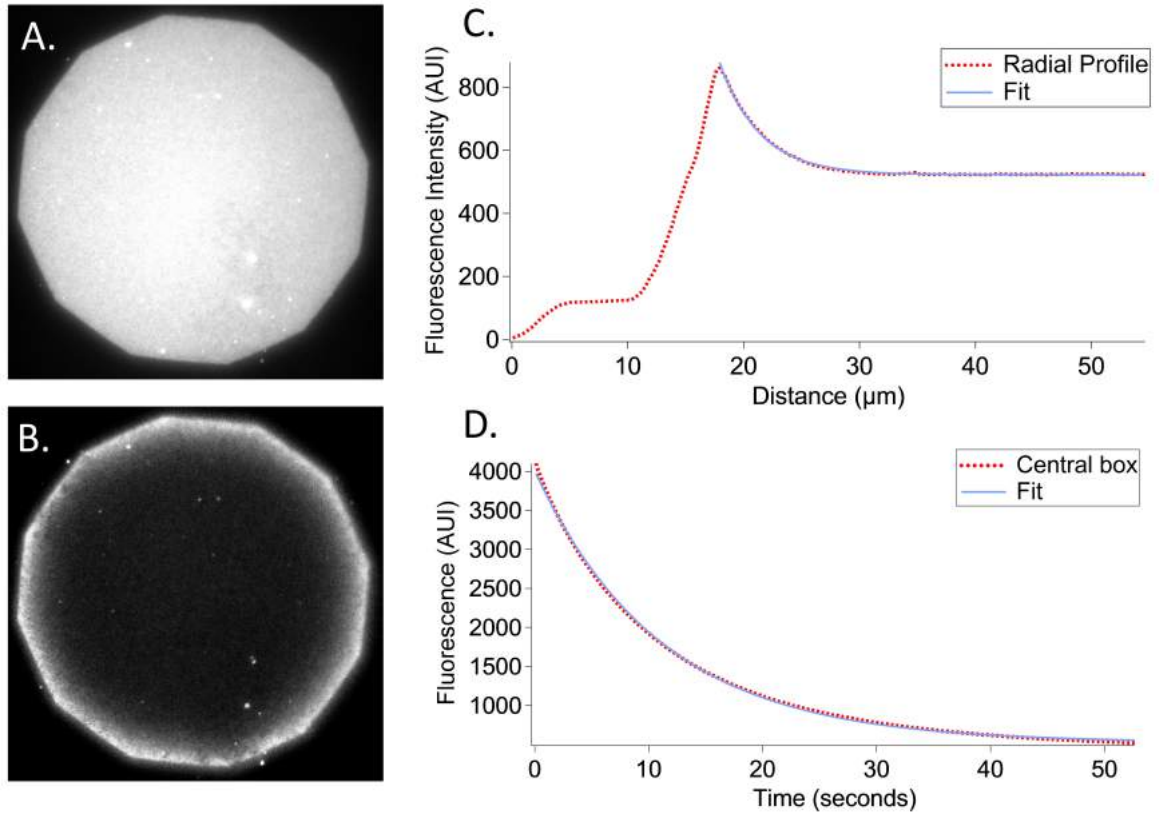
Figure 4.10: **Lateral molecular diffusion of YFP-hisTag measured by Continuous Photo-Bleaching** A: Epi-fluorescent image of a YFP-hisTag protein grafted on DOPC bilayer supplemented with 5% of NTA lipids before Photo-Bleaching. B: Epi-fluorescent image of a YFP-hisTag protein grafted on DOPC bilayer +5% of NTA lipids after 50 seconds of Continuous Photo-Bleaching. C: Average line profile across the limit of the field diaphragm. D extracted equals to 1.1 μm^2/sec. D: Intensity decay over time measured at the center. B extracted equals 0.09 sec^{-1}. (See section 2.6.1 for details of the analysis

patterned substrate $[\text{Bare}]_{SLB}$ $[\text{non-specific}]_{Dot}$ wich has a bare SLB surrounding dots of non specific proteins.

4.1.3.1 Characterization of dot size

As shown on Figure 4.11, the dot size did not change compared to the standard substrate regardless of the composition of the lipids bilayer.
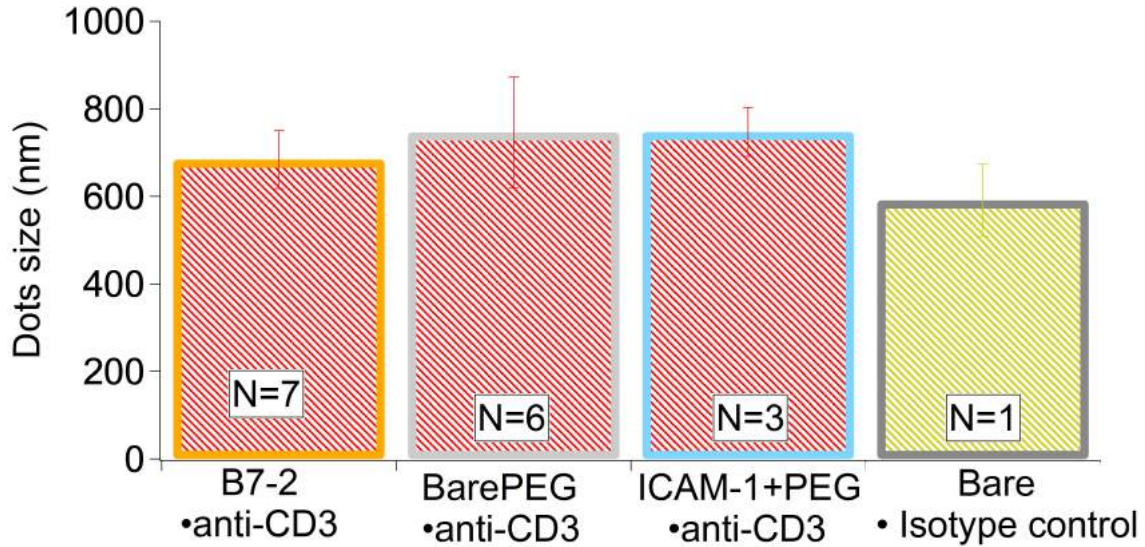
Figure 4.11: **Protein dot size measured from Full Width Half-Maximum for patterned substrates with anti-CD3 nano-dots.** Error bars represent standard deviations.

4.1.3.2 Characterization of NaV density and protein ratio

Figure 4.12 shows that $[\text{B7-2}]_{SLB}$ $[\alpha\text{CD3}]_{Dot}$ substrates had the same characteristics as $[\text{ICAM-1}]_{SLB}$ $[\alpha\text{CD3}]_{Dot}$ substrates in terms of NaV density and in terms of ratio between inside and outside the dots. This is not surprising because the SLB composition is the same (DOPC+ 5% NTA). This figure coupled with Figure 4.8 and Figure 4.9 shows that the addition of PEG molecules in the SLB decreased the NaV density outside and inside the dots whereas the ratio remained the same. This lower density outside the dots is due to the repulsive nature of the PEG molecules in the SLB which provide absorption of proteins. The decrease in density inside the dots could be explained by PEG preventing protein deposition in the dots by steric hindrance.

4.1.4 Patterned substrates with ICAM-1 dots in SLB

These substrates are composed of ICAM-1 nano-dots, surrounded by a Bare SLB or a SLB functionalized with anti-CD3.

(a) NaV density inside the nano-dots

(b) NaV density outside the nano-dots

(c) Average NaV density presented by the substrate

(d) Protein ratio on the subtrates
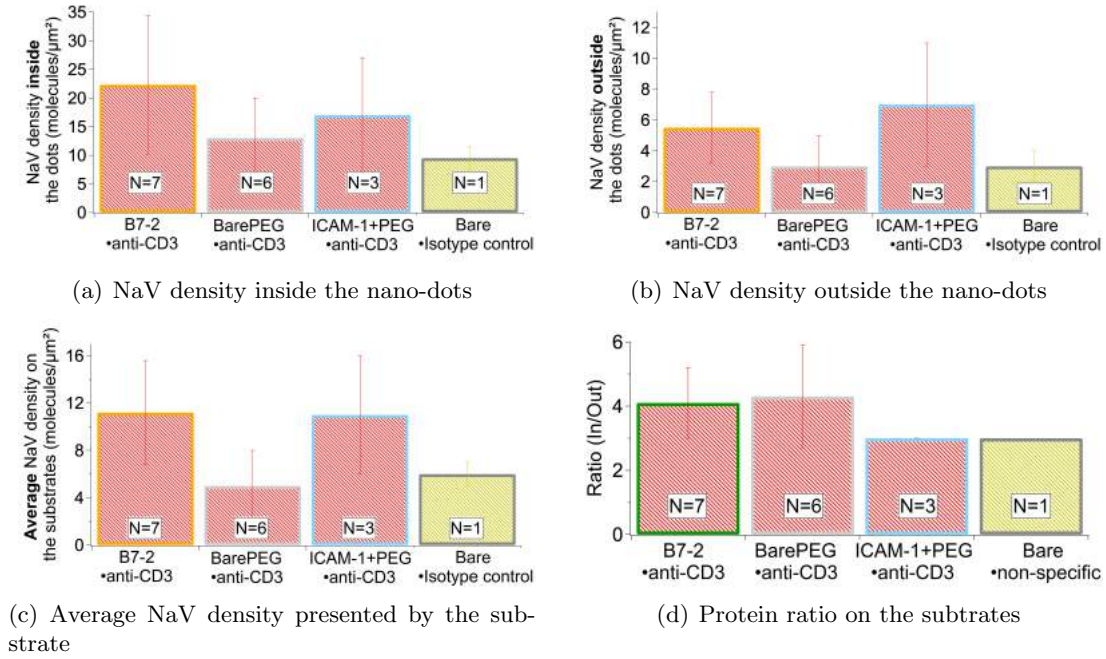
Figure 4.12: **Characterization of patterned substrates with anti-CD3 dots surrounded by SLB.** Error bars represent standard deviations.

4.1.4.1 Characterization of dot size

As shown in Figure 4.13, ICAM-1 nano-dots can be revealed by a fluorescence antibody against ICAM-1. Dot size was measured at 690 ± 130 nm, which is similar to the size obtained with anti-CD3 nano-dots (Figure 4.5).

4.1.4.2 Characterization of protein density

On these substrates, the average ICAM-1 density was estimated around 45 molecules/μm^2. When the SLB is functionalized with anti-CD3, NaV quantification showed an average density of 31 ± 14 molecules/μm^2.

4.1.5 Substrates with E-beam lithography

Another method to fabricate the nano-pattern was E-beam lithography as described in section 3.2. E-beam lithography was used to fabricate the standard substrate $[\text{Bare}]_{SLB}$ $[\alpha\text{CD3}]_{Dot}$. (Note that the color code is different compared of what used for substrates created using beads)

4.1.5.1 Characterization of protein dot size

With the E-Beam lithography technique, different zones were fabricated with different dot sizes and spacings. Two zones (C-D) had the same percentage of surface covered by the dots, this percentage was kept the same as with the one obtained with nano-sphere
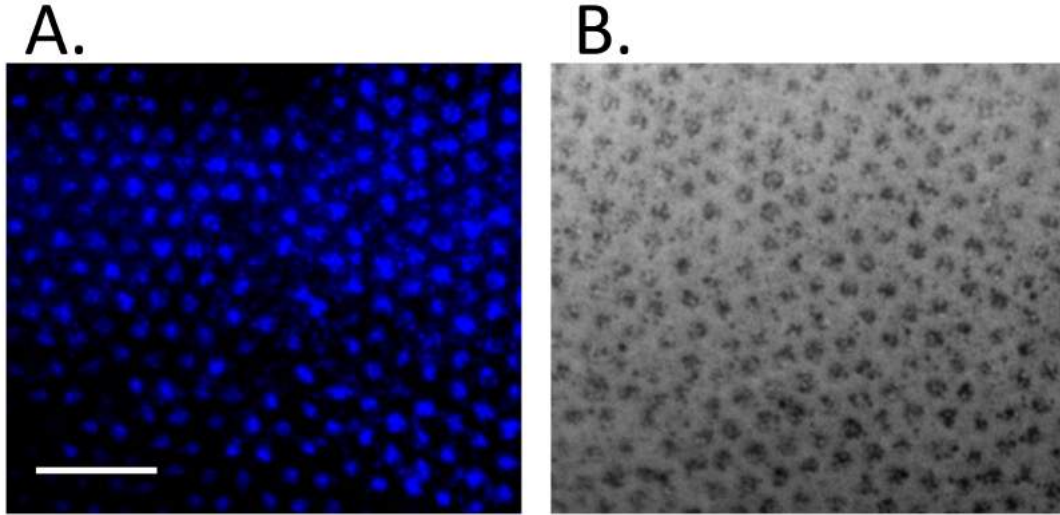
Figure 4.13: **ICAM-1 dots revealed by fluorescent anti-ICAM-1 surrounded by Bare SLB.** Dot size : 690± 130 nm. Scale bar= 10μm

lithography (11%) (see Table 8.1). Two other different patterns were drawn by changing the pitch between each dots and/or the dot size. Figure 4.14 shows epi-fluorescent images obtained for each zones. Figure 4.15(a) shows the dot sizes obtained for these zones. In accordance with what was expected, the dot sizes revealed by the fluorescent NaV fitted quite well with the size parameters of the E-beam design. For example, we obtained 570±140 nm for zone A where the dot size was set to 500 nm, 1200±40 nm for zone C where it was set for 1000 nm, and 320±55 for zone D where it was set for 300 nm. The overestimation of the dot size can be explained by the diffusion of the NaV fluorescence and/or the overestimation of ROIs during the automatic analysis of the epi-fluorescent images.

4.1.5.2 Characterization of NaV density and protein ratio

Figure 4.15(b) shows the NaV density in the different zones. The density inside the dots does not change with the dot size, even if the dots double in size (Zone A v/s Zone D). The average density measured in the four zones is quite similar (around 20 molecules/μm^2). With this technique the inside/outside protein ratio was found to be very low, this is due to a large amount of proteins outside the dots (Figure 4.15(b-c)). This last point needs to be further optimized.

4.2 Homogeneous substrates

Two kinds of homogeneous control substrates were fabricated. First, SLB controls, which consist of an homogeneous protein distribution on SLB. Second, dot controls, which consist of an homogeneous protein distribution directly on glass. These substrates were fabricated as described in section 3.5.
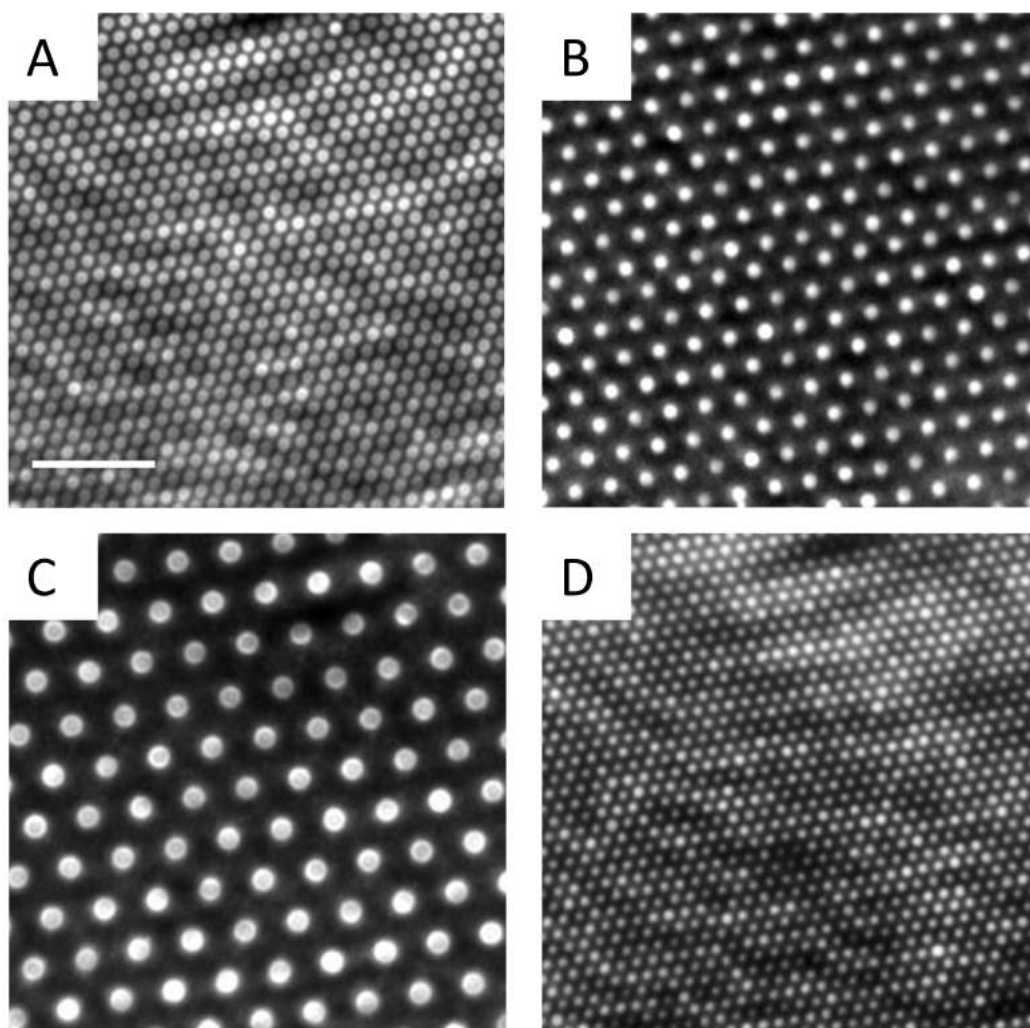
Figure 4.14: **Epi-fluorescent images of nano-dot arrays of NaV labeled with Dylight650 done with E-Beam lithography.** A: Zone A corresponds to a pattern expected to have a pitch of 1μm and dots size of 500nm. B: Zone B corresponds to a pattern expected to have a pitch of 2μm and dots size of 500nm. C: Zone C corresponds to a pattern expected to have a pitch of 3μm and dots size of 1000nm. D: Zone D corresponds to a pattern expected to have a pitch of 0.9μm and dots size of 300nm. Scale bar=10μm.

4.2.1 SLB controls

Two types of SLB controls were done. The first control, called Homogeneous SLB controls type 1, was done with a SLB treated as if it was on patterned substrates, which means that the SLB was incubated with the same proteins and in the same conditions as during the functionalization of patterned substrates. In this case, the protein functionalization of the substrates is due to non-specific absorption of proteins on the SLB. This type of control is useful for the study the impact of this phenomenon which also occurs during the functionalization of patterned substrates.

(a) Measured dot size.

(b) NaV density.

(c) NaV density ratio.

Zone	Pitch (μm)	Dots size (nm)
A	1	500
B	2	500
C	3	1000
D	0.9	300

(d) E-Beam size parameters for each zone
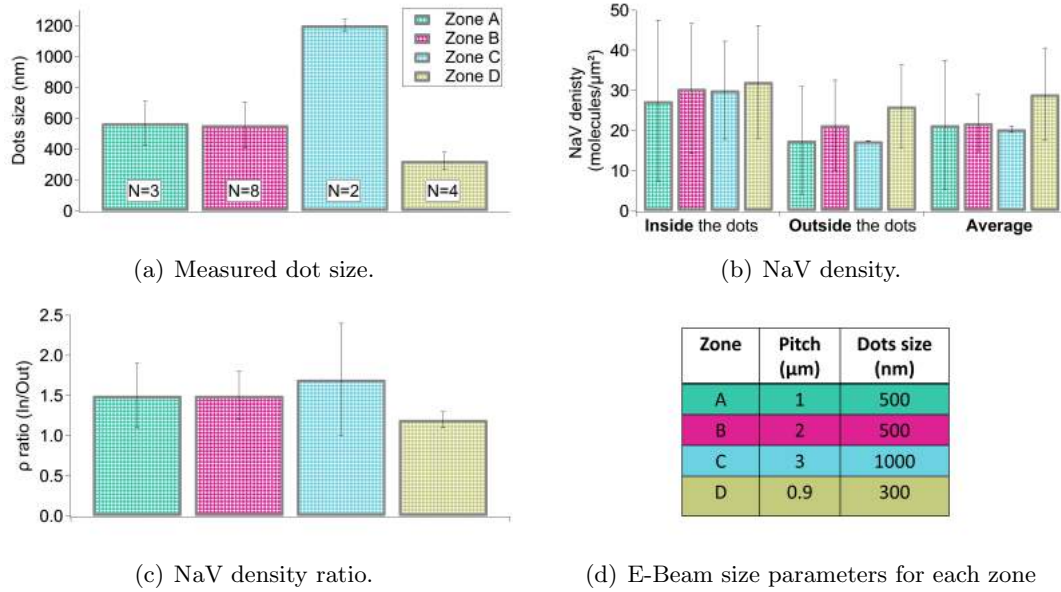
Figure 4.15: **Characterization of patterned substrates done with E-Beam lithography.** Note that the color code is different compared ot what used for substrate created using beads.

The second control, called Homogeneous SLB controls type 2, correspond to an homogeneous SLB with the same average protein density as measured on patterned substrates. These substrates were used as controls to study the impact of protein clustering. On these substrates, SLB fluidity and NaV density were characterized.

4.2.1.1   Characterization of SLB fluidity

Measurement of SLB fluidity on homogeneous SLB controls type 1 and 2 gave a diffusion constant of 4.2±0.3 μm²/sec. This value is similar to the diffusion constant measured in patterned substrates.

4.2.1.2   Characterization of NaV density

On Homogeneous SLB controls type 1, as expected, the protein density measured is equivalent to the one measured outside the dots on their corresponding patterned substrates (Figure 4.16(a)). The substrate control SLB ICAM-1 was also used as a control for patterned substrates $[B7\text{-}2]_{SLB}\ [\alpha CD3]_{Dot}$ as the lipid composition and the non-specific adsorption were the same in both.

For Homogeneous SLB controls type 2, the densities measured are presented in Figure 4.16(b). The density is quite similar to what was measured on the corresponding patterned substrates. In order to be able to compare homogeneous V/S patterned substrates, both need to present the same average proteins density on their surface. As the average density obtained with patterned substrates is very heterogeneous between sub-

strates, the density measured on these homogeneous SLB controls will serve as a reference to choose the corresponding patterned substrates to study the impact of clustering.
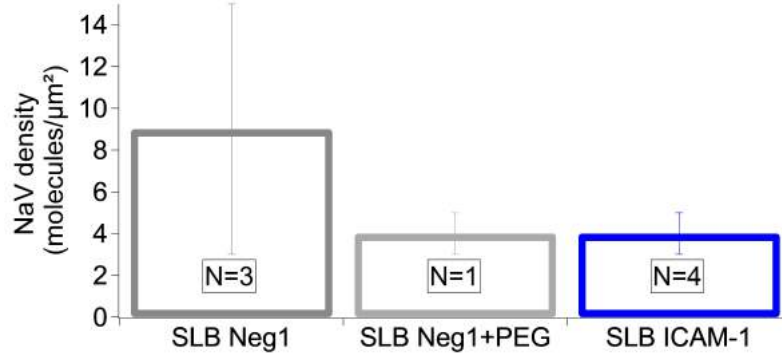
(a) Quantification of NaV density on homogeneous SLB controls type 1
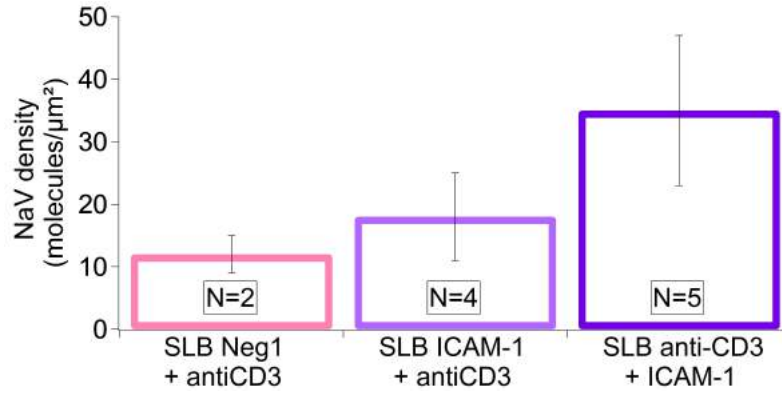
(b) Quantification of NaV density on homogeneous SLB controls type 2

Figure 4.16: **Quantification of NaV density on homogeneous SLB controls.** Error bars represent standard deviations.

4.2.2 Dot controls

These substrates mimic the protein situation in the dots of patterned substrates but in larger areas. As two kind of proteins are put in the dots, either anti-CD3 or ICAM-1, two controls substrates were used. The first one was POS antiCD3 where a NaV density of 115 ± 50 molecules/μm^2 was measured. The second one was POS-ICAM-1 where a ICAM-1 density of 159 molecules/μm^2 was estimated (see Figure 4.17).
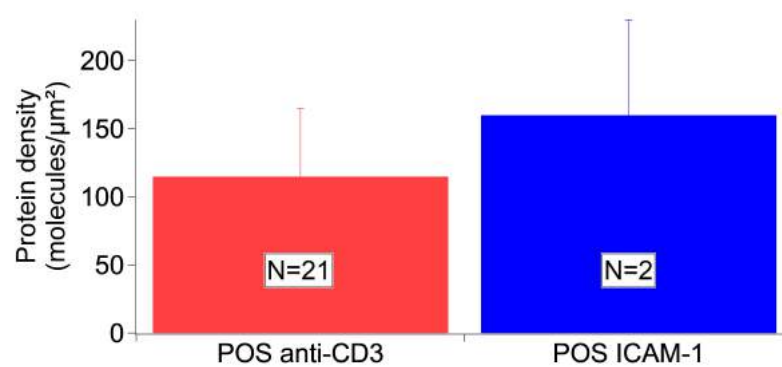
Figure 4.17:   **Quantification of NaV and ICAM-1 density on homogeneous glass controls.** Error bars represent standard deviations.

Chapter 5

T cells on clustered ligands

Contents

This chapter deals with the response of T-cells to the basic patterned substrates where anti-CD3 clusters are embedded in a bare SLB ([Bare]$_{SLB}$ [αCD3]$_{Dot}$ or Bare • anti-CD3). In most experiments, T-cells were studied after 30 minutes of engagement on substrates and PFA fixation. They were then imaged in RICM, and/or TIRF-M. The quantification of cell responses was done through the analyses of the cell spreading area (also called adhesion area), the T-cell membrane molecular distribution (TCR and ZAP-70), and the actin organization. For few cases, dynamic data is also presented. Preliminary results on behavior of primary mouse and human T cells are presented.

5.1 Cell spreading and adhesion area

Casual inspection of RICM images revealed that on [Bare]$_{SLB}$ [αCD3]$_{Dot}$ two major cell adhesion morphologies were observed - either patterned or homogeneous. In the first case, the cell membrane adheres mostly on the underlying pattern which induces a topography revealed by RICM images (Figure 5.1A). In this thesis, cells with this type of adhesion will be called "patterned". The proportion of such patterned cells equals to 43%. The second type of adhesion is called "homogeneous adhesion" or "non-patterned", and in this case the cell membrane is flat and adheres homogeneously to the surface (Figure 5.1B). Area measurements on this patterned substrate, yield a global cell adhesion area of 220±70 μm² (from 42 experiments spread over the three years of the thesis and totaling 860 cells). Cell adhesion area of patterned cells equaled 205±60 μm² and cells with homogeneous adhesion (refereed as non-patterned cells) had an adhesion area of 230±80 μm² (Figure 5.1C). Statistical tests showed that such patterning of the cell membrane does not impact the extent of spreading.

5.1.1 Impact of pattern characteristics

As shown previously in the chapter 4, within [Bare]$_{SLB}$ [αCD3]$_{Dot}$ substrates there is some variation of anti-CD3 dot size and protein density (quantified from analysis of fluoresce images of labeled neutravidin). The size variations were limited in range, whereas, in spite of keeping the preparation conditions unchanged, the protein density changed appreciably from sample to sample. Below we shall explore whether the dot size and protein density have an impact on the T-cells behavior, focusing on the adhesion area. Recall that as explained in the introduction chapter (see section 1.4.2.4,[103]), previous studies in our laboratory with similar patterns, where an inert polymer replaced the bare SLB, led us to expect the cell area to be independent of dot-size and be proportional to the average surface protein density.

Impact of dot size: First, the impact of anti-CD3 dot size on cell adhesion area was studied. As shown on Figure 5.2 for a range of dot size from 600 nm to 950 nm cell adhesion area does not change significantly. This result demonstrates that as expected, the dot size does not impact the cell adhesion area.

Impact of protein density: The analysis of the impact of protein density was done at two levels. First analysis was done on substrate-by-substrate basis by plotting the relation between protein density and cell adhesion area on different substrates. Then, for more

5.1 Cell spreading and adhesion area
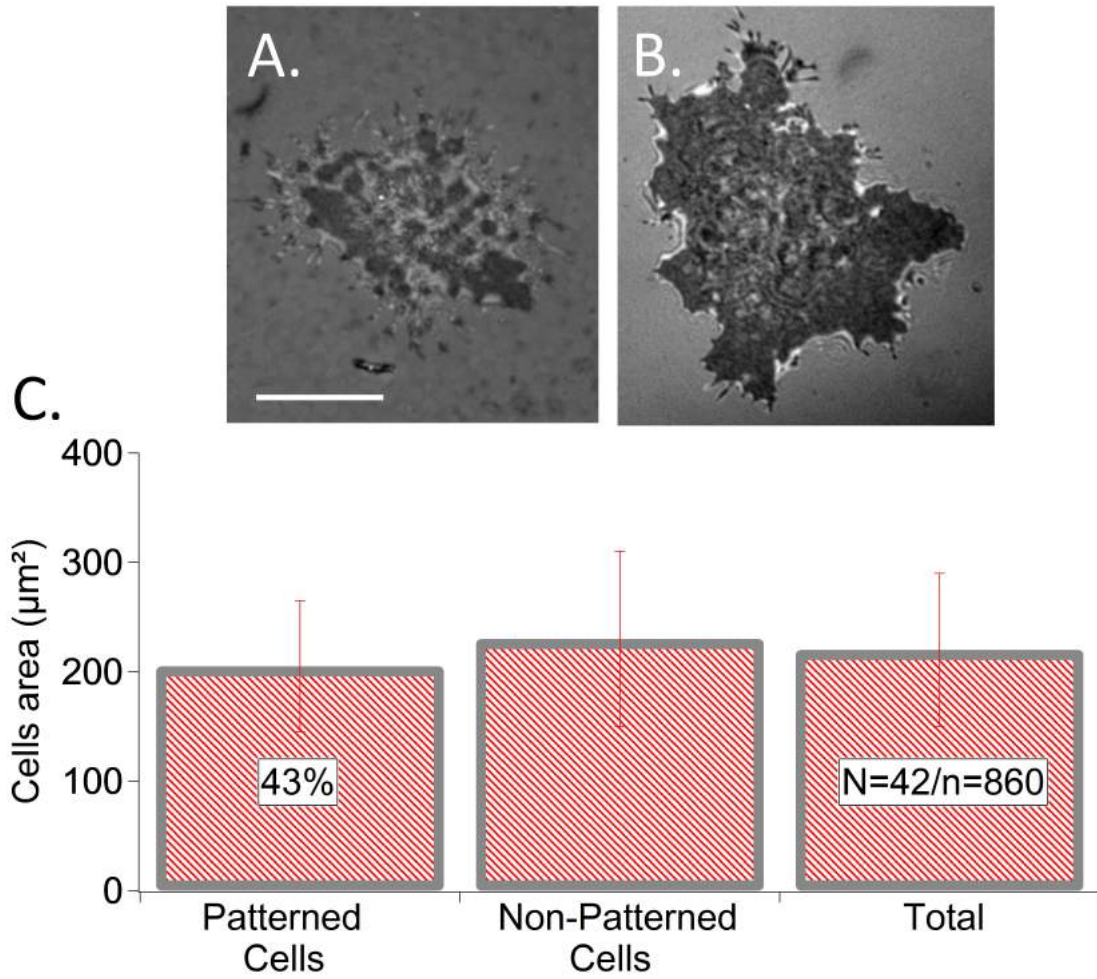
Figure 5.1: **Cell adhesion on [Bare]$_{SLB}$ [αCD3]$_{Dot}$ (also called Bare$\bullet$ anti-CD3).** A: RICM images of a patterned cell of Jurkat T-cell after 30 minutes engagement on substrate. B: RICM images of an homogeneous adhesion of Jurkat T-cell after 30 minutes engagement on substrates. Scale bar = 10μm. C: Cell adhesion area measurements of Jurkat T cells after 30 minutes engagement on substrates. Error bars represent standard deviations.

precision, the relation between protein density under each cells and the cell area was determined. Protein density was determined from epi-fluorescence images of NaV (for more details see 2.6.3).

Figure 5.3 presents a substrate-by-substrate analysis and shows that neither the protein density inside the dots(a), nor outside the dots(b), nor the average density on the substrate(c) has an influence on the average cell spreading area.

Given this unexpected result, more precise studies were performed by looking the density of proteins directly under each cell. To do so, the segmented ROI of each cell was superposed on the epi-fluorescence image of the underlying NaV pattern, then analyses of NaV density was done in the areas determined by the ROIs. Figure 5.4 presents cell-
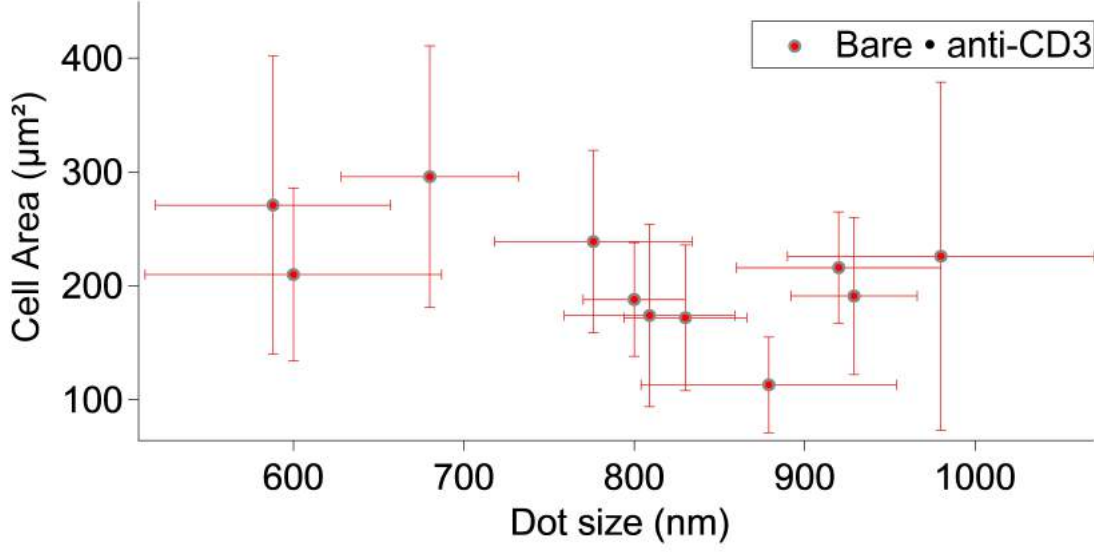
Figure 5.2: **Impact of dot-size on cell adhesion area on [Bare]$_{SLB}$ [αCD3]$_{Dot}$ (also called Bare • anti-CD3).** Each dot corresponds to one substrate with at least 20 cells. Area values are averaged over all the cells and the dot size is the average FWHM measured over all the fields, comprising hundreds of dots. Error bars are standard deviations.

by-cell analyses of four experiments with a total of 57 cells. These graphs show that even locally, neither the density inside(a) nor the average density(b) has an influence on the cell adhesion area. These results show that on [Bare]$_{SLB}$ [αCD3]$_{Dot}$ the cell spreading area is not influenced by the NaV proteins density and by extension not influenced by the anti-CD3 density presenting by the underlying pattern. One possible explanation is that the bare SLB does not adequately passivate the surface - a point discussed further in the next chapter 6.

5.1.2 Homogeneous controls

Two homogeneous controls correspond to this patterned substrate: POS anti-CD3 and SLB Neg1. POS anti-CD3 mimics the situation inside the dots of the patterned substrate [Bare]$_{SLB}$ [αCD3]$_{Dot}$ but over the entire substrate. SLB Neg1 is a SLB treated as if it was on the patterned substrate, which means that the SLB was incubated with the same proteins and in the same conditions as during the functionalization of [Bare]$_{SLB}$ [αCD3]$_{Dot}$. On these control substrates cells are homogeneously adhered and the cell adhesion area measured on RICM images for these controls equal 235±70 μm²(N=25,n=530) for POS anti-CD3 and 175±30 μm²(N=7;n=218) for SLB Neg1 (Figure 5.5). Thus, on POS, cells spreading is equivalent to spreading on [Bare]$_{SLB}$ [αCD3]$_{Dot}$ but the cells do spread much less on the bare SLBs.

5.1 Cell spreading and adhesion area
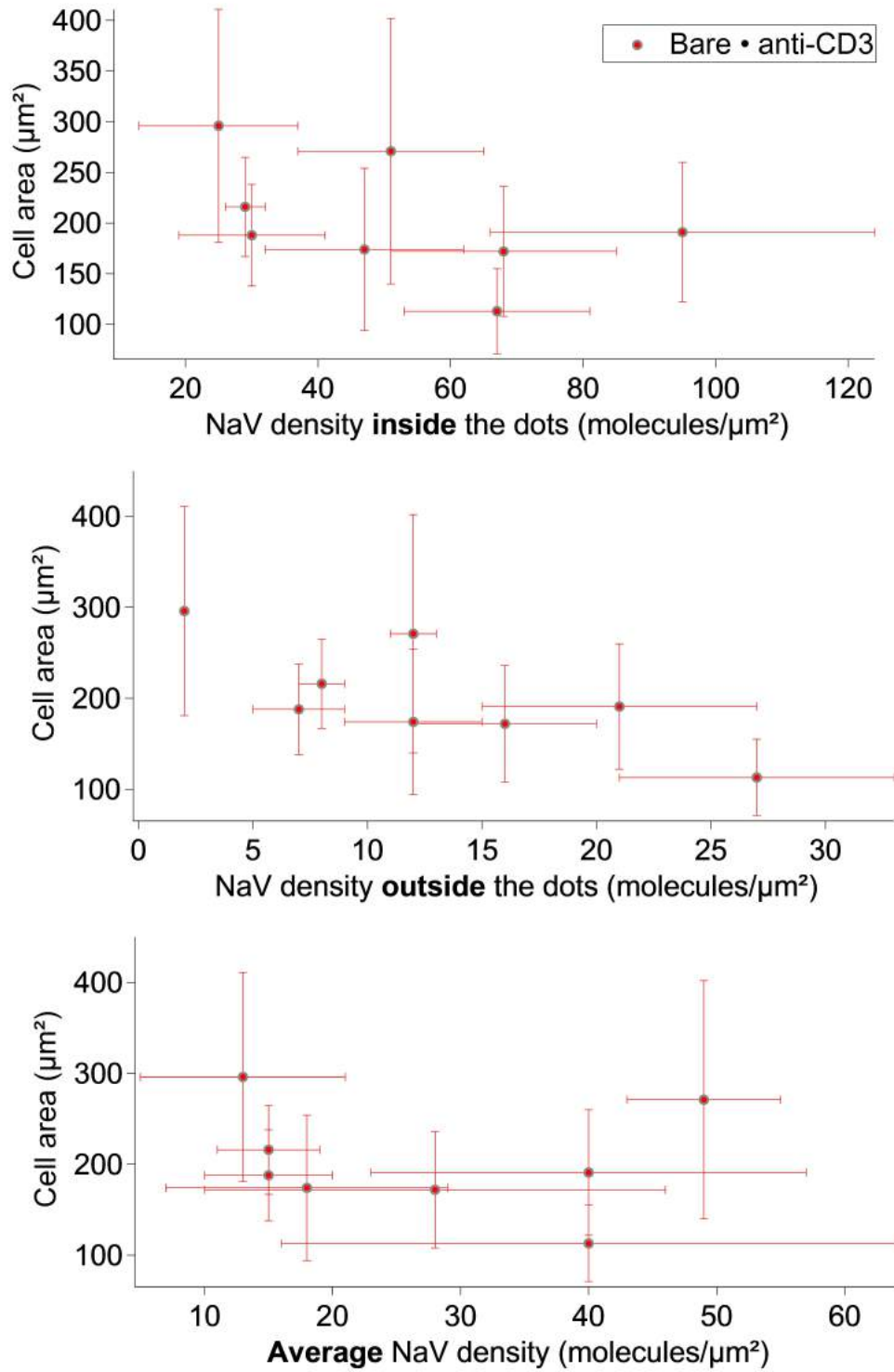
Figure 5.3: **Cell adhesion area as a function of the density of NaV inside the dots, or outside the dots, or averaged over the whole sample, on the underlying pattern [Bare]$_{SLB}$ [αCD3]$_{Dot}$ (also called Bare • anti-CD3).** Each point represents one experiment with error bars representing standard deviations. N=9;n=157
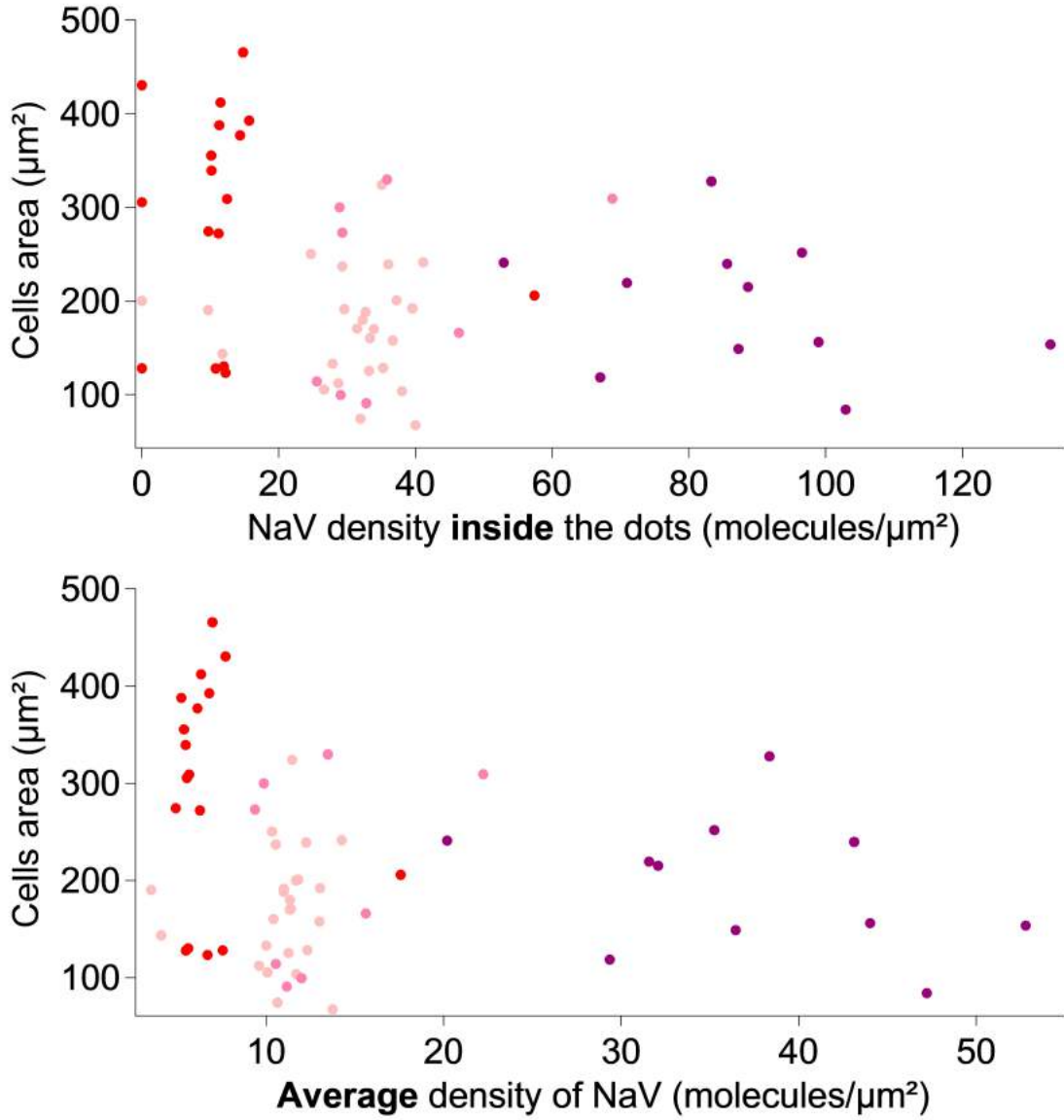
Figure 5.4: **Impact of variation of NaV density on cell area on [Bare]$_{SLB}$ [αCD3]$_{Dot}$ (also called Bare• anti-CD3).** Cell adhesion areas versus the NaV density under the cells are plotted. Each point represents one cell. N=4;n=57. Data from the four different experiments are shaded differently.
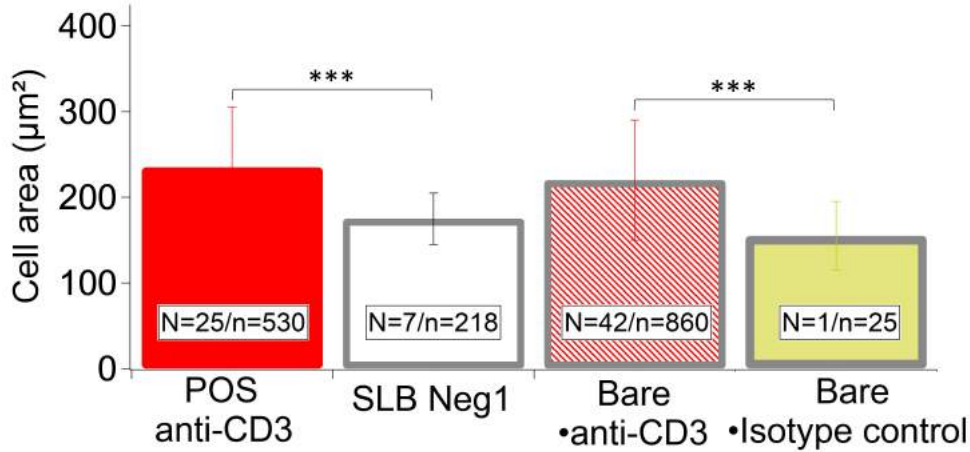
Figure 5.5: **Cell areas on controls substrates for [Bare]**$_{SLB}$ **[αCD3]**$_{Dot}$ **(also called Bare• anti-CD3).** Cell adhesion area measurements of Jurkat T cells were done after 30 minutes engagement on substrates. Error bars represent standard deviations.***=p<0.001.

5.1.3   Smaller dots

Smaller dots were obtained using the e-beam lithography process (see section 3.2). Preliminary experiments with Jurkat T-cell have not yielded any conclusive results. Indeed on the different designs cell area is quite similar (see Figure 5.6). As seen above, an important issues was insufficient passivation provided by the SLB leading to strong non-specific NaV adsorption outside the dots. This problem may be more severe for the samples prepared by e-beam lithography. NaV being present outside the dots greatly reduced the expected impact of the patterning ligand on the cell spreading area, bringing us closer to the homogeneous situation.

5.2   TCR and ZAP-70 distribution

As before, TCR and ZAP-70 distribution were analyzed for cell spreading after 30 minutes of engagement on the substrate. TCR molecules were revealed by labeling the β chain of the TCR molecules with an fluorescent antibody. And ZAP-70 signaling kinase was revealed with a fluorescent anti ZAP-70. Both were images in TIRF-M.

5.2.1   TCR clusters

Figure 5.7 presents comparative results of TCR distribution observed on T-cells spread on the homogeneous control POS anti-CD3 and on the patterned substrate Bare • anti-CD3. Visual inspection shows that on POS anti-CD3, TCR is in the form of small clusters randomly distributed whereas on patterned substrates, T-cells present TCR molecules in form of clusters which co-localized with the underlying anti-CD3 pattern (revealed by fluorescent NaV showed in third raw) (Figure 5.7A). Interestingly it should be pointed out that even if the membrane is flat, the TCR clusters still organize according the
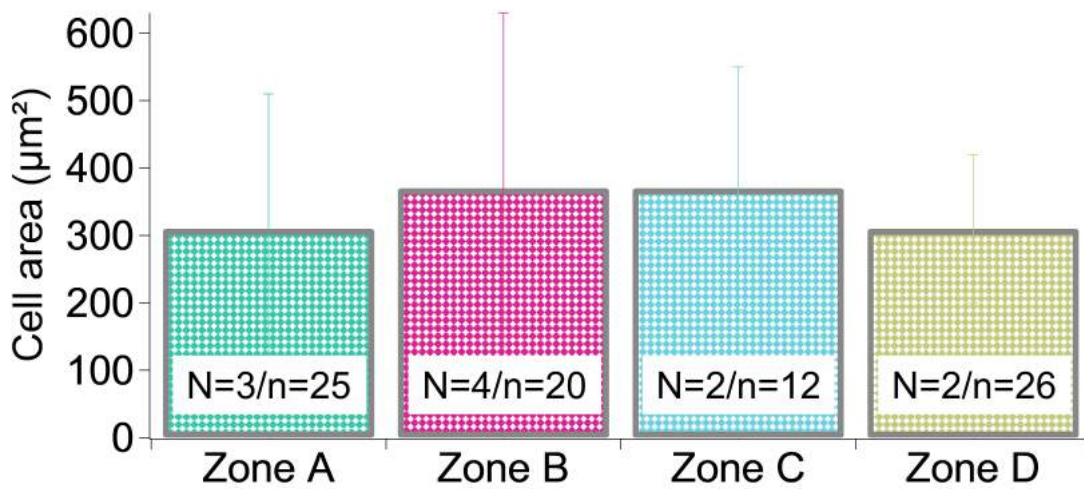
Figure 5.6: **Cell spreading area on patterned substrate with smaller dots.** Zone A corresponds to a pattern expected to have a pitch of 1μm and dots size of 500nm. Zone B corresponds to a pattern expected to have a pitch of 2μm and dots size of 500nm. Zone C corresponds to a pattern expected to have a pitch of 3μm and dots size of 1000nm. Zone D corresponds to a pattern expected to have a pitch of 0.9μm and dots size of 300nm. There is no statistical difference between the cell area on the different substrates. Note that the color code is different from substrate fabricate from NSL. In this case the colors correspond to one zone.

pattern which means that this observation is not due to a TIRF bias [1].

Cluster quantifications were performed by regrouping all TCR clusters for each kind of substrates, measured on at least 18 cells chosen randomly within 2 different substrates. Figure 5.7B presents a histogram of the apparent area of clusters normalized by the total number of clusters and it shows that on $[\text{Bare}]_{SLB}[\alpha\text{CD3}]_{Dot}$ (red dots with gray outline) there is an enrichment of large clusters (size superior to 0.3 to 0.4 μm^2 size range). This threshold value is quite close to the size of the underlying anti-CD3 dots (0.4 μm^2). Moreover T-cells on patterned substrates have a higher population of very large clusters (clusters superior to 1.3 μm^2) than on POS anti-CD3. In contrast, cells on POS anti-CD3 have a higher population of very small clusters (clusters inferior to 0.2 μm^2). These quantifications is in good agreement with visual inspections. Figure 5.7C presents a histogram of total area occupied by clusters normalized by the total cell area and the same conclusion can be drawn.

Figure 5.7D presents the density of TCR clusters (with detected size $>$ 200 nm^2) at the surface of T-cells spread on patterned and homogeneous surfaces. Density is higher on $[\text{Bare}]_{SLB}[\alpha\text{CD3}]_{Dot}$ compare to POS anti-CD3 as expected.

5.2.2 ZAP-70 clusters

ZAP-70 organization was imaged in TIRF-M in a similar way to TCR. ZAP-70 is a kinase which is one of the first activating molecules recruited by the TCR complex following the activation at the T-Cell membrane. Figure 5.8A shows that the distribution of ZAP-70 is similar to TCR. The kinase was randomly distributed on POS anti-CD3, whereas on $[\text{Bare}]_{SLB}[\alpha\text{CD3}]_{Dot}$, ZAP-70 clusters co-localized with the underlying anti-CD3 pattern.

Quantifications revealed that on POS anti-CD3, a majority of clusters have an area between 0.1 and 0.3 μm^2 (Figure 5.8B). As for TCR, on patterned substrates there is also an enrichment for clusters with a size superior to the 0.3-0.4 μm^2 size range which is a value quite close to the size of the underlying anti-CD3 dots (0.4 μm^2).

Density of ZAP-70 clusters is comparable for POS anti-CD3 and $[\text{Bare}]_{SLB}[\alpha\text{CD3}]_{Dot}$ but both are lower than the density of TCR clusters (Figure 5.8C). Taking together this means that this patterned substrate composed of anti-CD3 dots surrounded by an non functionalized fluid bilayer can influence the size and distribution of the TCR/ZAP70 clusters on T-cell membrane. T-cell membrane is locally enriched of TCR/ZAP-70 clusters with a area close to the underlying pattern. These clusters have the same pattern as the anti-CD3 presented by the surface.

5.3 Actin Cytoskeleton

The structure and dynamics of actin organization and its possible modification by the patterning of TCR ligands was studied either by staining fixed cells with FITC-conjugated phalloidin or by live observation of LifeAct-GFP transfected cells, both imaged in TIRF-M. As discussed in the introduction (see section 1.3.3), actin organization

---

[1]Since in TIRF-M, the illumination is confined to a thin layer close to the substrate, variations in membrane or actin topography, may show up as features in TIRF even if the fluorescent marker has an homogeneous organization over the interface; this is called the TIRF bias.
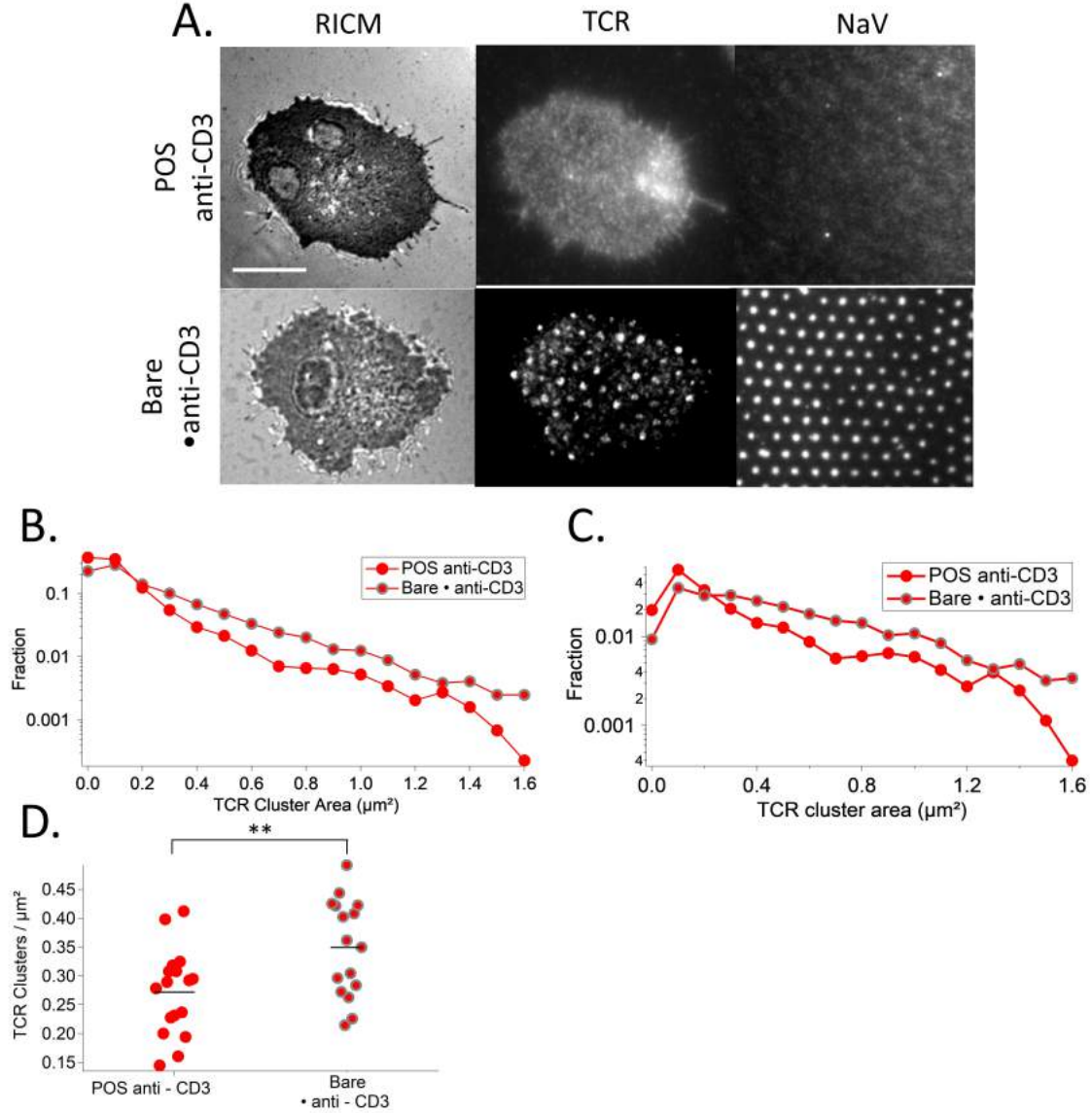
Figure 5.7: **TCR clusters of T-cells spreading POS anti-CD3 and on [Bare]$_{SLB}$ [αCD3]$_{Dot}$ (also called Bare• anti-CD3).** A: RICM, TIRF-M and epi-fluorescent images of Jurkat T-cells after 30 minutes engagement on homogeneous and patterned substrates. For TIRF-M images TCR was marked. Scale bar: 10μm. B: Histogram of the apparent area of clusters normalized by the total number of clusters. Clusters of size corresponding to the underlying anti-CD3 dots(0.4 μm^2) are enriched for [Bare]$_{SLB}$[αCD3]$_{Dot}$. C: Histogram of the total area occupied by clusters normalized by the total cell area. D: Scatter dot plot of the number of clusters per μm^2.**=0.001<p<0.01.
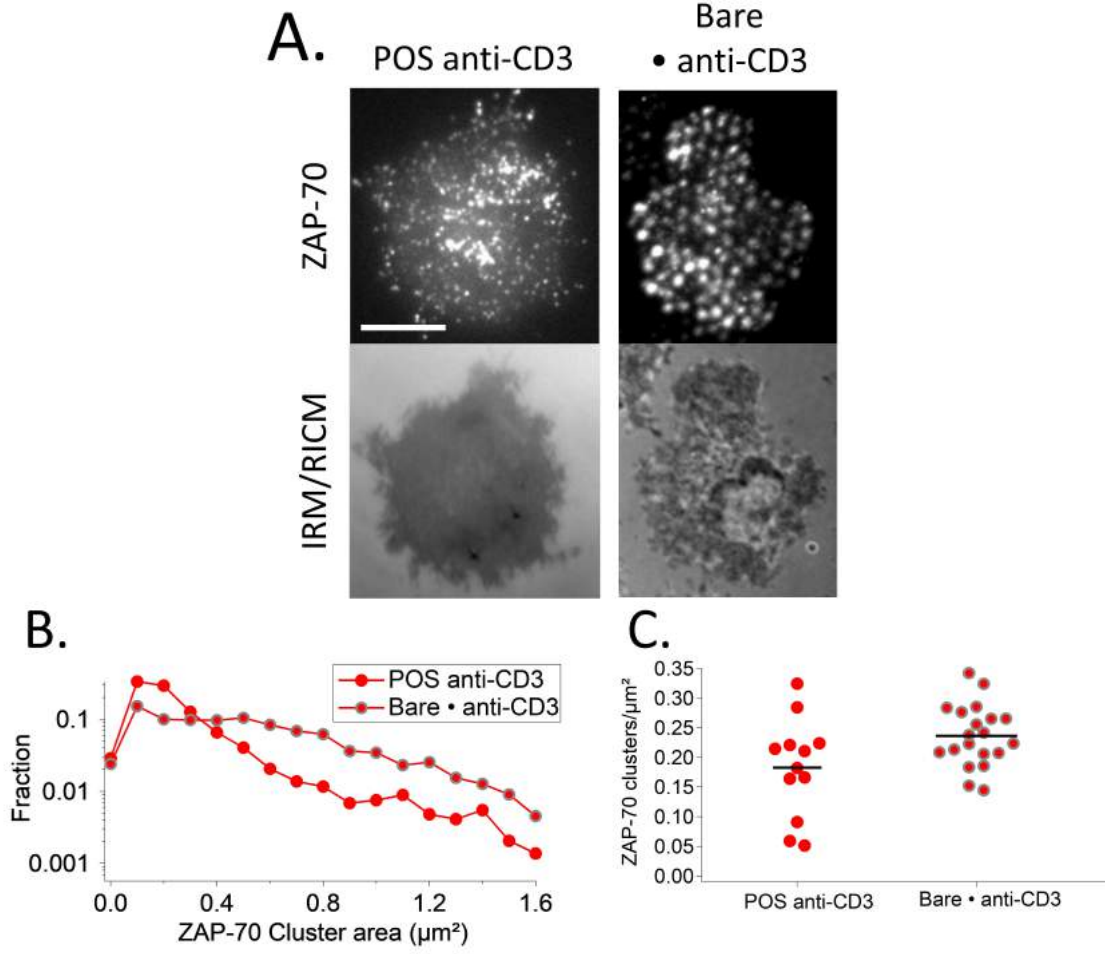
Figure 5.8: **ZAP-70 clusters of T-cells spreading on POS anti-CD3 and [Bare]$_{SLB}$ [αCD3]$_{Dot}$ (also called Bare• anti-CD3).** A:RICM and TIRF-M images of Jurkat T-cells after 30 minutes engagement on homogeneous and patterned substrates. For TIRF-M images ZAP-70 was marked. Scale bar: $10\mu m^2$. B: Histogram of the apparent area of clusters normalized by the total number of clusters. Clusters of size corresponding to the underlying anti-CD3 dots (0.4 μm^2) are enriched for[Bare]$_{SLB}$[αCD3]$_{Dot}$. C: Scatter dot plot of the number of clusters per μm^2.

in T cells is typically ring-like or peripheral. In order to qualitatively determine the organization of the actin (centralized, homogeneous or peripheral), fluorescence intensity at the center (I_{Center}) and in the rest of the cell ($I_{restCell}$) is measured and an actin parameter (p) is defined as:

$$p = \frac{I_{Center}}{I_{RestCell}} \tag{5.1}$$

We consider that if 0<p<0.5, the actin is peripherally distributed, if 0.5<p<1.5, the actin is homogeneously distributed and if p>1.5, the actin is centrally distributed.

5.3.1 Organization

Figure 5.9A shows the architectures of actin cytoskeleton observed on POS anti-CD3 and on $[\text{Bare}]_{SLB}[\alpha\text{CD3}]_{Dot}$. Visual inspection of the images reveals different architectures possible. On POS anti-CD3 the actin organization can be depleted at the center and enriched at the periphery (1.) or homogeneously distributed with a slight accumulation at the periphery (2.). The first type of organization is the most prevalently observed. On the other hand, on the patterned substrate $[\text{Bare}]_{SLB}[\alpha\text{CD3}]_{Dot}$, in a majority of cells, the actin architecture is in form of patches which are concomitant with the membrane topography and the underlying anti-CD3 pattern. Interestingly, sometimes even if the membrane topography is patterned, the actin may be homogeneous or peripheral - similar distributions as 1. et 2. but still with the presence of accumulation points which are concomitant with the membrane topography and the underlying anti-CD3 pattern (1'. and 2'.). When the membrane is flat (non-patterned cells), the actin is always either in the form of a ring or is homogeneously distributed.

Actin parameter on $[\text{Bare}]_{SLB}[\alpha\text{CD3}]_{Dot}$ is presented in Figure 5.9B and is compared to POS anti-CD3. Coherently with the visual inspections, T-cells spreading on POS anti-CD3 have an average actin parameter equal to 0.8 which correspond to an homogeneous organization. However the parameter has a large dispersion around this value due to the presence of the two kinds of organization described above. The presence of these populations can be observed in the histogram in Figure 5.9C. There are 36% of cells with an actin parameter between 0-0.5 and 53% with an actin parameter between 0.5-1.5 which correspond respectively to the actin architecture 1. and 2. presented in Figure5.9A. On $[\text{Bare}]_{SLB}[\alpha\text{CD3}]_{Dot}$ T-cells spreading have an average actin parameter equals to 1.2 which correspond to a homogeneous organization. However it should be pointed out that with this fluorescence intensity analyses method, the patterned actin distribution can not be differentiated from a homogeneous distribution, since the patches are regularly distributed. The parameter has also a large dispersion around this value due to the presence of several kinds of actin organization. In the histogram in Figure 5.9C presence of the architecture 1' does not appear as a predominant organization(3%), but there is a high proportion of cell with an actin parameter between 0.5-1.5 which correspond to the architecture 2' and 3 (73%). Next, relation between the actin parameter and the cell area or NaV density was tested. Figure 5.9D and C show that neither on POS anti-CD3 nor on $[\text{Bare}]_{SLB}[\alpha\text{CD3}]_{Dot}$ the actin architecture is related to the cell adhesion area or to the NaV average density.

5.3.2 Dynamics

Dynamics of actin was studied using Life-Act-GFP transfected cells expressing fluorescent actin. Cells were allowed to sediment on to POS anti-CD3 or $[\text{Bare}]_{SLB}[\alpha\text{CD3}]_{Dot}$ substrate and TIRF-M image sequence were recorded from as early times as possible, until saturation of the spreading area. Figure 5.10 shows that on POS anti-CD3, the actin appears as a growing patch which then develops a actin depleted center. The change of actin organization from homogeneous to peripheral according time is visible in Figure 5.10C. Figure 5.10B shows that in general actin parameter decreases as cell spreading area increases. TIRF-M time-sequence of actin presented in Figure 5.10A shows an example a actin organization dynamic which goes from homogeneous distributed to
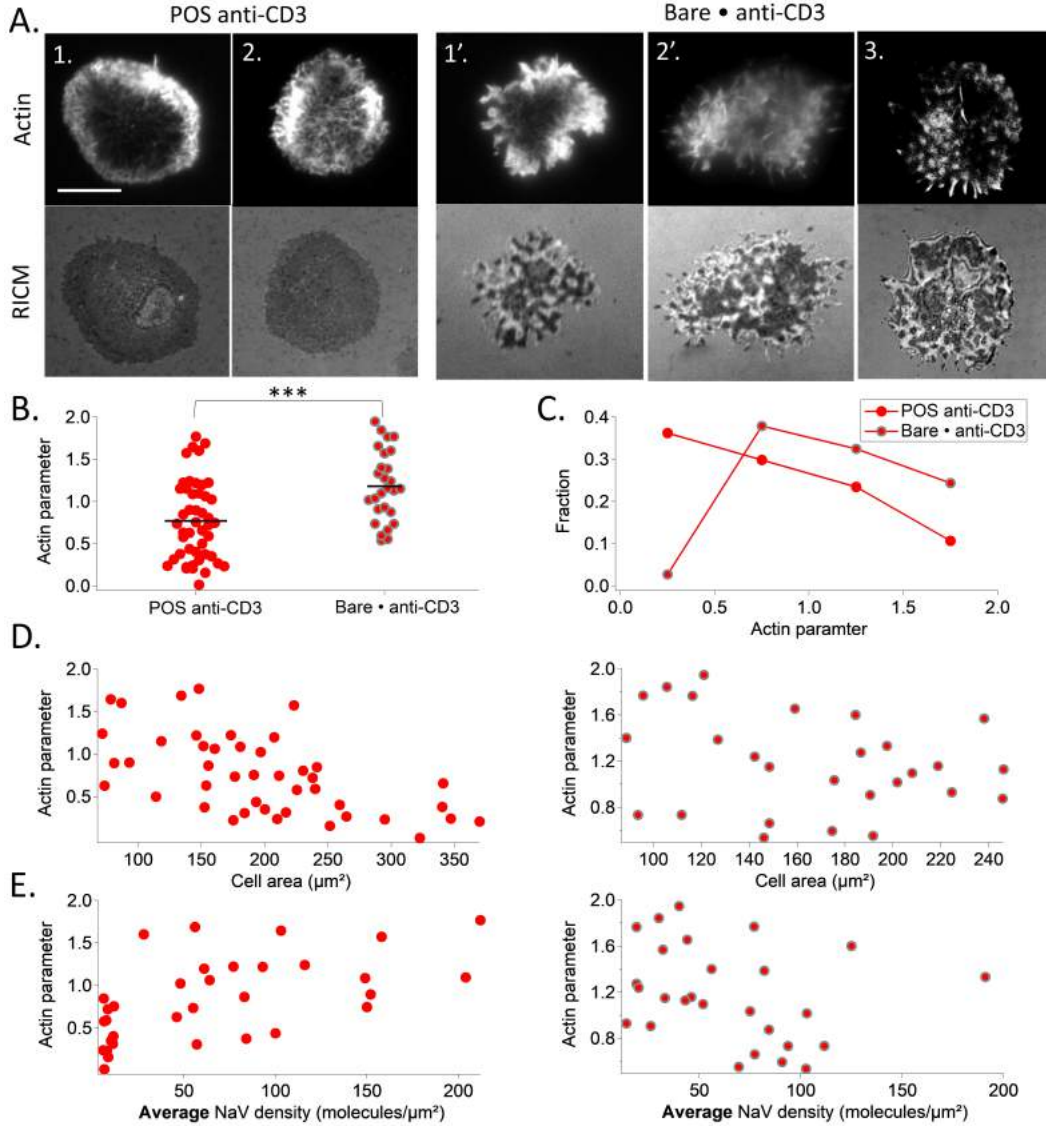
Figure 5.9: **Actin Cytoskeleton organization of T-cells spreading on POS anti-CD3 and [Bare]$_{SLB}$ [αCD3]$_{Dot}$ substrates (also called Bare• anti-CD3).** A: A:RICM and TIRF-M images of Jurkat T-cells after 30 minutes engagement on homogeneous and patterned substrates.For TIRF-M images Actin was marked. Scale bar: 10μm². B: Scatter dot plot of actin parameter. C: Histogram of the actin parameter normalized by the total number of analyzed cells. C: Scatter dot plot of the number of clusters per μm². D-E: Relation between actin parameter and cell adhesion area (D) or NaV average density (E) on POS anti-CD3 (left) and [Bare]$_{SLB}$[αCD3]$_{Dot}$ (right)A.

enriched in the periphery with a depletion at the center.

Figure 5.11 shows an example of T-cell spreading on Bare ● anti-CD3 with an peripheral actin architecture. Some accumulation of actin is visible during the spreading (brighter zones).

5.4 Clustered versus homogeneous distribution of anti-CD3

This section seeks to access the real impact of ligand clustering by comparing substrates with equivalent ligand densities but where the ligand distribution differs. To do so, T-cell behavior on patterned substrates is compared to their behavior on homogeneous SLB substrates which present the same density of proteins (homogeneous control type 2, see section 3.5.3). Results obtained for cell adhesion area, TCR clusters distribution and actin cytoskeleton architecture will be presented.

Adhesion area: As shown on Figure 5.12A-B, the cell spreading area slightly increases when anti-CD3 molecules are presented in clusters as compared to the homogeneous case. Cell-by-cell analysis shows the same trend (Figure 5.13).

TCR clusters distribution: As shown on Figure 5.14A TCR distribution is highly influenced by the patterning of anti-CD3. The presence of underlying nano-dots of TCR-ligand induced a reorganization of TCR molecules which change from homogeneous to co-localized with this underlying pattern. Histogram presented in Figure 5.14B shows an enrichment from cluster area of 0.2-0.3 μm^2.

Actin cytoskeleton organization: Actin labeled with fluorescent phalloidin shows different organization on patterned as compared to homogeneous substrates. Visual inspection of actin distribution on substrates with only anti-CD3 on SLB shows that actin is homogeneously distributed when the TCR ligand is homogeneously spread on the surface whereas when TCR ligands are presented in form of clusters actin forms patches which correspond to the pattern (Figure 5.15A). However the actin parameter is quite similar (Figure 5.15B). This analysis calculates the ratio between the fluorescence intensity at the center of the cell and the total fluorescence intensity of the cell. In cells with homogeneously spread patches, the fluorescence intensity in the center equals the mean intensity of the cell which results in an actin parameter around 1, the same as with an homogeneous distribution. Histogram of the actin parameter normalized by the total number of cells presented in Figure 5.15C indicates the same result. The fact that actin distribution changes when anti-CD3 are clustered demonstrate the impact of the patterning on the actin.

5.5 Pre-activated T-cells

In some experiments, cell were pre-incubated with anti-Vβ during 30 minutes prior the engagement of the cells on the substrate surface. This pre-incubation was previously demonstrated to lead to a pre-activation of the cells leading to the formation of a cS-MAC even if the ligands were fixed [86] (see Appendix C for detailed protocol of the T-cells pre-activation). These cells were used on $[\text{Bare}]_{SLB}[\alpha\text{CD3}]_{Dot}$ in order to see
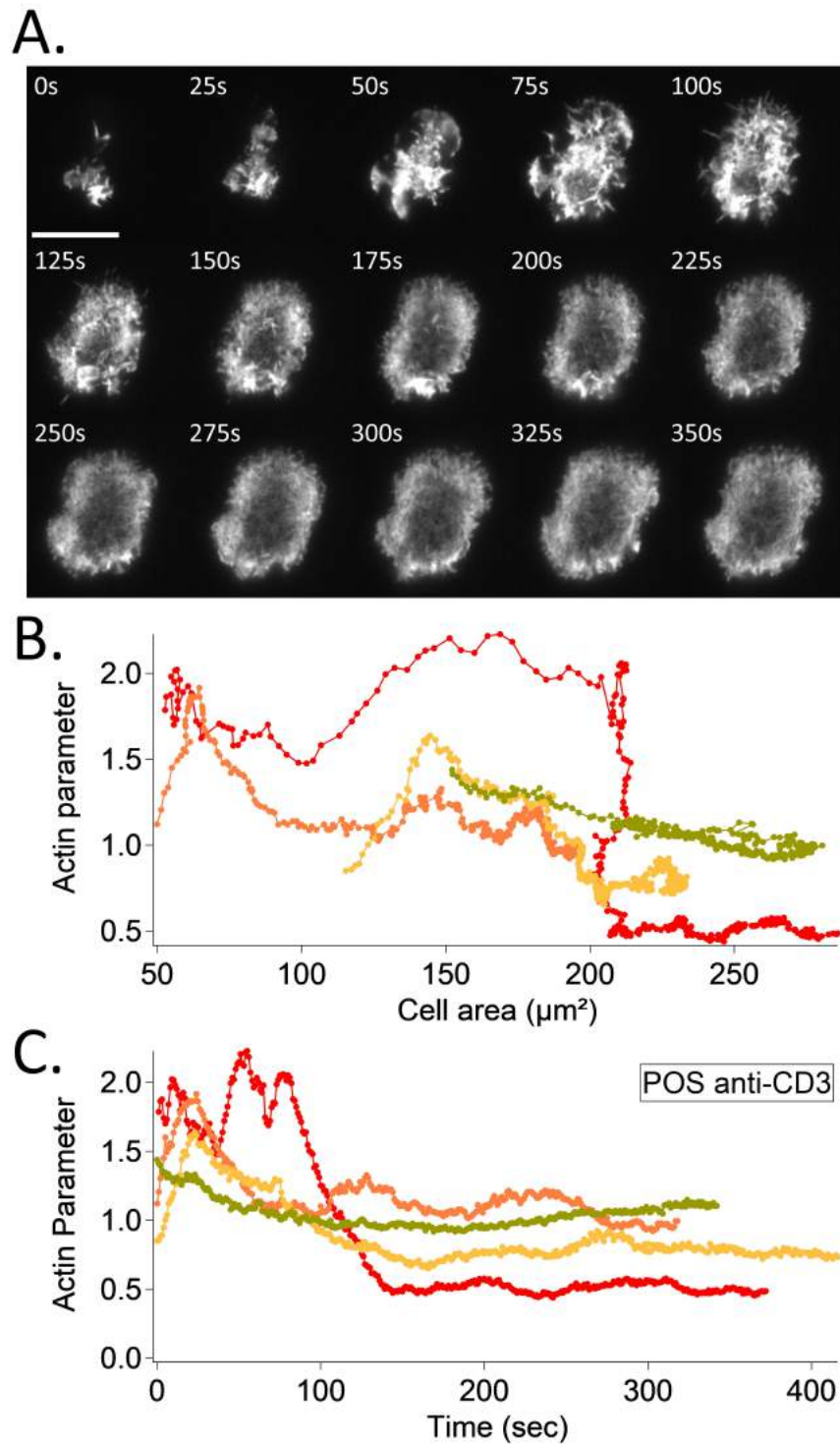
Figure 5.10: **Dynamic of actin organization of Life-Act cells during cells engagement on POS anti-CD3.** A:TIRF-M time-sequence of actin organization during Jurkat cell adhesion from first contact with the substrate to the stabilization of the cell spreading. Scale bar : 10 μm. B: Evolution of actin parameter with the cell spreading area. C: Dynamic of actin organization for 4 cells during cells engagement.
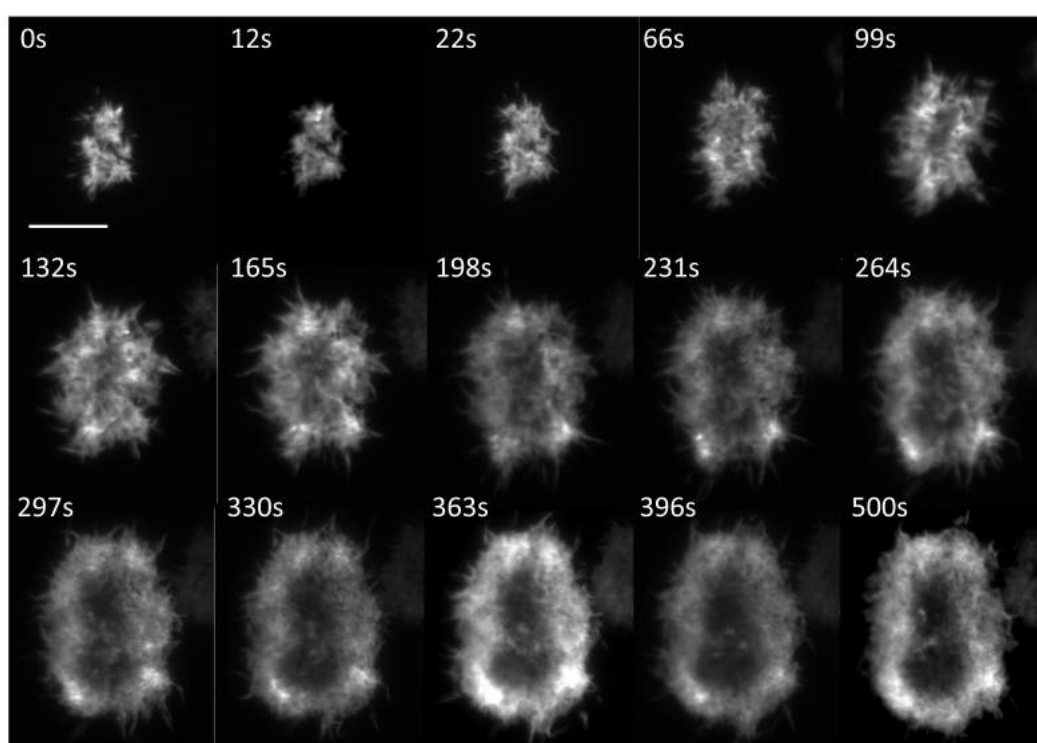
Figure 5.11: **Dynamic of actin organization of Life-Act cells during cells engagement on [Bare]$_{SLB}$[αCD3]$_{Dot}$.** Scale bar : 10 μm
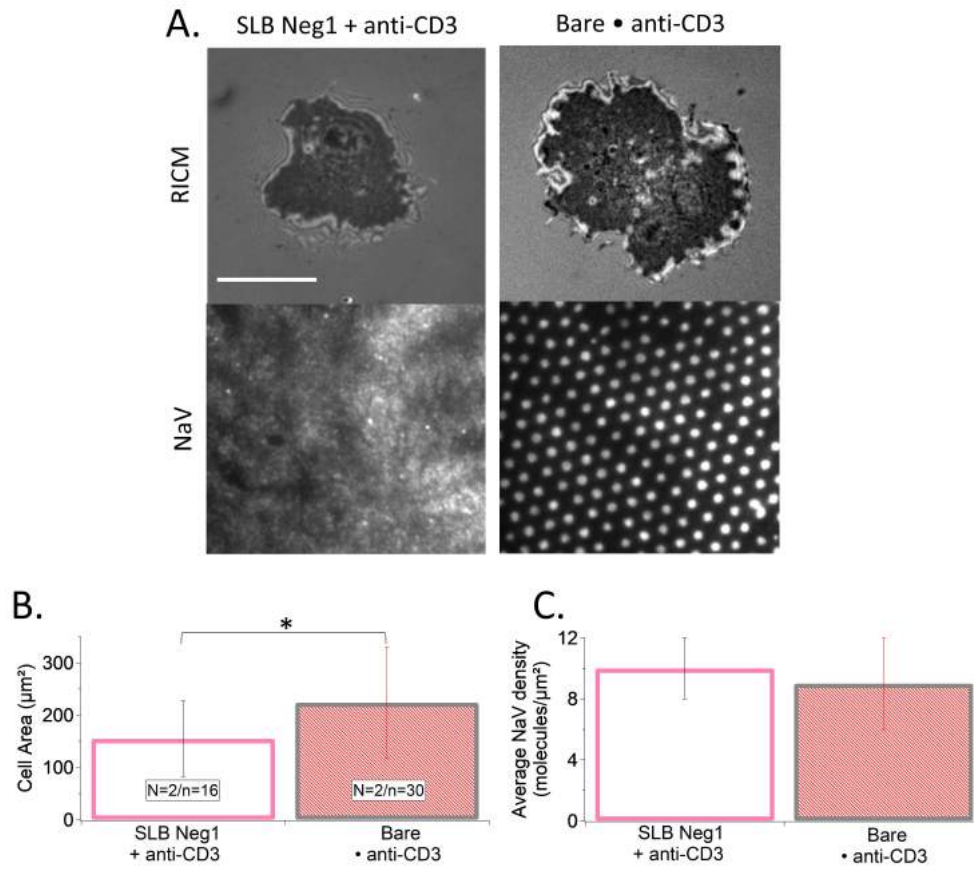
Figure 5.12: **Cell spreading area on patterned substrates [Bare]$_{SLB}$ [αCD3]$_{Dot}$ (also called Bare• anti-CD3) and on homogeneous substrates SLB Neg1 + anti-CD3.** A: A:RICM images of Jurkat T-cells after 30 minutes engagement on patterned substrates and epi-fluorescence images of the underlying organization of NaV. Scale bar: $10\mu m^2$. B: Cells area measurement. C: Quantification of Average NaV density. On both substrates the NaV density is around 10 molecules/μm^2. Error bars represent standard deviations. *=0.01<p<0.05.
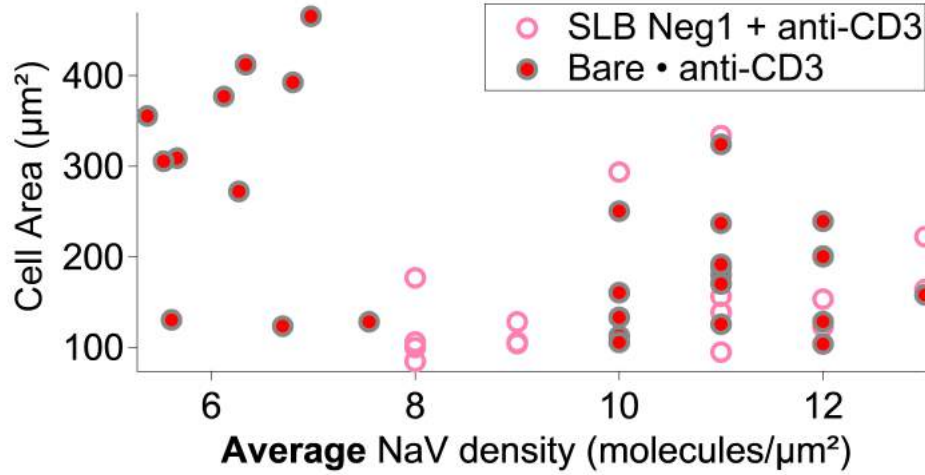
Figure 5.13: **Cell spreading area on patterned and homogeneous substrates according the NaV density.** Cell spreading area of Jurkat cell on $[\text{Bare}]_{SLB}$ $[\alpha\text{CD3}]_{Dot}$ (also called Bare• anti-CD3) and on homogeneous SLB Neg1 + anti-CD3 according NaV density under each cells. Each points represent one cell.

if this pre-activation affect the TCR clusters patterning and if the cSMAC can still be formed.

Cell adhesion area: As shown on Figure 5.16 the pre-activation induced a strong increase of the cell adhesion area to 360 ± 145 μm^2. Moreover the adhesion of pre-activated T-cells is always homogeneous without membrane patterning.

TCR cluster distribution As presented on TIRF-M images of Figure 5.17A, TCR clusters of pre-activated T-cells is regrouped into patches which co-localized with the underlying NaV patterned. Interestingly visual inspection show also that there is a centralization of TCR molecules comparable to a formation of the cSMAC. Quantification of the centralization of TCR reveals that non activated T-cells also have a weak centralization of the TCR but it is less pronounced than on pre-activated T-cells (Figure 5.17D). Concerning the apparent area of clusters there are no differences between the two populations. But the density of clusters is lower on pre-activated T-cells (Figure 5.17C).

Actin cytoskeleton organization: Pre-activated T-cells have different actin cytoskeleton architecture than non-activated T-cells.The morphology with patches of actin was never observed, only peripheral (1.) or homogeneous (2.) distributions were observed (Figure 5.18A). The average actin parameter equals to 0.5 for pre-activated T-cells which indicates an inclination to a peripheral actin distribution (Figure 5.18B). Moreover the histogram in (Figure 5.18C) indicates that 53% of the pre-activated cells present an peripheral distribution (actin parameter between 0-0.5) compared to 3% for the non-activated cells. Additionally, actin parameter of pre-activated cell seems to have no relation with the cell spreading area (Figure 5.18D.)
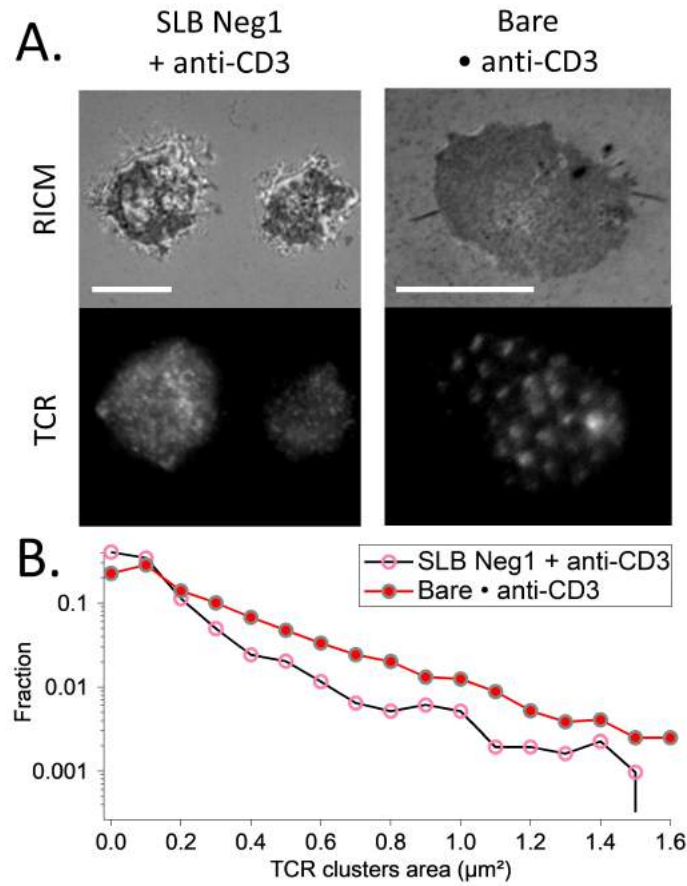
Figure 5.14: **TCR clusters of T-cells spreading on patterned and homogeneous substrates.** A: RICM and TIRF-M images of Jurkat T-cells after 30 minutes engagement on patterned substrates. Scale bar: 10μm. B: Histogram of the apparent area of clusters normalized by the total number of clusters.
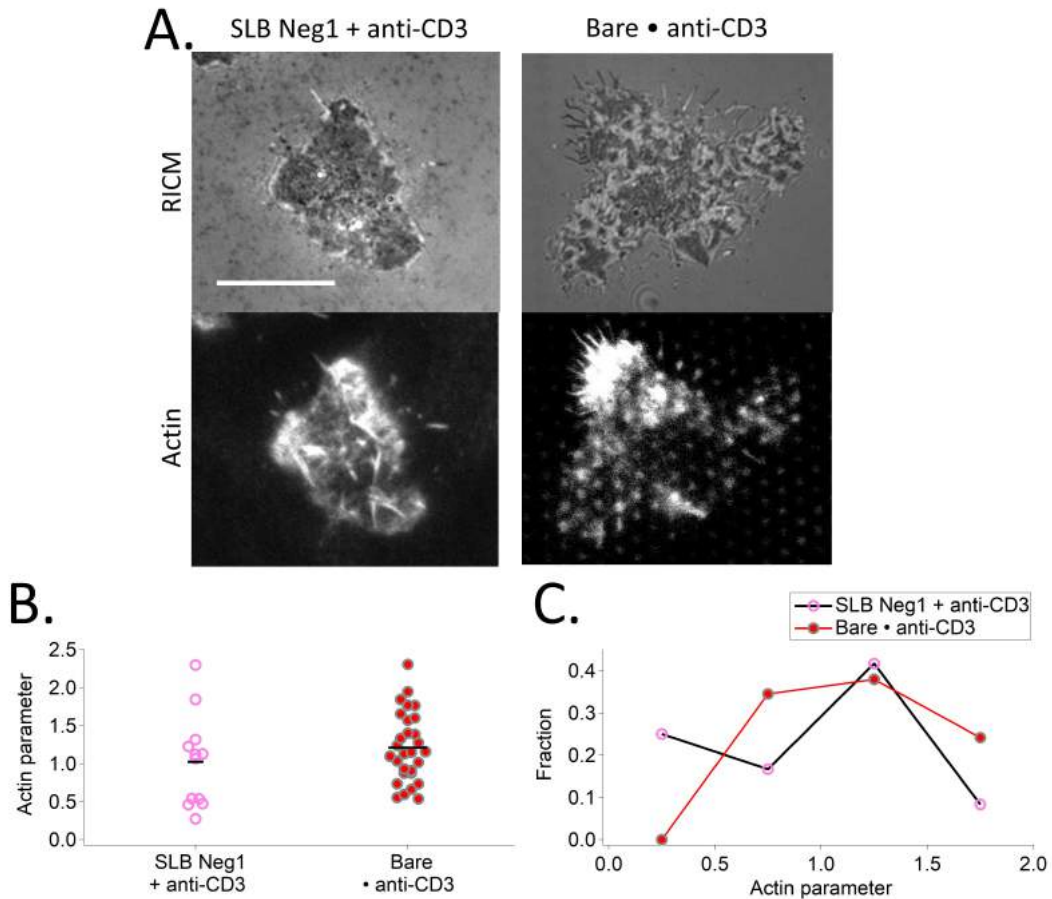
Figure 5.15: **Actin cytoskeleton organization on patterned substrates [Bare]$_{SLB}$ [αCD3]$_{Dot}$ (also called Bare• anti-CD3) and on homogeneous substrates SLB Neg1 + anti-CD3.** A: RICM images of Jurkat T-cells after 30 minutes engagement on patterned substrates and TIRF-M images of the actin cytoskeleton. Scale bar: 10μm². B: Scatter dot plot of actin parameter. C: Histogram of the actin parameter normalized by the total number of analyzed cells.
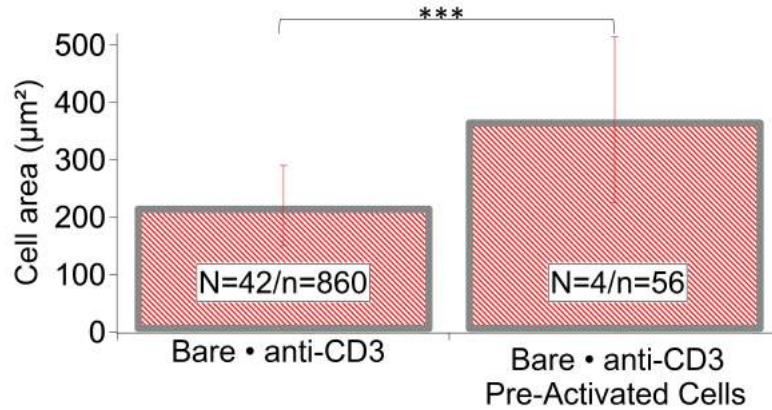
Figure 5.16: **Pre-Activated Cells area on [Bare]$_{SLB}$ [αCD3]$_{Dot}$ (also called Bare•** **anti-CD3) substrate.** Cell adhesion area measurement of Jurkat T cells pre-activated with anti-Vβ was done after 30 minutes engagement on substrates. Error bars represent standard deviations. ***=p<0.001.

5.6 Primary cells

Human and mouse primary cells were used to probe whether the results reported above for Jurkat T cells were also valid for primary T cells which are typically much smaller. Two types of primary cells were used: fresh human primary CD4+ cells from peripheral blood of healthy donors and mouse primary CD4+ T cells from wild-type B6 mice (pooled lymph nodes and spleens), amplified during 48 hours.

5.6.1 Human primary T-cells

Human T-cell were obtained in the context of collaboration with L.LIMOZIN (Laboratoire d'Adhesion et d'inflammation-LAI) and were isolated in LAI by Adeline QUERDRAY and Martine BIARNES. This were obtained from peripheral blood of healthy donors. Data from experiments that include naive and memory CD4+ cells, and from experiments where only CD4+ naive cells selected are pooled. They were seeded either on control POS anti-CD3 or on [Bare]$_{SLB}$ [αCD3]$_{Dot}$. A comparative study is presented below.

Cell adhesion area: As shown on Figure 5.19 human T-cells spread homogeneously on POS anti-CD3 as well as on [Bare]$_{SLB}$ [αCD3]$_{Dot}$ with a cell spreading area corresponding respectively to 45±20 μm^2 and 55±30 μm^2. This higher cell spreading on [Bare]$_{SLB}$ [αCD3]$_{Dot}$ than on POS anti-CD3 is observed in 2 of 3 comparative experiments. This result differs from cell spreading area of Jurkat where cell adhesion is similar on POS anti-CD3 and [Bare]$_{SLB}$ [αCD3]$_{Dot}$ (see Figure 5.5).
Unlike jurkat, topographical patterning of the membrane (patterned cells) were never observed. Note that the dot separation distance at 2 μm is about the third of the cell diameter, meaning that there are very few dots under any given cell.

TCR clusters distribution and Actin cytoskeleton architecture: As presented on Figure
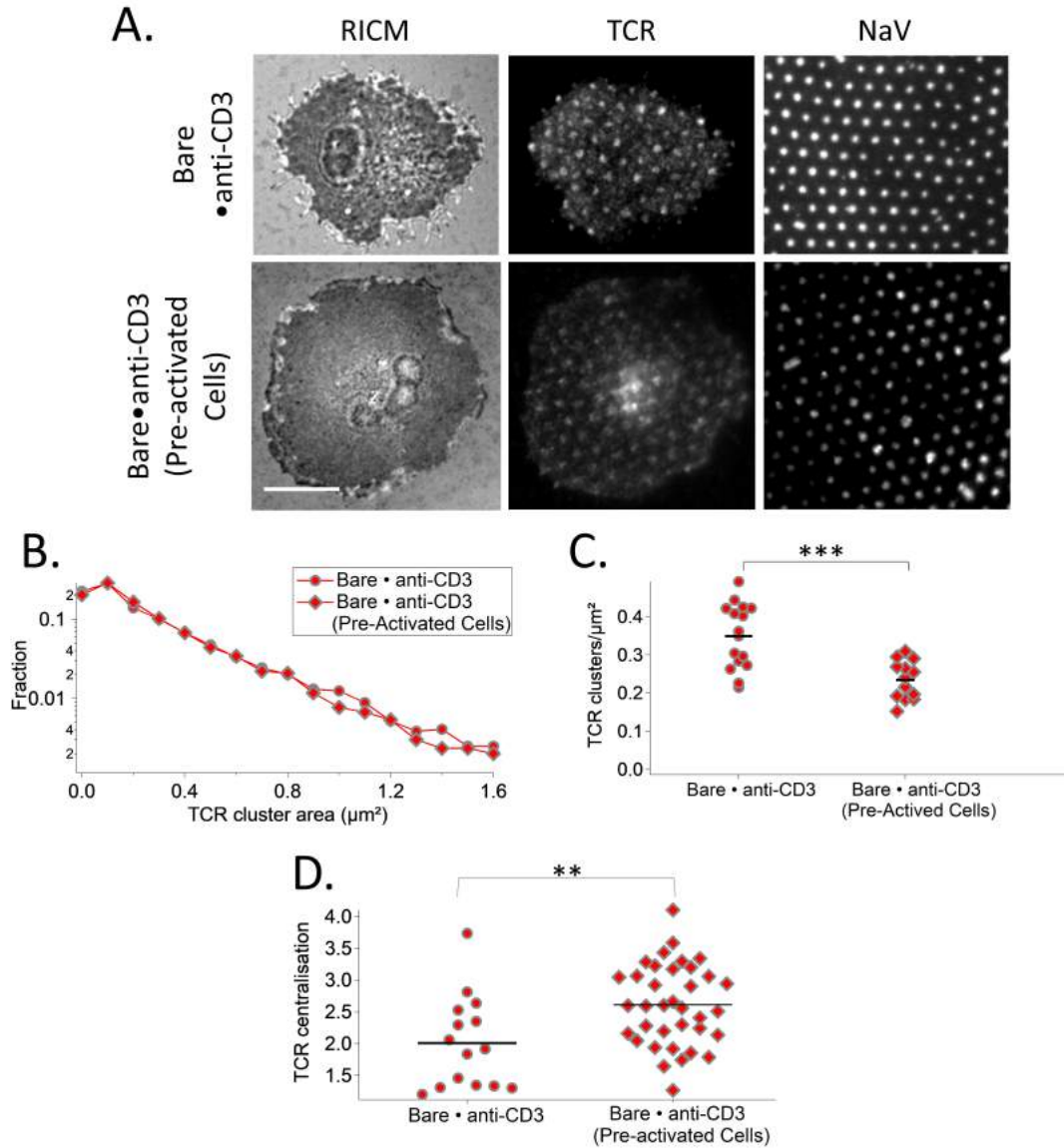
Figure 5.17: **TCR clusters of pre-activated T-cells spreading on** $[\mathbf{Bare}]_{SLB}$ $[\alpha\mathbf{CD3}]_{Dot}$ **(also called Bare• anti-CD3) substrate.** A: RICM, TIRF-M and epifluorescent images of Jurkat T-cells after 30 minutes engagement on patterned substrates. For TIRF-M images TCR was marked. Scale bar: 10μm. B: Histogram of the apparent area of clusters normalized by the total number of clusters. C: Scatter dot plot of the number of clusters per μm^2. D: Scatter dot plot of the TCR parameter. **=0.001<p<0.01, ***=p<0.001.
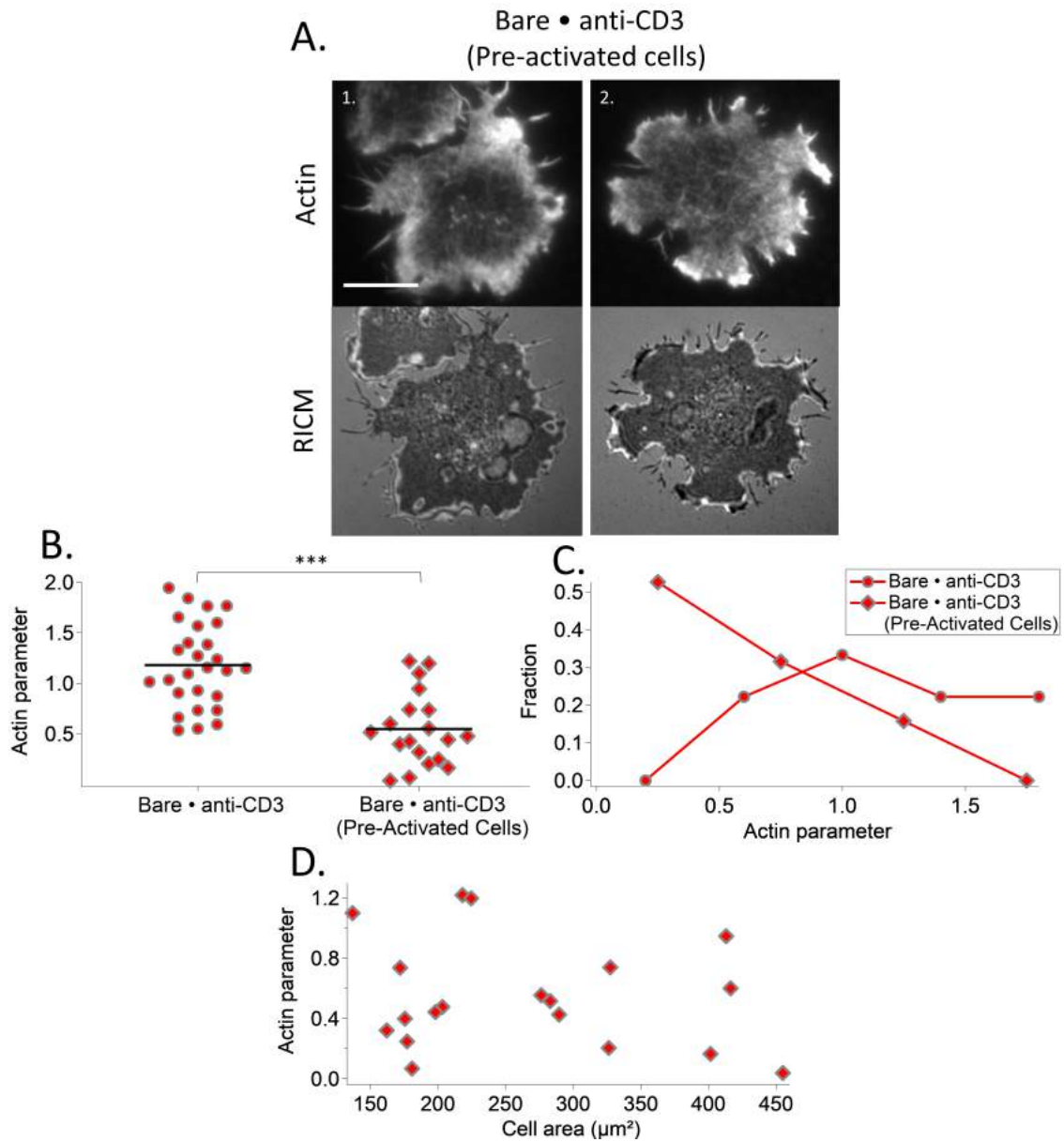
Figure 5.18: **Actin architecture of pre-activated T-cells spreading on [Bare]**$_{SLB}$ **[αCD3]**$_{Dot}$ **(also called Bare• anti-CD3) substrate.** A: RICM and TIRF-M images of pre-activated Jurkat T-cells after 30 minutes engagement on patterned substrates. Scale bar: 10μm. B: Scatter dot plot of the actin parameter. C. Histogram of the actin parameter normalized by the total number of analyzed cells. D: Scatter dot plot of the number of clusters per μm^2. D: Relation between actin parameter and cell adhesion area. ***=p<0.001

145

5.20 TCR clusters distribution remain homogeneously even on patterned substrate. On POS anti-CD3, the actin is enriched at the periphery and depleted in the center, moreover some puncta of actin can be also observed.

5.6.2   Mouse primary T-cells

Mouse T-cells were kindly gifted by Guillaume VOISINNE (team Malissen, Centre d'Immunologie de Marseille-Luminy - CIML). Studies were performed on standard substrates $[\text{Bare}]_{SLB}$ $[\alpha\text{CD3}]_{Dot}$ and POS anti-CD3 and also on substrates supplemented with αCD4. αCD4 is an activating ligand of the co-receptor CD4 on T-cell. As αCD4 used here is biotinyled, it binds to the NaV dots along with the anti-CD3 ($[\text{Bare}]_{SLB}$ $[\alpha\text{CD3} + \alpha\text{CD4}]_{Dot}$ substrate) or on homogeneous NaV (POS anti-CD3+ anti-CD4 substrate). These two types of substrates will be compare in terms of cell adhesion, TCR clusters distribution and actin organization.

Cell adhesion area: As shown on Figure 5.21, on $[\text{Bare}]_{SLB}$ $[\alpha\text{CD3}]_{Dot}$ substrates mouse primary T-cells adhere homogeneously on POS-anti-CD3 with a spreading area of 40 ± 20 μm^2 and on $[\text{Bare}]_{SLB}$ $[\alpha\text{CD3}]_{Dot}$ there are some cells with an patterned adhesion (40%). On this patterned substrate global spreading area equal $30\pm10\mu\text{m}^2$. This behavior is similar of the behavior of Jurkat T-cells. Addition of αCD4 induce a significantly increase of the cell spreading area for homogeneous and patterned substrates reaching 60 ± 40 μm^2 for POS anti-CD3 + anti-CD4 and 50 ± 20 μm^2 for $[\text{Bare}]_{SLB}$ $[\alpha\text{CD3} + \alpha\text{CD4}]_{Dot}$.

TCR clusters distribution: As presented in Figure 5.22, on homogeneous substrates with or without αCD4 TCR molecules are distributed homogeneously and on patterned substrates, patterned TCR distribution is observed as for jurkat when only anti-CD3 is present in the dots but not in the presence of the co-receptor ligand αCD4.

Actin cytoskeleton architecture: Since the primary cells are very small, precise actin architecture is difficult to quantify but on Figure 5.23 it can been seen that on homogeneous substrates actin is homogeneously distributed. On patterned substrate without anti-CD4 actin can form patched which co-localized with the underlying pattern whereas in presence of anti-CD4 the actin become homogeneous.

5.7   Conclusion

The experiments presented in this chapter were designed to probe the behavior of T cells when confronted with ligands that are clustered rather than being homogeneously distributed. The substrates used here were prepared identically using protocols described in chapter 3. The spacing and size of the dots are highly reproducible but the quantity of ligands inside and outside the dots is difficult to control, and may vary greatly (5 to 30 molecules/μm^2 outside and 20 to 100 molecules/μm^2 inside. We exploited this variation to explore the influence of local or average ligand density on cell spreading.
Previous work in the laboratory, using similar substrates where the supported bilayer was replaced by grafted polymers (PLL-PEG), has shown that at high polymer surface density, cell spreading was proportional to average ligand density, and not to any other
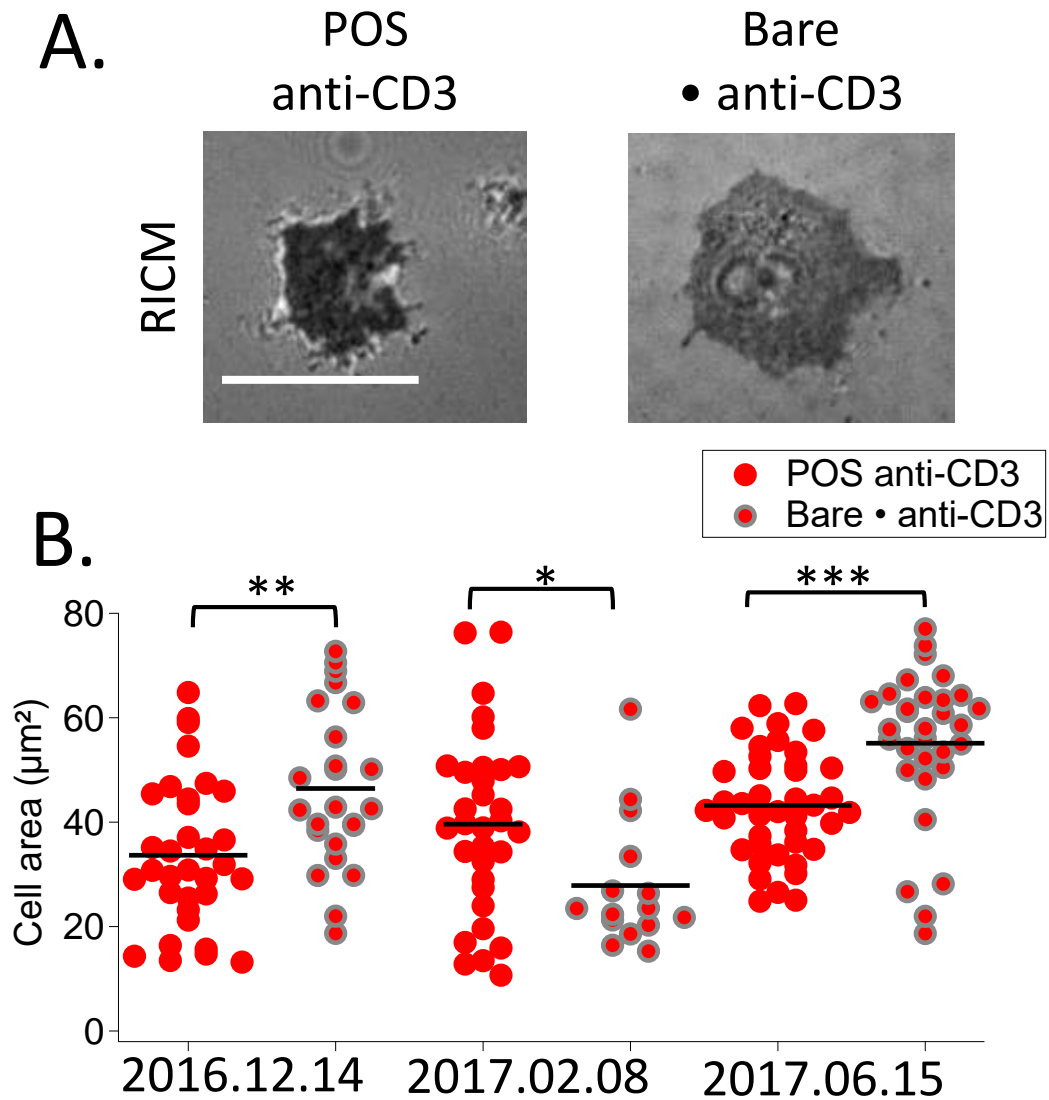
Figure 5.19: **Spreading area of human primary T-cell on homogeneous and patterned substrates.**A: RICM images of human primary T-cell after 30 minutes engagement on POS anti-CD3 and on $[\text{Bare}]_{SLB}$ $[\alpha\text{CD3}]_{Dot}$. Scale bar: 10μm. B: Spreading area measured on different substrates after 30 minutes of engagement.*$=0.01<$p<0.05, **$=0.001<$p<0.01 and ***$=$p<0.001.
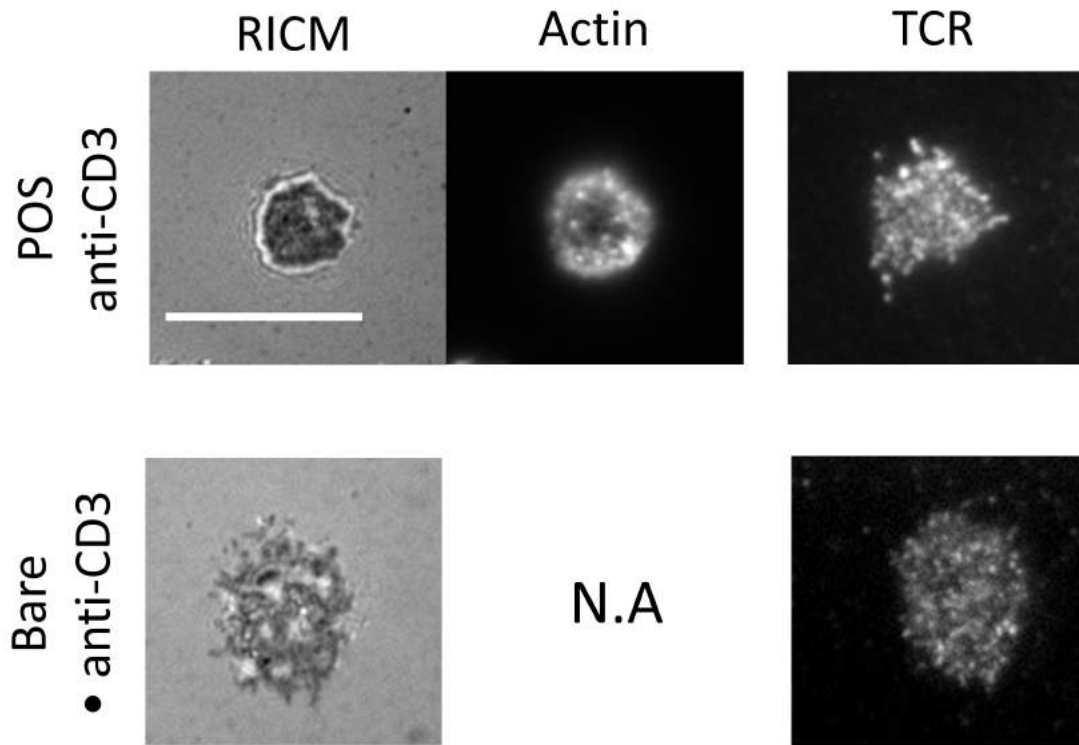
Figure 5.20: **TCR clusters and actin distribution of human primary T-cell after 30 minutes engagement on homogeneous and patterned substrates.**RICM and TIRF-M images of human primary T-cell on POS anti-CD3 and on $[\text{Bare}]_{SLB}\ [\alpha\text{CD3}]_{Dot}$ (also called Bare$\bullet$ anti-CD3). Scale bar: 10μm. N.A indicate data not available.
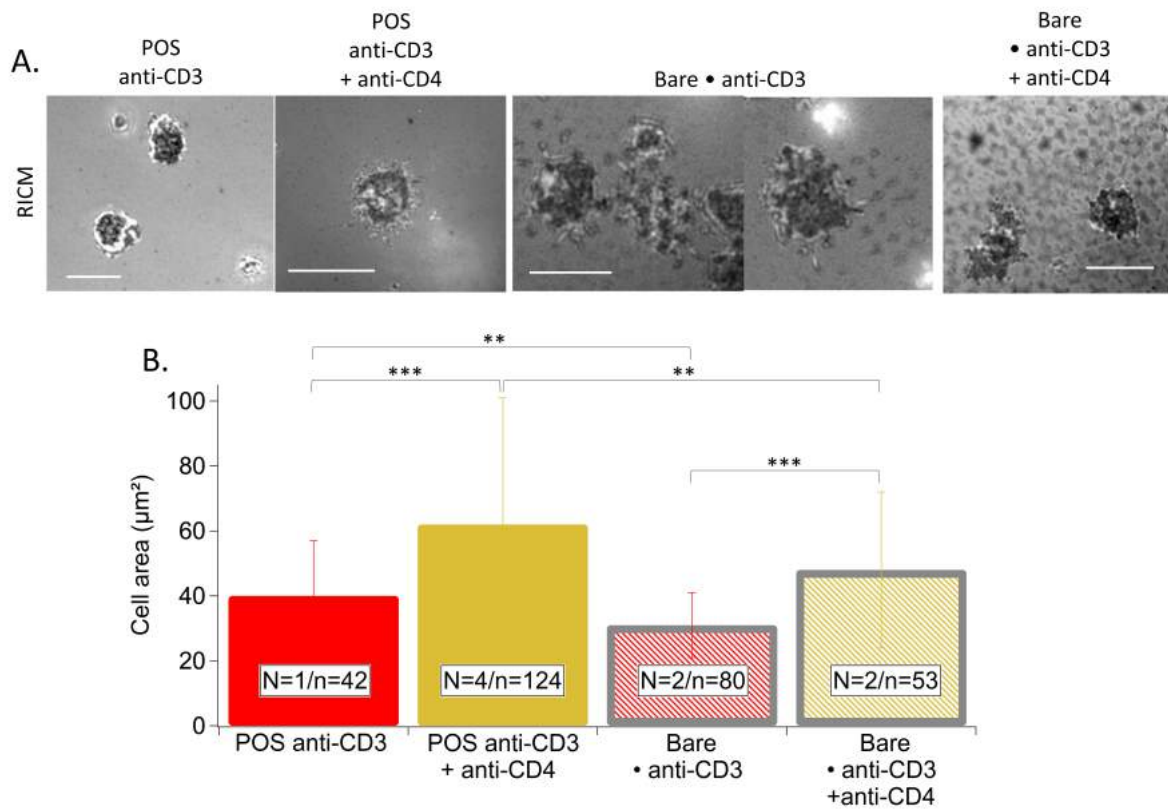
Figure 5.21: **Spreading area of mouse primary T-cell on different substrates.** A: RICM images of mouse primary T-cell on POS anti-CD3 and POS anti-CD3+CD4 and on $[Bare]_{SLB}$ $[\alpha CD3]_{Dot}$ (also called Bare• anti-CD3) and $[Bare]_{SLB}$ $[\alpha CD3 + \alpha CD4]_{Dot}$ (also called Bare• anti-CD3+CD4). Scale bar: 10μm. B: Spreading area measured on different substrates after 30 minutes of engagement.**=0.001<p<0.01 and ***=p<0.001.
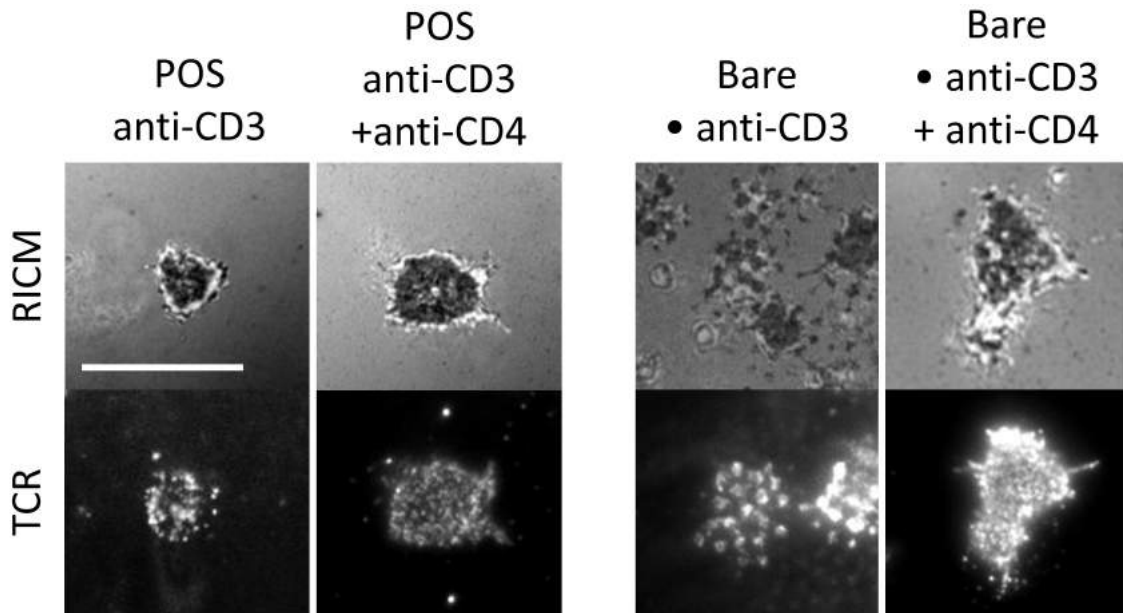
Figure 5.22: **TCR clusters distribution of mouse primary T-cell on different substrates.** RICM and TIRF-M images of mouse primary T-cell after 30 minutes of engagement on POS anti-CD3 and POS anti-CD3+CD4 and on $[\text{Bare}]_{SLB}$ $[\alpha\text{CD3}]_{Dot}$ (also called Bare• anti-CD3) and $[\text{Bare}]_{SLB}$ $[\alpha\text{CD3} + \alpha\text{CD4}]_{Dot}$ (also called Bare• anti-CD3+CD4). Scale bar: 10μm.
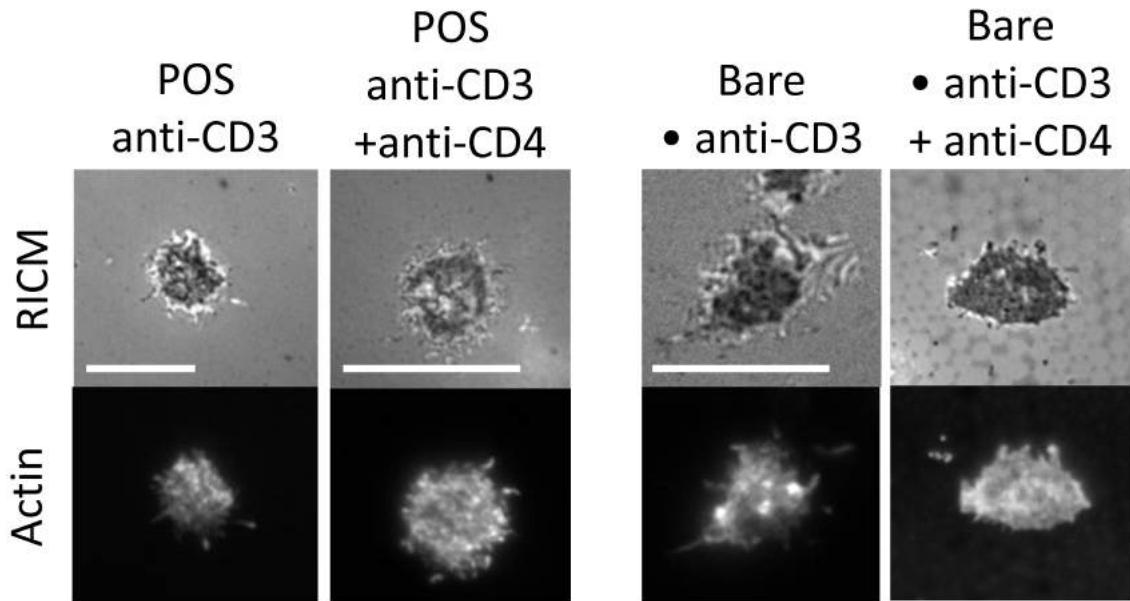
Figure 5.23: **TCR actin distribution of mouse primary T-cell on different substrates.** RICM and TIRF-M images of mouse primary T-cell after 30 minutes of engagement on POS anti-CD3 and POS anti-CD3+CD4 and on $[\text{Bare}]_{SLB}$ $[\alpha\text{CD3}]_{Dot}$ (also called Bare• anti-CD3) and $[\text{Bare}]_{SLB}$ $[\alpha\text{CD3} + \alpha\text{CD4}]_{Dot}$ (also called Bare• anti-CD3+CD4). Scale bar: 10μm.

parameter related to the patterning/clustering [103]. At low polymer surface density however, the cell spreading area was random with in a range and did not show any dependence on ligand density or any other parameter. We had concluded that the dependency of cell spreading on ligand density is masked if the substrate is not sufficiently passivated. In the present case of SLBs, this is probably the case. Nevertheless, cell area on the patterned substrates is larger than that on negative controls, including on a pattern where the active ligand anti-CD3 is replaced by its isotype control; Note that unexpectedly on POS anti-CD3, cells spread as much as on Bare • anti-CD3. We hypothesize that when stimulated by anti-CD3 alone, cells can spread only up to a limit. If there are enough anti-CD3 to attain this limit, addition of further anti-CD3 ligands do not elicit further spreading. This is supported by experiments with POS controls with a smaller anti-CD3 density (data not included).

In accordance with our previous work, the influence of clustering of anti-CD3 on cell spreading was limited. Furthermore, as was the case in previous work for both high and low density polymer substrates [143, 103], in spite of the high non-specific interactions, ligand clustering has dramatic impact on TCR and ZAP70 clusters, and to a smaller extent the actin cytoskeleton. The architecture of the actin cytoskeleton is variable - ranging from dots colocalized with the pattern to homogeneous or peripheral. It is still not clear what determines the specific actin architecture adapted by the cells - specifically whether this arises from intrinsic cell to cell variations in the population or whether it reflects undetectable small variations on the substrate. Live cell imaging with LifeAct transfected cells was undertaken but so far has not yielded definitive answers. In terms of area and TCR distribution, mouse primary T cells broadly show the same behavior as described above for Jurkat but for human primary T cells, the results are less clear. In the next chapter, the consequence of rendering the SLB surrounding the dots adhesive, stimulatory or repulsive is explored.

Chapter 6

T-cells on anti-CD3 clusters: role of adhesive and co-stimulatory molecules

Contents

The bulk of this chapter deals with the response of T-cells to substrates where anti-CD3 clusters are embedded in an SLB functionalized with the ligands of the T cell integrin LFA1, namely ICAM-1 ([ICAM-1]$_{SLB}$ [αCD3]$_{Dot}$). As in the previous chapter, in most experiments, T-cells were studied after 30 minutes of engagement on substrates and PFA fixation, followed by imaging in RICM, and/or TIRF-M. The quantification of cell response was done through the analyses of the cell spreading area (also called adhesion area), the T-cell membrane topography, membrane molecular distribution (TCR and ZAP-70), and the actin organization. Dynamics data is presented for some experiments. Comparison is made throughout with the results presented in the previous chapter on [Bare]$_{SLB}$ [αCD3]$_{Dot}$ and POS anti-CD3. After an in-depth analysis of the impact of having the adhesive molecules ICAM-1 on the SLB surrounding the anti-CD3 dots, the consequence of having ICAM-1 rather than anti-CD3 as clusters is explored. Finally, preliminary results for substrates where the surrounding SLB is functionalized with B7.2, which is a ligand of CD28 are presented.

6.1 Cell spreading on anti-CD3 clusters in presence of adhesive ligands

This section presents results on T-cell spreading area and membrane organization on patterned substrates [ICAM-1]$_{SLB}$ [αCD3]$_{Dot}$, composed of nano-dots of anti-CD3 surrounded by a fluid lipid bilayer functionalized with ICAM-1 which was shown to be fluid (see section 4.1.2.2).

6.1.1 Cell spreading area

On [ICAM-1]$_{SLB}$ [αCD3]$_{Dot}$, the cell membrane adheres homogeneously to the surface and forms an adhesion zone with area equal to 310$\pm$130 μm^2 (Figure 6.1), compared to the average area of 220$\pm$70 μm^2 on [Bare]$_{SLB}$[αCD3]$_{Dot}$. The uneven membrane topography seen previously in absence of integrin ligands (see Figure 5.1), is completely absent and in RICM, the membrane is seen to align with the underlying substrate, making a flat and uniformly adhered adhesion zone [1]

6.1.1.1 Impact of pattern characteristics

As for [Bare]$_{SLB}$ [αCD3]$_{Dot}$, variations within substrates were used to study the impact of the anti-CD3 dot size and protein density on the cell adhesion area.

Impact of dot size: As shown on Figure 6.2 for dot-size range of 510 nm to 900 nm, cell adhesion area does not change significantly. This result shows that as was the case for [Bare]$_{SLB}$ [αCD3]$_{Dot}$, the dot size does not impact the cell adhesion area even in the presence of ICAM-1.

Impact of protein density: As for [Bare]$_{SLB}$ [αCD3]$_{Dot}$ the study of the impact of protein density was done at two levels. First study was done substrate by substrate by looking

---

[1]The non-uniform fringes and darker/lighter zones sometimes formed in the adhesion zone are attributed to extra reflections from the nuclear membrane and scattering from small exo-vesicles.
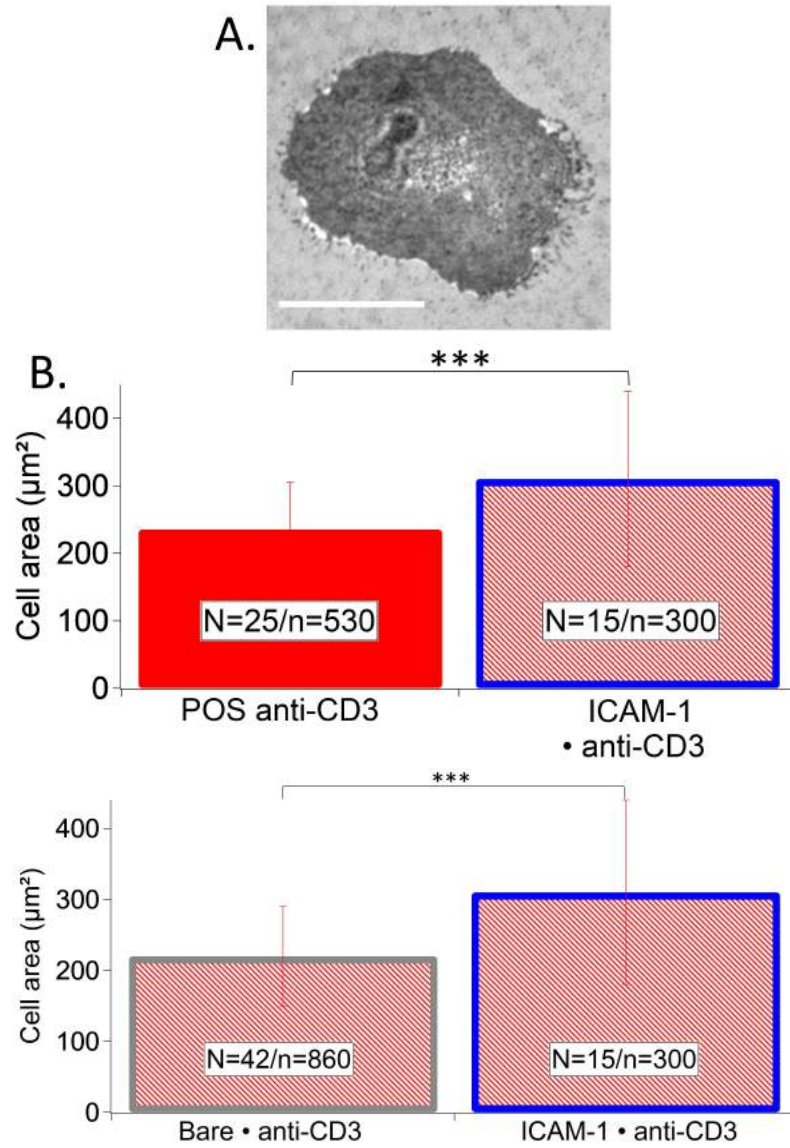
Figure 6.1: **Cell spreading area on $[\text{ICAM-1}]_{SLB}[\alpha\text{CD3}]_{Dot}$ (also called ICAM-1 • anti-CD3).** A: RICM images of homogeneous adhesion of Jurkat T-cell after 30 minutes engagement on substrates. Scale bare=10μm. B: Comparison of cell spreading area on $[\text{ICAM-1}]_{SLB}$ $[\alpha\text{CD3}]_{Dot}$ (=310±130 μm² average) with POS-anti-CD3. C: Comparison with $[\text{bare}]_{SLB}$ $[\alpha\text{CD3}]_{Dot}$. Errors bars are standard deviations.***=p<0.001.
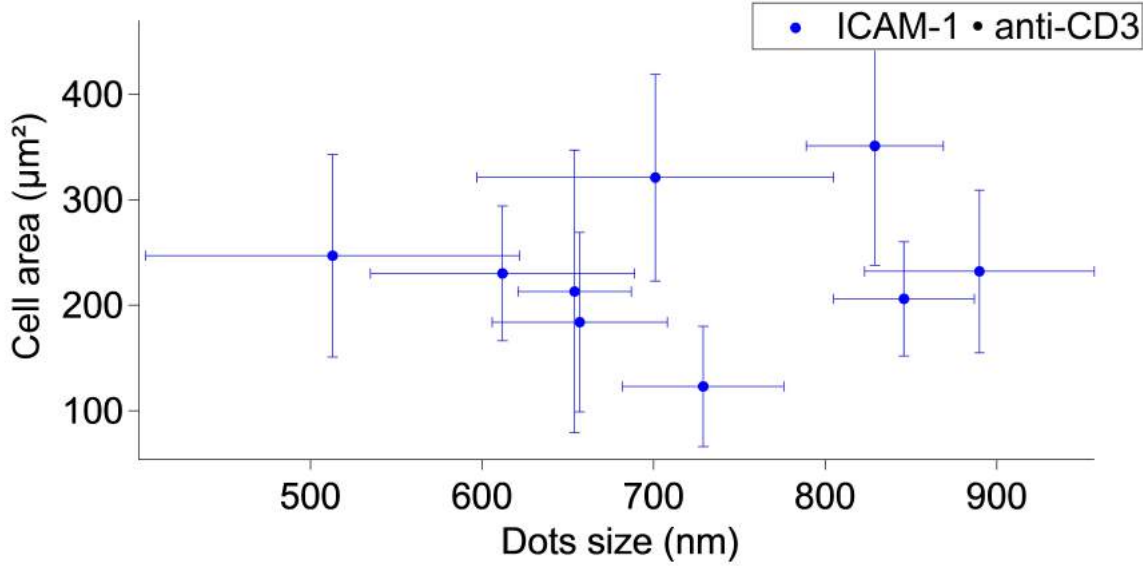
Figure 6.2: **Impact of dot-size on cell adhesion area on $[\text{ICAM-1}]_{SLB}$ $[\alpha\text{CD3}]_{Dot}$ substrate (also called ICAM-1 • anti-CD3).** Each dots correspond to one substrate with at least 20 cells area measured and the average dots size measured with FHWM (N=9/n=230). Error bars represent standard deviations.

the relation between the protein density and the average cell adhesion area on different substrates. Then, for more precision, relation between protein density under each cell and the cell area was evaluated. Reporting first on the substrate-by-substrate analysis, Figure 6.3 shows the dependence of the cell area on NaV density. Very unexpectedly, the area seems to decrease with the NaV density inside the dots. To a less extent, the same trend is observed for the NaV density outside the dots or for the average NaV density. To understand the origin of this discrepancy, we present in Figure 6.4, the area data from all experiments with ICAM-1 in the SLB (including those where the NaV density could not be determined due non-calibrated imaging conditions). As can be seen, in a majority of cases, the cell area is above 150 μm². In the following, we shall focus on cells with area at least 150 μm² and ignore this discrepancy, to solve which we need more statistics. Cell adhesion area versus the NaV density is plotted on a cell-by-cell basis in Figure 6.5, and shows that for the range of NaV density shown, the cell area is independent of protein density.

6.1.1.2 Homogeneous Controls

Two homogeneous controls correspond to this substrate: POS anti-CD3 and SLB ICAM-1. POS anti-CD3 is the same substrate presented in the previous section. SLB ICAM-1 is a SLB functionalized with ICAM-1 treated as if it was on patterned substrates, which means that the SLB was incubated with the same proteins and in the same conditions as during the functionalization of $[\text{ICAM-1}]_{SLB}$ $[\alpha\text{CD3}]_{Dot}$ substrate. Cell spreading area measured on RICM images for these controls were 235±70 μm² for POS anti-CD3 and 160±100 μm² for SLB ICAM-1 (Figure 6.6).
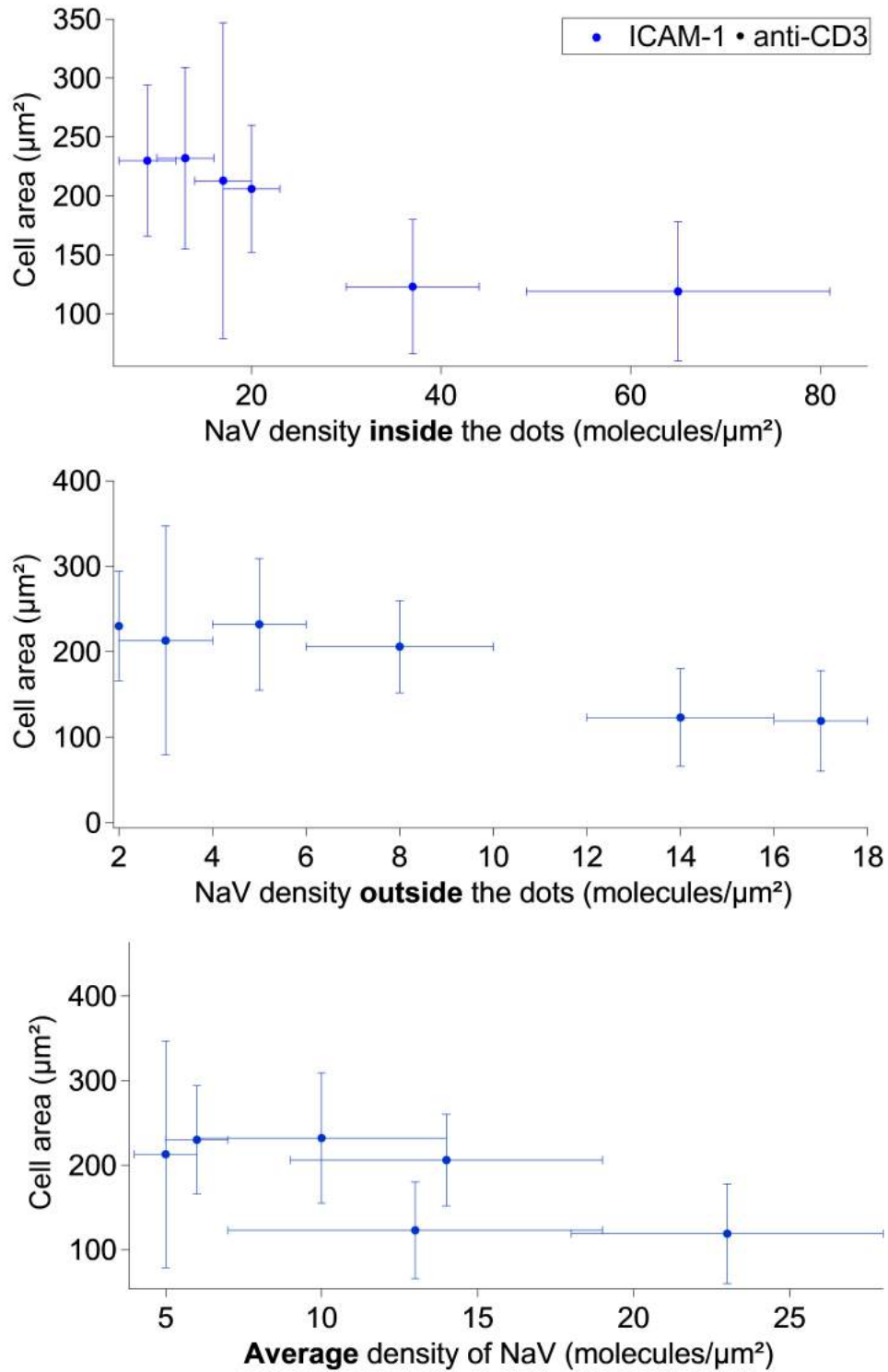
Figure 6.3: **Cell adhesion area according the average density of NaV on the underlying pattern on [ICAM-1]$_{SLB}$ [αCD3]$_{Dot}$ (also called ICAM-1 • anti-CD3).** Each point represent one experiment with error bars representing standard deviations. N=6;n=140.
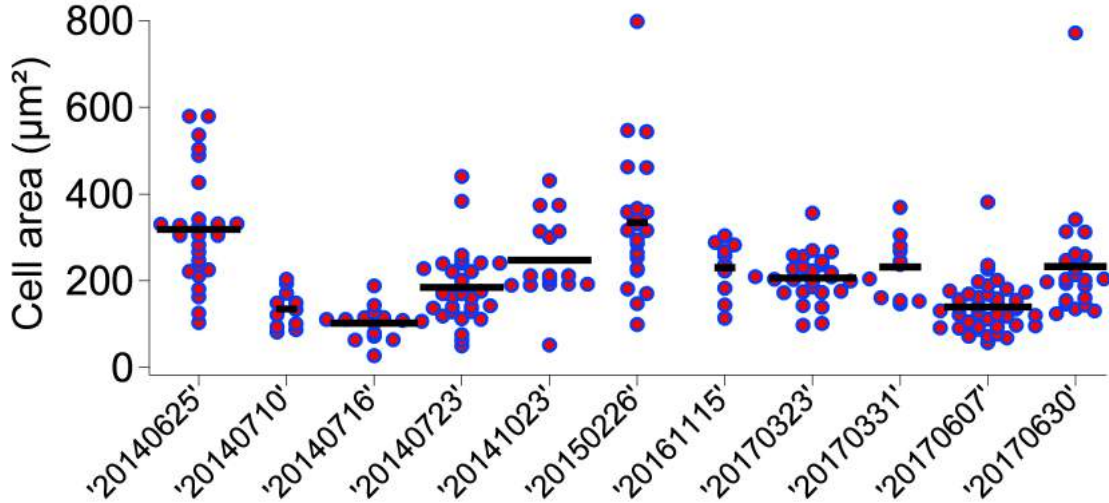
Figure 6.4: **Cell area on [ICAM-1]$_{SLB}$ [αCD3]$_{Dot}$ for all experiments.** Cell adhesion area of Jurkat T cells after 30 minutes engagement on [ICAM-1]$_{SLB}$ [αCD3]$_{Dot}$ reported as scatter dot plot for all experiments. Each point represents one cell, grouped into separate experiments. The date of the experiment is mentioned on the x-axis.

6.1.2 TCR and ZAP-70 distribution in presence of adhesive ligands

As before, TCR and ZAP-70 distribution were analyzed for cell spreading after 30 minutes of engagement on the substrate. TCR molecules were revealed by labeling the β chain of the TCR molecules with an fluorescent antibody. And ZAP-70 signaling kinase was revealed with a fluorescent anti ZAP-70. Both were images in TIRF-M.

6.1.2.1 TCR clusters

Figure 6.7 presents comparative results of TCR distribution observed on T-cells spread on the homogeneous control POS anti-CD3 and on the patterned substrate [ICAM-1]$_{SLB}$ [αCD3]$_{Dot}$. Visual inspection of images presented in Figure 6.7A shows that TCR on patterned substrates are in form of clusters which co-localized with the underlying anti-CD3 pattern (revealed by fluorescent NaV).

Cluster quantification was performed by regrouping all TCR clusters for each kind of substrates, measured on at least 18 cells chosen randomly within 2 different substrates. Figure 6.7B represent an histogram of the apparent area of clusters normalized by the total number of clusters and it shows that on patterned [ICAM-1]$_{SLB}$ [αCD3]$_{Dot}$ (red dots with blue outline) there is an enrichment for clusters with a size superior to the 0.5 to 0.6 μm^2 size range. This threshold value is higher than the size of the underlying anti-CD3 dots (0.4 μm^2). Moreover T-cells on patterned substrates have a higher population of very large clusters (clusters superior to 1.3 μm^2) compared to POS anti-CD3. This quantification is in good agreement with the visual inspection.

Figure 6.7C represent the density of TCR clusters (with detected size > 200 nm^2) at the surface of T-cells spread on patterned and homogeneous surfaces. Density is higher on [ICAM-1]$_{SLB}$[αCD3]$_{Dot}$ compare to POS anti-CD3 as expected.
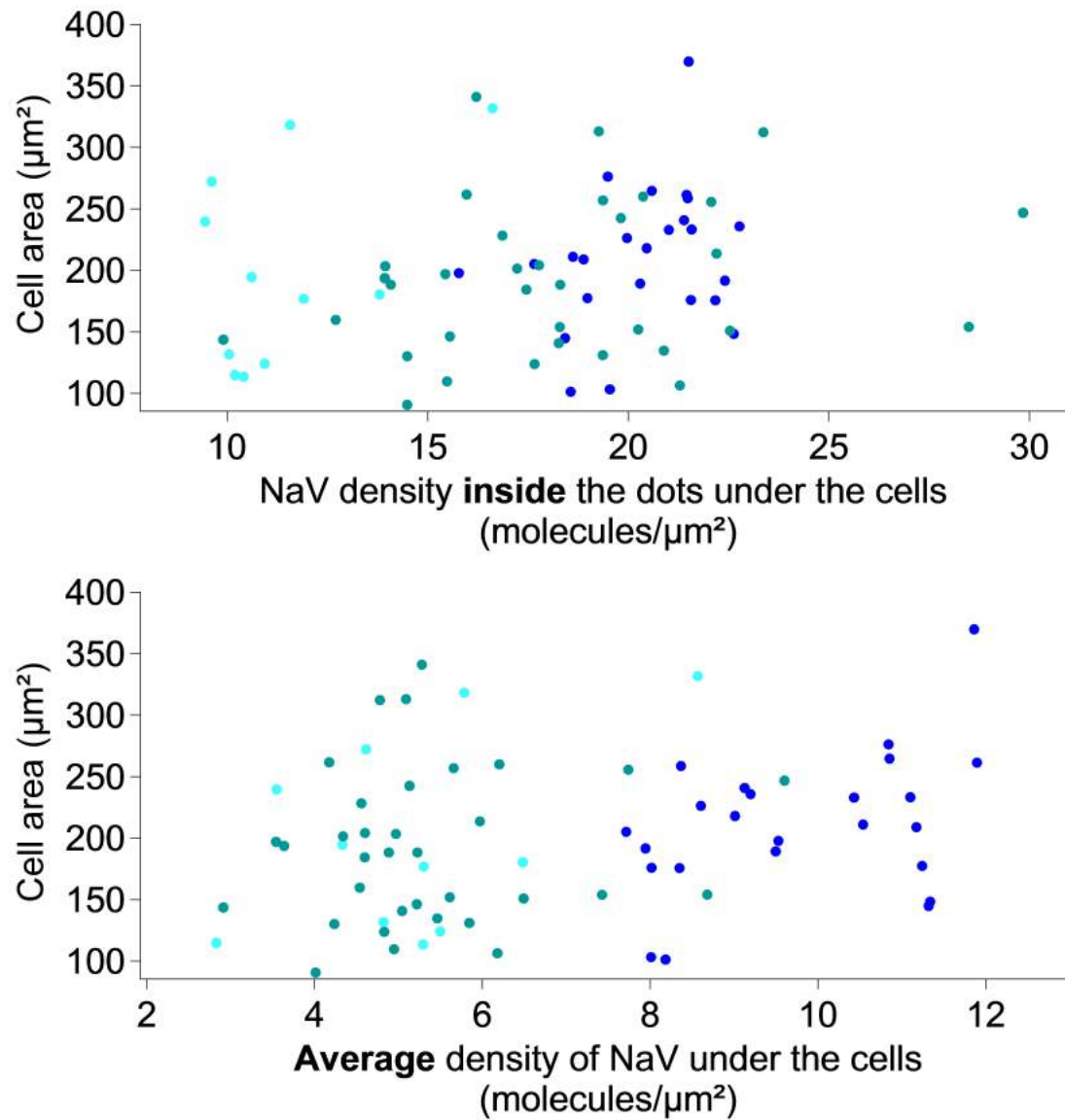
Figure 6.5: **Impact of variation of NaV density on cell area on [ICAM-1]$_{SLB}$ [αCD3]$_{Dot}$.** Cell adhesion area of Jurkat T-cells after 30 minutes engagement versus the NaV density under the cell is plotted. Each point represents one cell. N=3;n=59.
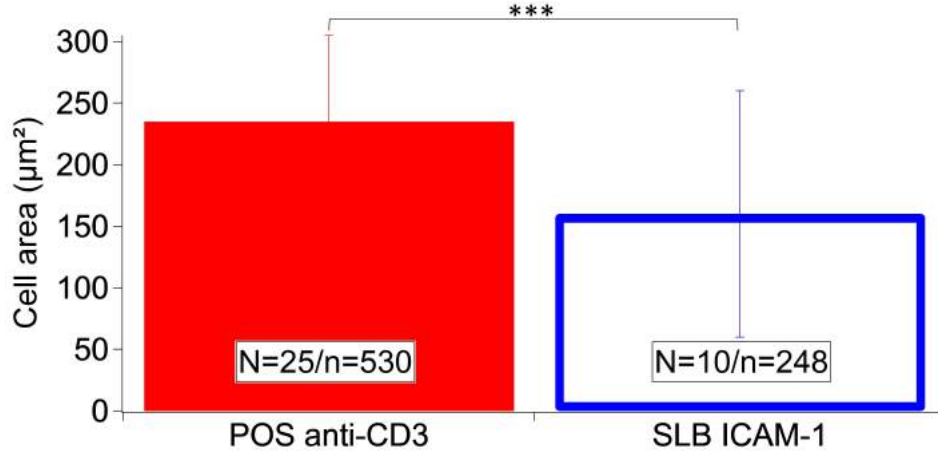
Figure 6.6: **Cells area on homogeneous controls for [ICAM-1]$_{SLB}$ [αCD3]$_{Dot}$ substrates (also called ICAM-1 • anti-CD3).** Area measurement of Jurkat T cells after 30 minutes engagement on substrates. Error bars represent standard deviations.***=p<0.001.
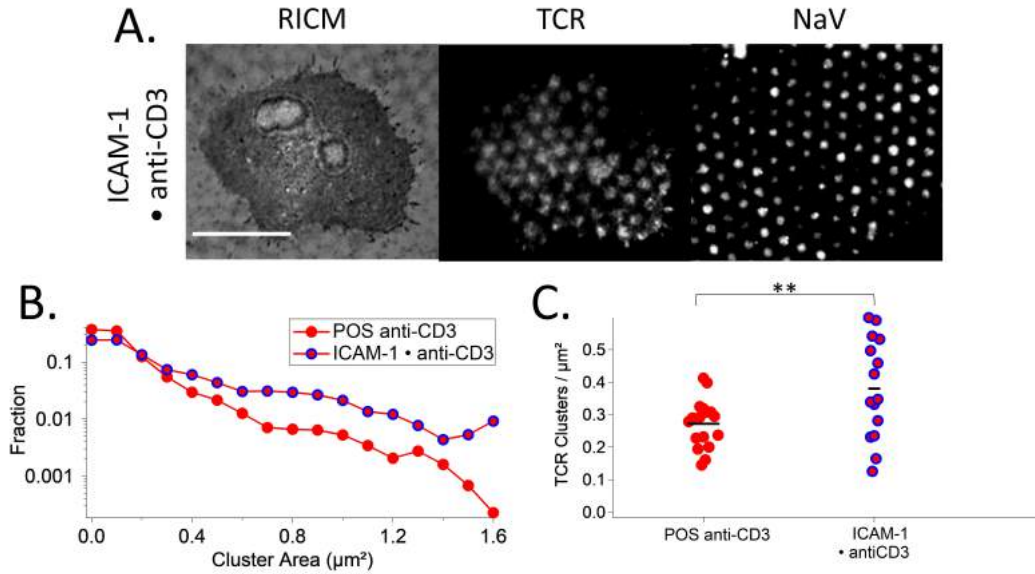
Figure 6.7: **TCR clusters of T-cells spreading POS anti-CD3 substrate and on [ICAM-1]$_{SLB}$ [αCD3]$_{Dot}$ substrate (also called ICAM-1 • anti-CD3).** A: RICM, TIRF-M and epi-fluorescent images of Jurkat cell after 30 minutes engagement on homogeneous and patterned substrates.For TIRF-M images TCR was marked. Scale bar: 10μm. B: Histogram of the apparent area of clusters normalized by the total number of clusters. Clusters of larger size corresponding to the underlying anti-CD3 dots(0.4 μm^2) are enriched for [ICAM-1]$_{SLB}$[αCD3]$_{Dot}$. C: Scatter dot plot of the number of clusters per μm^2. **=0.001<p<0.01..
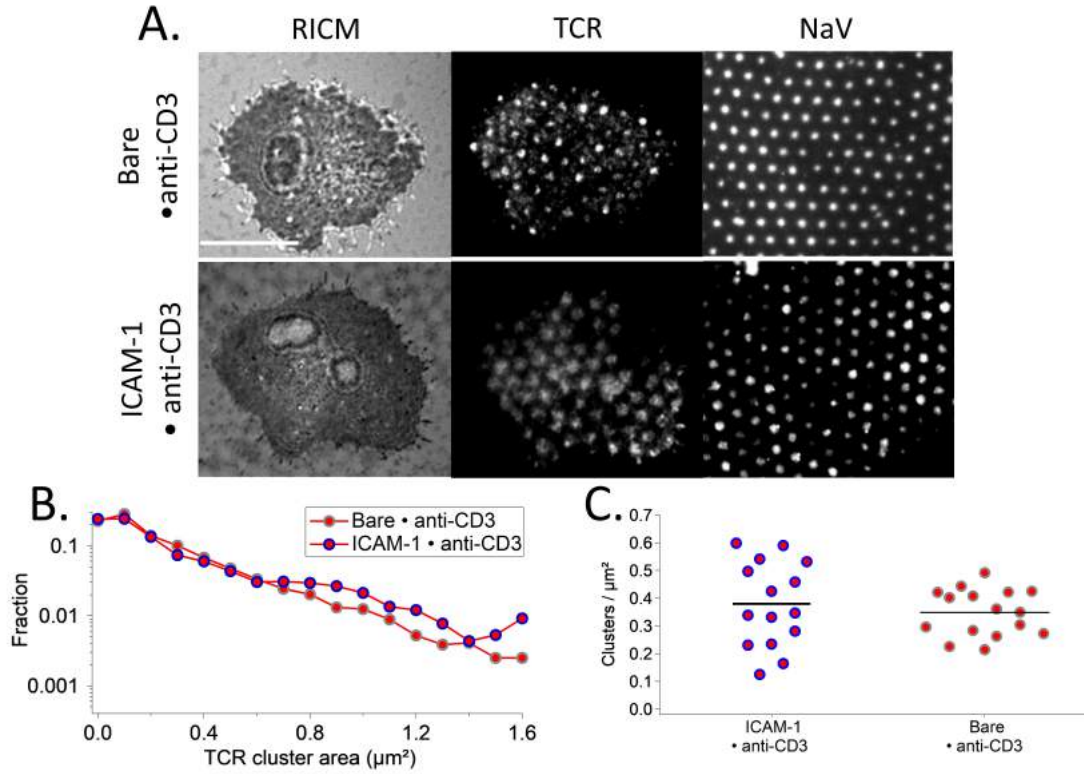
Figure 6.8: **TCR clusters of T-cells spreading on [Bare]$_{SLB}$ [αCD3]$_{Dot}$ and [ICAM-1]$_{SLB}$ [αCD3]$_{Dot}$ (also called Bare • anti-CD3) and ICAM-1 • anti-CD3.** A: RICM, TIRF-M and epi-fluorescent images of Jurkat cell after 30 minutes engagement on patterned substrates. Scale bar: 10μm. B: Histogram of the apparent area of clusters normalized by the total number of clusters. C: Scatter dot plot of the number of clusters per μm^2.

Figure 6.8 compares the substrates [ICAM-1]$_{SLB}$[αCD3]$_{Dot}$ and [Bare]$_{SLB}$[αCD3]$_{Dot}$ to explicit the effect of ICAM-1. In both cases, TCR clusters follow the pattern faithfully, independently of the presence of ICAM-1 on the SLB. Quantification on the histogram presented on Figure 6.8B shows that with ICAM-1 on the SLB there is an enrichment for TCR clusters with an area superior to the 0.7-0.8 μm^2. This threshold value is twice the size of the underlying pattern (0.4 μm^2) meaning that the presence of adhesion molecules outside the dots allows the TCR to form bigger clusters. Figure 6.8C shows that overall TCR cluster density is not influenced by the presence of ICAM-1 on the SLB.

6.1.2.2 ZAP-70 clusters

Visual inspection of the TIRF-M images show the presence of small as well as big clusters which are very bright (see an example in Figure 6.9A). Composite image of ZAP-70 (in red) and the underlying NaV pattern (in green) shows that the big and bright clusters co-localized well with the pattern (yellow spots) whereas the smaller dots are distributed randomly, showing that the ZAP-70 clusters are not completely co-localized with the
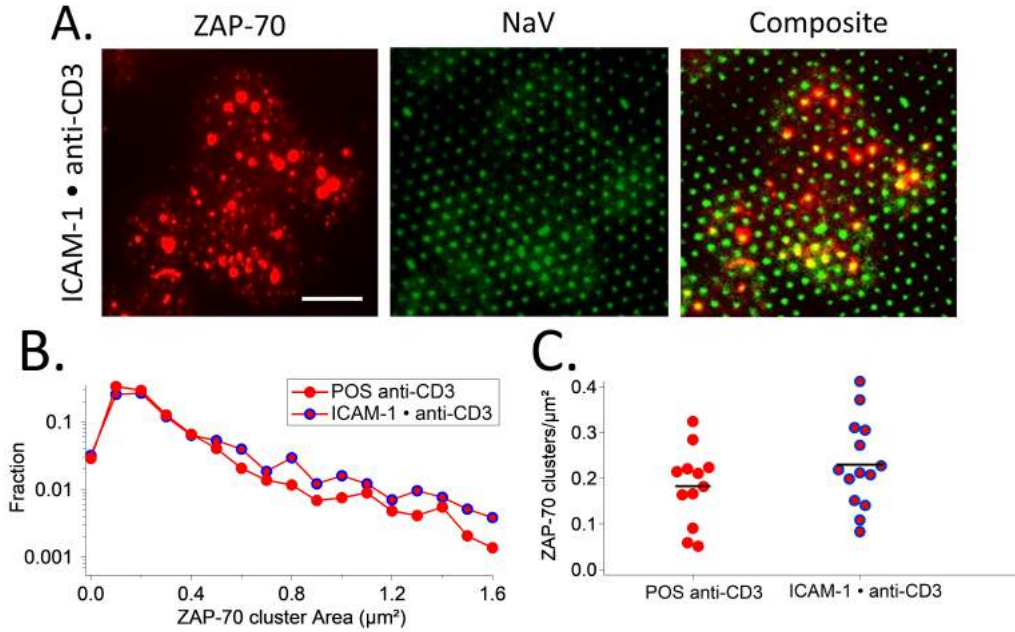
Figure 6.9: **ZAP-70 clusters of T-cells spreading on $[\text{ICAM-1}]_{SLB}$ $[\alpha\text{CD3}]_{Dot}$ (also called ICAM-1 • anti-CD3).**A: TIRF-M and epi-fluorescent images of Jurkat cell after 30 minutes engagement on $[\text{ICAM-1}]_{SLB}$ $[\alpha\text{CD3}]_{Dot}$. Composite image is constituated of the TIRF-M image of ZAP-70 in red and of epi-fluorescent image of NaV. Scale bar=$10\mu m$. B:Histogram of the apparent area of clusters normalized by the total number of clusters. C: Scatter dot plot of the number of clusters perμm^2.

underlying NaV pattern. Quantification demonstrated that as on POS anti-CD3 on $[\text{ICAM-1}]_{SLB}[\alpha\text{CD3}]_{Dot}$ there is a high fraction of cluster with an small area (comprise between 0-0.3μm^2), but there is also an enrichment of clusters with a size range of 0.8-0.9 μm^2. This size value is twice the size of the underlying pattern. These clusters correspond to the big and bright clusters observed during the visual inspection. Density of ZAP-70 clusters are comparable for POS anti-CD3 and $[\text{ICAM-1}]_{SLB}[\alpha\text{CD3}]_{Dot}$ but both are a bit lower than the density of TCR clusters.

Figure 6.10 compares the substrates $[\text{ICAM-1}]_{SLB}[\alpha\text{CD3}]_{Dot}$ and $[\text{Bare}]_{SLB}[\alpha\text{CD3}]_{Dot}$ to explicit the effect of ICAM-1. ZAP-70 clusters follow mostly the pattern on $[\text{Bare}]_{SLB}$ $[\alpha\text{CD3}]_{Dot}$ whereas on $[\text{ICAM-1}]_{SLB}$ $[\alpha\text{CD3}]_{Dot}$ only the bigger clusters co-localized with the pattern dots. Moreover, in presence of ICAM-1, the proportion of ZAP-70 molecules homogeneously distributed over the cell membrane is higher. These results differ with the result obtained previously concerning TCR clustering where the TCR clusters were highly co-localized with the underlying pattern. Quantification of the cluster area shown in Figure 6.10B shows an enrichment of small clusters for $[\text{ICAM-1}]_{SLB}$ $[\alpha\text{CD3}]_{Dot}$ (0.1-0.3 μm^2). For the clusters size range corresponding to the size of the underlying pattern (0.3-0.5 μm^2) no difference is observed, but for cluster size superior to 0.5-0.6 μm^2 range, there is an enrichment for $[\text{Bare}]_{SLB}$ $[\alpha\text{CD3}]_{Dot}$. Density of ZAP-70 clusters is similar with or without ICAM-1 in the SLB and is around 0.2 clusters/ μm^2. This value is half the density of TCR clusters which means that there is 1 ZAP-70 cluster for 2 TCR

162

clusters.

6.1.3   Actin Cytoskeleton organization in presence of adhesive ligands

Following chapter 5, the structure and dynamics of actin organization was studied either by staining fixed cells with FITC-conjugated phalloidin or by live observation of LifeAct-GFP transfected cells, both imaged in TIRF-M. The actin parameter is defined as before and it is considered that if $0<p<0.5$, the actin is peripherally distributed, if $0.5<p<1.5$, the actin is homogeneously distributed and if $p>1.5$, the actin is centrally distributed.

Figure 6.11A shows the 2 different types of actin architecture observed on the patterned substrate $[\text{ICAM-1}]_{SLB}$ $[\alpha\text{CD3}]_{Dot}$. The actin organization can be either peripheral (1.) or homogeneous (2.), as is the case for POS anti-CD3 (see section 5.3). However the predominance of the peripheral organization is shown in Figure 6.11B-C, where the actin parameter drops from 0.8 on POS anti-CD3 to 0.5 on $[\text{ICAM-1}]_{SLB}$ $[\alpha\text{CD3}]_{Dot}$ Figure 6.11(B), and where 71% of the cells have a actin parameter below 0.5 Figure 6.11(B). Next, relation between the actin parameter and the cell area or NaV density was tested. Figure 6.11D shows that on $[\text{ICAM-1}]_{SLB}$ $[\alpha\text{CD3}]_{Dot}$ the actin architecture is not related to the cell adhesion area or to the NaV average density.

We were next interested in the modification of the actin organization by the presence of adhesion molecule ICAM-1 in the SLB on patterned substrates. As presented on Figure 6.12A the actin changes its organization from patterned/homogenous to consistently peripheral in presence of ICAM-1 on the substrate. This shift is attested in Figure 6.12B and C where the actin parameter drop significantly from 1.2 to 0.5 with ICAM-1 (B.) and where the percentage of cells presenting peripheral actin architecture increase from 2% to 71% (C.).

Interestingly by looking to the actin dynamics on patterned substrate containing ICAM-1 in the SLB, formation of actin patches is observed which finally disappear to form a peripheral ring (cell A in Figure 6.13). These structures pointed to the fact that the actin structure is organized at early stage by the TCR ligand and at late time by LFA-1.

6.1.4   Clustered versus homogeneous distribution of anti-CD3 in presence of ICAM

In analogy with a similar approach in chapter 5, this section seeks to access the real impact of ligand clustering by comparing substrates with equivalent ligand densities on patterned or homogeneous substrates. As before, results obtained for cell adhesion area, TCR clusters distribution and actin cytoskeleton architecture will be presented.

Adhesion area: As shown on Figure 6.14, the cell spreading area increases significantly when anti-CD3 molecules are presented in clusters in a sea of ICAM-1. Comparing with results presented in the previous chapter (see section 5.4), in absence of ICAM-1 T-cell spreading is not affected by the TCR ligand clustering whereas with ICAM-1 on the SLB the fact that TCR ligand are presented as clusters induces clearly a larger spreading area. This means that the extent of spreading is determined by the clustering of TCR ligand rather than the average ligand-density. Cell by cell analysis was done and showed the
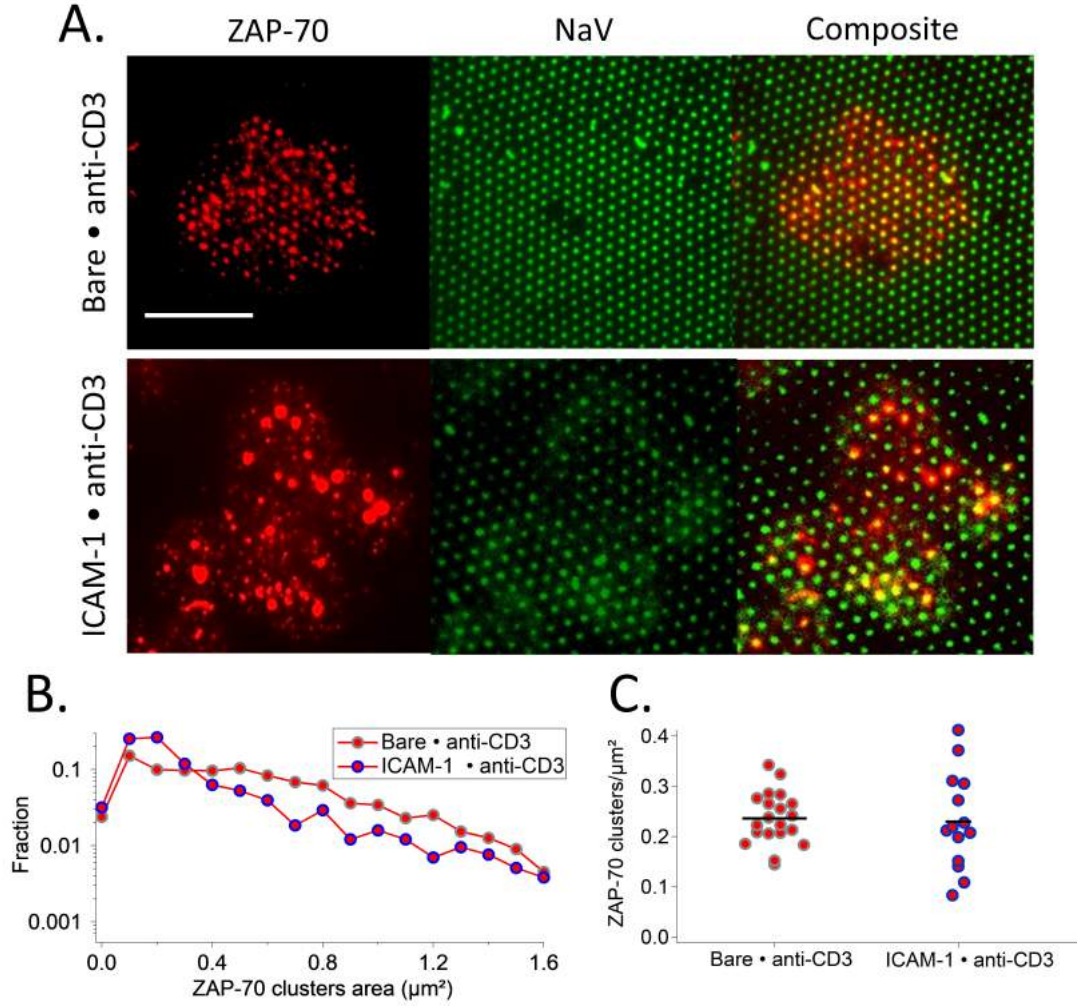
Figure 6.10: **ZAP-70 clusters of T-cells spreading on [ICAM-1]$_{SLB}$ [αCD3]$_{Dot}$ and on [Bare]$_{SLB}$ [αCD3]$_{Dot}$.** A:TIRF-M images of ZAP-70, epi-fluorescent images of NaV and merging images of ZAP-70 (in red) and NaV (in green) showing the colocalisation between the dots of the pattern and the ZAP-70 molecules on Jurkat cell after 30 minutes engagement on [ICAM-1]$_{SLB}$ [αCD3]$_{Dot}$ and [Bare]$_{SLB}$ [αCD3]$_{Dot}$. Scale bar=10μm. B:Histogram of the apparent area of clusters normalized by the total number of clusters. C: Scatter dot plot of the number of clusters perμm^2.
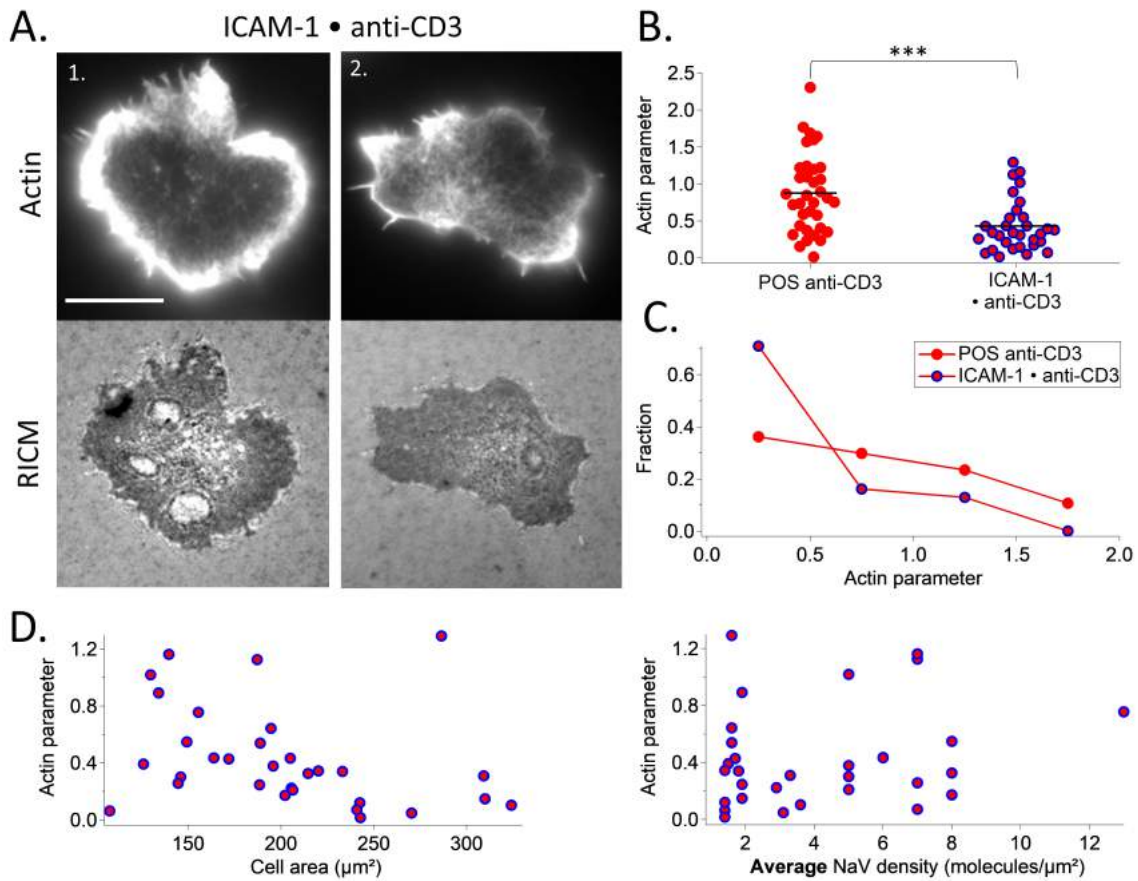
Figure 6.11: **Actin Cytoskeleton organization of T-cells spreading on POS anti-CD3 and [ICAM-1]$_{SLB}$ [αCD3]$_{Dot}$ substrates (also called ICAM-1 • anti-CD3).** A:RICM and TIRF-M images Jurkat cell after 30 minutes engagement on patterned substrates. For TIRF-M images Actin was marked. Scale bar: 10μm. B: Scatter dot plot of actin parameter. C: Histogram of the actin parameter normalized by the total number of analyzed cells. D: Relation between actin parameter and cell adhesion area and NaV average density on [ICAM-1]$_{SLB}$[αCD3]$_{Dot}$. ***=p<0.001.
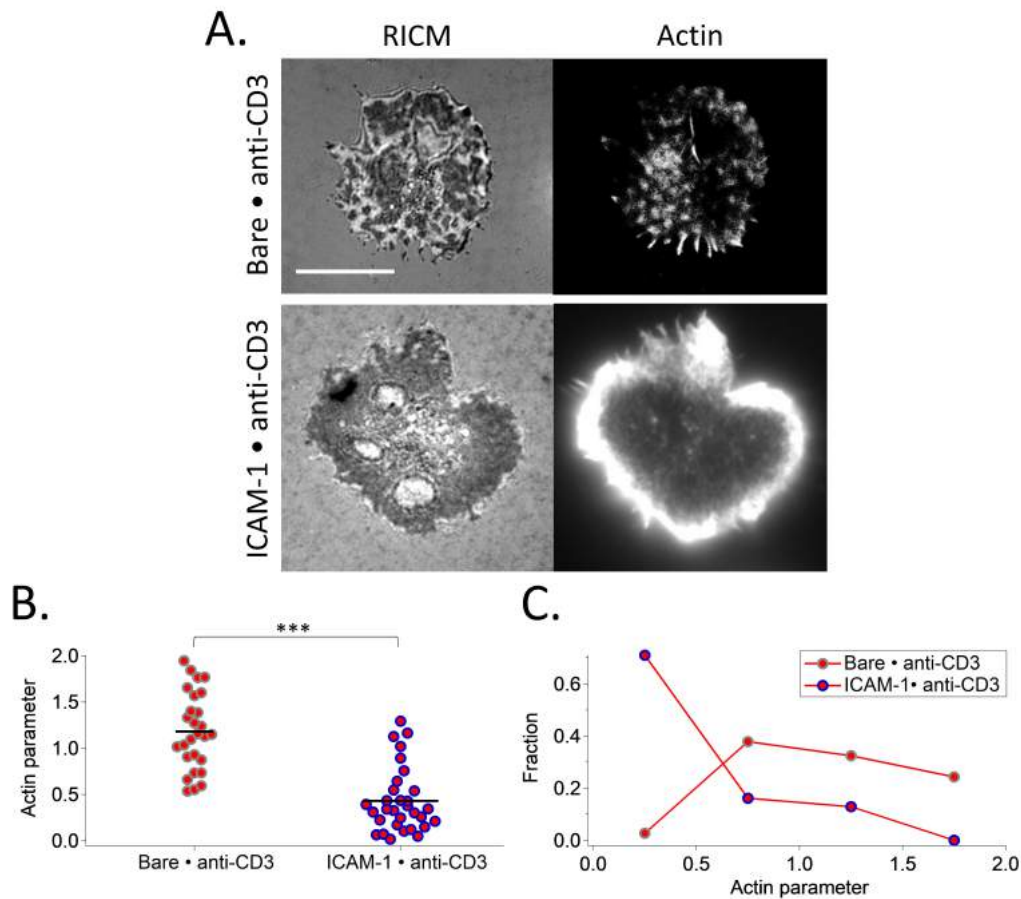
Figure 6.12: **Actin Cytoskeleton organization of T-cells spreading on [ICAM-1]$_{SLB}$ [αCD3]$_{Dot}$ and on [Bare]$_{SLB}$ [αCD3]$_{Dot}$ (also called ICAM-1 • anti-CD3 and Bare • anti-CD3).** A: A:RICM and TIRF-M images of Jurkat cell after 30 minutes engagement on patterned substrates. For TIRF-M images Actin was marked. Scale bar: 10μm. B: Scatter dot plot of actin parameter. C: Histogram of the actin parameter normalized by the total number of analyzed cells. ***=p<0.001.
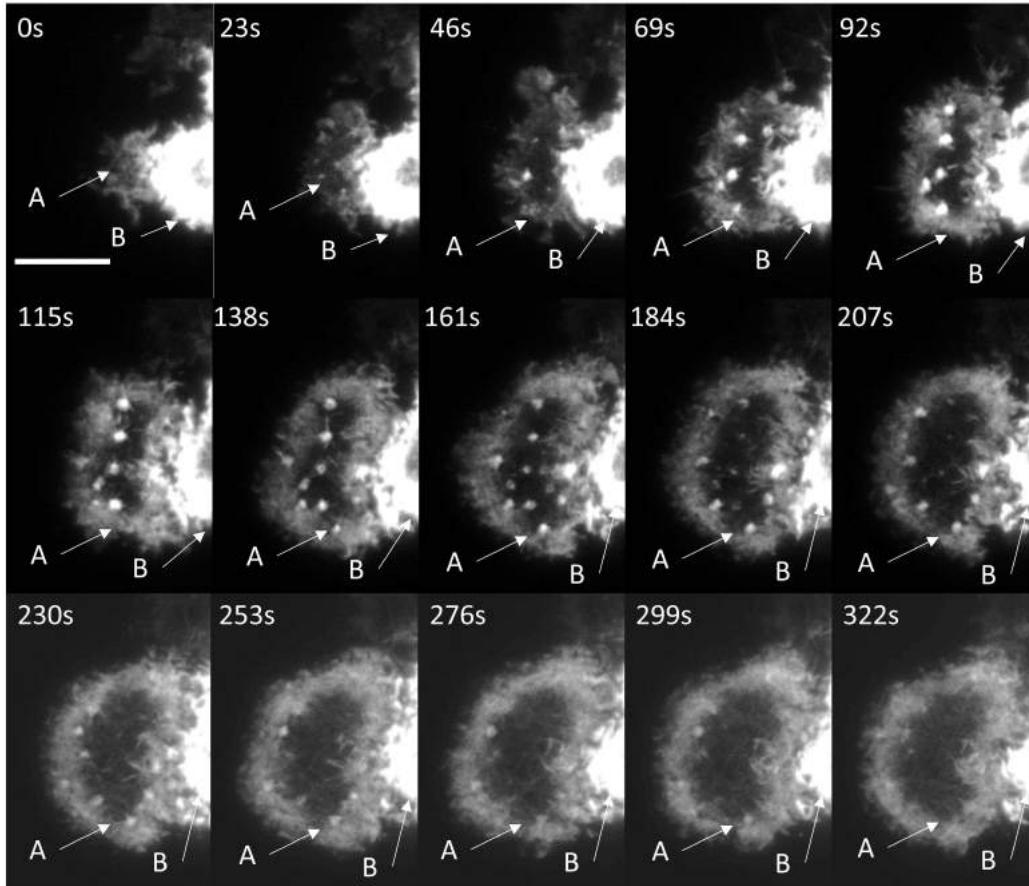
Figure 6.13: **Dynamics of actin organization of Life-Act cells during cells engagement on ICAM-1• anti-CD3.**TIRF-M time-sequence of actin organization during cell adhesion from first surface contact to the stabilization of the spreading (A). Actin patches appear and disappear during the interaction. Scale bar: 10 μm

Analyses / Substrates	Cell spreading area (μm^2)	Actin organization	TCR distribution
SLB Neg1+anti-CD3	155±70	Homogeneous	Homogeneous
Bare • αCD3	220±100 (↑)	Patterned	Patterned
SLB ICAM-1+anti-CD3	120±60	Homogeneous/Peripheral	Homogeneous
ICAM-1 • αCD3	207±60 (↑↑)	Peripheral	Patterned

Table 6.1: **Impact of anti-CD3 patterning** Summary of results obtained on homogeneous substrates and substrates presenting nano-clusters of anti-CD3, with (SLB Neg1+anti-CD3 and Bare •α CD3 respectively) or without ICAM-1 in the bilayer (SLB ICAM-1+anti-CD3 and ICAM-1 •α CD3 respectively). (↑) indicates a small significant difference for cell spreading area between SLB Neg1+anti-CD3 and Bare • anti-CD3. (↑↑) indicates a significant difference for cell spreading area between SLB ICAM-1 + anti-CD3 and ICAM-1 • anti-CD3. The number of experiments and cells are as followes: SLB Neg1+anti-CD3: N=2/n=16; Bare • anti-CD3 N=2/n=30, SLB ICAM-1+anti-CD3: N=4/n=69; ICAM-1 • anti-CD3: N=4/n=53.

same trend (Figure 6.15).

TCR clusters distribution: As shown on Figure 6.16A, TCR distribution is highly influenced by the patterning of anti-CD3 both in absence and in presence of ICAM-1. The presence of underlying nano-dots of TCR-ligand induced a reorganization of TCR molecules which change from homogeneous to co-localized with pattern. Histogram presented in Figures 6.16B-C shows an enrichment from cluster area of 0.2-0.3 μm^2 for substrates without ICAM-1 (Figure 6.16B, reproduced from previous chapter for convenience). For substrates with ICAM-1 there is a slight enrichment from cluster area of 0.4-0.5 μm^2 which increases from clusters of 0.6-0.7 μm^2.

Actin cytoskeleton organization: Visual inspection of the actin distribution on substrates where ICAM-1 and anti-CD3 are presented on the surface shows a small difference between the clustered and homogeneous case. In both cases the actin is depleted at the center and enriched at the periphery. Nevertheless this peripheral distribution is less clear in cells on homogeneous substrates (Figure 6.17A). Actin parameter supports this difference with an average actin parameter equals to 0.6 for homogeneous and to 0.4 for patterned substrates (Figure 6.17B). Moreover the histogram presented in Figure 6.17C indicates that for homogeneous substrates there are as many cells with an peripheral distribution (actin range 0-0.5) as with homogeneous distribution (0.5-1.5) whereas for patterned substrates the majority of cells present a peripheral distribution.

6.2 Adhesion and surface passivation

As reported in section 5.1.1 and 6.1.1.1, for both [Bare]$_{SLB}$ [anti-CD3]$_{Dot}$ and [ICAM-1]$_{SLB}$ [anti-CD3]$_{Dot}$, the cell area was independent of surface ligand density. This sur-
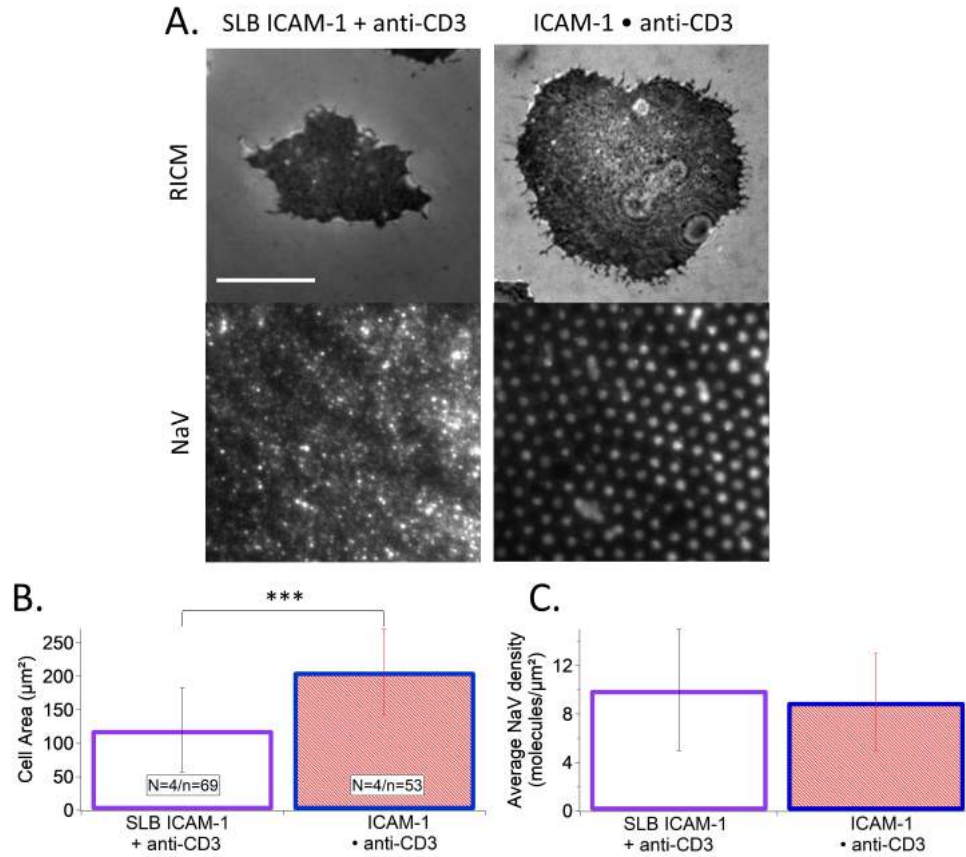
Figure 6.14: **Cell spreading area on patterned substrates [ICAM-1]**$_{SLB}$
[αCD3]$_{Dot}$ **(also called ICAM-1 • anti-CD3) and on homogeneous substrates**
SLB ICAM-1 + anti-CD3. A: A:RICM images Jurkat cell after 30 minutes engage-
ment on patterned substrates and epi-fluorescence images of the underlying organization
of NaV. Scale bar: $10\mu m^2$. B: Cells area measurement. C: Quantification of average
NaV density. On both substrates, NaV density is around 10 molecules/μm^2. Error bars
represent standard deviations. ***=p<0.001.
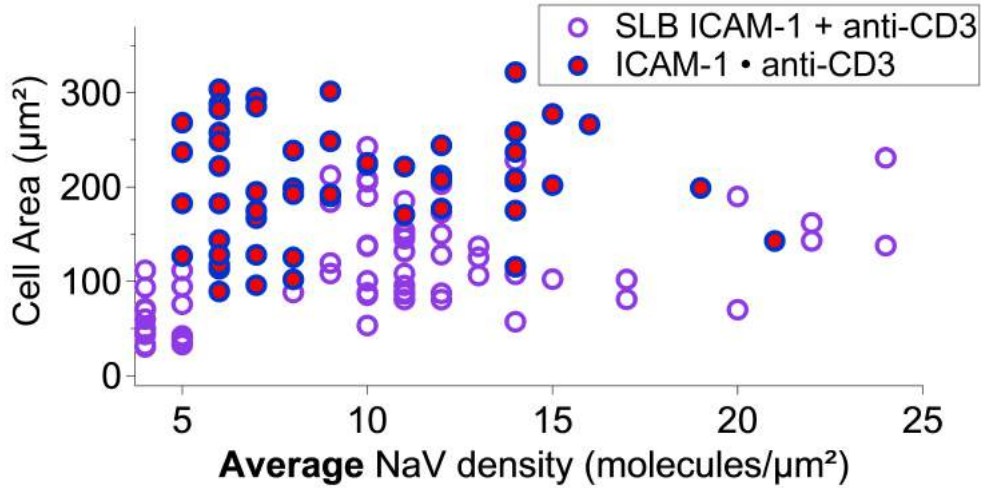
Figure 6.15: **Cell spreading area on patterned and homogeneous substrates according the NaV density.** Cell spreading area of Jurkat T-cell after 30 minutes engagement on [ICAM-1]$_{SLB}$ [αCD3]$_{Dot}$ (also called ICAM-1$\bullet$ anti-CD3) and on homogeneous SLB ICAM-1 + anti-CD3 according NaV density under each cells.Each points represent one cell.

prising result was attributed to a lack of adequate passivation of the area in-between the activating nano-dots. To study this point in detail, experiments with PEG molecule in the SLB were undertaken (see section 3.4.2.5 for details of SLB fabrication). PEG is known to enhance the passivating effect of the SLB and can be considered to mimic the glycocalyx [19]. In the previous chapter it was shown that on patterned substrates, cell adhesion can be either homogeneous or patterned. In the first case the cell membrane is flat and adheres completely to the surface, whereas in the second case cell membrane adheres mostly on the underlying pattern which induces a membrane topography revealed on RICM images. This section will focus on this modulation between repelling and adhesive area that can lead to membrane roughness detectable in RICM images. First analyses of dark area on different patterned substrates will be presented then impact of molecule PEG addition in the SLB will be presented.

Cell adhesion area: The area measured after 30 minutes of spreading is presented in Figure 6.18. For all substrates, addition of the repulsive polymer in the SLB induces a significantly decrease of the cell spreading area. This effect is present even in the presence of the adhesion molecule ICAM-1 outside the dots.

Cell membrane topography and TCR distribution: As shown previously, visual inspections of RICM images on [Bare]$_{SLB}$ [anti-CD3]$_{Dot}$ showed alternation of bright zones (corresponding to a weak adhesion of the cell to the substrate) and darker zones (corresponding to a strong adhesion) indicating an effect of the ligand patterning. But on [ICAM-1]$_{SLB}$ [anti-CD3]$_{Dot}$ this induced topography is not present. Dark area analysis was undertaken to quantify the RICM images. The dark area was determined by intensity thresholding of the segmented RICM image. The ratio dark Area/total cell area was
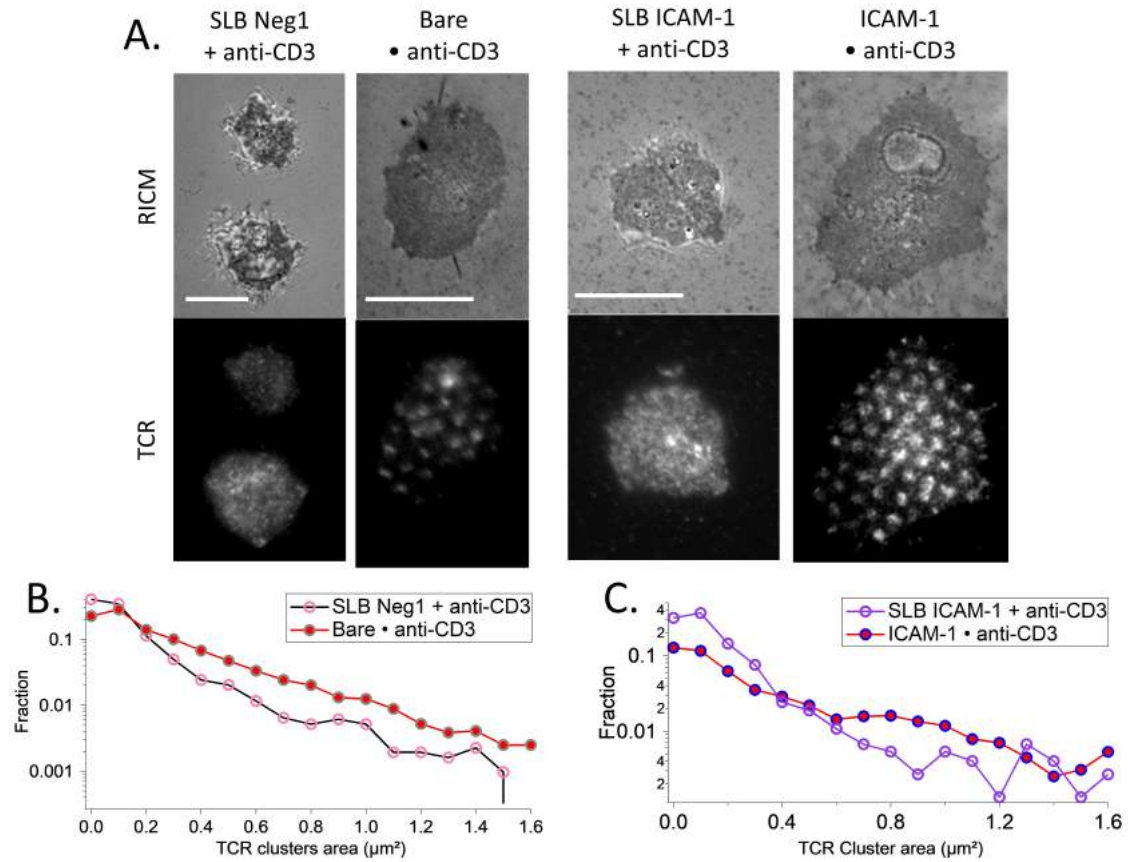
Figure 6.16: **TCR clusters of T-cells spreading on patterned and homogeneous substrates.** A:RICM and TIRF-M images of Jurkat cell after 30 minutes engagement on $[\text{ICAM-1}]_{SLB}$ $[\alpha\text{CD3}]_{Dot}$ and $[\text{Bare}]_{SLB}$ $[\alpha\text{CD3}]_{Dot}$ (also called ICAM-1• anti-CD3 and Bare• anti-CD3) and on homogeneous SLB ICAM-1 + anti-CD3 and SLB Neg1+anti-CD3. Scale bar: 10μm. B-C: Histogram of the apparent area of clusters normalized by the total number of clusters.
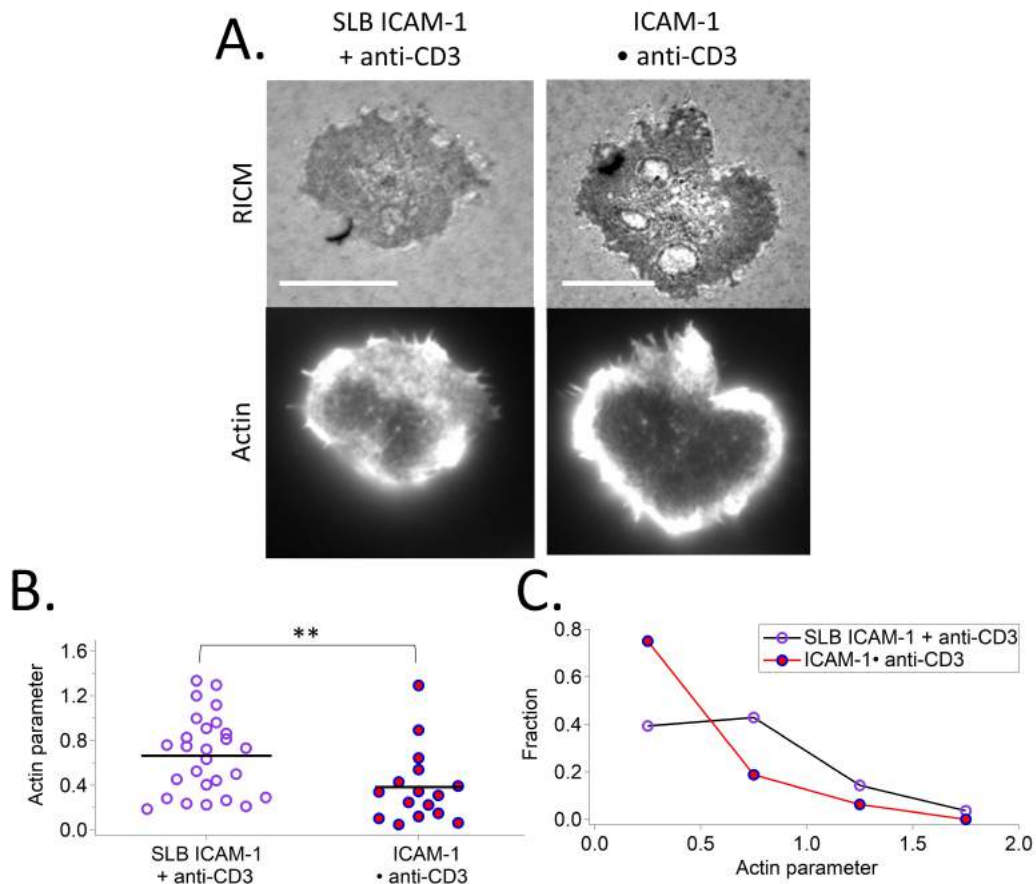
Figure 6.17: **Actin cytoskeleton organization on patterned substrates [ICAM-1]$_{SLB}$ [αCD3]$_{Dot}$ (also called ICAM-1 • anti-CD3) and on homogeneous substrates SLB ICAM-1 + anti-CD3.** A: RICM images Jurkat cell after 30 minutes engagement on patterned substrates and TIRF-M images of the actin cytoskeleton. Scale bar: $10\mu m^2$. B: Scatter dot plot of actin parameter. C: Histogram of the actin parameter normalized by the total number of analyzed cells.
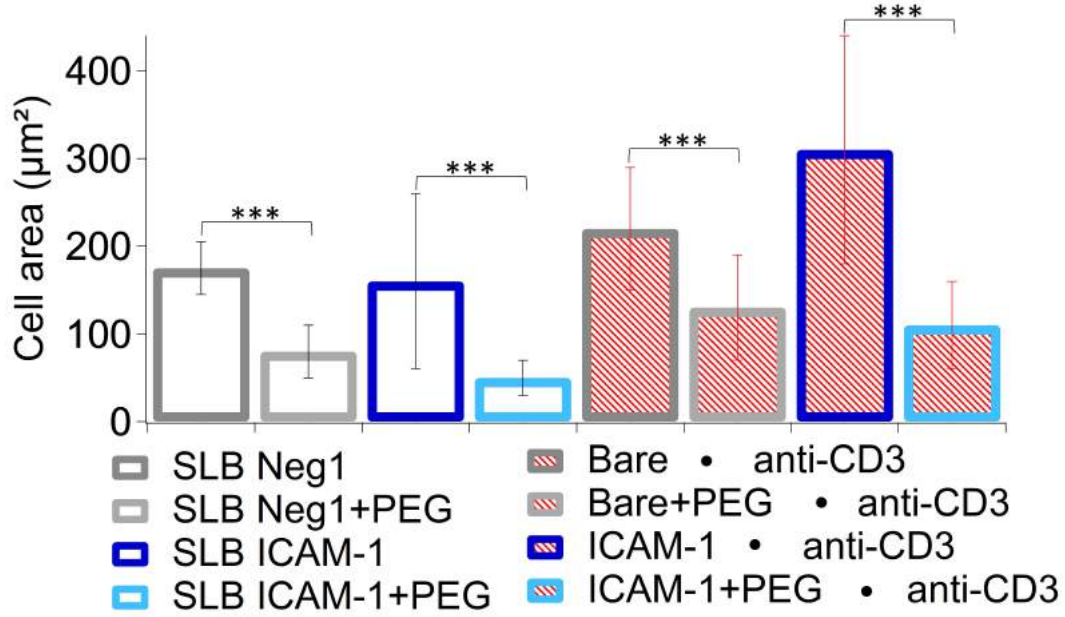
Figure 6.18: **Spreading area of Jurkat T-cells on substrates with or without PEG in the SLB.** Error bars represent standard deviations. ***=p<0.001.

calculated in order to normalize and compare each cell. Analyses were done on patterned substrates with non activating pattern (nano-dots were composed with an isotype control antibody or with BSA-biotin) and on patterned substrates with activating pattern ([Bare]$_{SLB}$ [anti-CD3]$_{Dot}$ and [ICAM-1]$_{SLB}$ [anti-CD3]$_{Dot}$). Visual inspection of RICM images (Figure 6.19A) shows an example where the membrane topography is visible when there is PEG in a bare SLB but not when there is PEG in SLB functionalized with ICAM-1. However, as is shown in Figure 6.20, quantification reveals that there is a large variation in dark-area ratio from preparation to preparation and PEG does not have a significant impact on the topography. There is however a significant difference between [Bare]$_{SLB}$ [anti-CD3]$_{Dot}$ and [ICAM-1]$_{SLB}$ [anti-CD3]$_{Dot}$. In presence of ICAM-1 as well as PEG, the membrane appears flat but the cell is adhered weakly at the edge which drives the dark-are ratio down in some cases.

As shown previously on [Bare]$_{SLB}$ [anti-CD3]$_{Dot}$ visual inspection indicated that there are 43% of patterned cells and addition of PEG in the SLB does not change a lot this proportion (40%). In term of dark area ratio there is also no difference with the addition of PEG in the SLB. However, addition of PEG induce a significant difference when there is ICAM-1 on the SLB. With only ICAM-1 on the SLB the dark area ratio is around 0.75 when with ICAM-1+PEG this ratio is around 0.66. This decrease can reflect the fact that with PEG the cell membrane is not totally flat.

As presented at the bottom left panel of the Figure 6.20 on substrates with non-activating pattern, the dark area ratio can vary between 0.3 and 0.8 and depending on the nature of the adhesive patch the dark area ratio is different. On substrates with anti-CD3 pattern there a difference between substrates with ICAM-1 on SLB or not. Indeed with ICAM-1 the ratio of Dark area is around 0.75 whereas with Bare SLB the ratio decrease
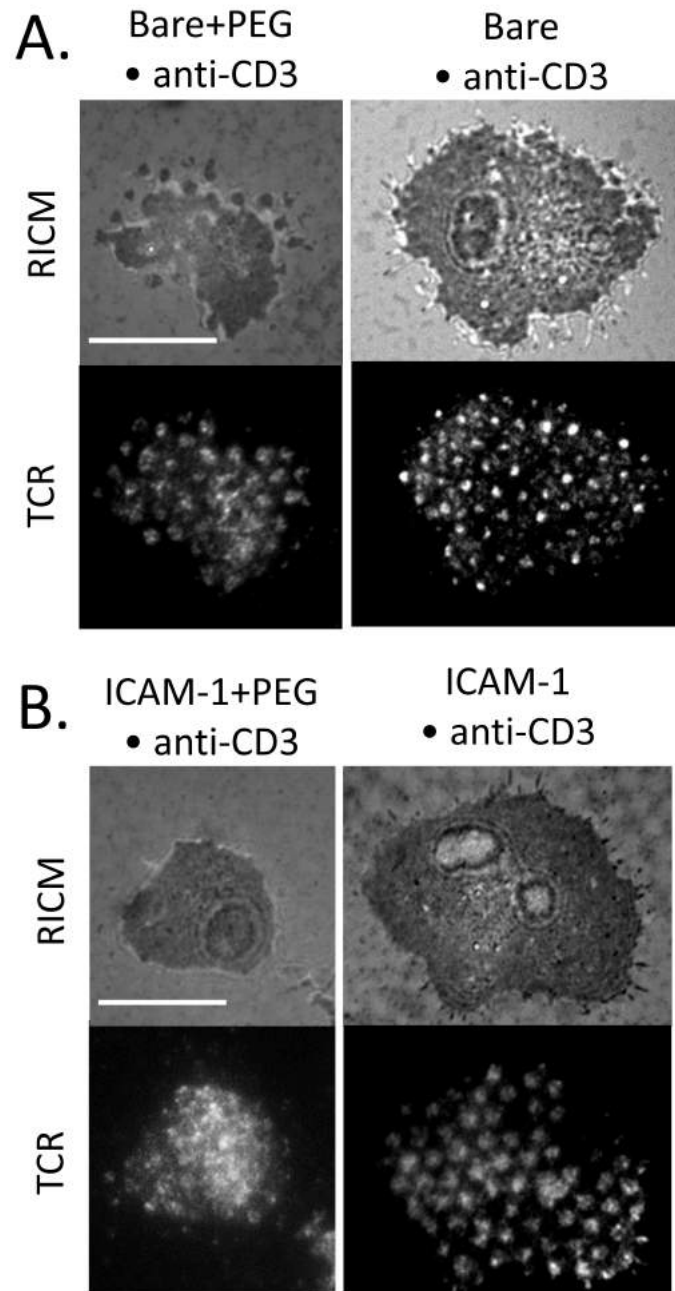
Figure 6.19: **RICM images and TCR clusters of T-cells spreading on patterned substrates with nano-dots of anti-CD3 surrounded by non-functionalized SLB and SLB functionalized with ICAM-1 and/or PEG.** A: RICM, TIRF-M and epi-fluorescent images of Jurkat cell after 30 minutes engagement on $[\text{Bare}]_{SLB}$ $[\alpha\text{CD3}]_{Dot}$ and $[\text{Bare+PEG}]_{SLB}$ $[\alpha\text{CD3}]_{Dot}$ (also called Bare • anti-CD3 and Bare+PEG • anti-CD3) . B: RICM, TIRF-M and epi-fluorescent images of cell spreading on $[\text{ICAM-1}]_{SLB}$ $[\alpha\text{CD3}]_{Dot}$ and $[\text{ICAM-1+PEG}]_{SLB}$ $[\alpha\text{CD3}]_{Dot}$ (also called ICAM-1 • anti-CD3 and ICAM-1+PEG • anti-CD3). As for A. for TIRF-M images TCR was marked. Scale bar: 10μm.
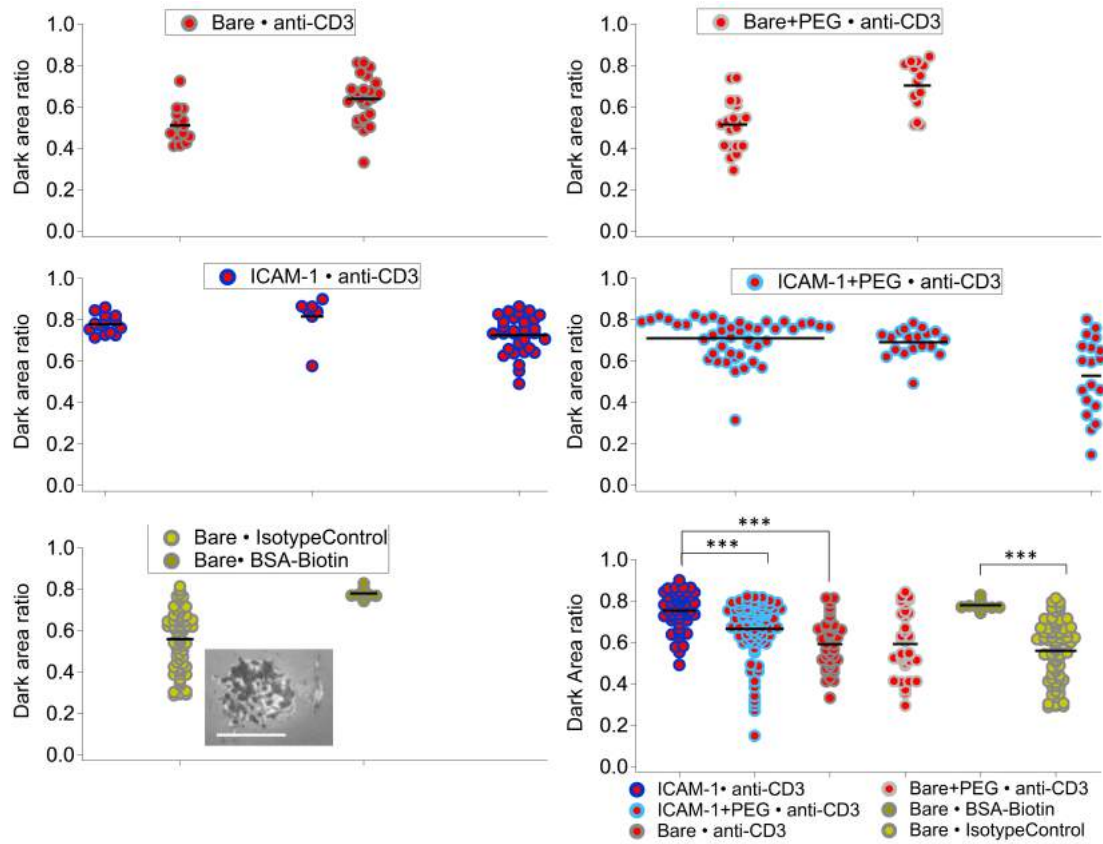
Figure 6.20: **Dark area analyses on different patterned substrates.** Analyses were made on RICM images ant the ratio Dark area/total cell area is calculated. Each scatter dot plot represents one experiment except for the one on below right where each scatter dot plots represent the total data of each substrates. In inset of the bottom left graph RICM image of a patterned T-cell on Bare• Isotype control is represented. ***=p<0.001.

to 0.66 (see Figure 6.20). This is a consistent result with the visual observation where on patterned substrate with ICAM-1 on the SLB cells are homogeneously spread with a flat membrane whereas with a Bare SLB a patterned topography of the membrane is observed meaning that the membrane strongly adhere only on the adhesive dots reducing the dark area.

In terms of TCR, as shown on Figure 6.19A with SLB with only PEG outside the dots TCR clusters still follow the underlying pattern of anti-CD3. Whereas with SLB functionalized with ICAM-1 the presence of PEG prevents good overlap between TCR and anti-CD3 dots.

Cell surface polymers: focus on CD45: After showing the impact of PEG on the cell membrane adhesion, the focus was on understanding the role of the polymers on the cell surface, focusing on the membrane molecular distribution of the glycoprotein CD45. CD45 is a large glycoprotein present normally in the dSMAC of the immune synapse (see Figure 1.14). We labeled the T-cell CD45 to see it's distribution on patterned substrate in presence of PEG. Visual inspection showed that CD45 is homogeneously distributed but if we look closer in the periphery of the cell where cell membrane adheres to the underlying dots (showing by red arrows on the images) it seems that there is a ring of CD45 around the dot (Figure 6.21), showing that CD45 may be excluded from the zone that adheres to the dots.

Actin organization: As shown on Figure 6.22 on $[\text{Bare+PEG}]_{SLB}$ $[\alpha\text{CD3}]_{Dot}$ actin distribution is quite similar as on $[\text{Bare}]_{SLB}$ $[\alpha\text{CD3}]_{Dot}$. There are actin organized in form of peripheral ring and actin organized in form of patches. Actin parameter is around 1 for the both type of substrates.

6.2.1 Cell membrane dynamics

In order to better understand the role of surface polymers, we also recorded the cell adhesion dynamics in RICM. First, records were done on $[\text{Bare}]_{SLB}$ $[\alpha\text{CD3}]_{Dot}$. On this substrate, the cell membrane may adhere to the underlying pattern alone, inducing a topography visible in RICM images. This was observed during the record as shown on the RICM time-sequence presented in Figure 6.23A. Examples of topography apparition are indicate with arrows. Moreover time-sequence presented in B. shows the spreading from the first contact to the stabilization of the spreading. It's shows that after 165 seconds of engagement the spreading is almost at the maximum (Table 6.2 summarized the data). This growth behavior is visible in Figure 6.23C. The growth curves were fitted with a tangent-hyperbolic function and the average time constant (τ) extracted from the fitting equals to 125±26 seconds. Note that it is very difficult to record the very first steps and therefore the zero of the time is variable and introduces errors.

Next, dynamics of cell spreading on $[\text{Bare+PEG}]_{SLB}$ $[\alpha\text{CD3}]_{Dot}$ was studied. On this substrate cell adhere slower than without PEG in the SLB with an average τ equals 280 ±76 seconds (Table 6.2. Moreover, cell have larger latency time before spreading facilitating a complete observation from first contact to stabilization of the spreading area. This can be observed on curves in Figure 6.24A, a red circle surround the part of a curve where a latency time is observed. Figure 6.24B shows RICM time-sequence where the image corresponding to a latency behavior is surrounded. Moreover, the cell
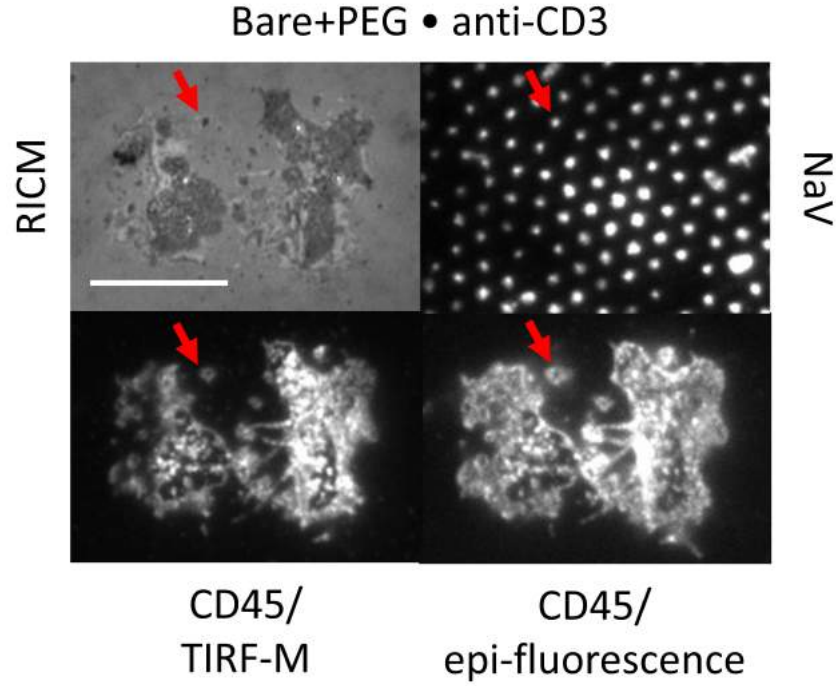
Figure 6.21: **CD45 distribution of T-cells spreading on [Bare+PEG]**$_{SLB}$ **[αCD3]**$_{Dot}$ **(also called Bare+PEG • anti-CD3) .**RICM, TIRF-M and epi-fluorescent images of Jurkat cell after 30 minutes engagement on [Bare+PEG]$_{SLB}$ [αCD3]$_{Dot}$. For TIRF-M images TCR was marked. Red arrows indicating an example where CD45 form a ring the dot. Scale bar: 10μm.
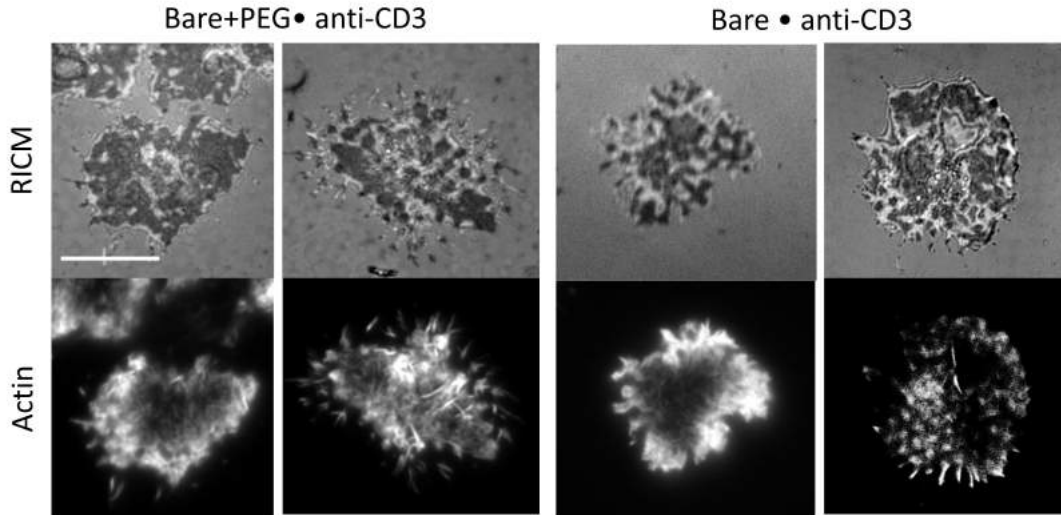
Figure 6.22: **Actin organization of T-cells spreading on [Bare]**$_{SLB}$ **[αCD3]**$_{Dot}$ **and [Bare+PEG]**$_{SLB}$ **[αCD3]**$_{Dot}$ **(also called Bare • anti-CD3 and Bare+PEG • anti-CD3).**RICM, TIRF-M and epi-fluorescent images of Jurkat cell after 30 minutes engagement on [Bare]$_{SLB}$ [αCD3]$_{Dot}$ and [Bare+PEG]$_{SLB}$ [αCD3]$_{Dot}$. For TIRF-M images Actin was marked. Scale bar: 10μm.
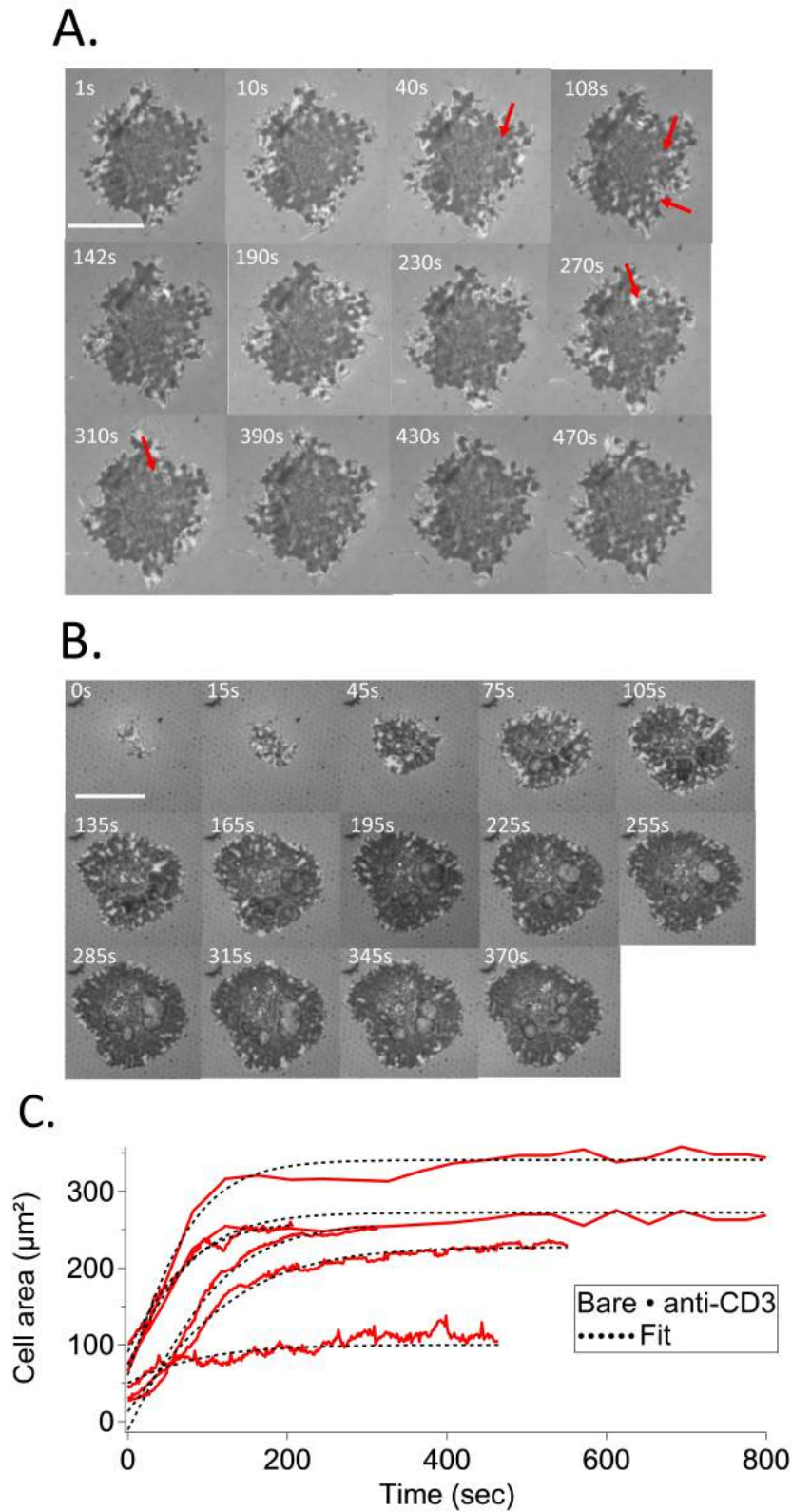
Figure 6.23: **Dynamics of cell spreading (RICM image sequence) on Bare •
anti-CD3.**A,B: RICM time-sequence during cell adhesion focusing on evolving mem-
brane topography (A) or the entire sequence (B). Red arrows show apparition of mem-
brane topography induce by the underlying pattern. Scale bar: 10 μm. C: Solid lines are
the cell area evolution and dashed lines are fits of the equation f(t) = A$_0$*tanh(t-t0/τ).
Average A$_0$ equals 240±80 μm² and τ equals 125±26 seconds.

Analyses Substrates	A_0 (μm^2) m±sd	τ (sec) m±sd	N/n
POS anti-CD3	233±24	125±63	3/4
Bare • anti-CD3	243 ±80	125 ±26†	5/6
Bare+PEG • anti-CD3	260 ±61	280 ±76 †	1/6

Table 6.2: **Summary of coefficients A_0 and τ from the fitting curve of area according time on different substrates** Curves of spreading area during engagement on substrate were fitted with the equation f(t) = A_0*tanh(t-t0/τ) and A_0 and τ were extracted. m: mean in μm^2, sd: standard deviation, N/n: number of independent experiments/number of cells, †= significant difference between substrate Bare • anti-CD3 and Bare+PEG • anti-CD3 with 0.001<p<0.01.

spreading area obtained in these dynamics observation is quite larger compared to the one obtained with fixed cells. This difference may be explained by the fact that due to the presence of filopodia around the live cells the adhesion area is overestimated. These delicate features are probably compromised during fixation.

6.3   Cell spreading on ICAM-1 clusters

After looking at the impact of anti-CD3 clustering, this section will focus on patterned substrates with nano-dots of ICAM-1 surrounded by SLB functionalized with anti-CD3 ([αCD3]$_{SLB}$ [ICAM-1]$_{Dot}$) or not ([Bare]$_{SLB}$ [ICAM-1]$_{Dot}$). In order to highlight the impact of ICAM-1 clustering behavior on patterned substrates will be compared to behavior on homogeneous substrates which have the same protein density as on patterned substrates. As before, for these substrates cell spreading area and actin organization were also analyzed.

Cell adhesion area: On [Bare]$_{SLB}$ [ICAM-1]$_{Dot}$ vs SLB Neg2+ICAM-1, as shown on Figure 6.25A, cells can adhere homogeneously or patterned (represent 20% of the total cells) while on the homogeneous substrates the membrane adheres uniformly. Cell adhesion area measurements indicate 100 ±50 μm^2 for patterned cells, 70 ±40 μm^2 for non-patterned cells and 65 ±45 μm^2 for average over all the cells. This value is similar to the cell spreading area on homogeneous substrate (Figure 6.25B-C).

Comparing these results with the ones obtained on [Bare]$_{SLB}$ [anti-CD3]$_{Dot}$ (see Figure 5.1) we can see that on both substrates there are patterned cells, but more often on [Bare]$_{SLB}$ [anti-CD3]$_{Dot}$ (43 % vs 20%). Cell spreading area is smaller on patterned substrates with clusters of ICAM-1 compared to clusters of anti-CD3.

Figure 6.26 shows that on [anti-CD3]$_{SLB}$ [ICAM-1]$_{Dot}$ there are 2 types of adhesion, either homogeneous or patterned like. On homogeneous substrate SLB anti-CD3+ICAM-1 there is only homogeneous adhesion. In contrast to [Bare]$_{SLB}$ [ICAM-1]$_{Dot}$, on this patterned substrate patterned cells have a smaller cell spreading area than non-patterned cells. Cell adhesion area measurements indicate 112 ±40 μm^2 for patterned cells, 185 ±80 μm^2 for non-patterned cells and 170 ±80 μm^2 for the total cells. This value is similar to the cell spreading area on homogeneous substrate SLB anti-CD3+ICAM-1 (Figure 6.26B-C).
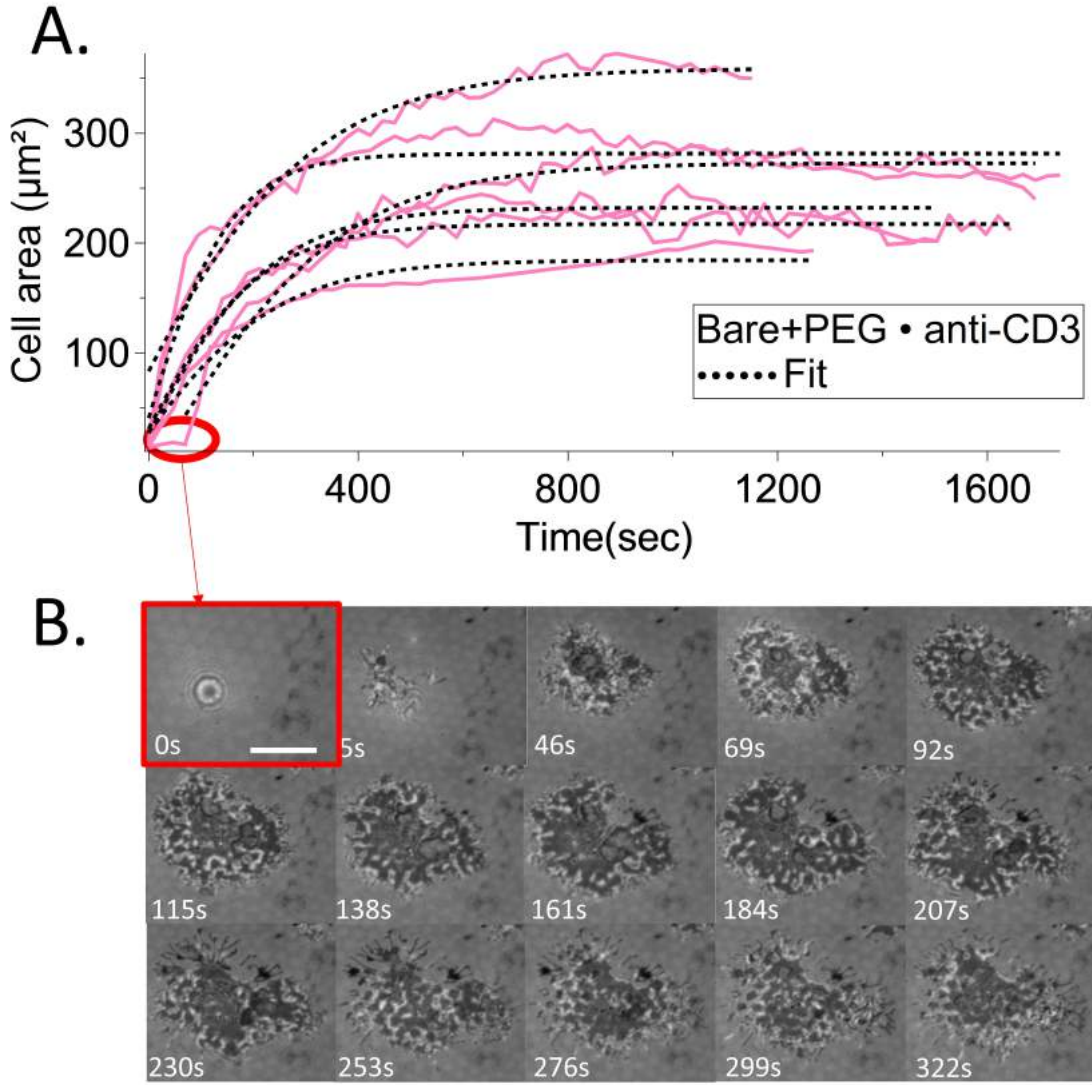
Figure 6.24: **Dynamic of cell spreading area of Jurkat T-cell measured on RICM image sequence during cells engagement on Bare+PEG • anti-CD3.**A: Solid lines represent the cell area evolution and dashed line represent fitting depending on the equation f(t) = A_0*tanh(t-t0/τ). Average A_0 equals 260±80 μm² and τ equals 280±76 seconds. Red circle surround the part of a curve where a latency time is observed. B: RICM time-sequence during cell adhesion from first surface contact to the stabilization of the spreading. RICM time-sequence where the image corresponding to a latency behavior is surrounded. Scale bar : 10 μm.
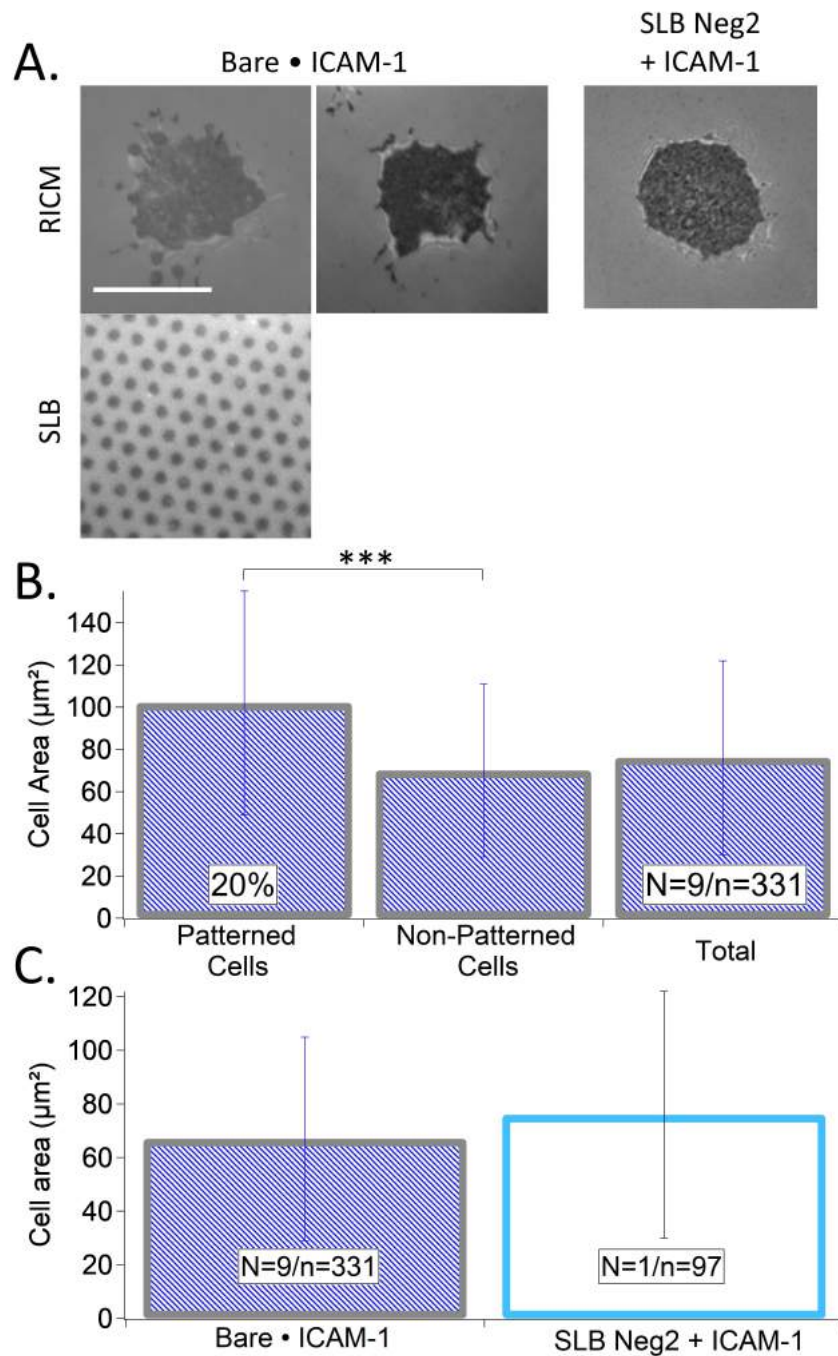
Figure 6.25: **T-cells on[Bare]$_{SLB}$ [ICAM-1]$_{Dot}$) (also called Bare • ICAM-1) and SLB Neg2+ICAM-1.** A: RICM images of Jurkat cell after 30 minutes engagement on patterned and homogeneous substrates and epi-fluorescence image of SLB. For epi-fluorescence image DOPC lipids was supplemented of 0.01% of fluorescent lipids. Scale bar: $10\mu m^2$. B-C: Cell adhesion area measurement of Jurkat T cells was done after 30 minutes engagement on substrates. ***=p<0.001.
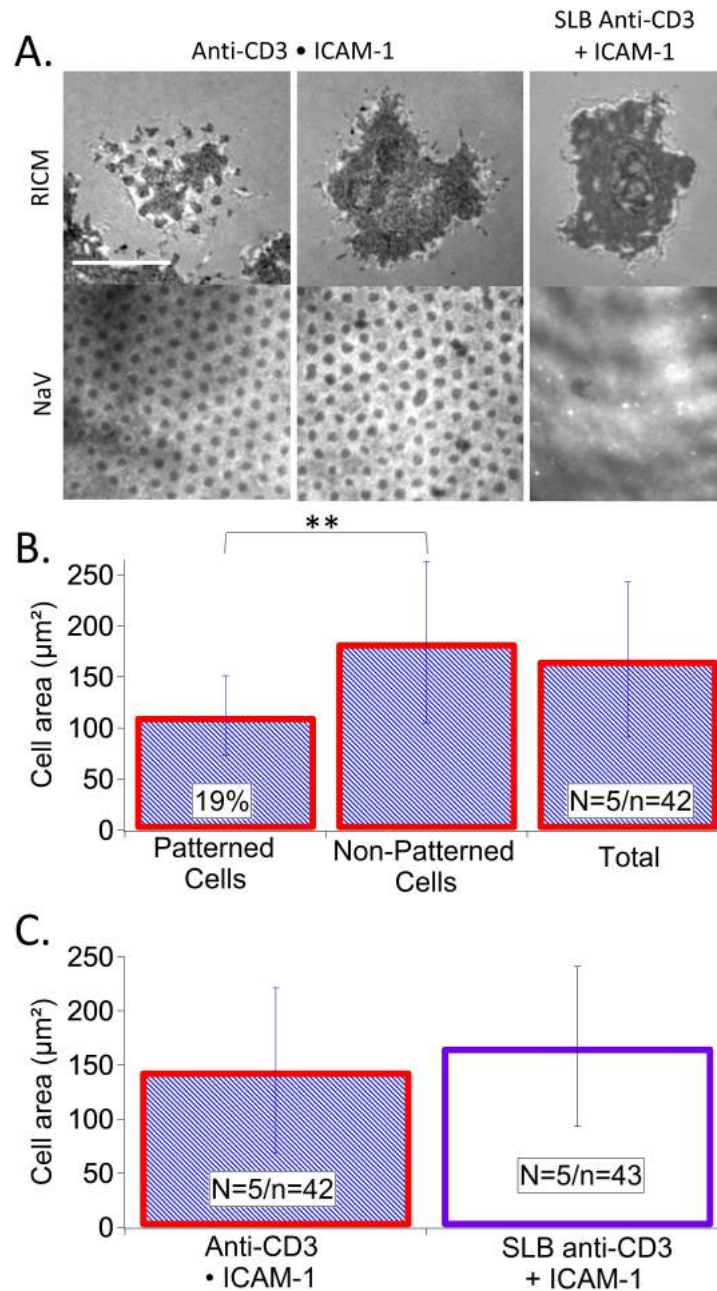
Figure 6.26: **T-cells on $[\text{Anti-CD3}]_{SLB}$ $[\text{ICAM-1}]_{Dot}$ (also called Anti-CD3 •
ICAM-1) and SLB Anti-CD3+ICAM-1.** A: RICM images of Jurkat cell after 30
minutes engagement on patterned and homogeneous substrates and epi-fluorescence im-
age of NaV. For epi-fluorescence images fluorescence NaV was used. Scale bar: $10\mu m^2$.
B-C: Cell adhesion area measurement of Jurkat T cells was done after 30 minutes en-
gagement on substrates. $** = 0.001 < p < 0.01$.
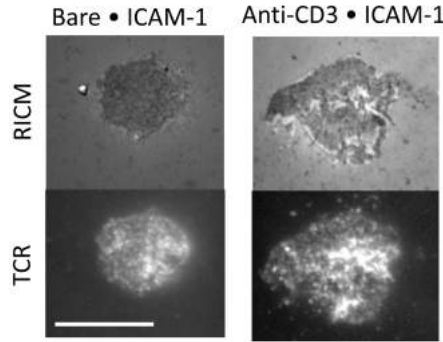
Figure 6.27: **TCR organization on T-cells on [Bare]$_{SLB}$ [ICAM-1]$_{Dot}$ and [Anti-CD3]$_{SLB}$ [ICAM-1]$_{Dot}$ (also called Bare • ICAM-1 and Anti-CD3 • ICAM-1).** Top row : RICM images of Jurkat cell after 30 minutes engagement on patterned substrates. Bottom row : TIRF-M images of TCR. Scale bar: $10\mu m^2$.

TCR cluster distribution: As shown on Figure 6.27 clustering of ICAM-1 in presence of TCR ligand or not, does not have an impact on the TCR organization which remains homogeneous.

The homogeneous control on glass corresponding to these patterned substrates is POS ICAM-1. This control represents the protein situation inside the dots, which mean molecules of ICAM-1 fixed on glass. Figure 6.28 shows results obtained for this substrate. As demonstrated on RICM images T-cells adhere homogeneously with an average cell spreading area equals 94 $\pm$40 μm^2 (A-B.). Moreover on this homogeneous substrate actin and TCR are homogeneously distributed (A.). Analyses give an average actin parameter of 1.2 (C.) and on the histogram of the TCR cluster area, population of very small clusters (0.1-0.2 μm^2) appear to be majority (D.).

Actin cytoskeleton organization: On the [Bare]$_{SLB}$ [ICAM-1]$_{Dot}$ vs SLB Neg2+ICAM-1 substrates, with only ICAM-1 present, clustering of ICAM-1 does have an impact on actin organization. On patterned substrate, actin can form patches (representing 15 % of cells) or is homogeneous. In both cases actin parameter is around 1.2. Moreover histogram of the actin parameter shows relatively the same distribution (Figure 6.29C). Additionally, actin parameter plot with cell spreading area shows no relation (Figure 6.29B-E). Dynamics observation was done on Bare • ICAM-1, and as presented in Figure 6.30A the actin parameter fluctuate between 1.2 and 2.7 during the engagement on the surface. Moreover as shown on the time-sequence in Figure 6.30B the actin structure is very dynamic and form patch structure which co-localized with the underlying pattern.

On [Anti-CD3]$_{SLB}$ [ICAM-1]$_{Dot}$ vs SLB anti-CD3+ICAM-1 substrates with both ICAM-1 and anti-CD3 presented, clustering of ICAM-1 does not have any impact on actin organization. Actin organization is homogeneous with an actin parameter around 1 on both substrates. Additionally histogram of the actin parameter is quite the same for patterned and homogeneous substrates (Figure 6.31). Moreover, there is no relation between cell area and actin distribution (Figure 6.31D-E).
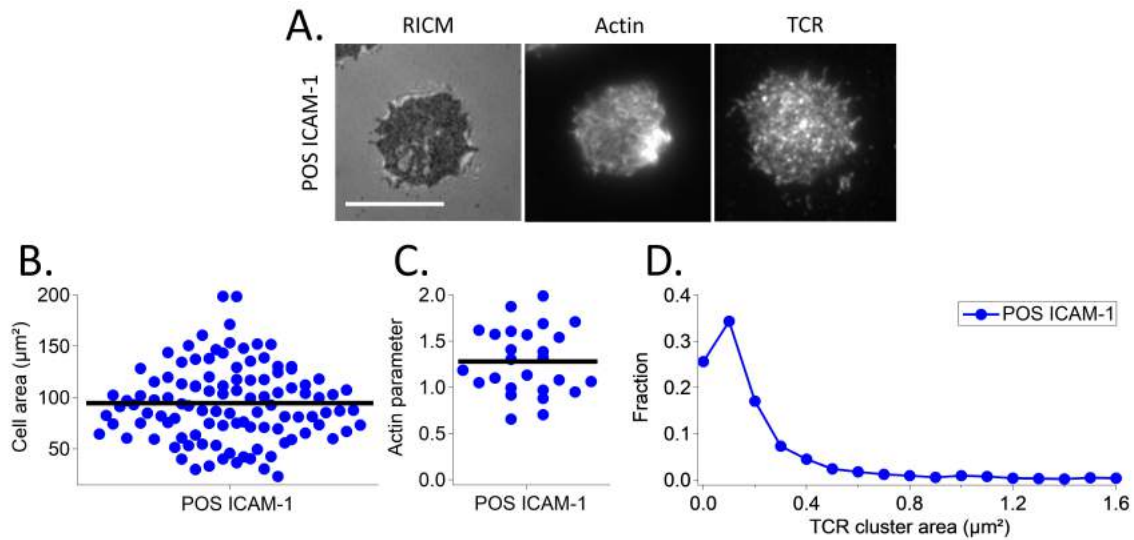
Figure 6.28: **T-cells on homogenous control on glass POS ICAM-1.** A: RICM and TIRF-M images of Jurkat cell after 30 minutes engagement on patterned substrates. For TIRF-M images Actin and TCR were marked. Scale bar: $10\mu m^2$. B:Scatter dot plot of cell spreading area (N=4;n=108). C: Scatter dot plot of actin parameter. C: Histogram of the TCR cluster area normalized by the total number of clusters.

Analyses Substrates	Cell spreading area (μm^2)	Actin organization
SLB Neg2+ICAM-1	70±40	Homogeneous
Bare • ICAM-1	80±50 (=)	Patterned
SLB anti-CD3+ICAM-1	145±70	Homogeneous/Peripheral
Anti-CD3 • ICAM-1	170±80 (=)	Peripheral

Table 6.3: **Impact of ICAM-1 patterning** Summarized results obtained on homogeneous substrates and substrates presenting nano-clusters of ICAM-1.(=) indicate no significative difference for cell spreading area between SLB Neg2+ICAM-1 and Bare • ICAM-1 and between SLB anti-CD3+ICAM-1 and Anti-CD3 • ICAM-1. The number of experiments and cells are as followes: SLB Neg2+ICAM-1: N=1/n=97; Bare • ICAM-1 N=9/n=331, SLB anti-CD3+ICAM-1: N=5/n=43; Anti-CD3 • ICAM-1: N=5/n=42.
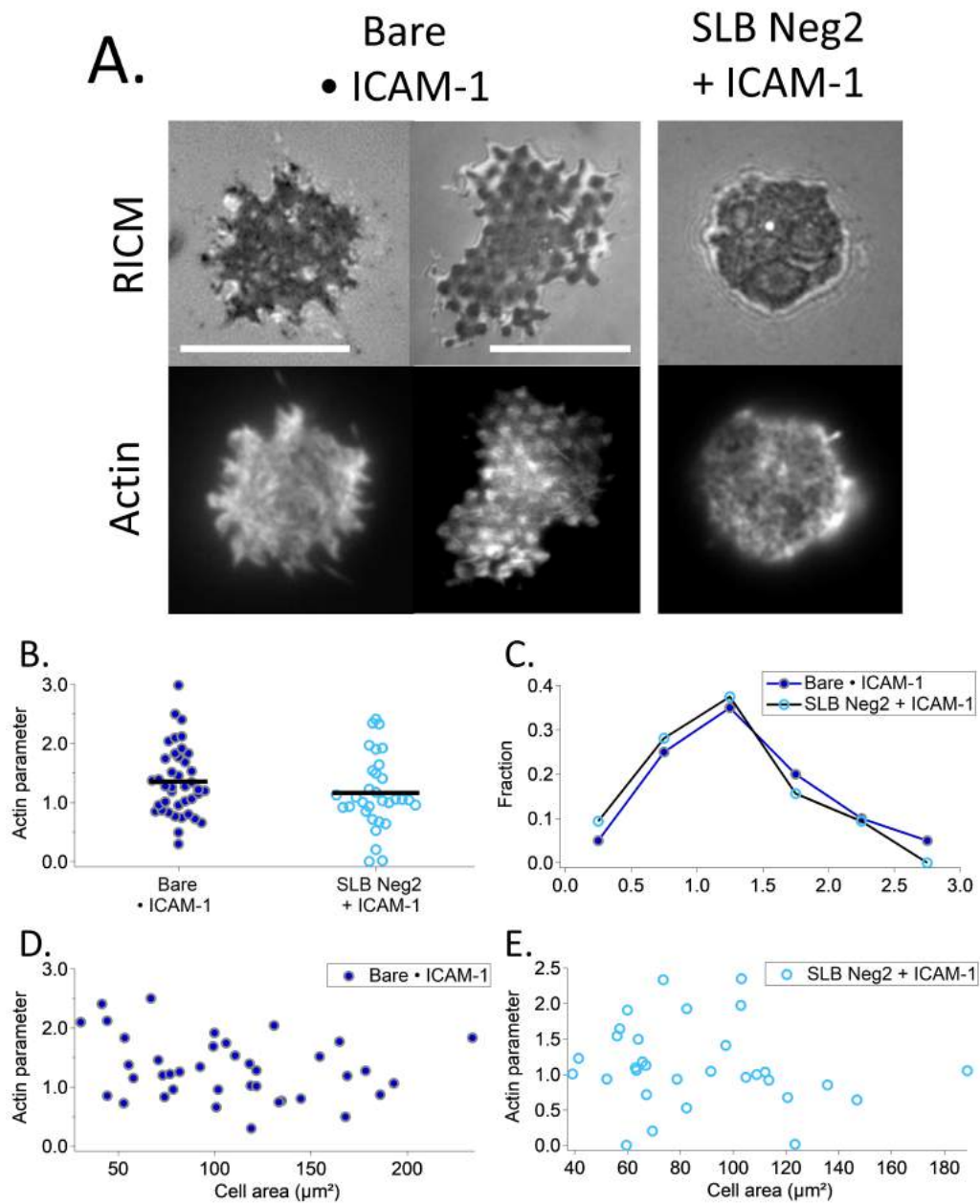
Figure 6.29: **Actin cytoskeleton architecture of T-cells on [Bare]$_{SLB}$ [ICAM-1]$_{Dot}$ (also called Bare • ICAM-1) and SLB Neg2+ICAM-1.** A: RICM and TIRF-M images of Jurkat cell after 30 minutes engagement on patterned and homogeneous substrates. For TIRF-M images actin was labeled. Scale bar: 10μm. B: Scatter dot plot of actin parameter. C: Histogram of actin parameter normalized by the total number of cells. D-E: Actin parameter according cell spreading area on [Bare]$_{SLB}$ [ICAM-1]$_{Dot}$ (D.) and on SLB Neg2+ICAM-1.
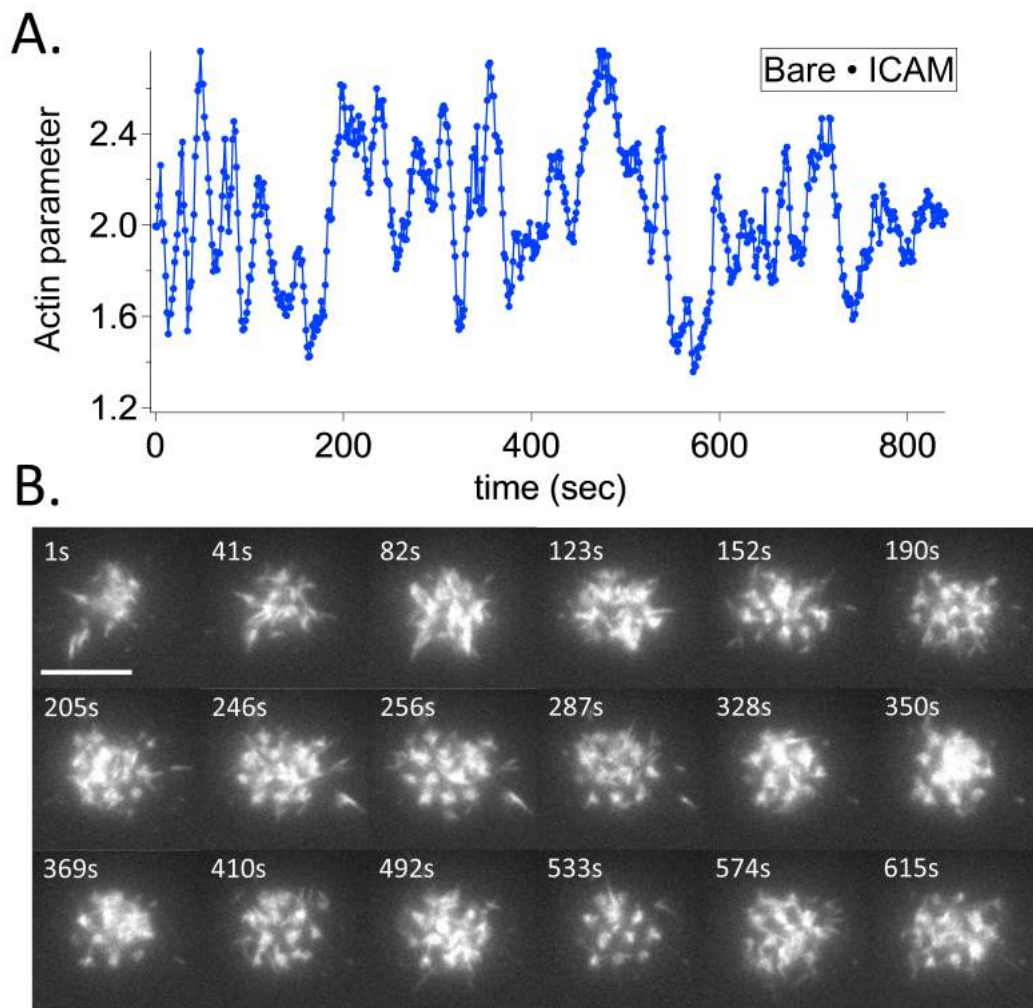
Figure 6.30: **Dynamic of actin organization of Life-Act cells during cell engagement on Bare • ICAM-1.**A: Dynamic of actin organization for 1 cell during its engagement. B: TIRF-M time-sequence of actin organization during cell adhesion from first surface contact to the stabilization of the spreading. Scale bar : 10 μm
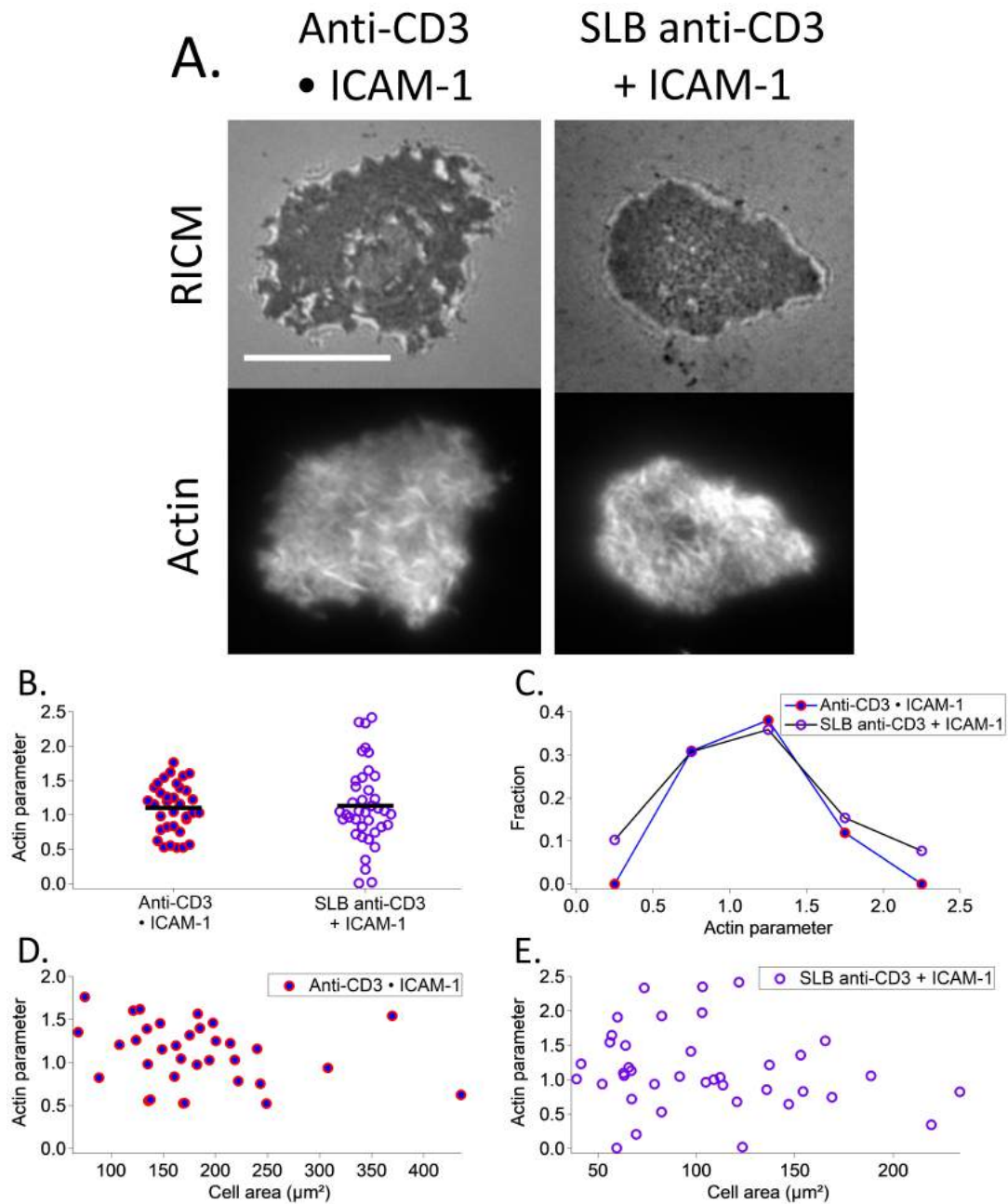
Figure 6.31: **Actin cytoskeleton architecture of T-cells on [Anti-CD3]$_{SLB}$ [ICAM-1]$_{Dot}$ (also called Anti-CD3•ICAM-1)and SLB Anti-CD3+ICAM-1.** A: RICM and TIRF-M images of Jurkat cell after 30 minutes engagement on patterned and homogeneous substrates. For TIRF-M images actin was labeled. Scale bar: $10\mu m^2$. B: Scatter dot plot of actin parameter. C: Histogram of actin parameter normalized by the total number of cells. D-E: Actin parameter according cell spreading area on [Anti-CD3]$_{SLB}$ [ICAM-1]$_{Dot}$ (D.) and on SLB Anti-CD3+ICAM-1.
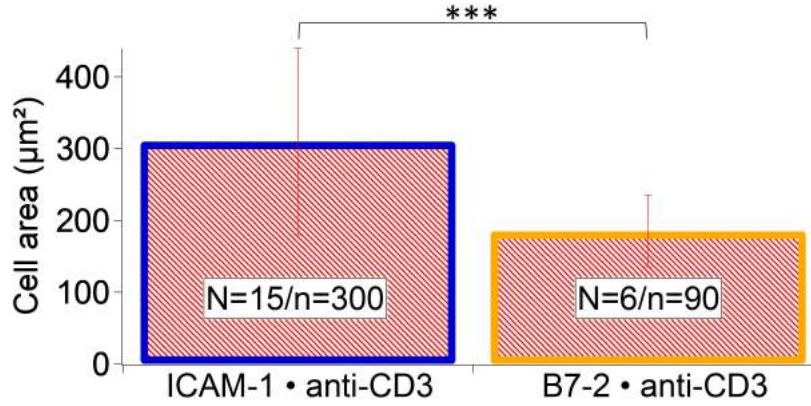
Figure 6.32: **Cell area on [B7-2]$_{SLB}$ [αCD3]$_{Dot}$ and [ICAM-1]$_{SLB}$ [αCD3]$_{Dot}$ (also called B7-2 • anti-CD3 and ICAM-1 • anti-CD3) .**Cell adhesion area measurement of Jurkat T cells after 30 engagement on substrate. Error bars represent standard deviations. ***=p<0.001.

6.4 Cell spreading on anti-CD3 clusters in presence of co-receptor ligands

After showing that presence of adhesion molecule ICAM-1 outside the anti-CD3 have an impact on T-cell membrane organization, there was an interest in the impact of the presence of co-stimulatory B7-2 in the SLB. B7-2 (or CD86) is a co-stimulatory molecule present on APC membrane which binds CD28 or CD152 on T-cell surface. B7-2/CD28 binding can produce a co-stimulatory signal which enhance T-cell activation. This section will compare results obtained on patterned substrates with either ICAM-1 or B7-2 in the SLB surrounding anti-CD3 dots ([ICAM-1]$_{SLB}$ [αCD3]$_{Dot}$ and [B7-2]$_{SLB}$ [αCD3]$_{Dot}$). These experiments were undertaken in collaboration with Jacques Nunes (CRCM).

6.4.1 Cell adhesion

Cell adhesion on [B7-2]$_{SLB}$ [αCD3]$_{Dot}$ for the majority of cells is homogeneous and flat like on [ICAM-1]$_{SLB}$ [αCD3]$_{Dot}$ (with 5% of patterned cells) but the cell spreading area is lower, 185±50 μm^2 versus 310±130 μm^2 (Figure 6.32).

As shown on Figure 6.33, the cell area may in this case increase with NaV (and threfore anti-CD3) density (linear coefficient superior to 0.8). While this result, seen in isolation, is encouraging, it is necessary to understand why in case of B7, lack of correct passivation is not an issue.

Homogeneous Controls: Two homogeneous controls correspond to this substrate: homogeneous control on glass called POS anti-CD3 and homogeneous control on SLB called SLB B7-2. Area measured on RICM images for these controls were 235±70 μm^2(N=25,n=530) for POS anti-CD3 and 90±20 μm^2(N=2;n=30) for SLB B7-2 (Figure 6.34).
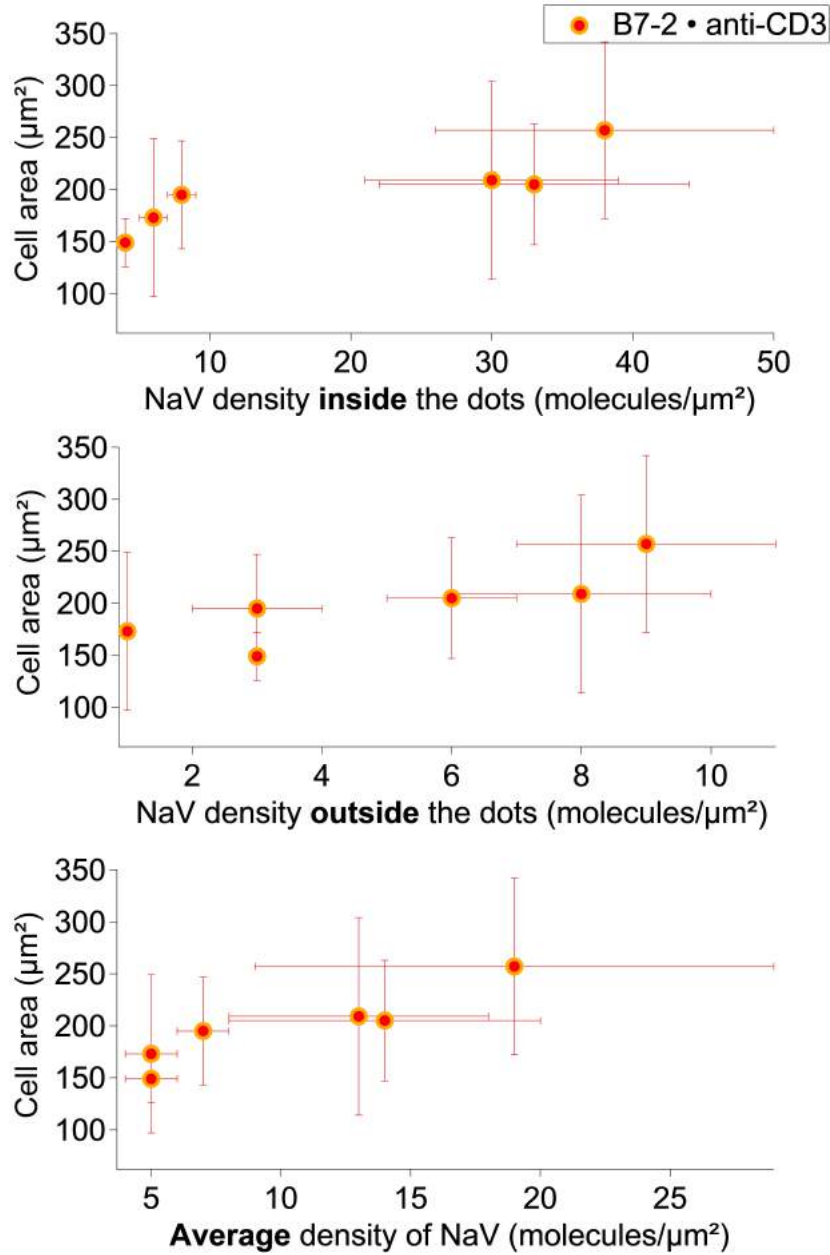
Figure 6.33: **Cell adhesion area according the average density of NaV on the underlying pattern on [B7-2]$_{SLB}$ [αCD3]$_{Dot}$ (also called B7-2 • anti-CD3).** Each point represent one experiment with error bars representing standard deviations. N=6;n=90. The linear correlation coefficient between cell area and NaV density inside equals to 0.9, between cell area and NaV density outside it equals to 0.8 and between cell area and NaV density inside it equals to 0.9
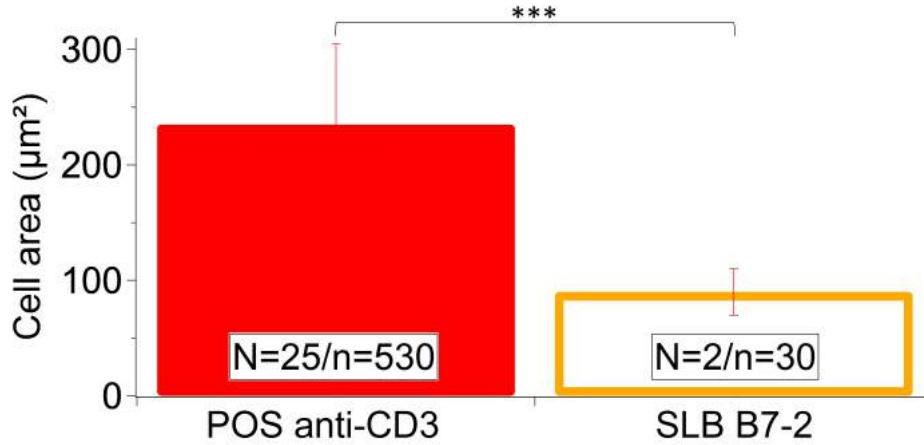
Figure 6.34: **Cell adhesion area on homogeneous controls type 1 for $[\text{B7-2}]_{SLB}$ $[\alpha\text{CD3}]_{Dot}$ substrate.** Cell adhesion area measurement of jurkat T cells was done after 30 minutes engagement on substrates. Error bars represent standard deviations. ***=p<0.001.

6.4.2 TCR clusters distribution

As shown on Figure 6.35A on patterned substrates with B7-2 in the SLB, TCR molecules are homogeneously distributed on T-cell membrane (1.). This result is quite surprising as on previous patterned substrates studied (with Bare SLB or ICAM-1 in the SLB) TCR clusters were always following the underlying pattern. However fews cells (13.5%) present the patterned distribution (2.) but the co-localization is not as much clear as on the previous substrates. In both distributions visual inspection suggests a centralization of the TCR. This result is confirmed by the analysis of the TCR centralization which give a TCR parameter equals to 2.4 (Figure 6.35B). This centralization was not observed in patterned substrates with ICAM-1 on the SLB whereas it was observed with pre-activated Jurkat T-cells on $[\text{Bare}]_{SLB}$ $[\alpha\text{CD3}]_{Dot}$ (see section 5.5) meaning that concerning the TCR the presence of B7-2 on SLB have the same effect as the T-cell pre-activation with anti-Vβ8.

Analyses of TCR cluster area in Figure 6.35C show an small enrichment on $[\text{B7-2}]_{SLB}$ $[\alpha\text{CD3}]_{Dot}$ for cluster size below the range 0.2-0.4 μm^2 whereas after 0.4μm^2 the enrichment is on $[\text{ICAM-1}]_{SLB}$ $[\alpha\text{CD3}]_{Dot}$. The critical value where the enrichment shift corresponds to the size of the underlying anti-CD3 pattern. These results match with the visual inspection.

Taking together these results show that in presence of the co-stimulatory B7-2 the TCR distribution is not imposed by the TCR ligand patterning. Moreover on this substrate TCR is able to move toward the center. As this situation is also observed with pre-activaed Jurkat, the formation of this kind of cSMAC may be explained by an activation of the T-cell through co-stimulatory B7-2/CD28 binding.
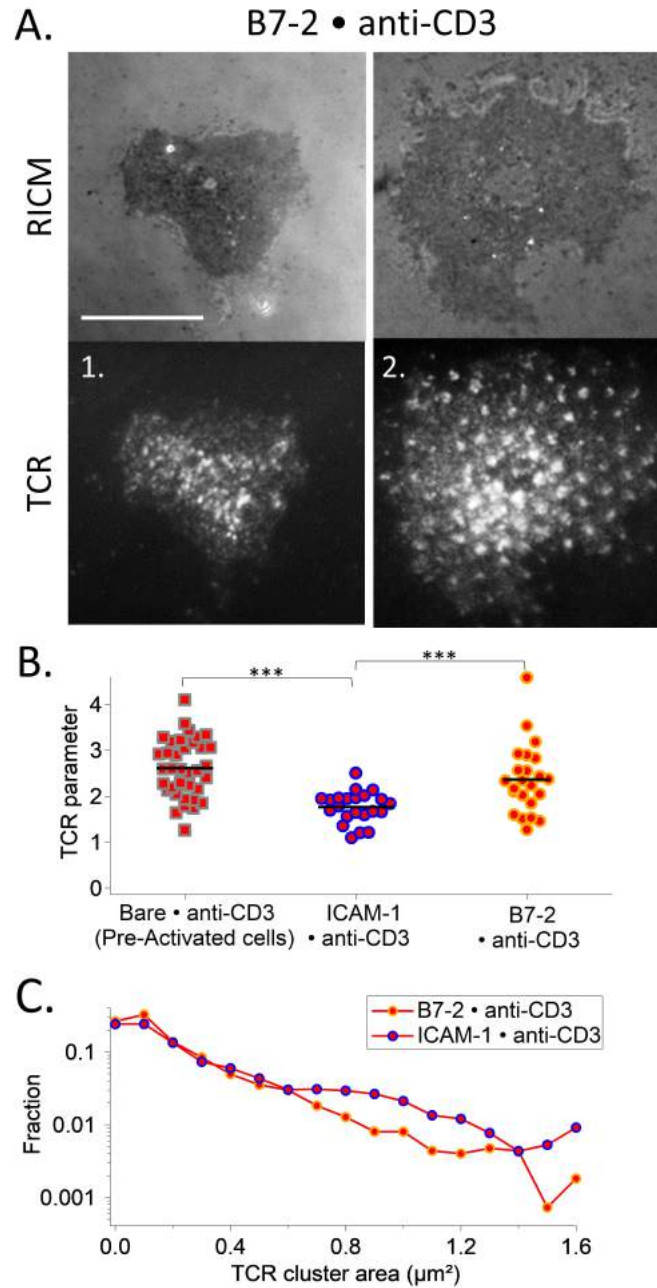
Figure 6.35: **TCR clusters of T-cells spreading on $[\text{B7-2}]_{SLB}$ $[\alpha\text{CD3}]_{Dot}$ (also called B7-2 • anti-CD3).** A: RICM and TIRF-M images of Jurkat cell after 30 minutes engagement on patterned substrates. Scale bar: 10μm. B: Histogram of the apparent area of clusters normalized by the total number of clusters. C: Scatter dot plot of the TCR parameter. ***=p<0.001.

6.4.3 Actin cytoskeleton architecture

As presented in Figure 6.36A, 2 actin distribution is observed on $[\text{B7-2}]_{SLB}\ [\alpha\text{CD3}]_{Dot}$, either homogeneous or peripheral. These organizations are similar to that found on patterned substrate with ICAM-1 or with Pre-activated cells on $[\text{Bare}]_{SLB}\ [\alpha\text{CD3}]_{Dot}$. Moreover on $[\text{B7-2}]_{SLB}\ [\alpha\text{CD3}]_{Dot}$ actin is mainly found to have an peripheral organization. Actin images analyses indicate a average actin parameter equals to 0.5. This value is close to the ones found on patterned substrates with ICAM-1 on the SLB or with Pre-activated cells on $[\text{Bare}]_{SLB}\ [\alpha\text{CD3}]_{Dot}$ (Figure 6.36B). Histogram of the actin parameter normalized by the total number of cells indicate 55% of cells with actin parameter between 0-0.5 (corresponding to peripheral organization) against 50 and 70% for the 2 other substrates (Figure 6.36C).

As shown on graphs in Figure 6.36D-E, actin parameter is not influenced by the cell spreading area or the NaV density.

6.4.3.1 Dynamics

Finally on $[\text{B7-2}]_{SLB}\ [\alpha\text{CD3}]_{Dot}$ the value of the actin parameter decreases during cell engagement and this decrease is related to the cell spreading on the surface (Figure 6.37C-D). TIRF-M time-sequence shows dynamics of the membrane at the periphery (Figure 6.37A) and a retrograde flow. Moreover kimograph across the cells shows this dynamics (Figure 6.37B)

6.4.4 Conclusion

In this chapter we presented dually functionalized substrates – those with anti-CD3 dots with additional ICAM-1 or B7.2 or those with ICAM-1 dots with additional anti-CD3. Taken together with results of the previous chapter, the most interesting point to emerge from this study is that at least for the specific surface densities probed, clustering of anti-CD3 has an impact on cell spreading only when ICAM-1 is also present, but clustering of ICAM-1, in presence or not of anti-CD3, has no effect on cell spreading. For the former case, the presence of ICAM-1 in the bilayer has no effect on TCR distribution, which co-localize with anti-CD3, but the actin architecture goes from being predominantly patchy or homogeneous to being mostly peripheral. Comparing the case of clustered or homogeneous ICAM-1 in the presence of not of anti-CD3, we see that ICAM-1 clustering has no effect on cell area and the TCR-distribution is always homogeneous. The actin architecture is either homogeneous or patterned in absence of anti-CD3 and always homogeneous in the presence of anti-CD3.

It must however be noted that the surface density of ICAM-1 for these experiments was very low (to match the standard dot geometry). Comparing homogeneous substrates with or without ICAM-1 (in presence of anti-CD3) shows no increase in area in presence of ICAM-1, clearly because of low ICAM1 doses. It will be interesting to test patterns with higher ICAM-1 density.

On B7.2, cell spreading was not appreciably impacted by the presence of B7-2 (compared with Bare • anti-CD3) but the colocalization of TCR and actin patches with underlying dots was impaired for the former and disappeared entirely for the latter. Our data is consistent with a different role for LFA-1 and CD-28 in modulating TCR
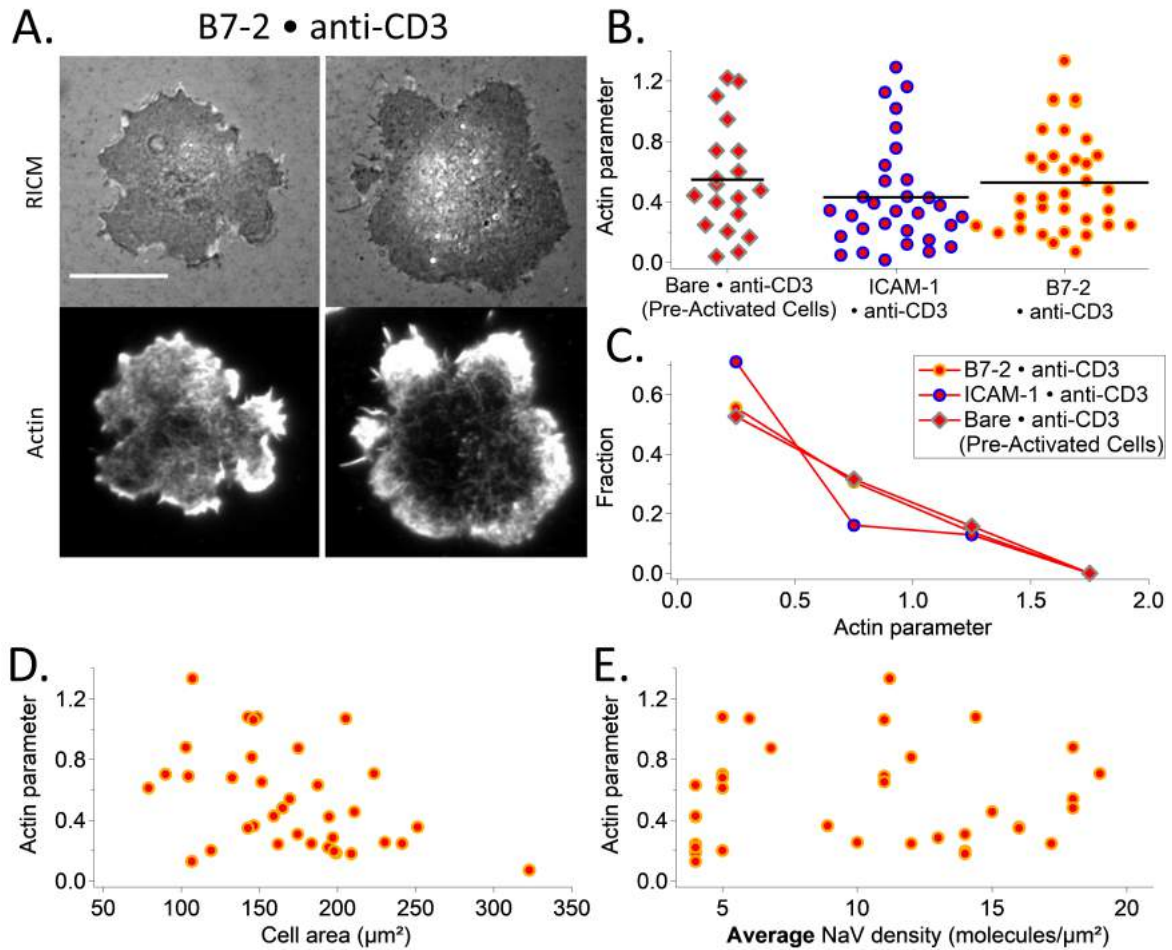
Figure 6.36: **Actin Cytoskeleton organization of T-cells spreading on $[\mathbf{B7\text{-}2}]_{SLB}$ $[\alpha\mathbf{CD3}]_{Dot}$ (also called B7-2 • anti-CD3).** A: RICM and TIRF-M images Jurkat cell after 30 minutes engagement on patterned substrates. For TIRF-M images Actin was marked. Scale bar: $10\mu m^2$. B: Scatter dot plot of actin parameter. C: Histogram of the actin parameter normalized by the total number of analyzed cells. D-E: Relation between actin parameter and cell adhesion area (D.) and NaV average density(E.).
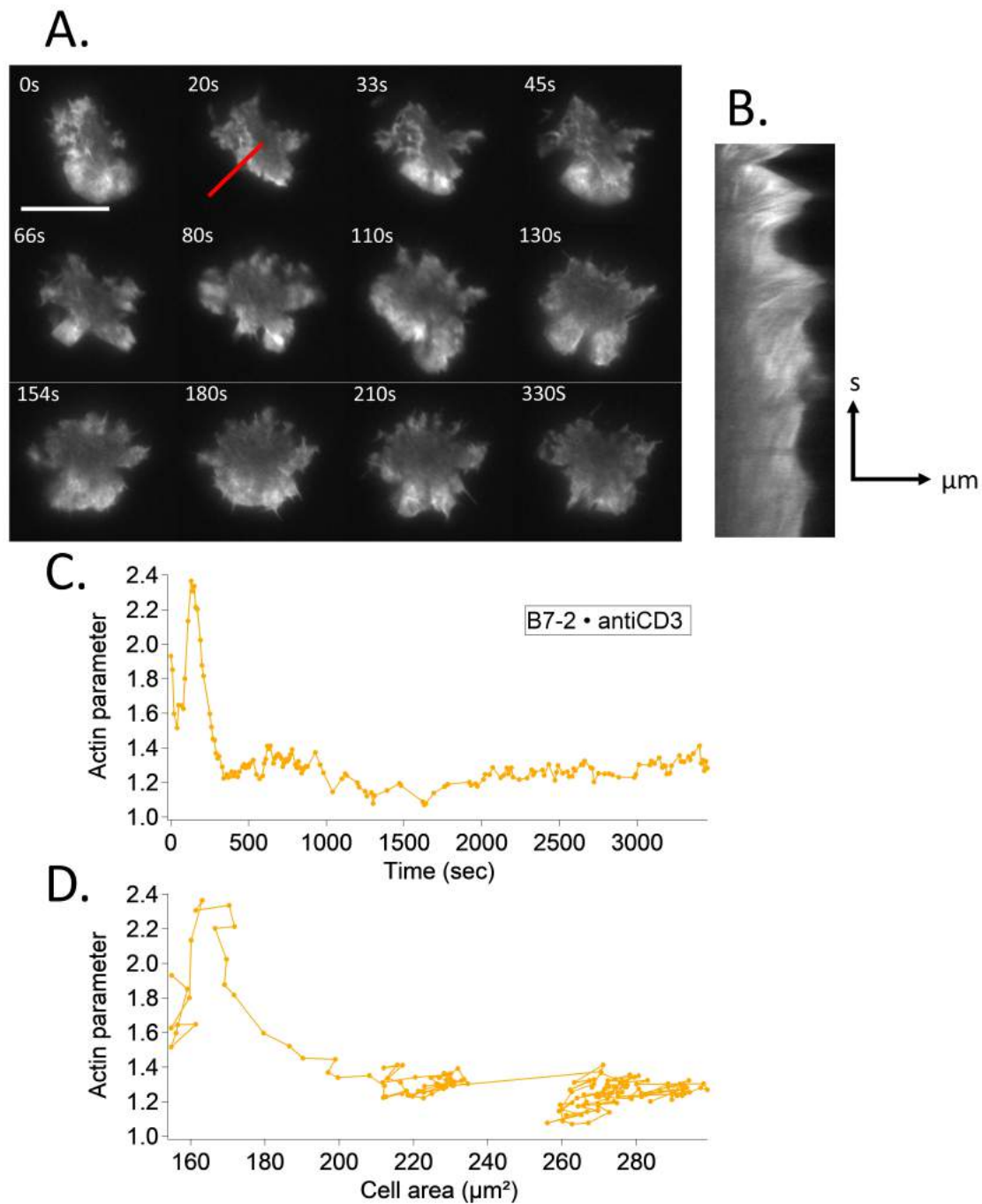
Figure 6.37: **Dynamic of actin organization of Life-Act cells during cell engagement on B7-2 • ICAM-1.** A: TIRF-M time-sequence of actin organization during cell adhesion from first surface contact to the stabilization of the spreading. Scale bar : 10 μm. B: Kimograph along the red line on A. C: Dynamic of actin organization for 1 cell during its engagement. D: Evolution of actin parameter with the cell spreading area.

activation.

A large part of this chapter was dedicated to experiments designed to understand the spread in data concerning membrane topography and actin architecture. Cells that exhibit membrane topography also exhibit patterned actin (with only one or two exceptional individual cells). On all substrates where cells are patterned, we also find a population of non-patterned cells. Clearly, the presence of adhesive dots in non-adhesive SLB promotes cell patterning even when the dots are not activating (iso-type or ICAM in absence of anti-CD3). However, only activating (anti-CD3) dots promote formation of TCR clusters, both for patterned and for flat membranes, which co-localize with the anti-CD3 dots. We had hypothesized that the presence of PEG in the SLB will passivate the SLB better and therefore drive the cells to being more consistently patterned in terms of membrane topography. However, this was not the case - the presence of PEG consistently reduces cell area but does not induce increased membrane topography. Conversely, usually when the SLB as well as the dots are adhesive (anti-CD3 dots in ICAM-1 or B7.2 SLB), the membrane is flat and the actin is either homogeneous or ring-like. Clearly having alternating adhesive/passive zones is important to generate membrane topography.

Analyses Substrates	Cell adhesion	Cell spreading area (μm^2) m±sd	N/n	TCR distribution	ZAP-70 distribution	Actin organization
Bare • αCD3	Patterned/ Homogeneous	220±70	42/860	Patterned	Patterned	Patterned
Bare • α CD3 (Pre-Activated cells)	Homogeneous	360±145	4/56	Patterned/ Centralized	N.A	Peripheral
ICAM-1 • αCD3	Homogeneous	310±130	15/300	Patterned	Only big clusters co-localized	Peripheral
B7-2 • αCD3	Homogeneous	185±50	6/90	Homogeneous/ Centralized	N.A	Homogeneous
Bare • ICAM-1	Patterned/ Homogeneous	65±45	9/331	Homogeneous	N.A	Patterned
Anti-CD3 • ICAM-1	Patterned/ Homogeneous	170±80	5/42	Homogeneous	N.A	Homogeneous

Table 6.4: **Summary of cell adhesion and area measured with RICM, TCR, ZAP-70 and Actin organization after 30 min of engagement of Jurkat on various substrates.** m: mean in μm^2, sd: standard deviation, N/n: number of independent experiments/number of cells, N.A: not applicable.

Chapter 7

Overview, discussion and perspective

The interaction of T cells with antigen presenting cells (APCs) plays a central role in adaptive immunity, one of whose salient features is the duality of exquisite sensitivity and strict discrimination in the context of recognition of antigen by T cells through the T cell receptor (TCR). To achieve this, the T cell membrane carries a variety of co-stimulatory and inhibitory molecules to complement the basic TCR mediated interaction. Following encounter with its antigen, a key step towards correct activation of the T cell is the reorganization of its membrane and its cytoskeleton. Concomitantly, the cell spreads on the APC, forming the so-called immunological synapse [44, 57]. The extent of spreading in T cells is a marker of their activation and eventual proliferation [144].

A very fruitful approach to dissect adhesion and membrane/cytoskeleton reorganization has been to replace the APC with a synthetic antigen presenting substrate (APS). The early APS were, typically, supported bilayers carrying ligands for the TCR/CD3 complex – either lipids coupled pMHC [44] or biotinyled anti-CD3 [63], and ligands for LFA-1 – often in the form of a GPI-anchored protein [63, 44] or connected to NTA functionalized lipids [145]. In the last decade, such substrates have been designed to carry, in addition, a host of co-receptors [145] to dissect specific aspects of T cell response.

Seminal work in the early 2000, from Dustin and Saito labs underlined the importance of TCR-clusters in initiation of T cell activation [146, 64]. Segregation of TCR into clusters is also at the heart of the currently most credible model for T cell activation, namely the kinetic segregation [33]. In this model, the membrane topography plays an important role. The pair TCR/pMHC being much shorter than ICAM-1/LFA1, the TCR clusters exclude the longer ICAM-1/LFA1 but also the long phosphatases like CD45. The absence of CD45 permits the phosphorylation of the ITAM-motifs associated with the TCR/CD3 domain, thus initiating T cell activation.

Simultaneously with activation and adhesion, actin polymerization is triggered at the cell edge to promote spreading [147]. The actin is organized roughly as a ring [148], whose fine structure was revealed recently [149, 150, 151]. It was shown recently that the peripheral nature of the actin ring is more pronounced for stronger pMHC ligands as compared to weaker ones where the distribution is more homogeneous [149]. The TCR as well as LFA1 get connected to the actin cytoskeleton: the molecular species connecting integrins like LFA1 to actin are well known, those connecting TCR to actin are yet to

be fully identified [152]. TCR-clusters that already exclude both LFA1 and long sugars, are carried by the actin retrograde flow towards the center where they eventually form the cSMAC [63, 153].

To address the question of the impact of ligand/receptor segregation or clustering two approaches have emerged – genetic modification to vary relevant molecular lengths [154, 37], or manipulation of the clustering itself – sometimes called spatial mutation [65]. The second approach was advanced by the Groves lab, who designed SLBs that are patterned with micron size corals which do not allow diffusion of molecules across their fence. This revealed the importance of ligands diffusion for the formation of a stable immunological synapse.

In parallel to the use of SLBs as APS, several groups also used protein coated glass as APS [148, 97]. Using this approach, Irvin and Doh explored the consequences of micro-clustering of TCR and/or LFA1, focusing on the formation of c-SMAC [97]. They showed that T-cells can be fully activated when focal spots of immobilized TCR ligand are in the center of the interacting surface but not if they are patterned differently. Later, Kam et al. [98] have shown that T-cells were able to produce IL-12 when anti-CD3 dots are surrounded by CD28 (co-stimulation molecule that binds to CD80/86) whereas when both are co-localized they did not. These studies emphasized the importance of the organization of the ligands on the formation of the immunological synapse and the activation of the T-cells.

A more recent article reported complementary roles of TCR and LFA-1 on cytoskeletal growth and contractility using micro-patterning. They found that Arp2/3 acts downstream of TCRs in order to nucleate dense actin foci and that LFA-1 is required for the propagation of the network. LFA-1 adhesion enhances actomyosin forces, which in turn modulate actin assembly downstream of the TCR [155].

More recently, T-cells were interrogated by nano-patterns of ligands [99, 100, 101]. This approach revealed that T cells respond globally to average density of TCR ligands, rather than details of the pattern [99]. Moreover, playing with the distance between TCR ligands, using similar patterns but with also ICAM-1 in the system, Declassian et al. showed that the nano-scale spatial structure can affect T-behavior. Indeed more the spacing increase more the T-cell responses decreased (to achieved a background level with a spacing of 69 nm). However, in this system, the density and ligand spacing are related [101].

In ongoing projects in the host lab, T cell interactions with designed surfaces are studied with advanced microscopy. The ligand of choice was anti-CD3 for two reasons. First, using anti-CD3 rather than pMHC allowed us to work with TCR/CD3 complex alone, in absence of ICAM – something not possible if pMHC was used since the TCR-pMHC bond is not strong enough to sustain adhesion. At the same time it should be pointed out that this is a legitimate approach since anti-CD3 is known to elicit the same signaling pathways as pMHC ligation [14] and the CD3 domain mediates T-cell mechanotransduction [156]. The second reason for use of anti-CD3 is linked to the choice of using the Jurkat cell line, for which the MHC peptide is not available [130].

In the group, we develop new strategies for patterning anti-CD3 on glass (or elastomer) surfaces. Colloidal bead lithography (see section 3.1) is the method of choice to simplify the patterning process. With this technique, so far, sub-micron sized features were achieved. The subsequent functionalization strategy involving only organic

molecules and proteins, and avoiding metals like gold, ensured that the substrates are fully compatible with advanced optical microscopy and this allowed us to go beyond the work reported in [100, 99, 101] and simultaneously observe global adhesion as well as local membrane/actin reorganization. This is the context in which this thesis was conceived and executed.

During *my PhD* work, I made advances in two parallel directions – improvement of substrates and understanding cellular response.

Concerning *substrates*, at the start of my work in the lab, a protocol for creating sub-micron size dots had been developed. The dots were surrounded by a repulsive polymer (PLL-PEG) [102]. We developed a new way to vary the dot size independent of spacing[102]. Simultaneously, I put in place the protocol to replace the PLL-PEG by a fluid SLB [102, 157]. This protocol yields very good control of the spacing and size of the anti-CD3 dots but, as discussed in chapter 4, the surface protein density is more difficult to control. However, this in itself is not prohibitive since we can measure the surface density inside as well as outside the dots, down to the resolution scale.

A more pressing issue proved to be that of passivation. As was shown in chapter 5 and 6, cell adhesion area was insensitive to surface protein density. The most logical explanation, especially in the light of our previous work [103] showing that cell area is directly proportional to average surface density of anti-CD3 in similar range as that studied here, is that uncontrolled non-specific interactions are dominating here over specific ligand/receptor mediated effects. However, some effects are still present as can be discerned by comparing the cell spreading on anti-CD3 patterns and on patterns where the antibody is replaced by its isotype (see Figure 5.5).

Even though the cells do not spread well on the isotype control pattern, close inspection of the RICM image of a cell on this pattern (see Figure 6.20) shows that the membrane adheres to the dots, implying that there is strong non-specific adhesive interaction between the cell membrane and the dots, which are presumably not passivated enough in this protocol. In addition, we believe that there is unspecific interaction coming from insufficient passivation of the SLB, and included PEG carrying lipids in the SLB to improve passivation. Inclusion of PEG decreased the overall adhesion but probably does not fully screen the non-specific interactions. Improving passivation and understanding the role of unspecific interactions is part of ongoing efforts.

I put in place an entirely new method combining e-beam lithography and surface functionalization ("declaration de invention" submitted for eventual patent). The idea was to produce smaller features whose shape and spacing can be perfectly controlled at will. This target was achieved to satisfaction (Figure 4.14) but the issue of passivation remained (Figure 4.15).

At the beginning of this work, one aim was to create SLBs that support diffusing anti-CD3. Previous work in the lab had revealed that for SLBs prepared with Langmuir-Blodgett technique (LB-SLB, as was done here), anti-CD3 (bound using a protocol similar to ours) is immobilized even though the lipids remain fluid. It was shown that SLBs prepared using vesicle spreading (VS-SLB), and using mono-biotinylated anti-CD3, the lipids as well as proteins can remain mobile [142]. A considerable part of my time was therefore spent in trying to combine VS-SLBs with patterning. This however did not succeed. Another small variation to the protocol involved adaptation for use of NTA-BSA instead of biotin-BSA, which was successfully achieved.

As a future *perspective*, the most immediate concern is to improve and understand the issue of passivation. Perfecting and exploiting the lithography protocol is another important opening. Finally, successful implementation of VS-SLB with patterning will open the possibility of new interesting experiments on tracking of ligands while cells spread on ligand-dots.

Cellular studies concentrated on accessing the role of different ligands. To do this, we fixed the dot separation and size to 2 μm and about 800 nm respectively. These choice of parameters ensured that there were enough dots under a spread cell and that optical imaging with TIRF was possible (without having to resort to super-resolution at this stage). The dot size also happens to be close to the best estimates of typical TCR cluster size reported in literature [145]. For the reasons explained before, we chose to work with anti-CD3 to target the TCR-CD3 complex.

The standard substrate for this thesis, against which all other modifications were compared, was anti-CD3 oots in a sea of non-functionalized SLB ([Bare]$_{SLB}$ [αCD3]$_{Dot}$ also called Bare$\bullet$ anti-CD3). These substrates are similar to those studied in the lab before [103], with the SLB replaced by a polymer ([PLL-PEG]$_{glass}$ [αCD3]$_{Dot}$ also called PLL-PEG$\bullet$ anti-CD3). As expected, Bare$\bullet$ anti-CD3 substrates reproduce many of the results reported for PLL-PEG$\bullet$ anti-CD3. Specifically the membrane topography and the TCR and actin organization which follow the underlying pattern of anti-CD3.

However, the global behavior of the cells, that cell spreading was proportional to average ligand density, was not reproduced here (as discussed above) probably because of inadequate passivation. This is consistent with the fact that even for PLL-PEG $\bullet$ anti-CD3, this result was valid only when the PEG layer was sufficiently dense and not when it was sparse [103].

Going beyond previously reported work [103], actin cytoskeleton was also studied here. Patterned actin was found almost systematically on cells that exhibit membrane topography. Otherwise the architecture of the actin cytoskeleton is variable - ranging from homogeneous to peripheral.

The most important result emerging from experiments on Bare$\bullet$ anti-CD3 and related controls, and consistent with previous reports [100, 103], is that when only the ligands of TCR-CD3 complex are involved, extent of receptor clustering is at best a weak control parameter for cell spreading.

LFA-1 and CD28 were the choice of secondary signaling targets. Traditionally, LFA-1 was believed to facilitate the functional triggering of TCRs solely by promoting adhesion of T cells to APCs but now it is accepted that ligation of LFA1 to ICAM-1 modifies the affinity of TCR for its ligands [158]. Post activation, LFA-1 forms its own (smaller) micro-clusters, segregated from TCR clusters [152, 153]. The co-receptor CD28 however is known to interact even more intimately with TCR, co-localizing in the same micro-clusters at least at early times [159].

In a first set of experiments, ICAM-1, which is the ligand of LFA-1, was incorporated into the supported bilayer which surrounded the anti-CD3 dots ([ICAM-1]$_{SLB}$ [αCD3]$_{Dot}$ also called ICAM-1 $\bullet$ anti-CD3). On this substrate the cell spread more than on Bare$\bullet$ anti-CD3, the membrane exhibited no topography, the TCRs did form clusters overlapping with the underlying anti-CD3 dots, and actin was systematically in the form of a peripheral ring. **Importantly, in presence of ICAM-1, the extent of anti-CD3 clustering clearly impacts cell spreading.**

Next, the positions of anti-CD3 and ICAM-1 were reversed – this time ICAM-1 was on the dots surrounded by either a bare SLB or a anti-CD3 containing SLB ([Bare]$_{SLB}$ [ICAM-1]$_{Dot}$ and [Anti-CD3]$_{SLB}$ [ICAM-1]$_{Dot}$ also called Bare • ICAM-1 and Anti-CD3 • ICAM-1). The cell area is lower than on substrates with anti-CD3 clustering, membrane topography is also observed but in less proportion (43% vs 20%). As expected, the TCRs did not form clusters overlapping with the underlaying pattern. The actin architecture is either homogeneous or patterned in absence of anti-CD3 and always homogeneous in the presence of anti-CD3.

We conclude that the clustering of ICAM-1 in dots does not impact cell spreading.

Next, as a variation of substrates with anti-CD3 dots, we functionalized the bilayer with B7.2 (or CD86). Here the ligand of CD28, B7.2 was in the bilayer and the TCR/CD3 ligands were in the dots, thus preventing the mixing of TCR and CD28 domains, except at the edges of the dots. Nevertheless, B7.2 had an impact on T cell behavior. Indeed, cell spreading was not appreciably impacted but the colocalization of TCR and actin patches with underlying dots was impaired for the former and disappeared entirely for the latter

To *interpret* the results described above, it is essential to consider the relative lengths of the involved molecules. Figure 8.10 schematizes the geometry in the vertical direction of all the patterns presented in this thesis. The lengths of the molecules are taken from literature as follows: BSA-biotin = 4 nm, NaV = 4 nm [160], anti-CD3=16 nm, [161], ICAM-1 = 19 nm [162], B7-2-CD28 complex = 14 nm [163], TCR = 7 nm and LFA-1= 20 nm [164].

Throughout this thesis, four parameters were reported: the cell adhesion area, which is a measure of cell activation in T cells [144], TCR clustering and membrane topography which together is thought to be essential for activation [33] and actin architecture which plays an important role in molecular transport as well as mechanosensing [156, 152]. Table 8.11 summarizes the effective height difference between the ligand/receptor pairs, molecular densities of the ligands, and the four measured parameters.

In terms of **area**, results are largely as expected. In presence of anti-CD3 only, the clustering of anti-CD3 does not have a big impact on the cell spreading (0.01<p<0.05 between Bare • anti-CD3 and SLB Neg1+anti-CD3). Compare to POS anti-CD3, spreading on Bare • anti-CD3 is the same which possibly indicates that in the Bare • anti-CD3 system, we already have enough anti-CD3 to attain maximum possible stimulation with anti-CD3 alone. Addition of B7-2 on the SLB induces no change in the area. This can be explained by the fact that while B7-2 is known to reduce the activation threshold level, it may not induce additional activation required for further spreading. With addition of the repulsive polymer PEG in the SLB cell spreading area decreases. This may partly due to the decrease of the ligand density (25±15 vs 5±3 molecules/µm^2). As expected, in presence of ICAM-1 on the SLB the cell area significantly increases and presence of PEG reduces this spreading. We showed here that the clustering of anti-CD3 in presence of ICAM-1 on the SLB does have a positive impact on cell spreading area. As anticipated, ICAM-1 alone, in the form of dots or not, does not induce cell spreading. Addition of anti-CD3 increases the spreading but not as much as on substrates with anti-CD3 in the dots surrounded by ICAM-1. Moreover, comparing patterned and homogeneous substrates ICAM-1 clustering does not have an impact on cell spreading area of T-cells.

It is seen that in terms of **topography**, whenever the height of the dots plus the receptor length (henceforth called h_d) is higher than the surrounding area, with or without ligands, plus the length of the receptors (henceforth called h_{SLB}), there is a high probability (20-40%) of detecting patterned cells. That is, high percentage of patterned membrane is seen if $h_d > h_{SLB}$ and no ligand (case of Bare•anti-CD3 and Bare•ICAM-1). We believe that the cell membrane above the ligand-free and distant SLB harbors long molecules of the glycocalyx, which are responsible for keeping the membrane away from the SLB. This was hinted at in our experiments labelling CD45 (Figure 6.21). As was reported in section 6.2 however, there is always a population of cells where the membrane is flat and no topography is detected. We speculate that in these cases the glycocalyx is pushed out of the contact zone. Whether the first case represents a kinetically trapped state or whether different cells have different amount of glycocalyx and hence behave differently remains to be explored. PEG molecules at 4 nm are too short to change this scenario.

However, clearly, the presence of adhesive ligands in the SLB (case of ICAM-1• anti-CD3 and B7-2•anti-CD3) drives out the long molecules and promotes homogeneous adhesion. One exception to the rule above is Anti-CD3 • ICAM-1 here, since $h_d > h_{SLB}$ topography is seen in about 20 % of the cells. Interestingly, pre-activating the cells also leads to a loss of patterning even on Bare•anti-CD3.

The co-localization of TCR with anti-CD3 dots occurs in all cases (where anti-CD3 is in form of dots) with a few exceptions. Whereas on POS anti-CD3, the anti-CD3 is distributed all over the surface and the TCR get bound and immobilized uniformly, on dot anti-CD3 (Bare• anti-CD3 with or without PEG) there is a pool of diffusive and non-bound TCR molecules that are able to diffuse over the SLB and co-localize with the anti-CD3 dots. On ICAM-1• anti-CD3, the ICAM-1 is diffusive and does not hinder the diffusion of TCR. However in presence of PEG, co-localization of TCR and anti-CD3 is hindered (see Figure 6.19), possibly because with 5% ICAM-1 carrying NTA-lipids and 2% PEG-lipid in the SLB, the surface may be too crowded to allow free diffusion of the ICAM-1 bearing lipids, which, when ligated to LFA-1 in turn act as fixed obstacles on the cell surface thus preventing free diffusion of the TCR. Two other cases where a centralization of the TCR in the form of a cSMAC, in addition to co-localization with anti-CD3 dots are seen, in presence of B7.2 or when cells are pre-treated with anti-TCR (anti-V$_\beta$8). We think that in both cases, TCR clusters are formed on the SLB due to the presence of their (co-)receptors on the SLB (B7-2) or in solution (anti-V$_\beta$8) and these then migrate over the dots to be centralized, as would happen if the ligands were free to move.

In terms of actin, patterned organization seems to be correlated with the membrane patterning describe above. Between homogeneous and peripheral organizations, the distribution broadly shows a correlation with binding strength, with stronger binding resulting in more peripheral organization [149]. For example, most cells present homogeneously distributed actin in absence of ICAM-1 but actin is peripherally distributed in presence of ICAM-1. In presence of B7-2 and in pre-activated cells, the actin architecture is peripheral and may be related to TCR centralization. Exception is observed for POS anti-CD3, on which non-specific interactions may lead to stronger interactions than expected [142].

To conclude, in this thesis the power of TIRF-compatible patterned substrates ex-

hibiting clusters of one ligand with or without the presence of another ligand was demonstrated. Based on our experimental results, we presented qualitative arguments to explain the observations which should now set the stage for a more quantitative model linking molecular parameters and ligand clustering to cell activation.
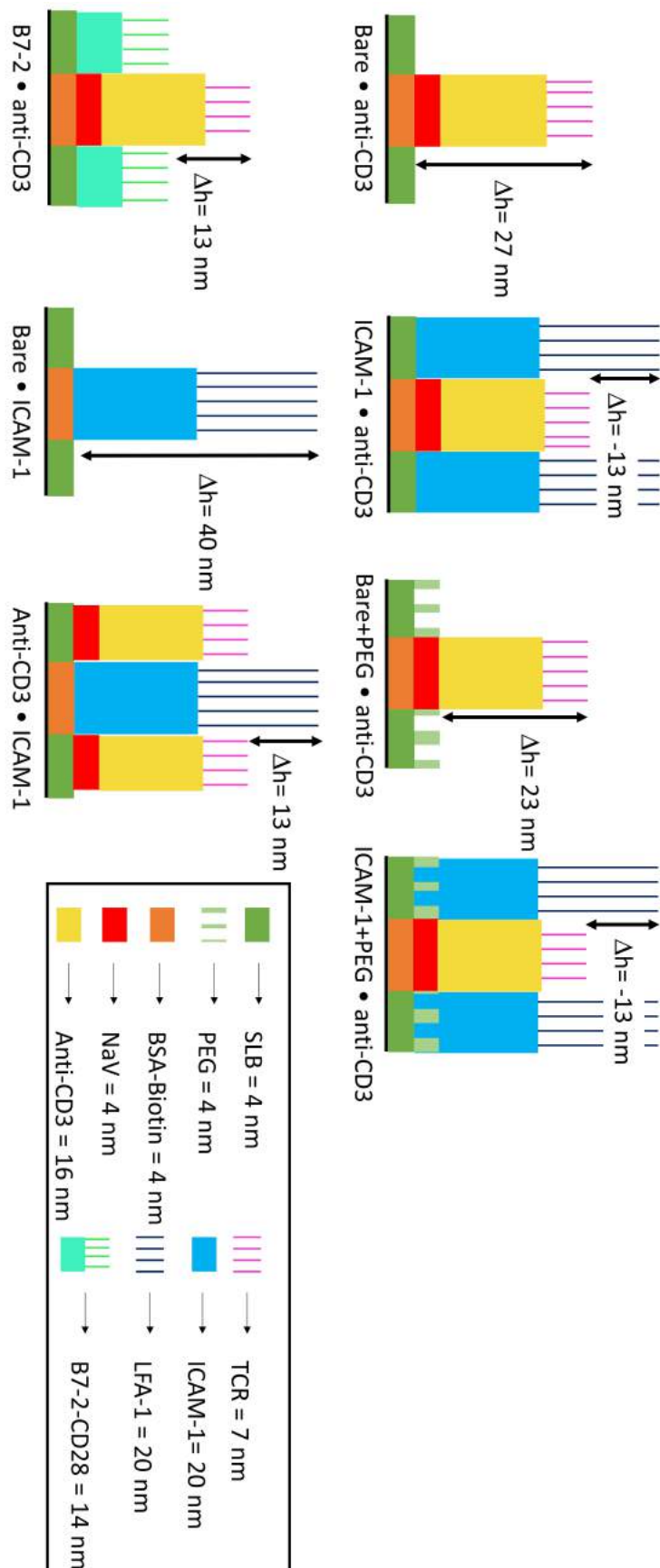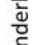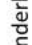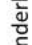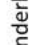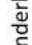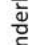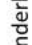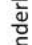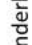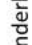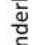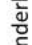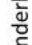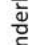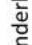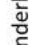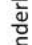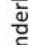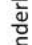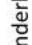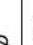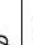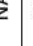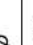
Figure 7.1: **Schematic of the molecular size and geometry in the vertical direction for all the patterns.**

Substrates	ρ NaV (molecules/μm²)	ρ ICAM-1 (molecules/μm²)	Δh ($h_d - h_{SLB}$) (nm)	Membrane topography	Cell Area (μm²) (m±std)	TCR	Actin
Bare • anti-CD3	25±15	Ø	27	Yes (43%)	220±70	(patterned)	(patterned / periphery)
ICAM-1 • anti-CD3	9±4	100	-13	No	310±130	(patterned)	(periphery)
B7-2 • anti-CD3	11±4	Ø	13	Yes (5%)	185±50	(centralization / homogeneous)	(periphery)
Bare • ICAM-1	Ø	45	40	Yes (20%)	65±45	(homogeneous)	(patterned)
Anti-CD3 • ICAM-1	31±14	45	13	Yes(20%)	170±80	(homogeneous)	(homogeneous)
Bare+PEG• anti-CD3	5±3	Ø	23	Yes (40%)	130±60	(patterned)	(patterned / periphery)
ICAM-1+PEG • anti-CD3	11±5	NA	-13	No	110±50	(homogeneous)	NA
Bare • anti-CD3 (Pre-activated cells)	25±15	Ø	27	No	360±145	(centralization)	(periphery)
POS anti-CD3	115±50	Ø	0	No	235±70	(homogeneous)	(periphery)
POS ICAM-1	Ø	160	0	No	93±40	(homogeneous)	(homogeneous)
SLB Neg1+anti-CD3	12±2	Ø	NA	No	155±70	(homogeneous)	(homogeneous)
SLB ICAM-1+anti-CD3	16±8	100	NA	No	120±60	(homogeneous)	(periphery)
SLB Neg2+ICAM-1	Ø	NA	NA	No	70±40	NA	(homogeneous)
SLB anti-CD3+ICAM-1	34±11	NA	NA	No	145±70	NA	(periphery)

Legend:
- ⋮ : patterned following the underlaying ligand
- ● : homogeneously distributed
- ☀ : centralization and patterned following the underlaying ligand
- ○ : enrichement in the periphery
- (green box) : Patterned substrates
- (blue box) : Homogeneous substrates

Figure 7.2: **Table resuming the substrates characteristic and cell results.** ρ NaV and ICAM-1 was determined from fluorescence images. Δ_h correspond to the height difference between the dot (h_d) and the SLB (h_{SLB}). In the columns corresponding to TCR and actin distribution, the most frequent geometry is entered first (leftmost) and so on. NA= Not available.

Chapter 8

Summary in French

L'interaction des cellules T avec les cellules présentatrices d'antigènes (CPA) joue un rôle central dans l'immunité adaptative. L'une des caractéristiques principales de cette interaction est d'être a la fois très sensible et de posséder une discrimination stricte dans le contexte de la reconnaissance de l'antigène par les lymphocytes T. Pour atteindre cet objectif, la membrane des cellules T porte une variété de molécules co-stimulantes et inhibitrices qui complètent l'interaction médiée par le TCR. Suite à la rencontre avec son antigène, une étape cruciale permettant une activation complète de la cellule T est la réorganisation de sa membrane et de son cytosquelette. De facon concomittante, la cellule se propage sur la CPA, formant ce qu'on appelle la synapse immunologique [44, 57]. L'étendue de l'étalement des cellules T est un marqueur de leur activation et de leur éventuelle prolifération [144].

Une approche très fructueuse pour étudier l'adhésion et la réorganisation membrane/cytosquelette a consisté à remplacer la CPA par un substrat synthétique présentant l'antigène. Ces premiers substrats étaient, typiquement, des bicouches lipidique supportées (BLS) portant des ligands pour le complexe TCR/CD3: soit des peptides couplés à des molécules de CMH (pCMH) couplées à des lipides [44] soit des molecules d'anti-CD3 biotinylé couplées a des lipides [63], et des ligands pour LFA-1 souvent sous la forme d'une protéine ancrée à du GPI [63, 44] ou connectée à des lipides fonctionnalisés avec du NTA [145]. Au cours de la dernière décennie, de tels substrats ont été conçus pour transporter, en plus, des co-récepteurs [145] pour disséquer des aspects spécifiques de la réponse des lymphocytes T.

Au début des années 2000, des travaux de Dustin et Saito ont souligné l'importance des clusters de TCR dans l'initiation de l'activation des cellules T [146, 64]. La ségrégation du TCR en grappes (ou clusters) est également au coeur du modèle actuellement le plus crédible pour l'activation des cellules T, à savoir la ségrégation cinétique [33]. Dans ce modèle, la topographie membranaire joue un rôle important. La paire TCR/pCMH étant beaucoup plus courte que ICAM-1/LFA1, les clusters de TCR excluent les plus longues molecules (ICAM-1/LFA1) mais aussi les longues phosphatases (comme CD45). L'absence de CD45 permet la phosphorylation des motifs ITAM associés au domaine TCR/CD3, initiant ainsi l'activation des lymphocytes T.

Simultanément avec l'activation et l'adhésion, la polymérisation de l'actine est déclenchée au bord de la cellule pour favoriser l'étalement [147]. L'actine est organisée comme un anneau en périphérie [148], dont la structure a été révélée récemment [149, 150, 151]. Il

a aussi été démontré récemment que la nature périphérique de l'anneau d'actine est plus prononcée pour les ligands pCMH avec une forte affinité que pour les ligands plus faibles où la distribution est plus homogène [149]. Le TCR ainsi que le LFA-1 sont connectés au cytosquelette d'actine et les espèces moléculaires reliant les intégrines comme LFA-1 à l'actine sont bien connues, cependant celles reliant le TCR à l'actine ne sont pas encore complètement identifiées [152]. Les clusters de TCR qui excluant à la fois LFA-1 et les long sucres, sont transportés par le flux retrograde d'actine vers le centre où ils forment le cSMAC [63, 153].

Pour aborder la question de l'impact de la ségrégation ou du regroupement des ligands/récepteurs, deux approches ont vu le jour: la modification génétique afin de varier les longueurs moléculaires, ou la manipulation des structures elles-mêmes, parfois appelée mutation spatiale [65]. La deuxième approche a été avancée par le laboratoire de Groves, qui a conçu des BLS confinées à l'intérieur de corrals de taille micrométrique ne permettant pas la diffusion des molécules entre deux corrals adjacents. Ceci a révélé l'importance de la diffusion des ligands pour la formation d'une synapse immunologique stable.

Parallèlement à l'utilisation de BLS comme susbtrat synthétique mimant la CPA, plusieurs groupes ont également utilisé directement une lame de verre fonctionnalisée par des protéines [148, 97]. En utilisant cette approche, Irvin et Doh ont exploré les conséquences de la micro-agrégation du TCR et/ou de LFA-1, en se concentrant sur la formation du cSMAC [97]. Ils ont montré que les lymphocytes T ne peuvent être complètement activés que lorsque les points focaux du ligand du TCR sont au centre de la surface d'interaction, mais pas quand ils sont configurés différemment. Plus tard, Kam et al. [98] ont montré que les lymphocytes T étaient capables de produire de l'IL-12 quand les ilots d'anti-CD3 sont entourés de CD28 (molécule de co-stimulation qui se lie à CD80/86) alors que lorsque ces deux molécules sont co-localisées, ils ne le font pas. Ces études ont souligné l'importance de l'organisation des ligands sur la formation de la synapse immunologique et l'activation des lymphocytes T.

Un article plus récent a rapporté des rôles complémentaires du TCR et de LFA-1 sur la croissance du cytosquelette et de sa contractilité en utilisant le micro-patterning. Ils ont en effet trouvé que l'adhésion à LFA-1 augmente les forces d'actomyosine, qui à leur tour modulent l'assemblage d'actine en aval du TCR [155].

Plus récemment, les lymphocytes T ont été interrogés par des nano-motifs de ligands [99, 100, 101]. En utilisant cette approche il a été révélé que les cellules T répondent globalement à la densité moyenne des ligands de TCR, plutôt qu'à des détails de la structure du substrat [99]. De plus, en jouant avec la distance entre les ligands du TCR, et en présence aussi d'ICAM-1 dans le système, Declassian et al. a montré que la structure spatiale à l'échelle nanométrique peut affecter le comportement des lymphocytes T. En effet plus l'espacement augmente, plus les réponses des cellules T diminuent (pour atteindre un niveau basal avec un espacement de 69 nm). Cependant, dans ce système, la densité et l'espacement des ligands sont liés [101]. Dans le cadre des projets en cours dans l'equipe, les interactions entre les cellules T et des surfaces synthetiques sont étudiées en utilisant des techniques de microscopie avancée (comme le RICM et TIRF-M). Le ligand de choix était l'anti-CD3 pour deux raisons. Premièrement, l'utilisation d'anti-CD3 plutôt que de pCMH nous a permis de travailler avec le complexe TCR/CD3 seul, en l'absence d'ICAM-1, chose impossible si le pCMH était utilisé puisque la liai-

son TCR-pCMH n'est pas assez forte pour maintenir l'adhésion. De plus, il convient de souligner qu'il s'agit d'une approche légitime depuis que l'on sait que l'anti-CD3 induit les mêmes voies de signalisation que la liaison de pCMH [14] et que le domaine CD3 intervient dans la mécanotransduction des cellules T [156]. La deuxième raison de l'utilisation de l'anti-CD3 est liée au choix de l'utilisation de la lignée cellulaire Jurkat, pour laquelle le peptide associé au CMH n'est pas disponible [130]. Dans le groupe, nous développons de nouvelles stratégies pour structurer l'anti-CD3 sur des surfaces en verre (ou en élastomère). La lithographie utilisant un masque colloïdal est la méthode de choix pour simplifier le processus de structuration. Avec cette technique, jusqu'à présent, des ilots de taille inférieure au micron ont été obtenus. La stratégie de fonctionnalisation impliquant uniquement des molécules et des protéines organiques, et évitant les métaux comme l'or, a permis de s'assurer que les substrats sont entièrement compatibles avec la microscopie optique avancée, ce qui nous a permis d'aller au-delà des travaux décrits dans [100, 99, 101] et d'observer l'adhésion cellulaire globale ainsi que la réorganisation locale de la membrane et de l'actine. C'est dans ce contexte que cette thèse a été conçue et exécutée.

Pendant le travail de ma thèse, j'ai fait des avancée dans deux directions parallèles – dans l'amélioration des substrats et dans la compréhension de la réponse cellulaire.

8.1   Fabrication du substrat

En ce qui concerne les substrats, au début de ma thése, un protocole d'ilots de taille inférieure au micron avait été développé. Les ilots fonctionnalisés avec de l'anti-CD3, étaient entourés d'un polymère répulsif (PLL-PEG) [102]. Nous avons développé une nouvelle façon de faire varier la taille des ilots indépendamment de l'espacement [102]. Simultanément, j'ai mis en place le protocole pour remplacer le PLL-PEG par une BLS fluide [102, 157]. Ce protocole donne un très bon contrôle de l'espacement et de la taille des ilots d'anti-CD3 mais la densité des protéines de surface est plus difficile à contrôler. Cependant, ceci n'est pas en soi prohibitif puisque nous pouvons mesurer la densité de surface à l'intérieur et à l'extérieur des ilots. La fabrication du substrat patterné consiste tout d'abord à créer un masque primaire soit par auto-assemblage de billes, soit par lithographie par faisceau d'électrons, sur lequel est déposée une couche d'aluminium. Puis, un masque secondaire est révélé en enlevant le masque primaire. Ensuite, une matrice constitué de BSA marquée par de la Biotine ou NTA est créé par dépôt à travers ce masque secondaire. Et enfin la BLS est déposée (Figure 8.1). Différentes combinaisons de protéines et de lipides ont été utilisées.
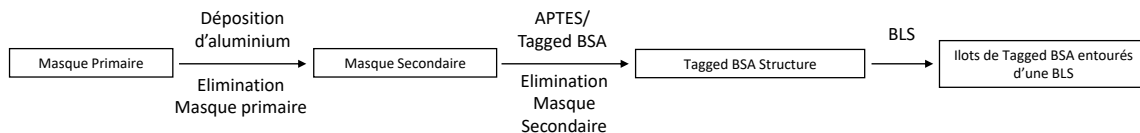
Figure 8.1: **Schéma général de la technique de structuration.**

8.1.1 Préparation du masque primaire

8.1.1.1 Preparation du masque primaire par auto-assemblage de billes

La principale technique utilisée lors de ma thèse pour créer le réseau de nano-agrégats a été l'auto-assemblage de billes colloïdales pour créer le masque primaire (voir Figure 8.2). Pour cela des billes de 2 μm de diamètre ont été utilisées. Dans cette technique la distance entre les billes (centre à centre) correspond au diamètre des billes utilisées. Après déposition d'une monocouche de billes sur une lamelle, une fine couche homogène d'aluminium est déposée par pulvérisation cathodique magnétron à fréquence radio (FR).
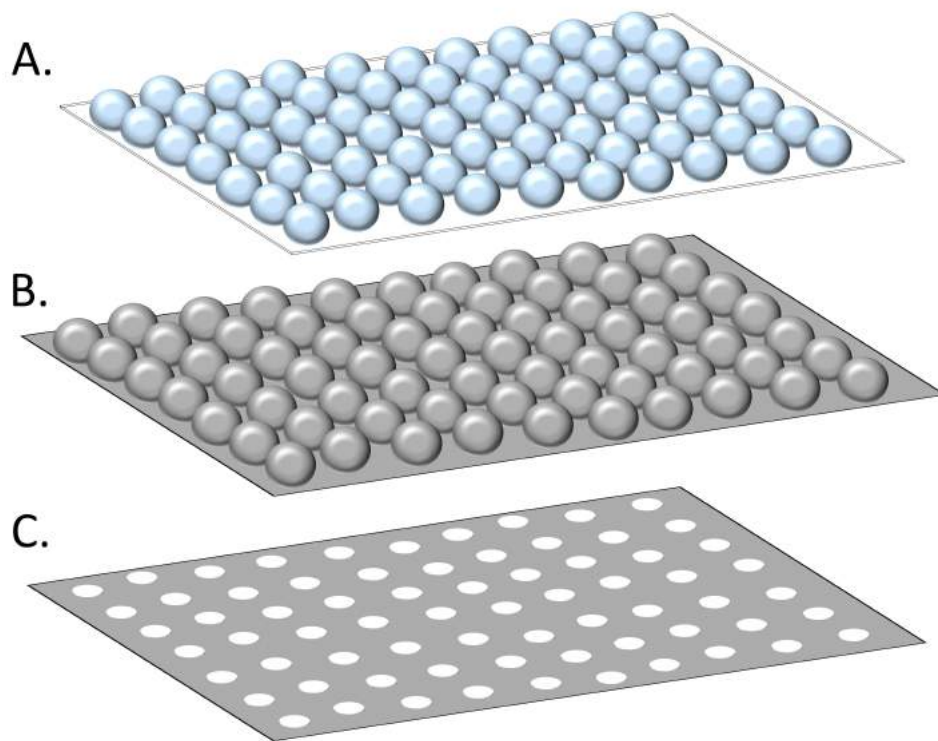
Figure 8.2: **Schéma de la technique d'auto-assemblage de nano-sphères.** A: Lamelle en verre avec un masque de billes colloïdales (notez que pour des raisons de simplicité, un motif carré est montré, en réalité le motif est hexagonal); B: L'aluminium est déposé par pulvérisation cathodique; C: Les billes sont enlevées par sonication. La surface résultante est constituée d'une couche mince d'aluminium avec des trous en lieu et place des billes.

8.1.2 Préparation de masques par lithographie par faisceau d'électrons

Nous avons développé une méthode alternative pour créer le substrat patterné, par lithographie par faisceau d'électrons (e-beam lithographie). L'avantage de cette tech-

nique est la reproductibilité et la résolution du motif (on s'attend à 20 nm). Voir la figure 8.3 pour le schéma général du protocole de lithographie par faisceau d'électrons. Pour cette technique, un faisceau d'électrons est utilisé pour créer le motif désiré a travers une résine négative et l'aluminium est déposé par évaporation. Nous avons décidé de tester différents types de motifs en changeant le pas et la taille des trous (voir la figure 8.1). Les différents motifs obtenus sont représentés sur la figure 8.4.
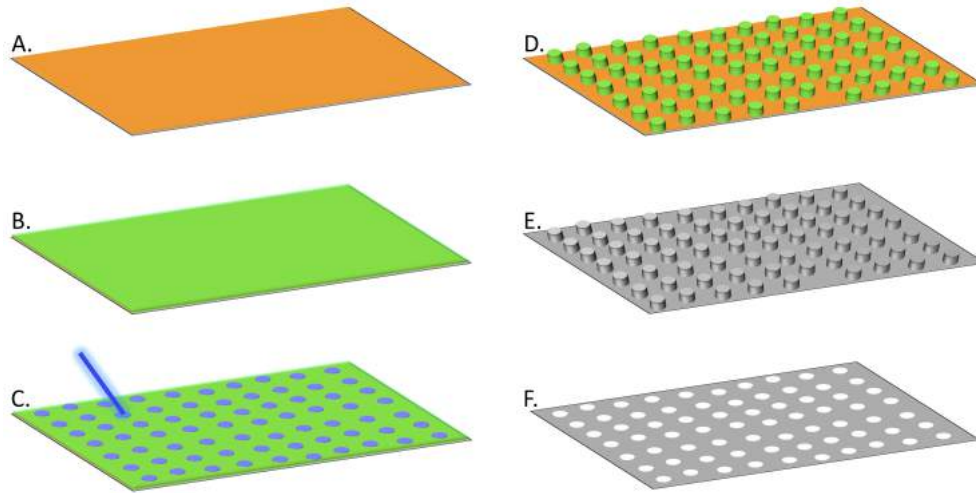
Figure 8.3: **Schéma du protocol de lithographie par faisceau d'électrons.**A: Lame de verre revêtues d'une couche de liaison. B: Une resine negative est déposée par centrifugation sur la lame de verre. C: Le motif est dessiné en exposant la résine au faisceau d'électrons. D: Après le développement, seule la résine exposée est laissée, laissant un reseaux de piliers de résine. E. L'aluminium est déposé par évaporation. F. La résine est dissoute, enlevant l'aluminium déposé sur le dessus. À la fin, une fine couche d'aluminium avec un reseau de trous vides est laissée.

Zone	Pas (μm)	Taille des trous (nm)
A	1	500
B	2	500
C	3	1000
D	0,9	300

Table 8.1: **Description de différents motifs dessinés avec la lithographie par faisceau d'électrons.**

8.1.3   Préparation de la matrice de protéines

Avant cette étape, les billes sont enlevées par ultrasons et la lamelle séchée à l'azote. A ce stade la lamelle est recouverte d'aluminium avec des trous vides exposant le verre. Afin de créer les ilots protéiques, la lamelle à travers les trous est d'abord fonctionalisée avec un

silane (APTES) permettant l'adsorbtion des protéines. La première couche de protéines est constituée de BSA marquée par de la Biotine ou NTA. Puis suite à l'élimination de l'aluminium (Figure 8.5 A-D) la BLS est déposée autour des ilots protéiques (Figure 8.5 E). La plupart des BLS ont été faites en utilisant la technique de Langmuir-Blodgett/ Langmuir Schaeffer (LB/LS). Cette technique permet d'obtenir une bicouche lipidique avec une vitesse moyenne de diffusion de 4.2 ±0.3 μm^2/sec. De plus, afin d'augmenter la fluidité de la BLS un dépôt utilisant des vésicules lipidiques a été testé. Cependant, cette technique n'a pas donné de résultats satisfaisant (BLS pas ou peu fluide).

8.1.4 Fonctionnalisation protéique

Les ilots protéiques et la BLS sont fonctionnalisés en même temps. Cependant avant de fonctionnaliser la BLS, une étape de passivation de la BLS est effectuée à l'aide de BSA. Les protéines utilisées pour fonctionnaliser les substrats au niveau des agrégats sont soit l'anti-CD3 soit l'ICAM-1 et pour la BLS soit l'anti-CD3 soit l'ICAM-1 ou soit B7-2. Dans le premier cas (fonctionnalisation avec l'anti-CD3), de la BSA-biotine suivie de neutravidine fluorescente sont préalablement déposées, alors que pour les deux derniers cas (functionnalisation avec ICAM-1 ou B7-2) la fonctionalisation est précédée d'un dépôt de BSA-NTA. Parallèlement aux substrats patternés, différents types de substrats contrôles homogènes sont été fabriqués. Il y a des contrôles pour les ilots protéiques (qui représentent la situation protéique au niveau des ilots mais à plus grande échelle) et des contrôles pour la BLS. Parmi ces derniers types de contrôles 2 types de situation protéique ont été crées : la situation dans laquelle l'absorption des protéines se fait de façon non-spécifique lors de la fonctionnalisation des ilots (appelé contrôle homogènes de type 1) et la situation dans laquelle la densité protéique est similaire à celle du substrat patterné (appelé contrôle homogène de type 2). La Table 8.2 liste les différents substrats préparés pour cette thése et la Figure 8.6 montre la composition et l'organisation des différentes protéines sur les différents substrats.

8.2 Caractérisation des substrats

Les substrats ont étés caractérisés en terme de fluidité de la BLS, de densité protéique (à l'intérieur et extérieur des ilots, et sur tout le substrat) et aussi par la mesure de la taille des ilots protéiques

8.2.1 Substrats patternés

La fluidité de la BLS est mesurée par la technique de photoblanchiment continu. Globalement il a été montré que la fluidité de la BLS sur des substrats patternés est autour de 5 μm^2/sec et qu'elle n'est pas affectée par la fonctionnalisation protéique. La taille des ilots et plus précisément leur diamètre est déterminé par l'épaisseur de la couche d'aluminium déposée par pulvérisation [143]. Elle est mesurée à partir des images fluorescentes du motif revelé par la neutravidine fluorescente (voir Figure 8.7 où pour chaque ilot un ilot médian est construit). Puis en utilisant le profil d'intensité de l'ilot son diamètre est déterminé en mesurant la largeur du pic a mi-hauteur. Il a été montré que le diamètre des ilots protéiques se situe entre 700-900 nm, quel que soit le type de fonctionnalisation (anti-CD3 ou ICAM-1). C'est aussi à l'aide de ce même profil d'intensité que la densité

protéique dans les ilots et à l'extérieur des ilots est déterminée à partir de respectivement le pic du profil d'intensité et de l'intensité entre les pics. En effet, on estime que l'intensité de fluorescence est proportionnelle à la densité de Neutravidine et donc d'anti-CD3. En moyenne, on retrouve quatre fois plus de protéines dans les ilots que sur la BLS, avec une moyenne de 20 ± 10 molécules/μm^2 sur la totalité du substrat. Concernant les substrats obtenus avec la technique de lithographie par faisceau d'électrons, le diamètre obtenu des ilots après fonctionnalisation correspond à celui dessiné avec le faisceau d'électrons. Cependant, sur ces substrats il y a une forte adsorption non spécifique des protéines sur la BLS.

8.2.2   Substrats Homogènes

Comme pour les substrats patternés la fluidité de la BLS est mesurée ainsi que la densité protéique. Sur les substrats contrôles pour la BLS, la fluidité de la bicouche est équivalente à celle trouvée sur les substrats patternés. La densité protéique mesurée sur les contrôles homogènes de type 1 correspond comme prévue à la densité mesurée à l'extérieur des ilots sur les substrats patternés. Pour les contrôles homogènes de type 2, la densité mesurée a servi de référence pour le choix du substrat patterné lors de l'étude de l'impact du regroupement des ligands.

8.3   Comportement des lymphocytes T sur des ligands agrégé

Les études cellulaires se sont concentrées sur le rôle de différents ligands. Pour ce faire, nous avons fixé la séparation des ilots protéiques et leur taille à 2 μm et environ 800 nm respectivement. Ces choix de paramètres ont permis de garantir le fait qu'il y avait suffisamment d'ilots sous une cellule étalée et que l'imagerie optique avec le TIRF était possible (sans avoir à recourir à la super-résolution à ce stade). La taille des ilots se trouve également proche des meilleures estimations de la taille des agrégats de TCR typiques rapportées dans la littérature [145]. Pour les raisons expliquées précédemment, nous avons choisi de travailler avec anti-CD3 pour cibler le complexe TCR-CD3.
Le substrat standard de cette thèse, contre lequel toutes les autres modifications ont été comparées, était composé d'anti-CD3 dans une BLS non fonctionnalisée ([Bare]$_{SLB}$ [anti-CD3] $_{Dot}$ aussi appelé Bare • anti-CD3). Ces substrats sont similaires à ceux étudiés précédement dans le groupe [103], avec la BLS remplacée par un polymère ([PLL-PEG]$_{verre}$ [anti-CD3]$_{Dot}$ aussi appelé PLL-PEG • anti-CD3). Comme prévu, les substrats Bare • anti-CD3 reproduisent un grand nombre des résultats rapportés comme pour PLL-PEG • anti-CD3. Spécifiquement, la topographie de la membrane et l'organisation du TCR et de l'actine qui suivent le motif sous-jacent d'anti-CD3 (voir Figure 8.8).

Cependant, le comportement global des cellules, plus particulièrement le fait que l'étalement des cellules est proportionnel à la densité moyenne des ligands, n'a pas été reproduit ici, probablement à cause d'une passivation inadéquate. Ceci est cohérent avec le fait que même pour PLL-PEG • anti-CD3, ce résultat n'était valable que lorsque la couche PEG était suffisamment dense et non lorsqu'elle était clairsemée [103]. Au-delà du travail précédemment rapporté [103], le cytosquelette d'actine a également été étudié ici. L'actine sous forme de patche a été trouvée presque systématiquement sur des

cellules présentant une topographie membranaire. Sinon, l'architecture du cytosquelette d'actine est variable - allant d'homogène à périphérique. Le résultat le plus important résultant des expériences sur Bare • anti-CD3 et des contrôles associés, et compatible avec les rapports précédents [100, 103], est que lorsque seuls les ligands du complexe TCR-CD3 sont impliqués, le regroupement des récepteurs à un faible impact sur l'étalement cellulaire.

Des expériences similaires ont été faites en utilisant des cellules T primaires provenant d'humains ou de souris. C'est avec ces dernières que les résultats obtenus se rapproche le mieux de ceux obtenus avec les Jurkats.

8.4   Roles des molécules d'adhésion et de co-stimulation

LFA-1 et CD28 étaient les choix de cibles de signalisation secondaires. Traditionnellement, on pensait que LFA-1 facilitait l'activation des TCR uniquement en favorisant l'adhérence des cellules T aux CPA mais maintenant il est accepté que la liaison de LFA-1 à ICAM-1 modifie l'affinité du TCR pour ses ligands [158]. Post-activation, LFA-1 forme ses propres micro-agrégats (plus petits), séparés des agrégats de TCR [152, 153]. Le co-récepteur CD28 est cependant connu pour interagir encore plus intimement avec TCR, et se co-localiser dans un premier temps dans les mêmes micro-agrégats clusters [159]. Dans un premier ensemble d'expériences, ICAM-1, qui est le ligand de LFA-1, a été incorporé dans la BLS qui entoure les ilots d'anti-CD3 ([ICAM-1]$_{SLB}$ [anti-CD3]$_{Dot}$ aussi appelé ICAM-1 • anti-CD3). Sur ce substrat la cellule s'est étalée plus que sur Bare • anti-CD3, et la membrane n'a présenté aucune topographie, les TCR ont formé des agrégats qui se co-localisent avec les ilots d'anti-CD3 sous-jacents, et l'actine a systématiquement pris la forme d'un anneau périphérique (voir Figure 8.9). Fait important, en présence de ICAM-1, l'ampleur de la mise en grappes anti-CD3 affecte clairement la propagation des cellules.

Ensuite, les positions d'anti-CD3 et d'ICAM-1 ont été inversées - cette fois ICAM-1 était dans les ilots entourés soit d'une BLS nue ou d'une BLS contenant de l'anti-CD3 ([Bare]$_{SLB}$ [ICAM- 1]$_{Dot}$ et [Anti-CD3]$_{SLB}$ [ICAM-1]$_{Dot}$ aussi appelé Bare *bullet* ICAM-1 et Anti-CD3 • ICAM -1). L'étalement cellulaire est plus faible que sur les substrats avec les ilots d'anti-CD3, la topographie membranaire est également observée mais en moindre proportion (43% vs 20%). Comme prévu, les TCR n'ont pas formé d'agrégats co-localisés avec le motif sous-jacent. L'architecture de l'actine est soit homogène, soit structurée en patches en l'absence d'anti-CD3 et toujours homogène en présence d'anti-CD3. Nous avons conclut que le regroupement de ICAM-1 en ilots n'a pas d'impact sur l'étalement cellulaire. Ensuite, en tant que variation de substrats structurés avec des ilots d'anti-CD3, nous avons fonctionnalisé la bicouche avec B7.2 (ou CD86). Ici, le ligand de CD28, B7.2 était dans la bicouche et les ligands du TCR/CD3 complexe étaient dans les ilots, empêchant ainsi le mélange des domaines TCR et CD28, sauf sur les bords des ilots. Néanmoins, B7.2 a eu un impact sur le comportement des cellules T. En effet, l'étalement cellulaire n'a pas été significativement impacté mais la co-localisation des patchs de TCR et d'actine avec les ilots sous-jacents a été altérée pour le premier et a complètement disparu pour le second.

8.5 Bilan, discussion et perspectives

Pour interpréter les résultats décrits ci-dessus, il est essentiel de considérer les longueurs relatives des molécules impliquées. La figure 8.10 schématise la géométrie dans le sens vertical de tous les substrats présentés dans cette thèse. Les longueurs des molécules sont tirées de la littérature comme suit: BSA-biotine = 4 nm, NaV = 4 nm [160], anti-CD3 = 16 nm, [161], ICAM-1 = 19 nm [162], complexe B7-2-CD28 = 14 nm [163], TCR = 7 nm et LFA-1 = 20 nm [164]. Tout au long de cette thèse, quatre paramètres ont été rapportés : l'aire d'adhésion cellulaire, qui mesure l'activation cellulaire dans les cellules T [144], le regroupement du TCR et la topographie membranaire qui sont considérés comme essentiels pour l'activation [33], l'architecture de l'actine qui joue un rôle important dans le transport moléculaire ainsi que la mécanosensibilité [156, 152]. La table 8.11 résume la différence de hauteur effective entre les paires ligand/récepteur, les densités moléculaires des ligands et les quatre paramètres mesurés. En termes d'aire d'adhésion, les résultats sont largement conformes aux attentes. En présence d'anti-CD3 seulement, le regroupement d'anti-CD3 n'a pas un grand impact sur l'étalement cellulaire ($0,01 < \mathrm{p} < 0,05$ entre Bare • anti-CD3 et SLB Neg1 + anti-CD3). Comparer avec POS anti-CD3, l'étalement sur Bare • anti-CD3 est le même ce qui indique peut-être que dans le système Bare • anti-CD3, nous avons déjà assez d'anti-CD3 pour atteindre la stimulation maximale possible avec anti-CD3 seul. L'ajout de B7-2 sur la BLS n'induit aucun changement pour l'aire d'adhésion. Cela peut s'expliquer par le fait que, bien que l'on sache que B7-2 réduit le niveau du seuil d'activation, il se peut qu'il n'induise pas d'activation supplémentaire requise pour un étalement plus important. Avec l'addition du polymère répulsif PEG dans la BLS, la zone d'étalement des cellules diminue. Cela peut être dû en partie à la diminution de la densité du ligand (25 ± 15 vs 5 ± 3 molécules/μm²). Comme prévu, en présence d'ICAM-1 sur la BLS, la surface cellulaire augmente significativement et la présence de PEG réduit cette propagation. Nous avons montré ici que le regroupement d'anti-CD3 en présence de ICAM-1 sur la BLS a un impact positif sur l'aire d'adhésion cellulaire. Comme prévu, l'ICAM-1 seul, sous forme d'ilots ou non, n'induit pas d'étalement cellulaire. L'addition d'anti-CD3 augmente l'étalement mais pas autant que sur les substrats avec anti-CD3 dans les ilots entourés par ICAM-1. De plus, en comparant les substrats présentant des ilots et les substrats homogènes, le regroupement d'ICAM-1 n'a pas d'impact sur la zone d'étalement cellulaire des lymphocytes T. On voit qu'en terme de topographie, chaque fois que la hauteur des ilots plus la longueur du récepteur (appelée désormais h_d) est plus élevée que la zone environnante, avec ou sans ligands, plus la longueur des récepteurs (dorénavant appelé h_{BLS}), il y a une probabilité élevée (20-40%) de détecter des cellules patternées. C'est-à-dire qu'un pourcentage élevé de membrane patternée est visible si $h_d > h_{BLS}$. Nous croyons que la membrane cellulaire au-dessus de la BLS sans ligand et éloignée abrite de longues molécules du glycocalyx, qui sont responsables de maintenir la membrane à l'écart de la BLS. Cela a été suggéré dans nos expériences marquant CD45. Cependant, il y a toujours une population de cellules où la membrane est plate et aucune topographie n'est détectée. Nous supposons que dans ces cas, le glycocalyx est expulsé de la zone de contact. Ce comportement différent reste à explorer pour savoir si le premier cas représente un état cinétiquement piégé ou si différentes cellules ont différentes quantités de glycocalyx et donc se comportent différemment. Les molécules

de PEG de 4 nm de haut sont trop courtes pour changer ce scénario. Cependant, il est clair que la présence de ligands adhésifs dans la BLS (cas d'ICAM-1 • anti-CD3 et B7-2 • anti-CD3) chasse les longues molécules et favorise une adhésion homogène. Une exception à la règle ci-dessus est le substrat Anti-CD3 • ICAM-1, puisque ici la topographie $h_d > h_{BLS}$ est observé dans environ 20% des cellules. Il est intéressant de noter que la pré-activation des cellules entraîne également une perte de topographie même sur Bare • anti-CD3. La co-localisation du TCR avec des ilots d'anti-CD3 se produit dans tous les cas (en présence d'ilots d'anti-CD3) avec quelques exceptions. Alors que sur POS anti-CD3, l'anti-CD3 est réparti sur toute la surface et les molecules de TCRs se lient et se fixent uniformément, sur les ilots d'anti-CD3 (Bare • CD3 anti-CD3 avec ou sans PEG) il y a un ensemble de molécules de TCRs non-liées capables de diffuser sur la BLS et de co-localiser avec les ilots d'anti-CD3. Sur ICAM-1 • anti-CD3, l'ICAM-1 est diffusif et n'entrave pas la diffusion du TCR. Cependant, en présence de PEG, la co-localisation du TCR avec l'anti-CD3 est entravée, peut-être parce que avec 5% de NTA-lipides transportant ICAM-1 et 2% de PEG-lipide dans la BLS, la surface peut être trop encombrée pour permettre la libre diffusion des lipides portant ICAM-1, qui, lorsqu'ils sont ligaturés à LFA-1 agissent à leur tour comme des obstacles fixes sur la surface cellulaire empêchant ainsi la diffusion libre du TCR. Dans deux autres cas on observe une centralisation du TCR sous la forme d'un cSMAC, en plus de la co-localisation avec les ilots d'anti-CD3. Il s'agit du substrat en présence de B7.2 ou lorsque les cellules sont pré-traitées avec un anti-TCR (anti-V_β 8). Nous pensons que dans ces deux cas, les agrégats de TCR sont formés sur la BLS en raison de la présence de leurs (co-)récepteurs sur la BLS (B7-2) ou en solution (anti-V_β 8) et ces agrégats migrent ensuite par-dessus les ilots pour ensuite centraliser, comme cela se passerait si les ligands étaient libres de se déplacer.

Concernant l'actine, l'organisation sous forme de patch semble être corrélée avec la structuration membranaire décrite ci-dessus. Entre les organisations homogènes et périphériques, la distribution montre globalement une corrélation avec la force de liaison, avec une liaison plus forte entrainant une organisation plus périphérique [149]. Par exemple, la plupart des cellules présentent une actine distribuée de manière homogène en l'absence de ICAM-1 mais l'actine est distribuée de manière périphérique en présence de ICAM-1. En présence de B7-2 et de cellules pré-activées, l'architecture de l'actine est périphérique et peut être liée à la centralisation des TCR. Une exception est observée pour POS anti-CD3, sur lequel des interactions non spécifiques peuvent conduire à des interactions plus fortes que prévu [142]. En conclusion, dans cette thèse, la puissance de substrats structurés compatibles avec la technique de TIRF-M présentant des groupes d'un ligand avec ou sans la présence d'un autre ligand a été démontrée. Sur la base de nos résultats expérimentaux, nous avons présenté des arguments qualitatifs pour expliquer les observations qui devraient maintenant ouvrir la voie à un modèle plus quantitatif reliant les paramètres moléculaires et le regroupement de ligands à l'activation cellulaire.
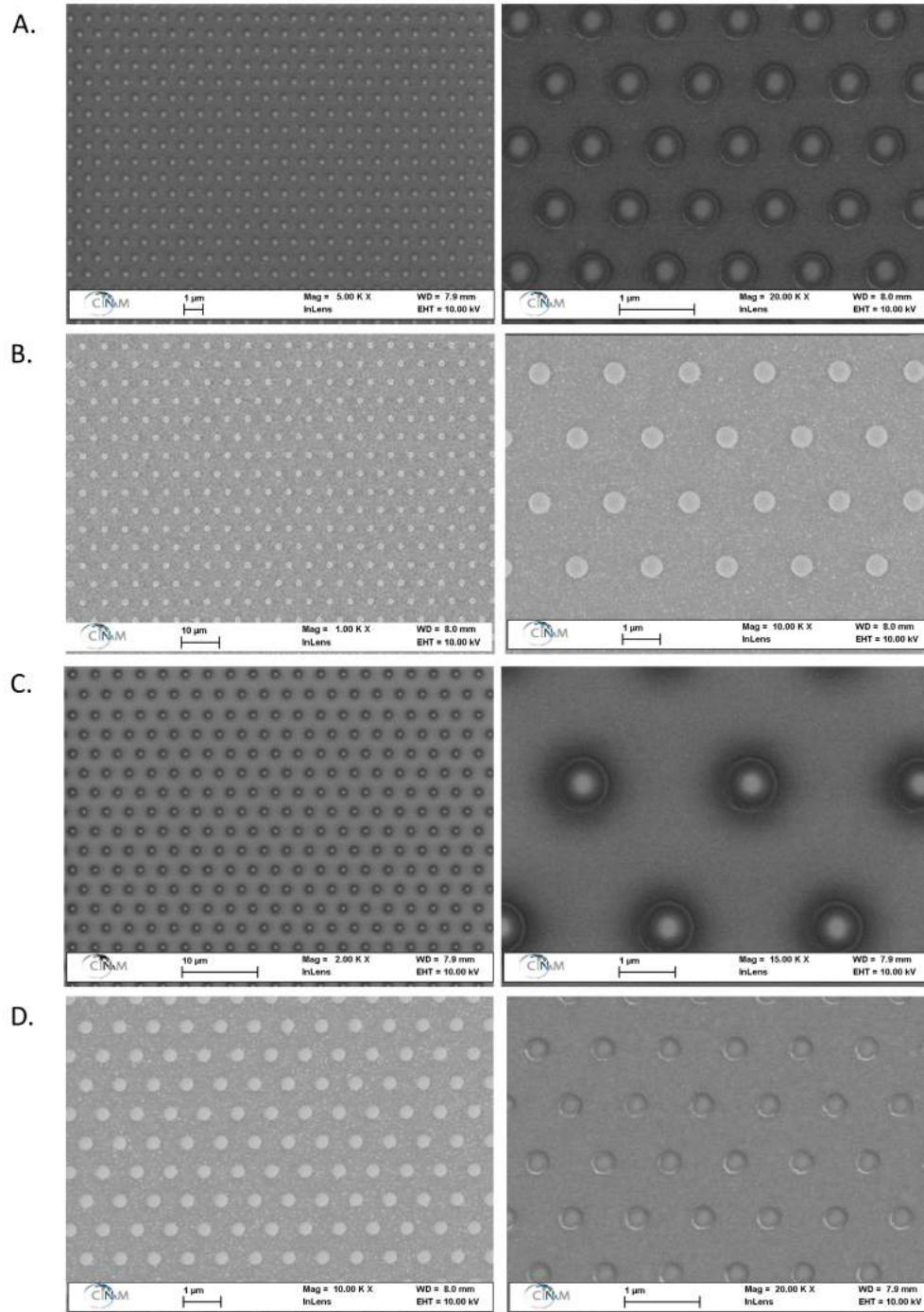
Figure 8.4: **Images en microscopie électronique à balayage des différents motifs (trous en aluminium) réalisés avec la technique du faisceau d'électrons décrit dans table 8.1.** A: Zone A avec un pas de 1μm et une taille de trous de 500 nm; B: Zone B avec un pas de 2μm et une taille de trous de 500 nm; C: Zone C avec un pas de 3μm et une taille de trous de 1000 nm; D: Zone D avec un pas de 0,9μm et une taille de trous de 300 nm.
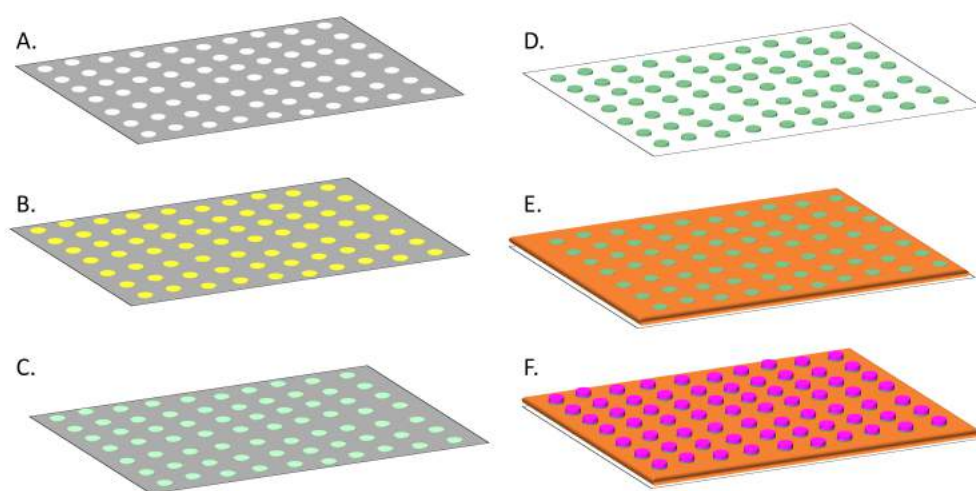
Figure 8.5: **Schéma général de fonctionnalisation du substrat structuré**. A: Lame en verre avec une fine couche d'aluminium avec des trous vides. B: Dépôt d'une couche d'APTES. C: Fonctionnalisation avec les premières couches de protéines dans les trous (BSA-Biotin ou BSA-NTA). D:Enlèvement de la couche d'aluminium ne laissant que les nano-ilots de protéine. E: Dépôt de la bicouche lipidique qui se depose autour des ilots. F: L'étape finale de la fonctionnalisation des ilots est typiquement avec soit de la NaV puis anti-CD3 ou avec ICAM-1-histag. La couche de lipides peut également être fonctionnalisée.

N°	Description		Noms	Nom abrégé
	BLS	ilots	$[\mathbf{BLS}]_{BLS}\ [\mathbf{ilots}]_{ilots}$	**BLS • ilots**
			Substrats structurés	
1	Neg1	α-CD3	$[\text{Bare}]_{SLB}\ [\alpha CD3]_{Dot}$	Bare • αCD3
2	ICAM-1	α-CD3	$[\text{ICAM-1}]_{SLB}\ [\alpha CD3]_{Dot}$	ICAM-1 • αCD3
3	B7-2	α-CD3	$[\text{B7-2}]_{SLB}\ [\alpha CD3]_{Dot}$	B7-2 • αCD3
4	Neg1+PEG	α-CD3	$[\text{Bare+PEG}]_{SLB}\ [\alpha CD3]_{Dot}$	BarePEG • αCD3
5	ICAM-1+PEG	α-CD3	$[\text{ICAM-1+PEG}]_{SLB}\ [\alpha CD3]_{Dot}$	ICAM-1+PEG • αCD3
6	Neg2	ICAM-1	$[\text{Bare}]_{SLB}\ [\text{ICAM-1}]_{Dot}$	Bare • ICAM-1
7	α-CD3	ICAM-1	$[\alpha\text{-CD3}]_{SLB}\ [\text{ICAM-1}]_{Dot}$	α-CD3 • ICAM-1
8	Neg1	BSA-Biotin	$[\text{Bare}]_{SLB}\ [\text{BSA-Biotin}]_{Dot}$	Bare • BSA-Biotin
9	Neg1	anti-rat IgG2b isotype control	$[\text{Bare}]_{SLB}\ [\text{anti-rat IgG2b isotype control}]_{Dot}$	Bare • non-specific
			Controles des ilots	
10		α-CD3	$[\alpha CD3]_{Dot}$	POS α-CD3
11		ICAM-1	$[\text{ICAM-1}]_{Dot}$	POS ICAM-1
12		anti-rat IgG2b isotype control	$[\text{non-specific}]_{Dot}$	POS non-specific
			Controles homogene de la BLS de type 1	
13	Neg1		$[\text{Neg1}]_{SLB}$	SLB Neg1
14	Neg1+PEG		$[\text{Neg1+PEG}]_{SLB}$	SLB Neg1+PEG
15	ICAM-1		$[\text{ICAM-1}]_{SLB}$	SLB ICAM-1
16	ICAM-1 +PEG		$[\text{ICAM-1+PEG}]_{SLB}$	SLB ICAM-1+PEG
17	B7-2		$[\text{B7-2}]_{SLB}$	SLB B7-2 1
18	Neg2		$[\text{Neg2}]_{SLB}$	SLB Neg2
19	α-CD3		$[\alpha\text{-CD3}]_{SLB}$	SLB α-CD3
			Controles homogene de la BLS de type 2	
20	Neg1+ α-CD3		$[\text{Neg1}+\alpha\text{-CD3}]_{SLB}$	SLB Neg1+ α-CD3
21	ICAM-1+ α-CD3		$[\text{ICAM-1}+\alpha\text{-CD3}]_{SLB}$	SLB ICAM-1+ α-CD3
22	Neg2+ICAM-1		$[\text{Neg2+ICAM-1}]_{SLB}$	SLB Neg2+ICAM-1
23	α-CD3+ICAM-1		$[\alpha\text{-CD3+ICAM-1}]_{SLB}$	SLB α-CD3+ICAM-1

Table 8.2: **Description des substrats, de leurs noms et de leurs noms abrégés.**
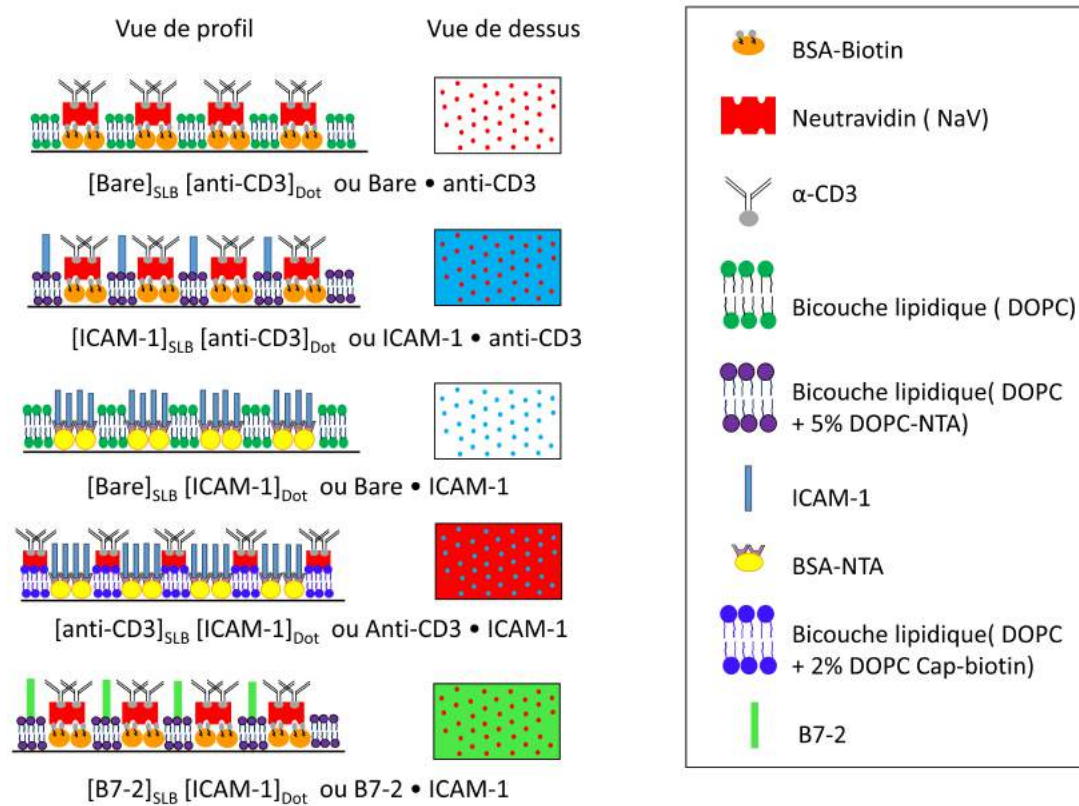
Figure 8.6: **Schéma de la composition protéique et de l'organisation des substrats structurés**. Représentation schématique des différents substrats utilisés durant cette thèse. Les substrats sont composés d'ilots d'anti-CD3 ou d'ilots d'ICAM-1 entourés soit d'une BLS non fonctionnalisé, soit d'une BLS fonctionnalisé avec ICAM-1, B7-2 ou anti-CD3. Une vue de profil et une vue de dessus sont représentées. Notez que l'échelle pour les protéines n'est pas respectée.
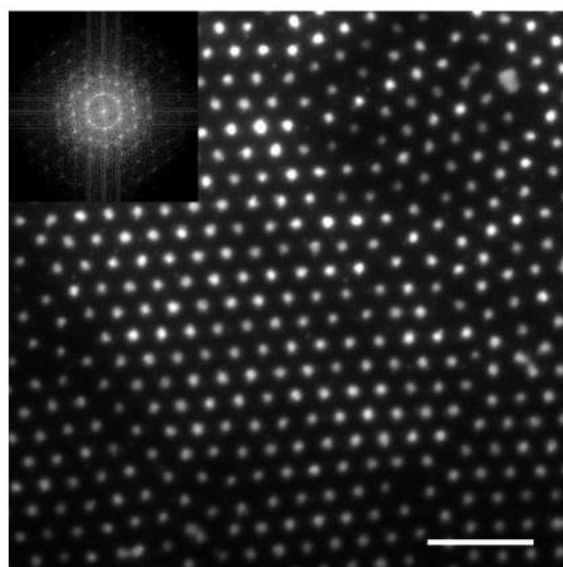
Figure 8.7: **Image d'épifluorescence du réseau d'ilots de NaV.** Les ilots de NaV fluorescents forment un réseau uniforme avec un treillis hexagonal. L'encart affiche la transformée de Fourier montrant l'ordre du réseau. Barre d'échelle $=10\mu$m.
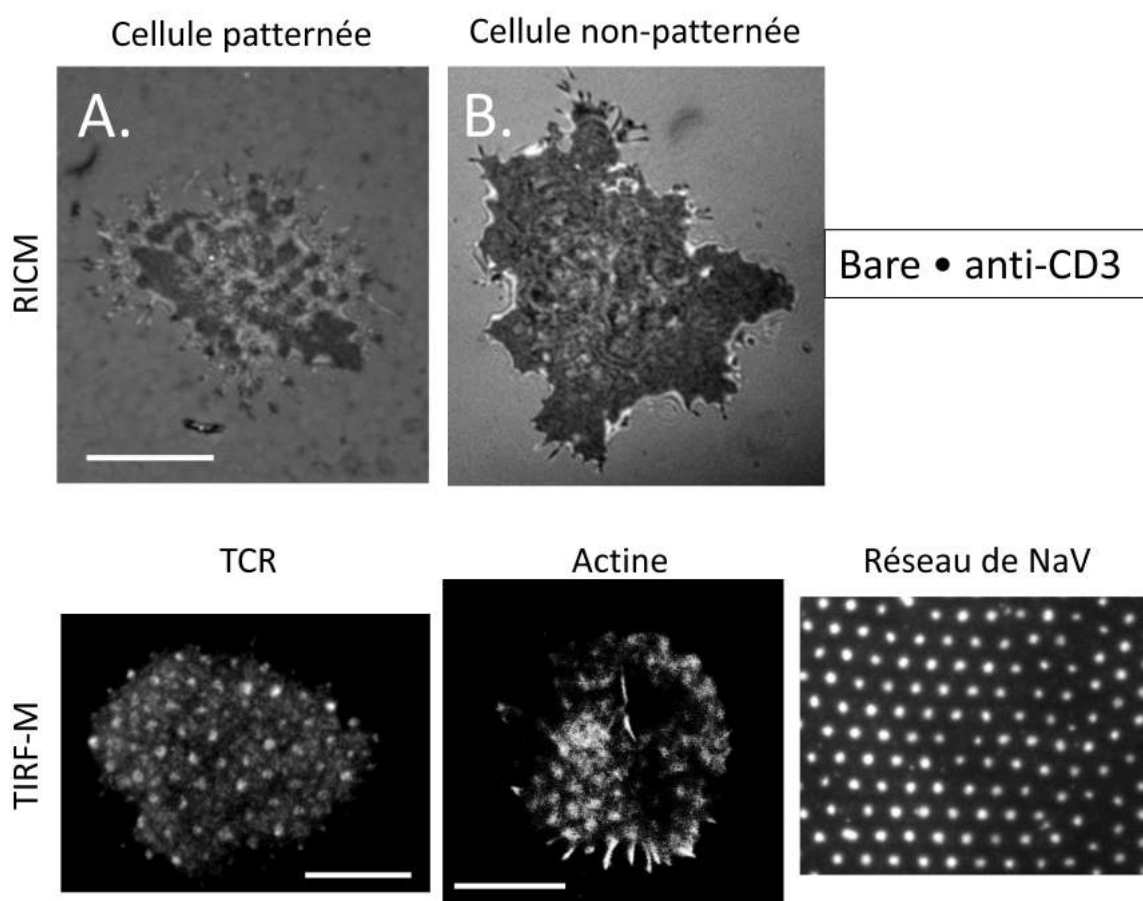
Figure 8.8: **Résultats cellulaires obtenus sur le substrat Bare • anti-CD3.** La première colonne représente les 2 types de topographie membranaire observés sur ce substrat en RICM. La deuxième colonne représente l'organisation du TCR et de l'actine sur ce substrat observés en TIRF-M. Ces deux molécules co-localisent avec le réseau de NaV sous-jacent. Barre d'échelle = 10 μm.
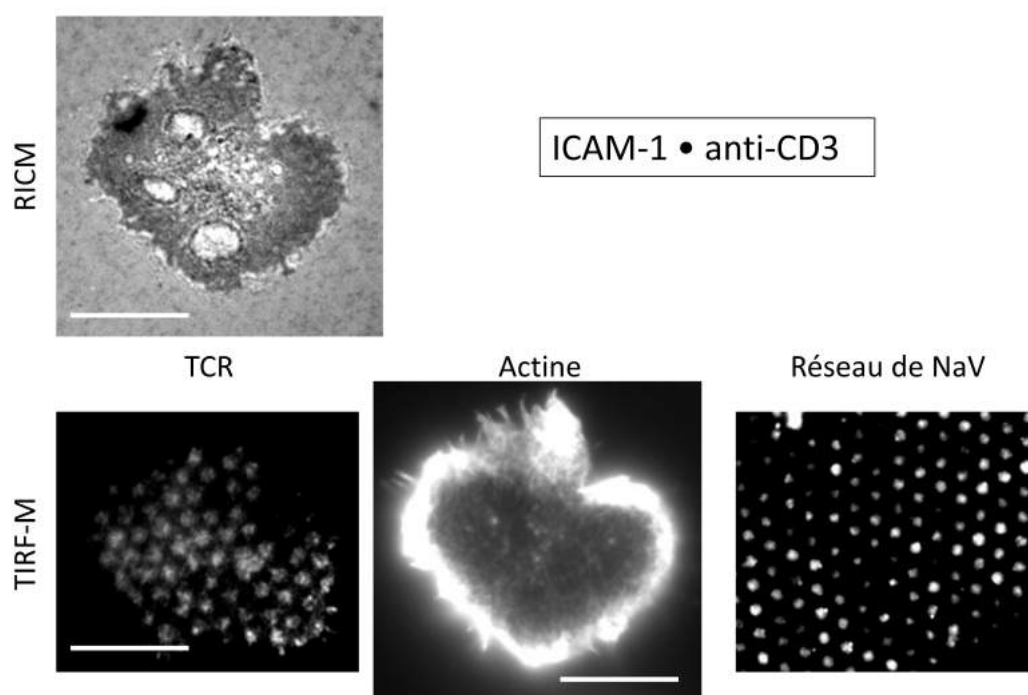
Figure 8.9: **Résultats cellulaires obtenus sur le substrat ICAM-1 • anti-CD3.**
La première colonne représente la topographie membranaire observé sur ce substrat.
L'adhésion cellulaire est homogène. La deuxième colonne représente l'organisation du
TCR et de l'actine sur ce substrat. Le TCR co-localisent avec le réseau de NaV sous-
jacent alors que l'actine s'organise sous forme d'un anneau en périphérie. Barre d'échelle
= 10 μm.
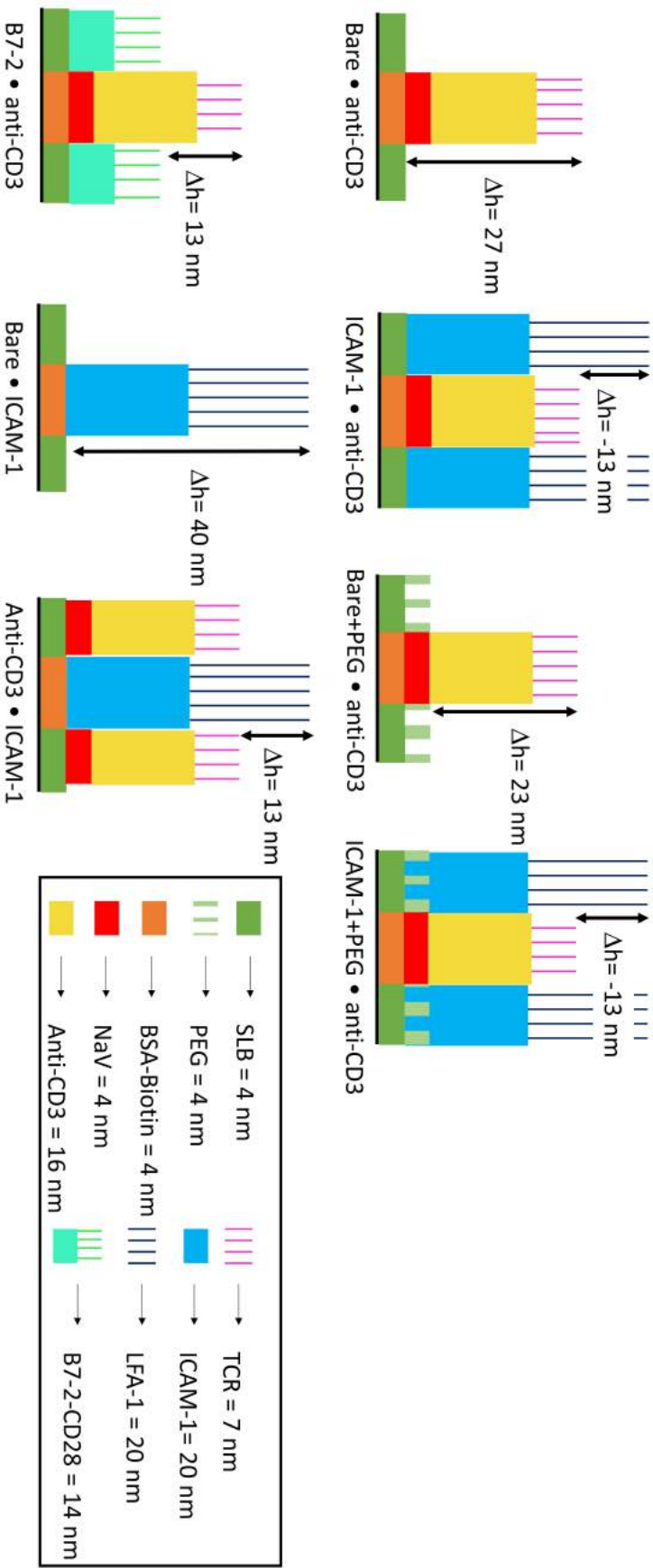
Figure 8.10: **Schéma de la taille et de la géométrie des molécules dans le sens vertical pour tous les substrats.**

Substrates	ρ NaV (molecules/μm²)	ρ ICAM-1 (molecules/μm²)	Δh (h_d - h_{SLB}) (nm)	Membrane topography	Cell Area (μm²) (m±std)	TCR	Actin
Bare • anti-CD3	25±15	Ø	27	Yes (43%)	220±70		
ICAM-1 • anti-CD3	9±4	100	-13	No	310±130		
B7-2• anti-CD3	11±4	Ø	13	Yes (5%)	185±50		
Bare • ICAM-1	Ø	45	40	Yes (20%)	65±45		
Anti-CD3 • ICAM-1	31±14	45	13	Yes(20%)	170±80		
Bare+PEG• anti-CD3	5±3	Ø	23	Yes (40%)	130±60		
ICAM-1+PEG • anti-CD3	11±5	NA	-13	No	110±50	NA	NA
Bare • anti-CD3 (Pre-activated cells)	25±15	Ø	27	No	360±145		
POS anti-CD3	115±50	Ø	0	No	235±70		
POS ICAM-1	Ø	160	0	No	93±40		
SLB Neg1+anti-CD3	12±2	Ø	NA	No	155±70		
SLB ICAM-1+anti-CD3	16±8	100	NA	No	120±60		
SLB Neg2+ICAM-1	Ø	NA	NA	No	70±40	NA	
SLB anti-CD3+ICAM-1	34±11	NA	NA	No	145±70	NA	

Patterned substrates

Homogeneous substrates

⋮ : patterned following the underlaying ligand

● : homogeneously distributed

☀ : centralization and patterned following the underlaying ligand

○ : enrichment in the periphery

Figure 8.11: **Tableau reprenant les caractéristiques des substrats et les résultats cellulaires.** ρ NaV et ICAM-1 ont été déterminée à partir d'images de fluorescence. Δ_h correspond à la différence d'hauteur entre les îlots (h_d) et la BLS (h_{SLB}). Dans les colonnes correspondant au TCR et à la distribution d'actine, la géométrie la plus fréquente est mise en premier (à gauche) et ainsi de suite. NA = Non disponible.

225

Appendix A

Cleaning procedure

This section summarizes all the cleaning procedure of chambers and glass slides to which we will refer in this thesis.

A.1   Procedure 1

This first procedure used a surfactant solution and was used to cleaned the open chambers, Teflon trays and glass slides. The cleaning protocol was the following :

- Ultrasonication in 2% (v/v) of Hellanex III(Sigma Aldrich, France) was performed during 30 minutes at 40°C.

- Items were rinsed 5 times with ultrapure water .

- A second ultrasonication in 2% (v/v) of Hellanex III(Sigma Aldrich, France) was performed during 30 minutes at 40°C.

- Rinsing 10 times with ultra-pure water

- Ultrasonication in ultra-pure water was performed during 30 minutes at 40°C.

- Rinsing 10 times with ultrapure water

- A second ultrasonication in ultra-pure water was performed during 30 minutes at 40°C.

- Rinsing 10 times with ultra-pure water.

After cleaning, all items were kept in ultra-pure water and protected from dust using aluminum foil. Items were used no longer than 48 hours after washing.

A.2   Procedure 2

This second procedure used pirahna acidic solution. This procedure was applied to glass slides used for experiments with Supported Lipid Bilayer by vesicles spreading. The slides were washed using the following protocol :

- The dust was remove from the slide with a Kim Tech

- Glass slides were washed with ethanol then ultra-pure water.

- Glass slides were dried with nitrogen.

- Incubation in a 1-1 ratio isopropanol-water solution in a ultrasonic bath at 40°C was performed during 30 minutes.

- Glass slides were rinsed 10 times with ultra-pure water

- Incubation in ultra-pure water in a ultrasonic bath at 40°C was performed during 15 minutes.

- Glass slides were rinsed 10 times with ultra-pure water

- Glass slides were dried using nitrogen.

- Incubation in piranha solution (70 % sulphuric acid 96 % concentrated and 30 % of hydrogen peroxide) was performed during 5 min.

- Glass slides were rinsed 10 times with ultra-pure water

- Glass slides were dried with nitrogen.

After cleaning, glass slides were kept in ultra-pure water and protected from dust using aluminium foil. They were used no longer than 48 hours after washing.

A.3   Film Balance cleaning

The presence of dust on the Film balance prior of lipids deposition will lead to faults in the bilayers. The following procedure of cleaning was applied for each new lipid deposition:

- Aspirate all the water on the Teflon enclosure using a water pump.

- Wash carefully with a Kimtech soak with chloroform.

- Pour and aspirate 4 times hot ultra-pure water (40 to 50°C)

- Pour and aspirate at least 6 times cold ultra-pure water until the apparent hydrophobicity of the Teflon enclosure is satisfactory enough.

Once the lipid deposition was finished, the Teflon trough was rinsed extensively with ultra-pure water to prevent the adsorption of remains on the Teflon that will lead to a loss of hydrophobicity over time.

Appendix B

Microscope settings

B.1 Epi-Fluorescence

For images using epi-fluorescence the settings for camera and microscope were the following :

1. For the Dansyl and Bodipy dye :
- Exposure time : 100 ms
- Pre-Amp gain : 2
- Electronic gain : 5

2. For the others dyes :

- Exposure time: 500 ms.
- Electronic gain: 100.
- Pre-Amp gain: 3.7.

Appendix C

T-cells pre-activation protocol

In some experiments, cell were pre-incubated with anti-Vβ
during 30 minutes prior the engagement of the cells on the substrate surface. The protocol was the following :

- 1 ml of the culture (containing about 0.6 millions of cells) was centrifuged during 4 minutes at 1100 rpm

- 950 μl of the supernatant was remove carefully

- The pellet was resuspend in the 50μl remaining and incubate with 5μl of 200 μg/ml of anti-Vβ8 during 5 min at 4°C

- 950 μl of of observation medium : composed with PBS+0.1% of BSA

- Cells were centrifuged during 4 minutes at 1100 rpm

- 950 μl of the supernatant was remove carefully

- The pellet was resuspend in 950 μl of observation medium : composed with PBS+0.1% of BSA (which was previously incubate at 37°C for at least 15 minutes).

Appendix D

Color codes for substrate

Each type of characterization is presented in the form of bar charts where the colors correspond to nature of the dot proteins. If it's a pattern substrate, the color outline of the bar chart or symbol corresponds to nature of the SLB and the color of the stripe inside correspond to the nature of the dots (see an example bellow). If it's a homogeneous SLB substrates there is only the outline of the bar charts and if it's a Dot control the bar chart will be homogeneous with a color corresponding to the nature of the SLB.
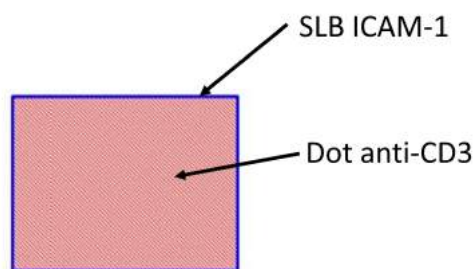
Figure D.1:
Example of a bar chart with a color code corresponding to the substrate [ICAM-1]$_{SLB}$ [αCD3]$_{Dot}$.

Functionalization nature	Color code
Bare	
Anti-CD3	
ICAM-1	
B7-2	
Bare+PEG	
ICAM-1+PEG	
Anti-CD3+ICAM-1	
ICAM-1+anti-CD3	
Neg1+anti-CD3	
Isotype control	
anti-CD3+anti-CD4	

Table D.1:
Color code corresponding to the protein functionalization nature.

Appendix E

Articles and patent

1. **Size-Tunable Organic Nanodot Arrays: A Versatile Platform for Manipulating and Imaging Cells.** Pi F, Dillard P, Alameddine R, <u>Benard E</u>, Wahl A, Ozerov I, Charrier A, Limozin L, Sengupta K. *Nano Lett.* 2015 Aug 12;15(8):5178-84.

2. **Ligand Nano-cluster Arrays in a Supported Lipid Bilayer.** <u>Benard E</u>, Pi F, Ozerov I, Charrier A, Sengupta K. *J Vis Exp.* 2017 Apr 23;(122).

3. **Metal free, Nano-size protein motif compatible with advanced optical microscopy for stimulation of living cells (NanoStim).** <u>Benard E</u>, Sengupta K, Ozerov I, Bedu F and Dallaporta H. ("declaration de invention" submitted for eventual patent submitted in to SATT sud-est in July 2017)

Video Article

Ligand Nano-cluster Arrays in a Supported Lipid Bilayer

Emmanuelle Benard[1], Fuwei Pi[1,2], Igor Ozerov[1], Anne Charrier[1], Kheya Sengupta[1]

[1]Aix-Marseille Université, CNRS, UMR 7325, CINaM

[2]State Key Laboratory of Food Science and Technology, School of Food Science of Jiangnan University

Correspondence to: Kheya Sengupta at sengupta@cinam.univ-mrs.fr

Abstract

Currently there is considerable interest in creating ordered arrays of adhesive protein islands in a sea of passivated surface for cell biological studies. In the past years, it has become increasingly clear that living cells respond, not only to the biochemical nature of the molecules presented to them but also to the way these molecules are presented. Creating protein micro-patterns is therefore now standard in many biology laboratories; nano-patterns are also more accessible. However, in the context of cell-cell interactions, there is a need to pattern not only proteins but also lipid bilayers. Such dual proteo-lipidic patterning has so far not been easily accessible. We offer a facile technique to create protein nano-dots supported on glass and propose a method to backfill the inter-dot space with a supported lipid bilayer (SLB). From photo-bleaching of tracer fluorescent lipids included in the SLB, we demonstrate that the bilayer exhibits considerable in-plane fluidity. Functionalizing the protein dots with fluorescent groups allows us to image them and to show that they are ordered in a regular hexagonal lattice. The typical dot size is about 800 nm and the spacing demonstrated here is 2 microns. These substrates are expected to serve as useful platforms for cell adhesion, migration and mechano-sensing studies.

Video Link

The video component of this article can be found at https://www.jove.com/video/55060/

Introduction

Cell adhesion takes place through specialized cell adhesion molecules (CAMs), proteins present on the cell membrane that are capable of binding to their counterpart on the extra cellular matrix or on another cell. On adhered cells, most adhesion molecules including the ubiquitous integrin and cadherin, are found in the form of clusters [1]. The interaction of T lymphocytes (T cells) with antigen presenting cells (APCs) provides a particularly striking illustration of the importance of receptor clusters formed at the interface between the two cells — often called an immunological synapse. Upon forming the first contact with the APC, T cell receptors (TCRs) on the surface of the T cell form micron scale clusters that serve as signaling platforms [2,3,4], and are eventually centralized to form a larger central supramolecular cluster (cSMAC) [5,6,7]. Recently, it was shown that on the APC side, the ligands of the TCR are also clustered [8].

In the context of T cell-APC interaction, the deployment of hybrid systems, where the APC is mimicked by an artificial surface functionalized with relevant proteins, has greatly advanced our understanding of the synaptic interface [2,3,4,5,6,7]. In this context, it is highly relevant to design APC mimetic surfaces that capture one or more aspects of the target cell. For example, if ligands are grafted on supported lipid bilayers, they can diffuse in the plane of the bilayer, mimic the situation on the APC surface and at the same time allow the formation of the cSMAC [6,7]. Similarly, the clusters on the APC have been mimicked by creating islands of ligands in a sea of polymers [9,10,11,12,13,14]. However, these two features have so far not been combined.

Here we describe a novel technique to create nano-dots of anti-CD3 (an antibody that targets the TCR complex) surrounded by a lipid bilayer with diffusing lipids. The bilayer is deposited using Langmuir-Blodgett/Langmuir-Schaefer technique [7,15,16] and if desired, could be functionalized with a specific protein — for example, the ligand of the T cell integrin (called ICAM1). In addition, the anti-CD3 protein dots could be replaced with another antibody or CAM. While we have chosen the proteins for future use as platform for T cell adhesion studies, the strategy detailed here can be adapted for any protein and even DNA.

Protocol

1. Cleaning Glass Cover-slides and Observation Chambers

1. Arrange the glass cover-slides on a multi-slide tray made of an inert material like Polytetrafluoroethylene (PTFE).

2. Immerse the tray with slides and the observation chamber in a surfactant solution (any product recommended for cleaning quartz cuvettes is suitable).
3. Using an ultrasonic bath, ultra-sonicate in the surfactant solution for 30 min at room temperature (between 20 and 30 °C).
4. Rinse 5 times with ultrapure water (18.2 MΩ.cm, 0.059 μS/cm).
5. Ultra-sonicate in surfactant solution for 30 min at room temperature (between 20 and 30 °C).
6. Rinse 10 times with ultrapure water.
7. Repeat steps 1.5 and 1.6 twice.
8. Store in water at room temperature (between 20 and 30 °C) for up to one week.

2. Fabrication of Protein Nano-dots

1. Deposition of beads
    1. Deposit the suspension of silica beads (2% v/v, 70 μL) drop by drop on a cover-slide (24 x 24 mm, thickness 170 μm) held at an inclination of 15 degrees.
    2. Let the suspension spread for about 1 min while flipping the glass by 90° every 15 s.
    3. Allow the liquid to evaporate under ambient conditions.
    4. Store in a clean glass or PTFE chamber at ambient conditions for up to 2 days.

2. Deposition of aluminum
    1. Place the slides (prepared in section 2.1) inside a radio frequency (RF) magnetron sputtering equipment [8], on a rotating table at a distance of about 105 mm from an aluminum (99%) : silicon (1%) target.
    2. Pump down the deposition chamber to 2.6×10^{-4} Pa using a turbo-molecular pump. This step is important for the removal of possible gaseous impurities.
    3. Introduce pure Argon atmosphere (5N, 99.999%) with a flux of 10 s.c.c.m. at a pressure of 0.8 Pa (6.6 mTorr).
    NOTE: The incoming argon flux is controlled by a mass flow controller and the process pressure is monitored using a pressure gauge. The argon gas flow is continuous and is controlled by a balance between the inlet and outlet opening valves.
    4. Switch on the RF power generator.
    NOTE: Here, a typical range of 400-600 W radiofrequency power at 13.56 MHz frequency was used. The RF generator is used with a matching network in a capacitive plasma coupling mode. The reflected power is monitored and minimized using the network adaptation.
    5. After the plasma is stabilized, sputter for 2 min keeping the shutter closed to remove possible impurities from the surface of the target.
    6. Open the shutter and allow the sputtering to continue for 60 min to deposit aluminum on the glass slide to a thickness of 200 nm.
    7. Cut the flow of argon, close the gate valve to isolate the turbomolecular pump from the deposition chamber and vent the chamber with clean nitrogen to obtain the room pressure. Recover the aluminum-coated slides. Store for up to a month in a clean and hermetically sealed glass or PTFE box under ambient conditions.

3. Vapor deposition of Organosilane
    1. Immerse the aluminum-coated slide prepared in step 2.2.6 in ultrapure water at room temperature and ultra-sonicate for 30 s in an ultrasonic bath (50 W, 50/60 Hz, between 20 and 30 °C).
    2. Deposit 0.5 mL of (3-aminopropyl)-triethoxysilane (APTES) at the bottom of a desiccator.
    CAUTION: APTES is an organosilane, which evaporates easily and is toxic. APTES should be handled only under a flow-hood and with gloves.
    3. Put the glass slides (prepared in 2.3.1) on a ceramic grid and place inside the desiccator.
    4. Connect the desiccator to a membrane pump and run at maximum power for 30 min to generate a low vacuum.
    5. Close the valve of the desiccator and switch off the pump.
    6. Heat the desiccator to about 50 °C for 1 h.
    7. Open the desiccator and collect the slides.
    8. Transfer to another clean desiccator for storage for up to 48 h at room temperature (20 to 30 °C).

4. Deposition of first layer of protein - bovine serum albumin labelled with biotin (BSA-biotin)
    1. Place one of the slides prepared in section 2.3 on a PTFE support.
    2. Deposit 1 mL of 25 μg/mL BSA-biotin dissolved in Phosphate Buffered Saline (PBS). Leave for 30 min at room temperature (20 to 30 °C).
    3. Rinse 10 times with PBS. Store the sample for up to 24 h at 4 °C away from light source.

5. Removal of aluminum mask
    1. Incubate the slides in a solution of NaOH in PBS (prepared by dropwise addition of 1 M NaOH to about 100 mL PBS to obtain pH≈12) over-night at room temperature (between 20 and 30 °C).
    CAUTION. NaOH is corrosive and should be handled using gloves.
    2. Rinse 10 times in ultrapure water.

3. Deposition of Supported Lipid Bilayer (SLB)

1. Cleaning the Langmuir trough
    1. Remove the water in the PTFE enclosure of the Langmuir trough using a pump.
    2. Clean with a lint-free non-woven disposable towel soaked in chloroform.
    CAUTION. Chloroform is toxic and should be manipulated in a well-ventilated area, with a mask (or under a flow-hood) and with appropriate gloves.

3. Clean 4 times with lukewarm ultrapure water (40 to 50 °C).
4. Clean at least 6 times with cold ultrapure water.

2. Deposition of the first lipid layer
   1. Place PTFE trays in the PTFE enclosure of the Langmuir trough and then fill it with ultrapure water.
   2. Use the control software of the Langmuir apparatus to set the measured pressure to 0 mN/m.
   3. Use a gastight glass/metal syringe to deposit 30 µL of a 1 mg/mL lipid solution (1,2-dioleoyl-*sn*-glycero-3-phosphocholine (DOPC) in chloroform) on the surface of the water. The chloroform evaporates and the lipid molecules spontaneously form a monolayer.
   4. Use the control software to compress the lipid monolayer by closing the PTFE barrier till the desired pressure (27 mN/m for DOPC) is reached.
   5. Use the control software to dip the glass slide prepared in the section 2.5.2 into the PTFE enclosure using a motorized clamp.
   6. Hold the slide, in the clamp, perpendicular to the air-water interface. Use the control software to raise it slowly (15 mm/min) through the interface, while maintaining a constant pressure at 27 mN/m.
   7. Place in a dry environment for either immediate use or for storage up to 24 h at room temperature (between 20 and 30 °C).

3. Deposition of the second lipid layer
   1. Maintain the surface pressure in the Langmuir trough at the desired value of 27 mN/m. Compress using the control software of the Langmuir apparatus and/or add a small amount of lipid to achieve the desired pressure.
   2. Place the glass slides carrying the lipid monolayer, prepared in section 3.2.6, horizontally on the surface of the water. Ensure that each slide is floating above a PTFE tray.
   3. Push the glass slides down, one slide at a time, into its corresponding PTFE tray using PTFE or metal tweezers such that they are immersed in the water. Avoid tilting the slides while pushing.
   4. Use PTFE or metal tweezers to transfer the PTFE trays containing the slides into a crystallizer filled with ultrapure water making sure that the slides are not exposed to air.
   5. Use PTFE or metal tweezers to transfer, while working underwater, a bilayer coated glass slide into an observation chamber.
      NOTE: The observation chamber is placed under water inside the crystallizer. The observation chamber is custom made and consists of a PTFE ring with a rubber gasket and steel casings, which can be assembled underwater to make a water-tight chamber whose bottom surface is made from the glass slide previously coated with the lipid bilayer.
   6. Close the chamber while continuing to work under water and ensuring that about 1 mL of water is trapped inside the chamber.
   7. Take the assembled chamber out of the water. Make sure that it is water-tight and leakage free.
   8. Replace the 1 mL of ultrapure water present in the observation chamber with PBS by adding and removing 500 µL of PBS 10 times. Ensure that the chamber is never devoid of liquid.

4. SLB blocking step
   1. Introduce 100 µg/mL of bovine serum albumin (BSA) in the observation chamber containing the slide prepared in section 3.3.6 and incubate for 30 min at room temperature (between 20 and 30 °C).
   2. Rinse the bilayer by removing and adding 500 µL of PBS 10 times. The bilayer can be kept 24 h at 4 °C.

4. Functionalization with Ligands

1. Add fluorescent or non-fluorescent neutravidin (NAV, a deglycosylated version of avidin not charged at pH 7) at 2 µg/mL into the chamber containing the slide prepared in section 3.4.2 for 30 min at room temperature (between 20 and 30 °C).
2. Rinse by adding and removing 500 µL of PBS 10 times.
3. Add biotinylated anti-CD3 at 2 µg/mL to the chamber containing the slide prepared in section 3.4.2. For double functionalization of the SLB and the dots, add Fc-ICAM1 His-tag at 5 µg/mL (here, the bilayer is made of DOPC + 1% of nitrilotriacetic acid (NTA) lipids). Leave for 30 min at room temperature (between 20 and 30 °C).
4. Rinse by adding and removing 500 µL of PBS 10 times
5. Replace the PBS with cell medium (PBS + 0.1% BSA) by adding and removing 500 µL of the cell medium 10 times.
6. Leave 200 µL of cell medium in the chamber with the slide.
7. Place the chamber for 10 min at 37 °C before adding cells.

5. Cell Deposition (see reference 7 for details)

1. Carefully deposit 400 µL of the cell suspension into the chamber. Incubate the cells for 30 min at 37 °C.
2. Fix the cell with 2% of paraformaldehyde (PFA) for 15 min at 37 °C. Replace the PFA with PBS by repeated removal and addition of 500 µL of PBS.

6. Observation

1. Proteo-lipidic Nano-pattern and SLB fluidity
   1. Use a fluorescence microscope to image the protein pattern in epi-fluorescence mode using appropriate illumination wavelength (639 nm) and filter cubes (*e.g.* here, EX TBP 483+564+642; BS TFT 506+582+659; EM TBP 526+601+688).
      NOTE: The intensity of the signal can be quantified to estimate the amount of protein inside and outside the dot. Use an appropriate illumination wavelength (330 nm) and filter cube to image the bilayer (BP 365/12, FT 395, LP 397), which appears bright with dark holes.
   2. Use continuous photo bleaching (CPB) technique[13,15] to measure the diffusion constant of tracer lipids in the bilayer. This observation is preferably made just after the SLB deposition.

NOTE: In order to quantify the diffusion constant, two parameters are measured during CPB process: the specific bleaching time of the dye (tauT) and the decay length of the fluorescent profile of the halo formed around the bleached area (tauD). The first is obtained by plotting the time evolution of the fluorescence intensity at the center of the illuminated field during the CPB process. The second is obtained by plotting the intensity profile at the edge of the illuminated zone (averaged over 12 lines and 5 images after steady-state is reached). The curves are fitted to obtain tauT and tauD. The diffusion constant is given by tauD^2/ tauT (D=$\frac{\tau_d^2}{\tau_t}$).

Representative Results

The fluorescence images were analyzed to measure the spacing and size of the dots. Typical spacing was found to be 1,900 ± 80 nm and typical dot-size was 600 ± 100 nm (**Figure 1g**). The spacing is set by the size of the beads used for the mask. The dot-size is set by the bead-size as well as deposition conditions. The SLB is deposited uniquely around the protein dots and not on them (**Figure 2**), with perfect complementarity between the holes seen in SLB imaging channel and the dots seen in the NAV imaging channel. Analysis of continuous photo bleaching data shows that the lipids in the patterned bilayer remain fluid and have a typical diffusion constant of 5 µm²/s (**Figure 3**).
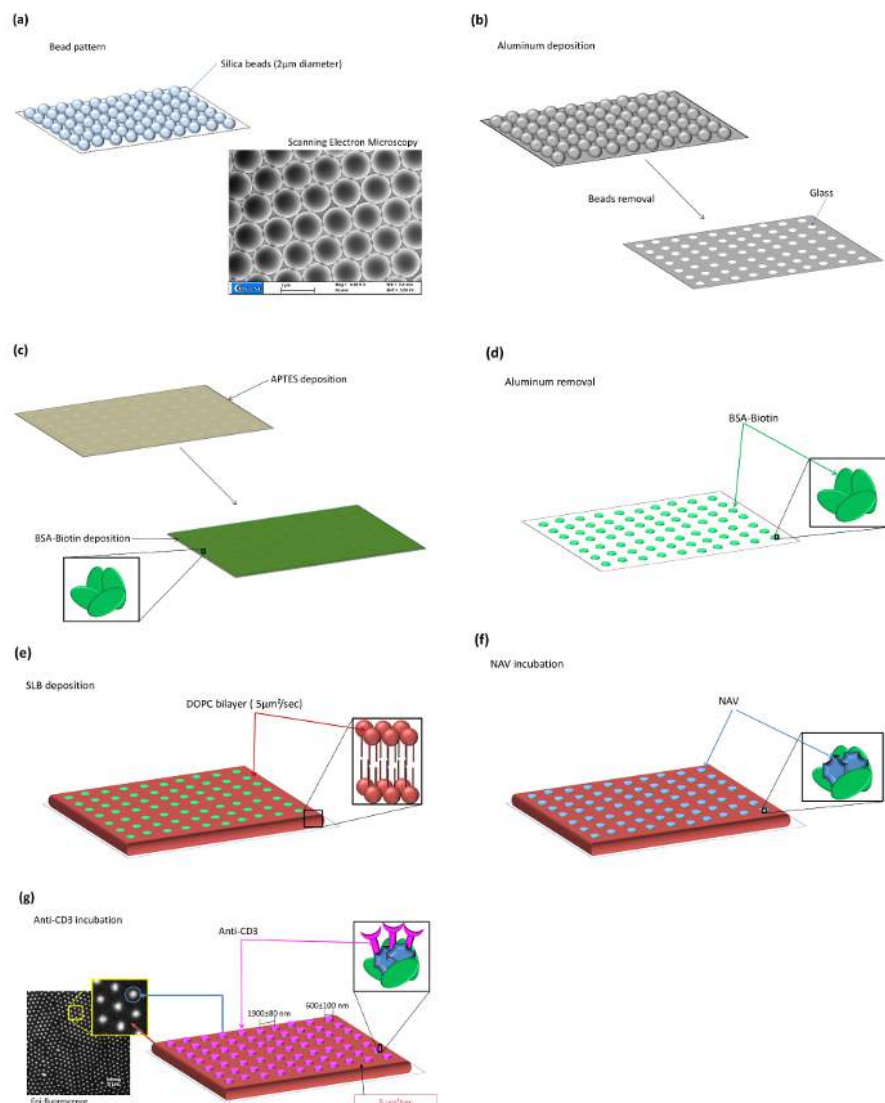
Figure 1: Schematic representation of fabrication steps. (**a**) Primary bead mask. Inset shows a scanning electron microscopy (SEM) image of the mask, made with beads of 2 µm diameter and covered with a thin layer of aluminum. Parameters used in this image are: nominal aluminum thickness 200 nm deposed at 400 W RF, initial pressure of 9 x 10^{-7} Torr, Argon flux 10 sccm, process pressure 6.2 mTorr, imaged at acceleration voltage of 5 kV. The images confirm observation made with optical microscopy (image not included) before aluminum deposition that the beads are arranged in a monolayer centered hexagonal lattice on the glass-slide. (**b**) Secondary mask of aluminum created by the sputter deposition after removal of the primary bead-mask. (**c**) Deposition of organosilane and BSA-biotin though the secondary mask. (**d**) Removal of aluminum revealing nano-dots of BSA-biotin. (**e**) Deposition of SLB. (**f**) Binding NaV to BSA-biotin. (**g**) Binding anti-CD3 to NaV.

Inset shows epi-fluorescence image of the nano-dots arrays. Here the NaV is fluorescently labelled. Typical dot-size is 600±100 nm and typical spacing is 1,900 ± 80 nm. Please click here to view a larger version of this figure.
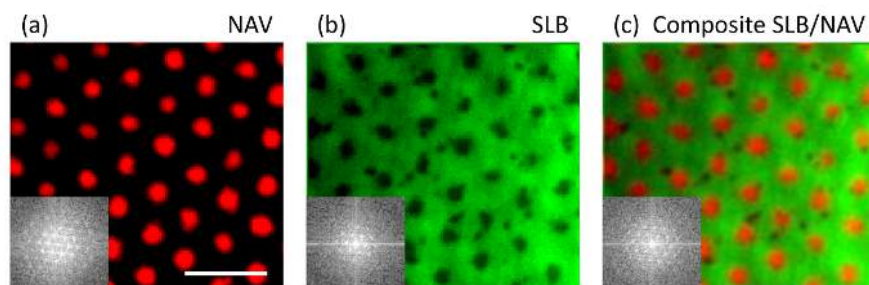
Figure 2: Complementarity of the nano-dot and SLB pattern. (**a**,**b**) Epi-fluorescence images of fluorescent NaV nano-dots and of SLB with fluorescent tracer lipids. (**c**) Composite image of the NaV dots (red) in the sea of SLB (green) shows perfect complementarity of the NaV and SLB. Fast Fourier Transform (FFT) image in the inset indicates long-range order. Scale bar: 4 µm. Please click here to view a larger version of this figure.
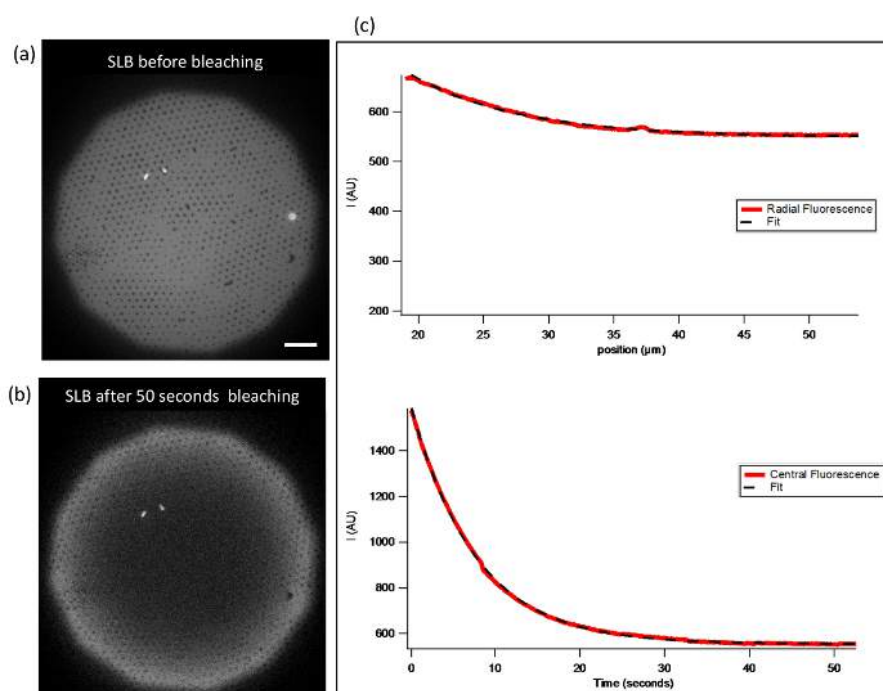
Figure 3: Quantification of lipid diffusion in the SLB. (**a**) Epi-fluorescence image of a SLB before bleaching. The protein dots show up as dark holes in a bright sea of lipids. The field-diaphragm limits the illuminated area. (**b**) Epi-fluorescence of SLB after bleaching continuously for 50 s. The halo visible inside the region delimited by the field-diaphragm indicates that the lipids are mobile. Scale bar: 10 µm. (**c**) Average intensity profile along the edge of the field-diaphragm (top) and the decay of intensity over time during the beaching process (bottom). This data is analyzed to extract the diffusion constant, which is typically 5 µm²/s.

Discussion

The critical steps within the protocol described above are related to the formation of the protein nano-dots or the back-filling of the space around the dots by a supported lipid bilayer. The first critical step with respect to protein nano-dots is the preparation of the bead-mask. The cleaning of the cover-slide is critical. The slides need to be either cleaned with a detergent solution that is recommended for cleaning quartz cuvettes, or with oxygen plasma. Other cleaning techniques like immersion in ethanol or iso-propanol treatment do not render the glass sufficiently hydrophilic and therefore do not support the formation of a large-coverage bead monolayer. At the same time, the surface of the slide needs to be compatible with the subsequent step of formation of the SLB by Langmuir-Blodgett technique [7,15,16]. The next critical step is the deposition and removal of aluminum. If the deposition is via sputtering technique, as done here, the target should to be doped with silicon (at 1%). Otherwise, if the target is made of pure aluminum, the deposited layer is hard to remove with the alkali hydroxide solution as described above, probably due to the formation of aluminum oxide and interpenetration between deposited aluminum layer and glass slide substrate. The duration of deposition determines the size of the protein dots [9], however, here we have worked with a single deposition time and therefore single dot size. The sample can be stored under ambient conditions for several months after aluminum deposition and for about a week after the deposition of BSA-biotin.

The second crucial step concerns the deposition of the SLB. Cleaning of the glass cover-slide is again a crucially important point. As is the case for any Langmuir-Blodgett deposition work, all the material used should be made of glass or Polytetrafluoroethylene (PTFE) and should be scrupulously clean. After deposition of the first lipid monolayer, the cover-slides can be stored for a couple of days but after the deposition of the second monolayer, they need to be used immediately.

While we have demonstrated the protocol for creating anti-CD3 nano-dots for use in T lymphocyte adhesion studies [9,13], the procedure is highly flexible and can be adapted for any biotinylated protein. The composition of the lipid bilayer can be easily changed and it can be further functionalized if desired. One important point to consider is the possible unspecific absorption of proteins, especially on the lipid bilayer surrounding the dots.

The main limitation of the technique arises from the use of colloidal-bead self-assembly for the primary mask. Being a bottom-up technique, it shares some of the problems of all such approaches for example, lack of flexibility and full control over the pattern shape. The pattern lattice necessarily reflects the symmetry of the bead mask and is therefore always hexagonal. The shape of the pattern motif is a circle and is determined by a combination of bead-size and the duration of aluminum deposition [9,13]. Alternative techniques for controlling the dot size have also been suggested [14,17,18].

Substrates nano-patterns with proteins, protein-fragments or peptides have been extensively used in the past to probe cell-surface interactions, especially adhesion [19] and migration [20]. Pioneering work has shown that tissue-forming cells fail to spread on patterns with a pitch greater than a given threshold [21], and further investigation showed that the length-scale of this phenomenon is set by the size of talins, which are instrumental in linking integrin receptors to the actin cytoskeleton [22]. However, in all these studies, the proteins were linked to gold nano-particles, which were themselves immobilized on glass.

In the context of T cells, proteo-lipidic membranes, typically mimicking antigen presenting cells, have been extensively used to understand fundamental aspects of T cell function [6]. Ingenious nano-patterning techniques have been used to create corrals with metal barriers separating protein functionalized SLB patches, which have provided insight into the structure and connectivity of the T cell/APC interface [23]. This kind of nano-patterning is however very different from the protein nano-dots proposed here. Recently, nano- clusters were created using chemical linkage of the protein functionalized lipids [3], which shed light on the consequence of receptor clustering. The advantage was that, unlike the present case, the clusters could in principle be themselves mobile. However, such spontaneously formed clusters are necessarily less well controlled in terms of size and density than pre-formed protein nano-dots described here.

We envisage that the protein nano-dot decorated SLBs presented here can be used to investigate different aspects of cell-cell adhesion. One obvious question that arises is whether, as described above for tissue forming cells [19], lymphocytes too have an intrinsic length-scale associated with adhesion. Preliminary results seem to indicate that at least when the adhesion is mediated by the TCR complex, the density of ligands rather than spacing is the defining parameter for spreading and activation [10,11,12,13]. Whether inclusion of mobile ligands in the surrounding SLB impacts this observation and how the mobile and immobile fractions work together is a possible question, which was partly addressed using self-assembled SLB bound clusters [24]. Another interesting application will be in the context of mechano-sensing where cell adhesion/activation on mobile and immobilized ligands were shown to be different not only for T cells [7,25] but also for cells that habitually adhere to the extra cellular matrix [26].

The two main advantages of these proteo-lipidic patterns are the compatibility of the substrates with advanced optical microscopy and the ease of preparation which makes them compatible with use-and-throw applications. Subsequent to aluminum deposition, all the preparation steps can be carried out on a standard wet-lab bench. In the future, it can be envisaged that the aluminum-coated and glass-supported bead-masks produced in a specialized facility are transferred and stored in biology laboratories for use as and when required. With this in view, we believe that these substrates have the potential to become the platform of choice for studying the interaction of cells with controlled nano-patterned proteo-lipidic membranes.

Disclosures

The authors have nothing to disclose.

Acknowledgements

References

1. Alberts, B., Johnson, A., Lewis, J., *et al.* Molecular Biology of the Cell. 4th edition. New York: *Garland Science.* (2002).
2. Varma, R., Campi, G., Yokosuka, T., Saito, T., Dustin, M.L. T Cell Receptor-Proximal Signals Are Sustained in Peripheral Microclusters and Terminated in the Central Supramolecular Activation Cluster. *Immunity.* **25**(1), 117-27, (2006).
3. Kaizuka, Y. *et al,* Mechanisms for segregating T cell receptor and adhesion molecules during immunological synapse formation in Jurkat T cells. *Proc Natl Acad Sci USA.* **104**(51), 20296-301 (2007).
4. Dustin, M.L., Groves, J.T. Receptor signaling clusters in the immune synapse. *Annu Rev Biophys.* **41**, 543-56 (2012).
5. Huppa, J.B. and Davis, M.M. T-cell-antigen recognition and the immunological synapse. *Nat Rev Immunol.* **3**(12), 973-83, (2003).
6. Grakoui, A., *et al.* The Immunological Synapse: A Molecular Machine Controlling T Cell Activation **.** *Science .* **285**, 221-228 (1999).
7. Dillard, P., Varma, R., Sengupta, K., Limozin, L. Ligand-mediated friction determines morphodynamics of spreading T cells. *Biophys J.,* **107**(11), 2629-38 (2014).

8. Lu, X., *et al.* Endogenous viral antigen processing generates peptide-specific MHC class I cell-surface clusters. *Proc Natl Acad Sci U S A.* **109**(38), 15407-12 (2012).
9. Pi, F., Dillard, P., *et al.* Size-Tunable Organic Nanodot Arrays: A Versatile Platform for Manipulating and Imaging Cells. *Nano Lett.* **15** (8), 5178-5184 (2015).
10. Deeg, J. *et al.* T cell activation is determined by the number of presented antigens. *Nano Lett.* **13**(11), 5619-26 (2013).
11. Delcassian, D., *et al.* Nanoscale ligand spacing influences receptor triggering in T cells and NK cells. *Nano Lett.* **13**(11), 5608-14 (2013).
12. Matic, J., Deeg, J., Scheffold, A., Goldstein, I., Spatz, J.P. Fine tuning and efficient T cell activation with stimulatory aCD3 nanoarrays. *Nano Lett.* **13**(11), 5090-7 (2013).
13. Dillard, P., Pi, F., Lellouch, A.C., Limozin, L., Sengupta, K. Nano-clustering of ligands on surrogate antigen presenting cells modulates T cell membrane adhesion and organization. *Integr Biol.* **8**(3), 287-301 (2016).
14. Pi, F., Dillard, P., Limozin, L., Charrier, A., Sengupta, K. Nanometric protein-patch arrays on glass and polydimethylsiloxane for cell adhesion studies. *Nano lett.*, **13**(7), 3372-8 (2013).
15. Fenz, S. F., Merkel, R., and Sengupta, K. Diffusion and intermembrane distance: case study of avidin and E-cadherin mediated adhesion. *Langmuir.* **25** (2), 1074-1085 (2009).
16. Sengupta, K., *et al.* Mimicking tissue surfaces by supported membrane coupled ultra-thin layer of hyaluronic acid. *Langmuir.* **19** (5), 1775-1781, (2003).
17. Taylor, Z.R., Keay, J.C., Sanchez, E.S., Johnson, M.B., Schmidtke, D.W. Independently controlling protein dot size and spacing in particle lithography. *Langmuir.* 28(25), 9656-63 (2012).
18. Massou, S. *et al.* Large scale ordered topographical and chemical nano-features from anodic alumina templates. *Appl. Surf. Sci.* 256(2), 395-398 (2009).
19. Selhuber-Unkel, C., Lopez-Garcia, M., Kessler, H., Spatz, J.P. Cooperativity in adhesion cluster formation during initial cell adhesion. *Biophys J.* 95(11), 5424-31 (2008).
20. Arnold, M., *et al.* Induction of cell polarization and migration by a gradient of nanoscale variations in adhesive ligand spacing. *Nano Lett.* 8(7), 2063-9 (2008).
21. Cavalcanti-Adam, E.A., *et al.* Cell spreading and focal adhesion dynamics are regulated by spacing of integrin ligands. *Biophys J.* 92(8), 2964-74 (2007).
22. Schvartzman, M., *et al.* Nanolithographic Control of the Spatial Organization of Cellular Adhesion Receptors at the Single-Molecule Level. *Nano Lett.*, 11 (3), 1306-1312 (2011).
23. Mossman, K., Groves, J. Micropatterned supported membranes as tools for quantitative studies of the immunological synapse. *Chem.Soc.Rev.* 36(1), 46-54 (2007).
24. Furlan, G. *et al.*, Phosphatase CD45 both positively and negatively regulates T cell receptor phosphorylation in reconstituted membrane protein clusters. *J Biol Chem.* 289(41), 28514-25 (2014).
25. Hsu, C.J., *et al.* Ligand mobility modulates immunological synapse formation and T cell activation. *PloS One.* 7(2), e32398 (2012).
26. Yu, C. *et al.* Early integrin binding to Arg-Gly-Asp peptide activates actin polymerization and contractile movement that stimulates outward translocation. *Proc Natl Acad Sci U S A.* 108(51), 20585-90 (2011).

Size-Tunable Organic Nanodot Arrays: A Versatile Platform for Manipulating and Imaging Cells

Fuwei Pi,[†] Pierre Dillard,[†,‡] Ranime Alameddine,[†] Emmanuelle Benard,[†] Astrid Wahl,[†] Igor Ozerov,[†] Anne Charrier,[†] Laurent Limozin,[‡] and Kheya Sengupta*,[†]

[†]Aix-Marseille Université, CNRS, CINaM-UMR 7325, Marseille 13288, France

[‡]Laboratoire Adhésion and Inflammation, Aix-Marseille Université/Inserm U1067/CNRS-UMR7333, Marseille13288, France

S Supporting Information
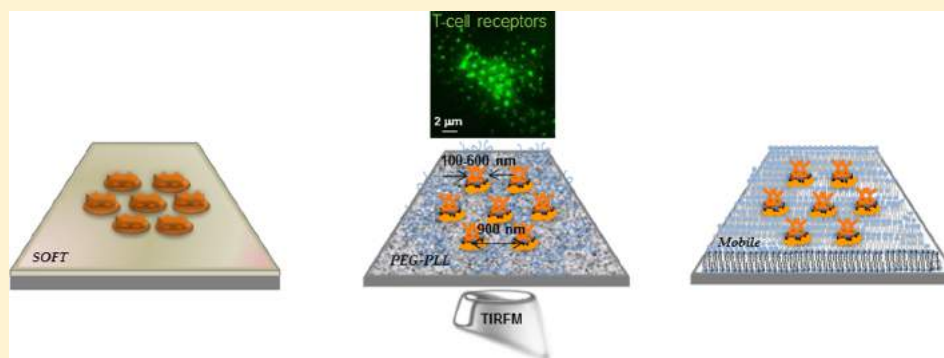
ABSTRACT: Arrays of protein nanodots with dot-size tuned independently of spacing (e.g., ~100 to 600 nm diameter for 900 nm spacing) are fabricated. The mechanism of size control is demonstrated, by numerical simulations, to arise from shadow effects during deposition of a sacrificial metal mask. We functionalize the nanodots with antibodies and embed them in a polymer-cushion or in lipid-bilayers or transfer them to soft elastomers. Their ability to influence cell architecture and local membrane organization is demonstrated in T-lymphocytes, using reflection interference contrast and total internal reflection fluorescence microscopy.

KEYWORDS: Nanobiopatterning, antibody nanodots, nanosphere lithography, T lymphocyte

Nanopatterning of biomolecules on surfaces is currently an important tool for bioengineering and cutting-edge cell biology studies.[1−9] Experiments on cellular interactions with such patterned surfaces provide insights into the mechanisms of cell adhesion, and this knowledge in turn is used to optimize the performance of artificial soft tissue grafts and prosthesis (see refs 10−12 and references therein). In the context of cell biology and bioengineering, arrays of solid-supported, sub-micro/nano scaled protein dots are currently used to influence cell architecture and to decipher cell function.[1−10]

Some of the most successful strategies for creating biochemically funtionalized nanodots are based on gold chemistry.[1−10] However, gold interacts strongly with light and as a consequence, advanced optical imaging techniques, such as total internal reflection fluorescence microscopy (TIRFM), reflection interference contrast microscopy (RICM), or optical super-resolution microscopy, which are essential tools for cell biology, are often not practicable, especially at high dot density. Replacing gold with organic molecules can overcome this problem.[13]

Organic-molecule based nanopatterning, covering large surface area, has been implemented via nanosphere lithography (NL).[13−15] NL is widely used in diverse applications, including for optical meta-materials and plasmonic sensors.[16−20] However, in NL, as applied to organic molecule deposition, so far the dot-size could not be varied independently of the dot-spacing, which is an important requirement for any systematic cellular study. One reported strategy to overcome this problem was heat treatment of polystyrene beads to increase the foot-print,[13,21] but this process is difficult to control and has not been implemented yet for any reported biological study. Another strategy is to reduce the bead size by reactive ion etching, but it is applicable only for areas of few tens of microns (see ref 22 for an overview). An additional challenge in cellular context comes from the fact that cells are sensitive to the compliance of their immediate environment.[23] Further, because in cell−cell interactions the relevant proteins are embedded in the cell membrane, synthetic supported lipid bilayer (SLBs) membranes are often used as surrogate cells.[24−27] Patterning of soft substrates at the nanoscale,[28−30] or an SLB even at the microscale,[31−36] is a current engineering challenge.
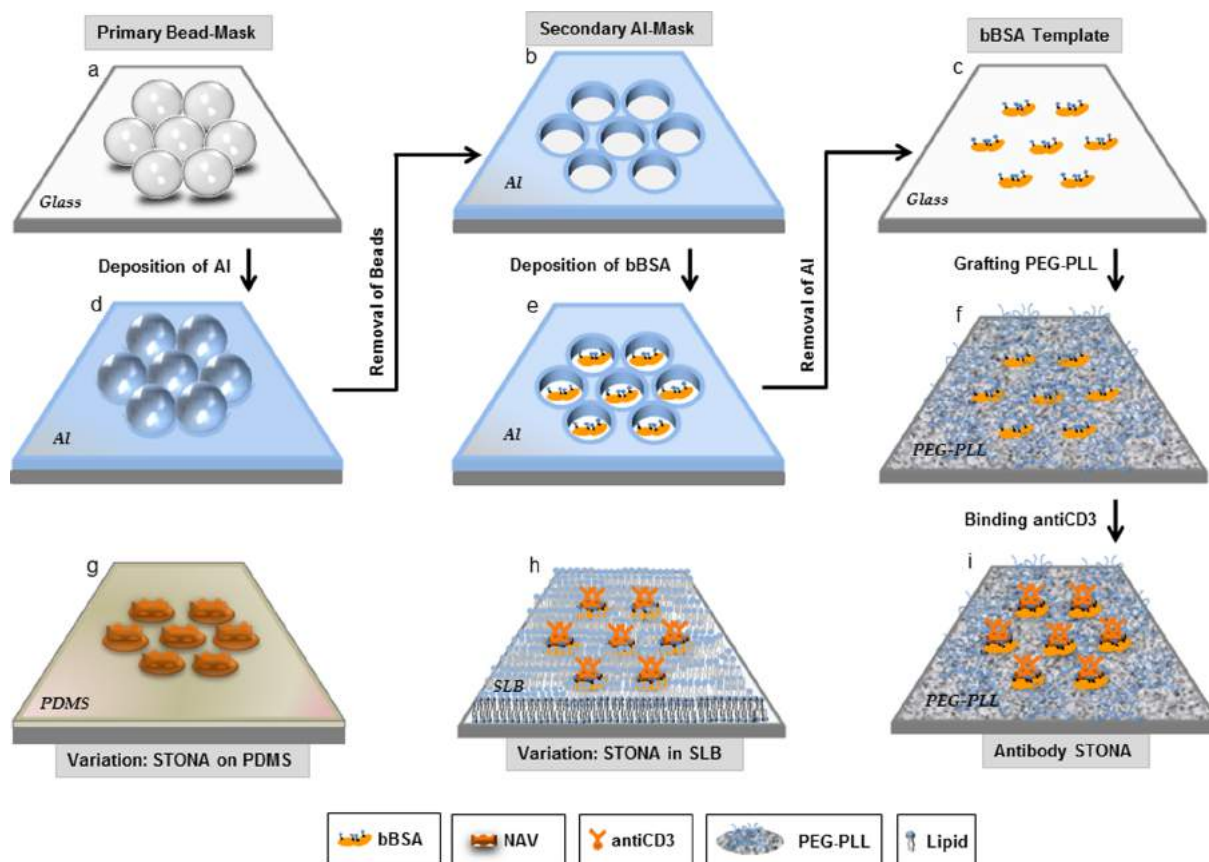
Figure 1. Schematic representation of fabrication steps to create size-tunable organic nanodot arrays (STONAs). A primary colloidal bead-mask is self-assembled on glass (a), aluminum (Al) is sputter deposited (d), the beads are mechanically removed to obtain the secondary aluminum mask (b), an organic molecule, biotinylated BSA (bBSA), is bound to the exposed bare glass (e), and Al is chemically lifted off to produce the bBSA template (c). Subsequent passivation of the bare glass with PEGPLL (f) and appropriate functionalization of the bBSA (with neutravidin, NAV, and the antibody antiCD3) yields antibody STONA surrounded by a polymer cushion (i). Alternatively, a supported lipid bilayer (SLB) can be used for the passivation step (h). NAV-STONA can be transferred to a soft elastomer, PDMS (g). Note that the drawings are not to scale; the square glass slide is 24 × 24 mm, the bead diameter ranges from 0.5 to 4 μm, the thickness of the aluminum varied from ~15 to ~500 nm, and the molecular dimensions of the proteins and lipids are in the range of few nanometers. The spacing of the dots is roughly equal to the diameter of the beads used in the primary masks and the diameter of the dots, tuned independently during creation of aluminum masks, could be varied from ~100 nm to ~2 μm.

Here we report an NL-based technique to create nanodots whose size can be tuned independently of spacing and use it to pattern not only glass but also soft substrates and SLBs. As summarized in Figure 1, our strategy relies on successive creation of two masks, a primary bead-mask that sets the lattice spacing and a secondary sacrificial aluminum mask, deposited through the primary mask, which sets the size of the motifs. The primary bead-mask is a self-assembled, two-dimensional monolayer of colloidal beads (see Supporting Information for method of preparation and Figure S1 for an image of the mask), through which aluminum is sputter-deposited from an aluminum target doped with silicon, using a standard radio frequency (RF) magnetron sputtering system, to create the secondary mask (see Supporting Information for details and Figure S2a for the geometry of deposition). The thickness of the aluminum layer (Al thickness), defined as the thickness of the deposited aluminum layer in an area well outside the bead-mask, was experimentally determined for each deposition run and was found to depend linearly on the duration of metal deposition (Supporting Information Figure S2b) for a given RF power. After metal deposition, the bead-mask was removed mechanically by ultrasonication, revealing the secondary aluminum mask, with a well-defined array of pits giving access to the glass underneath (Figures 1b and 2a, Supporting Information Figure S3) for further deposition. This glass supported metal-mask can be stored almost indefinitely (tested for up to several months without any degradation).

We observed that the lateral size of the pits can be tuned by tuning Al thickness (see scanning electron microscopy images in Supporting Information Figure S3). The mechanism that links the thickness of the deposited metal layer to the size of the pits can be understood in terms of shadow-effects during the process of deposition. In the present setup, the mean free path of aluminum atoms in the plasma at the operating pressure is estimated to be about 10 mm, smaller than the target to sample distance. Thus, multiple collisions ensure that atoms reach the bead-mask from all directions. However, at the scale of a microbead the trajectory of the sputtered aluminum atoms in the ambient argon gas is ballistic, and the rules of optical geometry applicable to standard NL[16,17] should be valid. Accordingly, the deposition pattern is calculated by summing over all the angles the shadow cast by an array of beads for a given illumination direction. Outside the mask, there are no shadows and the metal thickness is equal to Al thickness
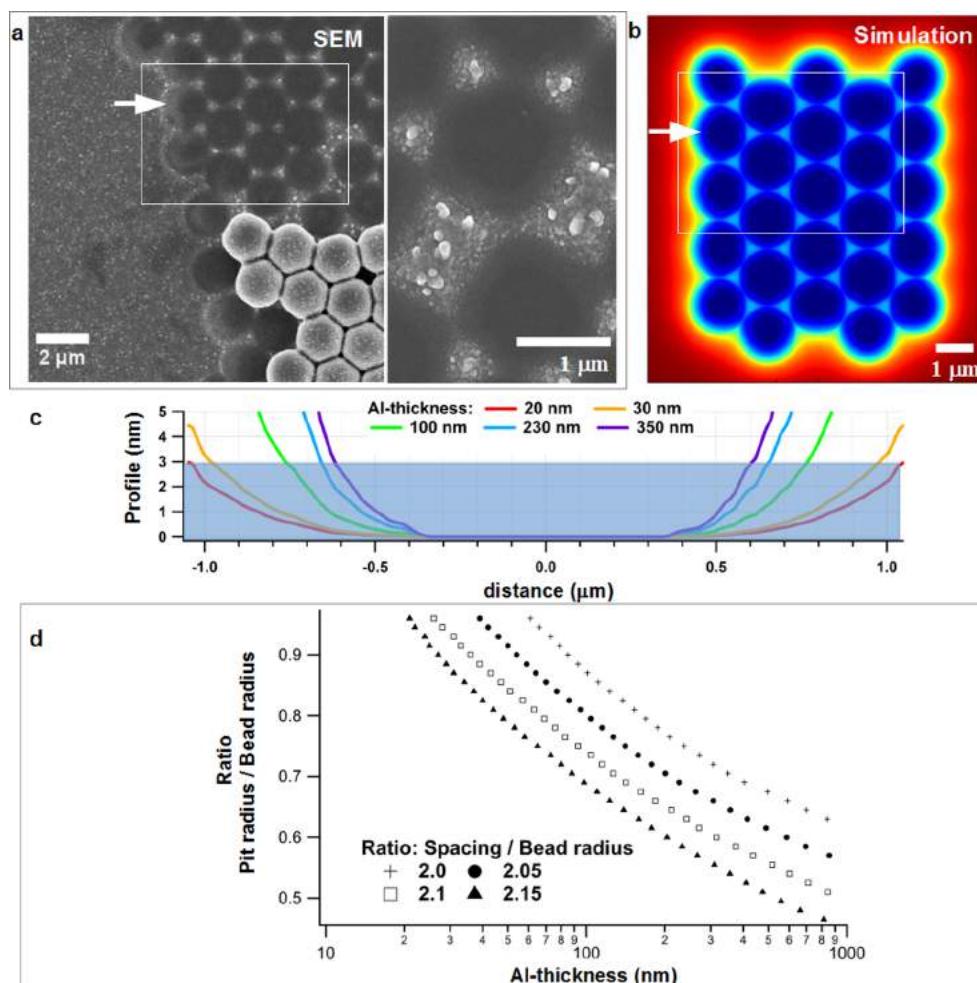
Figure 2. Tuning pit-size with Al thickness. (a) SEM image of the secondary aluminum mask after removal of the primary bead-mask (2 μm beads, 350 nm Al thickness). Hexagonal pattern of aluminum free pits are clearly visible as black circles and few remaining beads from the primary mask are also seen. High-resolution zoom of two pits are shown. (b) Simulated pattern of aluminum deposition, color coded from dark blue (no deposition) to dark red (maximum deposition, outside mask region, corresponds to Al thickness). Equivalent regions on the SEM and simulated images are marked by white box. The white arrow points to characteristic shadow effect at the edge of the mask seen both in SEM and simulations. (c) Simulated profiles of the pits close to the substrate, showing the height profile of the deposited aluminum, calculated for various Al thicknesses. The pit-size can be read off as the radius at which the profile is at least 3 nm thick. (d) The dependence of the simulated pit-size (normalized by the radius of the beads of the mask) on Al thickness, calculated for various bead separations.

defined above. Under the beads, at the contact point between the bead and the surface the shadow is absolute and therefore there is no aluminum deposition. The theoretical pattern therefore consists of an array of pits with sloping walls (Figure 2b, Supporting Information Figure S4). The radial profiles of the pits show that the steepness of the pit-wall strongly depends on Al thickness (as defined above). In Figure 2c, it is seen that as the Al thickness is increased from a low (20 nm) to a high (350 nm) value, the gradient becomes more pronounced (calculated for 2 μm bead size and 2.1 μm spacing).

A direct comparison of the theoretical profile of metal deposition with experiments is nontrivial. On the theoretical side, the simulation ignores the discrete nature of the deposition of aluminum atoms and any possible reorganization after the deposition, which may give rise to roughness and graininess in experiments. On the experimental side, scanning electron microscopy (SEM) usually provides a means to probe metal layers at the required spatial resolution but here is rendered difficult by the fact that the samples are non-conducting, and therefore charging by electrons can signifi-

cantly distort the images, especially for very thin films. Nevertheless, high-resolution SEM images of the pits (Figure 2a) show that as expected, there are different shadow regions that strongly resemble the simulations. Comparing Figure 2, panels a and b, it is seen that the characteristic asymmetric shadow at the edge of the mask (white arrow) is visible both in SEM images and in the simulated image. Similarly, in the interior of the mask, the shadow is symmetric in both images.

To correlate the pit-size and geometry to the final size of the protein nanodots, we need to consider that the aluminum is deposited atom by atom and therefore a certain thickness is needed to achieve full surface coverage. However, for the subsequent biofunctionalization steps, complete surface coverage of the aluminum layer is essential, because otherwise the underlying surface is not adequately masked. This is achieved at an average aluminum deposition of 3 nm (as explained in Supporting Information). The effective pit-size calculated with this threshold of 3 nm has a strong dependence on Al thickness and a weak dependence on the bead spacing (Figure 2d). The simulated pit-size will be compared below to the experimentally
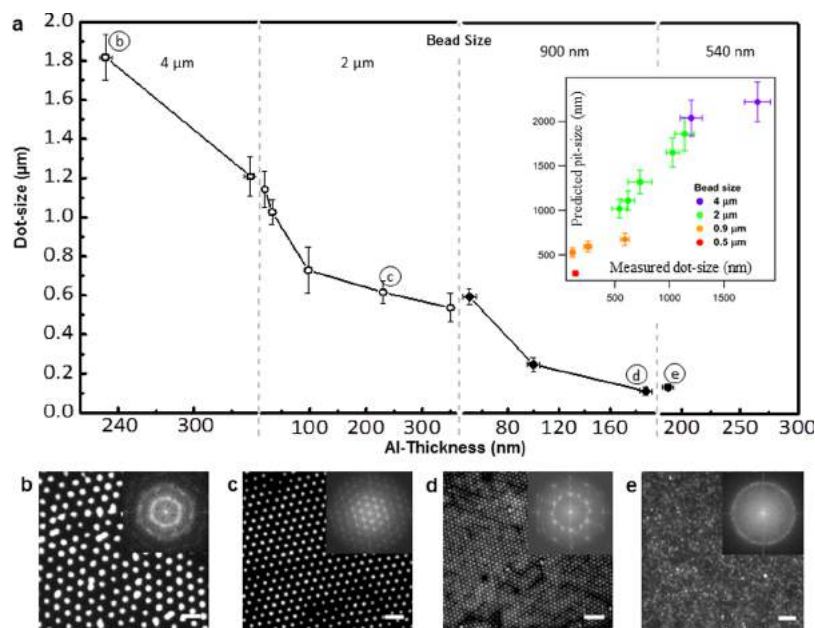
Figure 3. Tuning STONA dot-size. (a) The size of FluoNAV-STONA plotted as a function of Al thickness. For bead size 4 and 2 μm, the dot-size is the fwhm of intensity profiles from fluorescence images. For bead sizes 900 and 540 nm, the reported dot-size is the edge-to-edge distance measured from AFM images. Symbols are data, solid line is guide to the eye. Error bars for dot-size are standard deviations (at least 30 dots for 3 image-fields), and for Al thickness correspond to the full range of data (three independent measurements). Inset: comparison of pit-size predicted from simulations and protein dot-size measured as above. (b–e) Examples of fluorescence images for different spacing and dot-size, corresponding letters are marked in the graph above. Insets are corresponding FFT, performed on image fields of about 100 μm. Scale bars: 4 μm.

determined size of the protein nanodots obtained after biofunctionalization.

For biofunctionalization, first an organosilane (APTES) is deposited through the glass supported metal-mask from the vapor phase. It is subsequently functionalized with biotin conjugated bovine serum albumin (bBSA) from an aqueous phase. The aluminum is removed by chemical lift-off, taking care to retain the functionality of the biotin moiety of bBSA,[36] revealing size-tunable organic nanodot arrays of bBSA (bBSA-STONA) on glass (Figure 1c, see Supporting Information Figure S5 for atomic force microscopy images). The bare glass background is then covered with a passive material, here chosen to be a copolymer of polyethylene-glycol and poly-L-Lysin (PEGPLL), to prevent further protein absorption.[37–39] After passivation, the bBSA dots are functionalized with the biotin binding protein neutravidin (NAV), which serves as a versatile linker for further functionalization (Figure 1f).

The NAV-STONA, created with beads of diameter 4, 2, 1, or 0.5 μm, and various Al thickness were characterized by optical microscopy (OM) or atomic force microscopy (AFM) (Figure 3a, Supporting Information Figure S6). In each case, the fast Fourier transform (FFT) of the images (insets in Figure 3b–e) indicates long-range order in the system. As expected, the dot separation is set by the diameter of the beads used and the dot size gradually decreases with increasing Al thickness for each type of bead mask. By correct selection of bead-size and Al thickness, the dot-size could be varied from ~1800 nm (1800 ± 100 nm, OM data) down to ~100 nm (110 ± 20 nm, AFM data). Plotting the pit-size from simulations against the experimental dot-size shows a linear correspondence (inset Figure 3a). Note that the theoretical pit-size is systematically larger than the dot-size because the former is the diameter of the holes in the aluminum mask whereas for the latter we report the size as full width at half-maximum (fwhm) from

fluorescence images. Most importantly, we show that the spacing and size can be varied independently (similar dot-sizes are obtained for different dot-spacing and different sizes are obtained for same spacing); this was not hitherto possible with NL technology, especially when applied to biopatterning of molecules.

The ability of STONA to influence cell behavior and their compatibility with advanced optical imaging were tested on T lymphocytes (T cells). T cells play a central role in the acquired immune system. Supramolecular organization at the adhesive interface of T cells with antigen presenting cells is thought to have a direct impact on the subsequent signaling, activation, and function of these cells.[26,27,31,32] Influence of micron scale patterning of ligands in T cell has shed light on the importance of subcellular scale molecular organization in these cells.[41,42] Recent work with gold nanodot-based patterning revealed sensitivity of cellular activation to ligand organization at nanoscale but cells could not be imaged in detail.[1,43,44]

Here we imaged T cells interacting with STONA decorated with the biotinylated antibody antiCD3, which on one hand binds specifically to the NAV dots created above, and on the other hand targets the T cell receptor (TCR) complex. The antiCD3-STONA influences the membrane topography as seen in RICM, which looks roughly uniform on nonpatterned surfaces[26,27] but has a clear structuring on STONA (Figure 4a). Moreover, the cell surface TCR molecules, which appear as randomly distributed puncta on homogeneously coated antiCD3,[27,40] are rearranged to follow closely the underlying antibody pattern (Figure 4b). To our knowledge, this is the first time that such protein reorganization on the membrane of a lymphocyte was demonstrated at the submicron scale. There is also an impact on the architecture of the actin cytoskeleton as seen in TIRFM, which goes from the commonly observed
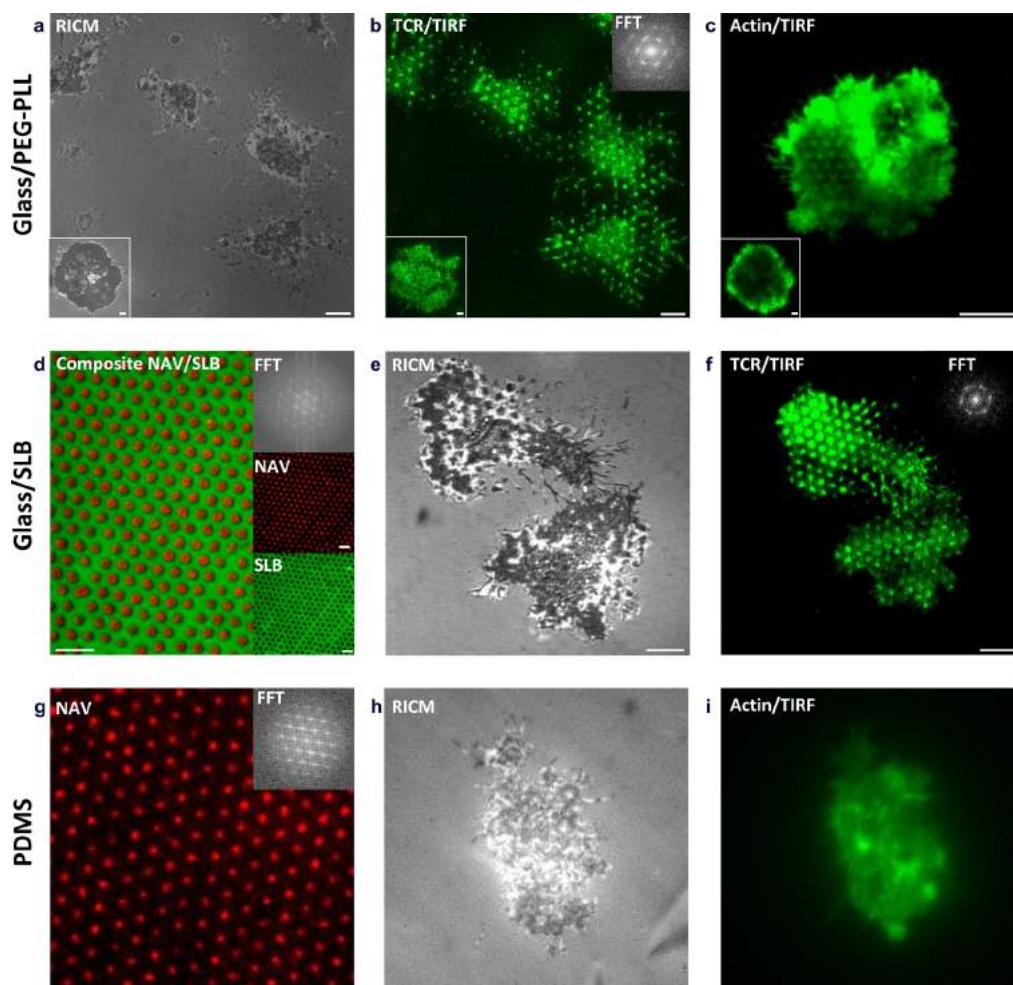
Figure 4. T cells on antibody STONA. (a) RICM image of T lymphocytes interacting with antiCD3-STONA (spacing 2 μm, size ~700 nm), showing modified membrane topography, as compared to cells on homogeneous antiCD3 under equivalent conditions (inset). (b) Corresponding TIRFM image of labeled T cell receptors (TCR), showing that the TCR are organized according to underlying antibody STONA pattern, corresponding FFT (inset, top) indicates long-range order in the TCR organization; compare with random distribution on homogeneous antiCD3 (inset, bottom). (c) TIRFM of actin shows that the cytoskeletal structure is influenced by the presence of the STONA, as compared to homogeneous antiCD3 (inset). (d) FluoNAV-STONA (inset, NAV, red) in a sea of supported lipid bilayer (inset, SLB, green). The main image shows perfect complementarity of the NAV and SLB pattern. The FFT in the inset indicates long-range order. (e,f) T cell interacting with STONA/SLB shows patterned membrane topography in RICM and organized TCR in TIRFM. (g) NAV-STONA on an elastomer (PDMS, Young modulus 300 kPa). (h,i) RICM and TIRFM of a T cell interacting with PDMS supported STONA. Scale bars: 4 μm.

peripheral organization[26,27,40] to partial colocalization with the dots (Figure 4c).

To illustrate the versatility of the technique, we present two variations. First, antibody-STONA were created in a sea of SLB (Figure 1h, 4d) mimicking a cell membrane.[24] Such SLBs have previously been patterned by fabrication of metal grids[31,32,35,36] or by protein stamping;[31,33] however these studies were mostly on micron-scale motifs. Here, we introduce the nanoscale STONA in the SLB such that the lipids in the SLB remain mobile in the plane of the bilayer even after nanopatterning (Supporting Information Figure S7). As before, the STONA impacts the cell membrane topography as seen in RICM (Figure 4e) and the TCR distribution as seen in TIRFM (Figure 4f). The second variation is STONA supported on an elastomeric substrate, which better mimics soft cells and also lend themselves to eventual use as a tool for force measurements.[43−46] NAV-STONA were transferred by reverse-contact-printing[13] to silicone rubber coated on glass with a measured elasticity of 300 kPa (Figures 1g and 4g, Supporting Information Figure S8). Remarkably, cells could be imaged in both RICM and TIRFM through the PDMS in the presence of the STONA (Figure 4h,i).

In all the cases, the obtained STONA are fairly homogeneous. Within each sample, or for different samples for the same deposition run, the size varied by about 5−10% (Supporting Information Table S1). The size variation from one deposition run to the other was slightly higher because the aluminum thickness was not exactly the same for each run. Another important characteristic of the STONA is the contrast or the amount of protein on the dots as compared to the amount absorbed outside the dots. Depending on the quality of metal deposition, this contrast, defined as the ratio of fluorescence intensities inside and outside the dots, is about 2 to 5.

The STONA method presented here relies on the combination of three key factors: (a) the use of self-assembly to create the primary-mask so that large area coverage is achieved in a simple manner, (b) metal-free strategies for

coupling the biomolecules ensuring compatibility with advanced optical microscopy, and (c) the use of shadow-effect in sputter deposition to lift the interdependence of dot size and spacing that hitherto limited applications of NL. The STONA protocol removes these constrains and truly fulfils the requirements of cell biologists interested in using nano-biopatterning as a tool to probe cellular interactions. The numerical simulations elucidate the underlying principle and provide an estimation of the size of the holes in the metal mask as a function of bead separation and metal layer thickness, making the method easily adaptable to other usage. Because the secondary metal-mask can be stored indefinitely, and the subsequent functionalization can be performed in a standard wet-laboratory, the metal-masks can potentially be prepared in specialized facilities and be made available for cell biological experiments on as-required basis. The simplicity of the STONA technology, including the linking-chemistry employed, makes it very versatile in terms of choice of material for the dots as well as the background. The feasibility of transfer by reverse-contact-printing on to elastomers further broadens the potential impact of STONA in the fast growing field of nano-biopatterning.

■ ASSOCIATED CONTENT

ⓢ Supporting Information

Details of experimental methods, simulations, imaging and analysis, table of data corresponding to Figure 3, SEM image of primary bead mask, schematic of metal deposition and SEM images of metal mask, simulated pattern, OM and AFM images of dots, diffusion measurement on SLB, images of nanodot transfer to PDMS, and schematic to demonstrate versatility of the technique. The Supporting Information is available free of charge on the ACS Publications website at DOI: 10.1021/acs.nanolett.5b01400.

■ AUTHOR INFORMATION

Corresponding Author

*E-mail: sengupta@cinam.univ-mrs.fr.

Author Contributions

F.P. developed the concept, put in place the protocol, fabricated and characterized the basic STONA, was involved in all experiments, and participated in writing the article, P.D. participated in all the cell related work, R.A. was responsible for patterning and characterization of PDMS, A.W. for cells on PDMS, E.B. for SLB-STONA, and I.O. for sputtering and SEM. A.C. cosupervised all PDMS related work and AFM measurements, and participated in project conception, L.L. cosupervised all T cell and optical microscopy work, did the simulation of sputtering, participated in project conception, and manuscript preparation, and K.S. conceived and supervised the entire project and wrote the article.

Notes

The authors declare no competing financial interest.

■ REFERENCES

(1) Deeg, J. A.; Louban, I.; Aydin, D.; Selhuber-Unkel, C.; Kessler, H.; Spatz, J. P. *Nano Lett.* **2011**, *11*, 1469−1476.

(2) Cavalcanti-Adam, E. A.; Volberg, T.; Micoulet, A.; Kessler, H.; Geiger, B.; Spatz, J. P. *Biophys. J.* **2007**, *92*, 2964−2974.

(3) Schwab, E. H.; Pohl, T. L. M.; Haraszti, T.; Schwaerzer, G. K.; Hiepen, C.; Spatz, J. P.; Knaus, P.; Cavalcanti-Adam, E. A. *Nano Lett.* **2015**, *15*, 1526−1534.

(4) Wang, X.; Li, S.; Yan, C.; Liu, P.; Ding, J. *Nano Lett.* **2015**, *15*, 1457−1467.

(5) Gautrot, J. E.; Malmström, J.; Sundh, M.; Margadant, C.; Sonnenberg, A.; Sutherland, D. S. *Nano Lett.* **2014**, *14*, 3945−3952.

(6) Coyer, S. R.; Singh, A.; Dumbauld, D. W.; Calderwood, D. A.; Craig, S. W.; Delamarche, E.; García, A. J. *J. Cell Sci.* **2012**, *125*, 5110−5123.

(7) Malmström, J.; Christensen, B.; Jakobsen, H. P.; Lovmand, J.; Foldbjerg, R.; Sørensen, E. S.; Sutherland, D. S. *Nano Lett.* **2010**, *10*, 686−694.

(8) Schvartzman, M.; Palma, M.; Sable, J.; Abramson, J.; Hu, X.; Sheetz, M. P.; Wind, S. J. *Nano Lett.* **2011**, *11*, 1306−1312.

(9) Kristensen, S. H.; Pedersen, G. A.; Nejsum, L. N.; Sutherland, D. S. *Nano Lett.* **2012**, *12*, 2129−2133.

(10) Geiger, B.; Spatz, J. P.; Bershadsky, A. D. *Nat. Rev. Mol. Cell Biol.* **2009**, *10*, 21−33.

(11) Tay, C. Y.; Irvine, S. A.; Boey, F. Y. C.; Tan, L. P.; Venkatraman, S. *Small* **2011**, *7*, 1361−1378.

(12) Yao, X.; Peng, R.; Ding, J. *Adv. Mater.* **2013**, *25*, 5257−5286.

(13) Pi, F.; Dillard, P.; Limozin, L.; Charrier, A.; Sengupta, K. *Nano Lett.* **2013**, *13*, 3372−3378.

(14) Hulteen, J. C.; Van Duyne, R. P. *J. Vac. Sci. Technol., A* **1995**, *13*, 1553−1558.

(15) Singh, G.; Gohri, V.; Pillai, S.; Arpanaei, A.; Foss, M.; Kingshott, P. *ACS Nano* **2011**, *5*, 3542−3551.

(16) Kosiorek, A.; Kandulski, W.; Chudzinski, P.; Kempa, K.; Giersig, M. *Nano Lett.* **2004**, *4*, 1359−1363.

(17) Kostinski, S. V.; Chen, E. R.; Brenner, M. P. *Phys. Rev. Lett.* **2014**, *112*, 235502.

(18) Nemiroski, A.; Gonidec, M.; Fox, J. M.; Jean-Remy, P.; Turnage, E.; Whitesides, G. M. *ACS Nano* **2014**, *8*, 11061−11070.

(19) Bai, C.; Liu, M. *Nano Today* **2012**, *7*, 258−281.

(20) Ai, B.; Yu, Y.; Möhwald, H.; Zhang, G.; Yang, B. *Adv. Colloid Interface Sci.* **2014**, *206*, 5−16.

(21) Taylor, Z. R.; Keay, J. C.; Sanchez, E. S.; Johnson, M. B.; Schmidtke, D. W. *Langmuir* **2012**, *28*, 9656−9663.

(22) Yang, S. M.; Jang, S. G.; Choi, D. G.; Kim, S.; Yu, H. K. *Small* **2006**, *2*, 458−475.

(23) Discher, D. E.; Janmey, P.; Wang, Y.-L. *Science* **2005**, *310*, 1139−1143.

(24) Sackmann, E. *Science* **1996**, *271*, 43−48.

(25) Boxer, S. G. *Curr. Opin. Chem. Biol.* **2000**, *4*, 704−709.

(26) Grakoui, A.; Bromley, S. K.; Sumen, C.; Davis, M. M.; Shaw, A. S.; Allen, P. M.; Dustin, M. L. *Science* **1999**, *285*, 221−227.

(27) Dillard, P.; Varma, R.; Sengupta, K.; Limozin, L. *Biophys. J.* **2014**, *107*, 2629−2638.

(28) Aydin, D.; Louban, I.; Perschmann, N.; Blümmel, J.; Lohmüller, T.; Cavalcanti-Adam, E. A.; Haas, T. L.; Walczak, H.; Kessler, H.; Fiammengo, R.; Spatz, J. P. *Langmuir* **2010**, *26*, 15472−15480.

(29) Kim, B. C.; Matsuoka, T.; Moraes, C.; Huang, J.; Thouless, M. D.; Takayama, S. *Sci. Rep.* **2013**, *3*, 3027.

(30) Platzman, I.; Gadomska, K. M.; Janiesch, J. W.; Louban, I.; Cavalcanti-Adam, E. A.; Spatz, J. P. *Method Cell Biol.* **2014**, *119*, 237−260.

(31) Groves, J. T.; Ulman, N.; Boxer, S. G. *Science* **1997**, *275*, 651−653.

(32) Mossman, K. D.; Campi, G.; Groves, J. T.; Dustin, M. L. *Science* **2005**, *310*, 1191−1193.

(33) Perez, T. D.; Nelson, W. J.; Boxer, S. G.; Kam, L. *Langmuir* **2005**, *21*, 11963−11968.

(34) Tsai, J.; Sun, E.; Gao, Y.; Hone, J. C.; Kam, L. C. *Nano Lett.* **2008**, *8*, 425−430.

(35) Lohmüller, T.; Xu, Q.; Groves, J. T. *Nano Lett.* **2013**, *13*, 3059−3064.

(36) Jackson, B. L.; Groves, J. T. *Langmuir* **2007**, *23*, 2052−2057.

(37) Huang, N.-P.; Michel, R.; Voros, J.; Textor, M.; Hofer, M.; Rossi, A.; Elbert, D. L.; Hubbell, J. A.; Spencer, N. D. *Langmuir* **2001**, *17*, 489−498.

(38) Théry, M.; Piel, M. Adhesive micropatterns for cells: a microcontact printing protocol. *Cold Spring Harb Protoc.* **2009**, *2009*, 5255.

(39) Reymann, A. C.; Martiel, J. L.; Cambier, T.; Blanchoin, L.; Boujemaa-Paterski, R.; Théry, M. *Nat. Mater.* **2010**, *9*, 827−832.

(40) Kaizuka, Y.; Douglass, A. D.; Varma, R.; Dustin, M. L.; Vale, R. D. *Proc. Natl. Acad. Sci. U. S. A.* **2007**, *104*, 20296−20301.

(41) Doh, J.; Irvine, D. J. *Proc. Natl. Acad. Sci. U. S. A.* **2006**, *103*, 5700−5705.

(42) Shen, K.; Thomas, V. K.; Dustin, M. L.; Kam, L. C. *Proc. Natl. Acad. Sci. U. S. A.* **2008**, *105*, 7791−7796.

(43) Delcassian, D.; Depoil, D.; Rudnicka, D.; Liu, M.; Davis, D. M.; Dustin, M. L.; Dunlop, I. E. *Nano Lett.* **2013**, *13*, 5608−5614.

(44) Matic, J.; Deeg, J.; Scheffold, A.; Goldstein, I.; Spatz, J. P. *Nano Lett.* **2013**, *13*, 5090−5097.

(45) Balaban, N. Q.; Schwarz, U. S.; Riveline, D.; Goichberg, P.; Tzur, G.; Sabanay, I.; Mahalu, D.; Safran, S.; Bershadsky, A.; Addadi, L.; Geiger, B. *Nat. Cell Biol.* **2001**, *3*, 466−472.

(46) Merkel, R.; Kirchgeßner, N.; Cesa, C. M.; Hoffmann, B. *Biophys. J.* **2007**, *93*, 3314−3323.

Bibliography

[1] Charles A Janeway, Paul Travers, Mark Walport, and Mark Shlomchik. *Immunobiology. 6th.* 2005.

[2] Kenneth Murphy, Paul Travers, and Mark Walport. Janeway's immunobiology. *GarlandScience*, pages 611–668, 2012.

[3] CHARLES A Janeway, PAUL Travers, MARK Walport, and MARK Shlomchik. Immunobiology (5th edn). *Garland, NY*, page 505, 2001.

[4] P. Grasso, S. Gangolli, and Ian Gaunt. Essentials of pathology for toxicologists. *CRC Press*, 2002.

[5] Bruce Alberts, Alexander Johnson, Julian Lewis, Martin Raff, Keith Roberts, and Peter Walters. Molecular biology of the cell; fourth edition. *New York and London: Garland Science*, 2002.

[6] http://slideplayer.com/slide/10780579/. Immune system. *Slideplayer*, Accessed june 5, 2016.

[7] http://www.cours pharmacie.com.

[8] Carl G Gahmberg, Susanna C Fagerholm, Susanna M Nurmi, Triantafyllos Chavakis, Silvia Marchesan, and Mikaela Grönholm. Regulation of integrin activity and signalling. *Biochimica et Biophysica Acta (BBA)-General Subjects*, 1790(6):431–444, 2009.

[9] Amoura Z. and Piette JC. Nouvelles approches thérapeutiques des maladies auto-immunes. *Revue Neurol*, 162 Spec No 1:3S7–3S11, Jun 2006.

[10] D. D. Billadeau, J. C. Nolz, and T. S Gomez. Regulation of t-cell activation by the cytoskeleton. *Nature Review Immunology*, 7:131–143, 2007.

[11] Francis J.Alenghat and David E.Golan. Membrane protein dynamics and functional implications in mammalian cells. *Curr Top Membr*, 72:89–120, Sept 2013.

[12] Nathalie Bufi, Michael Saitakis, Stéphanie Dogniaux, Oscar Buschinger, Armelle Bohineust, Alain Richert, Mathieu Maurin, Claire Hivroz, and Atef Asnacios. Human primary immune cells exhibit distinct mechanical properties that are modified by inflammation. *Biophysical journal*, 108(9):2181–2190, 2015.

[13] Lu X., Gibbs J.S., Hickman H.D., David A., Dolan B.P., Jin Y., Kranz D.M., Bennink J.R. Yewdell J.W., and Varma R. Supported planar bilayers for the formation of study of immunological synapses and kinapse. *International Journal of Energy Research*, 19, 2008.

[14] Gary A. Koretzky Jennifer E. Smith-Garvin and Martha S. Jordan. T cell activation. *Annu Rev Immunol*, 27:561–619, Jan 2009.

[15] Rudd C.E., Trevillyan J.M., Dasgupta J.D., Wong L.L., and Schlossman S.F. The cd4 receptor is complexed in detergent lysates to a protein-tyrosine kinase (pp58) from human t lymphocytes. *Proceedings of the National Academy of Sciences of the United States of America*, 85:5190–5194, 1988.

[16] Barber E.K., Dasgupta J.D., Schlossman S.F., Trevillyan J.M., and Rudd C.E. The cd4 and cd8 antigens are coupled to a protein-tyrosine kinase (p56lck) that phosphorylates the cd3 complex. *Proceedings of the National Academy of Sciences of the United States of America*, 86:3277–3281, 1989.

[17] Woodgett JR Truneh A Olive D Cantrell DA. Nunes JA, Battifora M. Cd28 signal transduction pathways. a comparison of b7-1 and b7-2 regulation of the map kinases: Erk2 and jun kinases. *Mol Immunol*, 33:63–70, 1996.

[18] Sackmann E. Lecture notes on biological physics: Physics of cell adhesion. 2013.

[19] Robert P., Limozin L., Benoliel A.M., Pierre A., and Bongrand P. *Glycocalyx regulation of cell adhesion*. 2006.

[20] K. Sengupta and L. Limozin. Adhesion of soft membranes controlled by tension and interfacial polymers. *Physical Review Letters*, 104, 2010.

[21] Limozin L. and Sengupta K. Modulation of vesicle adhesion and spreading kinetics by hyaluronan cushions. *Biophysical Journal*, 93:3300–3313, 2007.

[22] Sadir R Pleiner T Baleux F Lortat-Jacob H Coche-Guerente L Richter RP. Migliorini E, Thakar D. Well-defined biomimetic surfaces to characterize glycosaminoglycan-mediated interactions on the molecular, supramolecular and cellular levels. *Biomaterials*, 32:8903–15, 2014.

[23] Robert P., Sengupta K., Puech P.H., Bongrand P., and Limozin L. Tuning the formation and rupture of single ligand receptor bonds by hyaluronan induced repulsion. *Biophysical Journal*, 95:3999–4012, 2008.

[24] Sabri S., Soler M., Foa C., Pierres A., Benoliel A.M., and Bongrand P. Glycocalyx modulation is a physiological means of regulating cell adhesion. *Journal of Cell Science*, 113:1589–1600, 2000.

[25] Dustin M.L. Science cover. *Science*, 285, 1999.

[26] Matsui K., Boniface J.J., Reay P.A., Schild H., Fazekas de St Groth B., and Davis MM. Low affinity interaction of peptide-mhc complexes with t cell receptors. *Science*, 254:1788–1791, 1991.

[27] Weber S., Traunecker A., Oliveri F., Gerhard W., and Karjalainen K. Specific low-affinity recognition of major histocompatibility complex plus peptide by soluble t-cell receptor. *Nature*, 254:1788–1791, 1991.

[28] Jun Huang, Veronika I. Zarnitsyna, Baoyu Liu, Lindsay J. Edwards, Ning Jiang, Brian D. Evavold, and Cheng Zhu. The kinetics of two-dimensional tcr and pmhc interactions determine t-cell responsiveness. *Nature*, 464:932–936, 2010.

[29] Huppa J.B., Axmann M., Mörtelmaier M.A., Lillemeier B.F., Newell E.W., Brameshuber M., Klein L.O., Schütz G.J., and Davis M.M. Tcr-peptide-mhc interactions in situ show accelerated kinetics and increased affinity. *Nature*, 463:963–967, 2010.

[30] Boryana N. Manz, Bryan L. Jackson, Rebecca S. Petit, Dustin M.L., and Jay Groves. T-cell triggering thresholds are modulated by the number of antigen within individual t-cell receptor clusters. *Proceedings of the National Academy of Sciences of the United States of America*, 108:9089–9094, 2011.

[31] D. J. Irvine, M. A. Purbhoo, M. Krogsgaard, and M. M. Davis. Direct observation of ligand recognition by t cells. *Nature*, 419:845–849, 2002.

[32] S. Stoll, J. Delon, T. M. Brotz, and R. N. Germain. Dynamic imaging of t cell–dendritic cell interactions in lymph nodes. *Science*, 296:1873–1876, 2002.

[33] Simon J Davis and P Anton van der Merwe. The kinetic-segregation model: Tcr triggering and beyond. *Nature immunology*, 7(8):803–809, 2006.

[34] P. Anton van der Merwe and Omer Dushek. Mechanisms for t cell receptor triggering. *Nature Reviews Immunology*, 11:141–142, 2011.

[35] Tobias Zech, Christer S Ejsing, Katharina Gaus, Ben De Wet, Andrej Shevchenko, Kai Simons, and Thomas Harder. Accumulation of raft lipids in t-cell plasma membrane domains engaged in tcr signalling. *The EMBO journal*, 28(5):466–476, 2009.

[36] Thomas Harder and Dhaval Sangani. Plasma membrane rafts engaged in t cell signalling: new developments in an old concept. *Cell Communication and Signaling*, 7(1):21, 2009.

[37] John R. James and Ronald D. Vale. Biophysical mechanism of t cell receptor triggering in a reconstituted system. *Nature*, 487:64–69, Jul 2013.

[38] Weiss A. Abraham RT. Jurkat t cells and development of the t-cell receptor signalling paradigm. *Nat Rev Immunol*, 4:3001–8, 2004.

[39] B.M. Gumbiner. Cell adhesion: The molecular basis of tissue architecture and morphogenesis. *Cell*, 84:345–357, 1996.

[40] National University of Singapore Mechanobiology Institute. *http://www.mechanobio.info/topics/cytoskeleton-dynamics/go-0030027/go-0030032.*

[41] Benoit Ladoux and Alice Nicolas. Physically based principles of cell adhesion mechanosensitivity in tissues. *Reports on Progress in Physics*, 75:116601–116626, 2012.

[42] Beemiller P Beppler C Rubashkin MG Weaver VM Gérard A-Liu TL Chen BC Betzig E Bartumeus F Krummel MF Cai E, Marchuk K. Visualizing dynamic microvillar search and stabilization during ligand detection by t cells. *Science*, 356:6338, May 2017.

[43] Dustin M.L., Shannon K. Bromley, Zengyan Kan, Daniel A. Peterson, and Emil R. Unanue. Antigen receptor engagement delivers a stop signal to migrating t lymphocytes. *Proceedings of the National Academy of Sciences of the United States of America*, 94:3909–3913, 1997.

[44] A. Grakoui, S. K. Bromley, C. Sumen, M. M. Davis, A. S. Shaw, P. M. Allen, and Dustin M.L. immunological synapse: a molecular machine controlling t cell activation. *Science*, 285:221227, 1999.

[45] Lee K.H., Dinner A.R., Tu C., Campi G., Raychaudhuri S., Varma R., Sims T.N., Burack W.R., Wu H. Wang J., Kanagawa O., Markiewicz M., Allen P.M., Dustin M.L., Chakraborty A.K., and Shaw A.S. The immunological synapse balances t cell receptor signaling and degradation. *Science*, 94:1218–1222, 2003.

[46] F Mazerolles, C Barbat, C Hivroz, and A Fischer. Phosphatidylinositol 3-kinase participates in p56 (lck)/cd4-dependent down-regulation of lfa-1-mediated t cell adhesion. *The Journal of Immunology*, 157(11):4844–4854, 1996.

[47] Linsley P.S., Bradshaw J., Greene J., Peach R., Bennett K.L., and Mittler R.S. Intracellular trafficking of ctla-4 and focal localization towards sites of tcr engagement. *Immunity*, 4:535–543, 1996.

[48] M.A. Norcross. A synaptic basis for t-lymphocyte activation. *Annual Review of Immunology*, 135:113–134, 1984.

[49] Spatz J.P. and Geiger B. Molecular engineering of cellular environments: cell adhesion to nano-digital surfaces. *Methods in Cell Biology*, 83:89–111, 2007.

[50] Mempel T.R., Henrickson S.E., and Von Andrian U.H. T-cell priming by dendritic cells in lymph nodes occurs in three distinct phases. *Nature*, 427:154–159, 2004.

[51] Miller M.J., Safrina O., Parker I., and Cahalan M.D. Imaging the single cell dynamics of cd4+ t cell activation by dendritic cells in lymph nodes. *Journal of Experimental Medicine*, 200:847–856, 2004.

[52] Bousso P. and Robey E. Dynamics of cd8+ t cell priming by dendritic cells in intact lymph nodes. *Nature Immunology*, 4:579–585, 2003.

[53] Huppa J.B., Gleimer M., Sumen C., and Davis M.M. Continuous t cell receptor signaling required for synapse maintenance and full effector potential. *Nature Immunology*, 4:749–755, 2003.

[54] C.-J. Hsu, W.-T. Hsieh, A. Waldman, F. Clarke, E. S. Huseby, J. K. Burkhardt, and T. Baumgart. Ligand mobility modulates immunological synapse formation and t cell activation. *PLOS One*, 7:e32398, 2012.

[55] P. Friedl, A.T. den Boer, and M. Gunzer. Tuning immune responses: diversity and adaptation of the immunological synapse. *Nature Reviews Immunology*, 5:532–545, 2005.

[56] Dustin M.L. T-cell activation through immunological synapses and kinapses. *Immunological Reviews*, 221:77–89, 2008.

[57] C. R. Monks, B. A. Freiberg, H. Kupfer, N. Sciaky, and A. Kupfer. Three-dimensional segregation of supramolecular activation clusters in t cells. *Nature*, 395:82–86, 1998.

[58] Cell membrane. *http://aisdvs.aldine.k12.tx.us/mod/book/view.php?id=179201*.

[59] Borowitz MJ, Weidner A, Olsen EA, and Picker LJ. Abnormalities of circulating t-cell subpopulations in patients with cutaneous t-cell lymphoma: cutaneous lymphocyte-associated antigen expression on t cells correlates with extent of disease. *Leukemia*, 7:859–863, 1993.

[60] Fletcher D.A. and Mullins D. Cell mechanics and the cytoskeleton. *Nature*, 463:485–492, 2010.

[61] O. Dushek, S. Mueller, S. Soubies, D. Depoil, I. Caramalho, D. Coombs, and S. Valitutti. Effects of intracellular calcium and actin cytoskeleton on tcr mobility measured by fluorescence recovery. *PLOS One*, 2008.

[62] Yan Yu, Nicole C Fay, Alexander A Smoligovets, Hung-Jen Wu, and Jay T Groves. Myosin iia modulates t cell receptor transport and casl phosphorylation during early immunological synapse formation. *PloS one*, 7(2):e30704, 2012.

[63] Yoshihisa Kaizuka, Adam D Douglass, Rajat Varma, Michael L Dustin, and Ronald D Vale. Mechanisms for segregating t cell receptor and adhesion molecules during immunological synapse formation in jurkat t cells. *Proceedings of the National Academy of Sciences*, 104(51):20296–20301, 2007.

[64] R. Varma, G. Campi, T. Yokosuka, T. Saito, and Dustin M.L. T cell receptor-proximal signals are sustained in peripheral microclusters and terminated in the central supramolecular activation cluster. *Immunity*, 25:117–127, 2006.

[65] Dustin M.L. and Groves J.T. Receptor signaling clusters in the immune synapse. *Annual Review of Biophysics*, 41:543–556, 2012.

[66] Bunnell S.C. *Multiple Microclusters: Diverse Compartments Within the Immune Synapse*, volume 340. 2010.

[67] Yamamoto Y Ma Y Bridgeman JS Cohnen A Benzing C-Gao Y Crowther MD Tungatt K Dolton G Sewell AK Price DA Acuto O Parton RG Gooding JJ Rossy J Rossjohn J Gaus K. Pageon SV, Tabarin T. Functional role of t-cell receptor

nanoclusters in signal initiation and antigen discrimination. *PNAS*, 37:E5454–63, Sep 2016.

[68] Cuche C Danckaert A Thoulouze MI de Chaumont F Duong T Perrault N Varin-Blank N Olivo-Marin JC Etienne-Manneville S Arpin M Di Bartolo V Alcover A. Lasserre R, Charrin S. Ezrin tunes t-cell activation by controlling dlg1 and microtubule positioning at the immunological synapse. *EMBO J*, 14:2301–14, Jul 2010.

[69] 1 Min Zhang Viresh Patel Stephen P. Schoenberger June L. Round, Tamar Tomassian and M. Carrie Miceli. Dlgh1 coordinates actin polymerization, synaptic t cell receptor and lipid raft aggregation, and effector function in t cells. *J Exp Med*, 3:419–430, Feb 2005.

[70] Alcover A. Charrin S. Role of erm (ezrin-radixin-moesin) proteins in t lymphocyte polarization, immune synapse formation and in t cell receptor-mediated signaling. *Front Biosci*, 11:1987–97, May 2006.

[71] Alcover A Soares H, Lasserre R. Orchestrating cytoskeleton and intracellular vesicle traffic to build functional immunological synapses. *Immunol Rev*, 256:118–32, Nov 2013.

[72] Burkhart JK Comrie WA. Action and traction: Cytoskeletal control of receptor triggering at the immunological synapse. *Front Immunol*, pages 7–68, Mar 2016.

[73] Safran SA. Nicolas A. Limitation of cell adhesion by the elasticity of the extracellular matrix. *Biophys J*, 1:61–73, 2006.

[74] Adam J. Engler, Shamik Sen, H. Lee Sweeney, and Dennis E. Discher. Matrix elasticity directs stem cell lineage specification. *Cell*, 126:677–689, 2006.

[75] Basta L Anseth KS Yang C, Tibbitt MW. Mechanical memory and dosing influence stem cell fate. *Nat Mater*, 6:645–52, 2014.

[76] Janmey P.A., Winer J.P., Murray M.E., and Wen Q. The hard life of soft cells. *Cell Motility Cytoskeleton*, 66:597–605, 2009.

[77] Brugge JS. Ng MR. A stiff blow from the stroma: collagen crosslinking drives tumor progression. *CancerCell*, 16:455–457, 2009.

[78] R. G. Wells. Cellular sources of extracellular matrix in hepatic fibrosis. *Clinics in liver disease*, 12:759–768, 2008.

[79] Solon J., Levental I., Sengupta K., Georges P.C., and Janmey P.A. Fibroblast adaptation and stifness matching to soft elastic substrates. *Biophysical Journal*, 93:4453–4461, 2007.

[80] P. C. Georges I. Levental and P. A. Janmey. Soft biological materials and their impact on cell function. *Soft Matter*, 3:299–306, 2007.

[81] S. Sen C. G. Bonnemann H. L. Sweeney A. J. Engler, M. A. Griffin and D. E. Discher. Myotubes differentiate optimally on substrates with tissue-like stiffness pathological implications for soft or stiff microenvironments. *J Cell Biol*, 166:877–887, 2004.

[82] S. Kumari M. L. Dustin E. Judokusumo, E. Tabdanov and L. C. Kam. Mechanosensing in t lymphocyte activation. *Biophs Journal*, 102:L5–L7, Jan 2012.

[83] K. Shen K. Bashour T. Akimova W. W. Hancock L. C. Kam R. S. O'Connor, X. Hao and M. C. Milone. Substrate rigidity regulates human t cell activation and proliferation. *J Immunol*, 189:1330–9, Aug 2012.

[84] Pi F Bouzalmate K Limozin L Charrier A Sengupta K Alameddine R, Wahl A. Printing functional protein nanodots on soft elastomers: From transfer mechanism to cell mechanosensing.. *Nano Lett*, 17:4284–4290, Jul 2017.

[85] Michael Saitakis, Stéphanie Dogniaux, Christel Goudot, Nathalie Bufi, Sophie Asnacios, Mathieu Maurin, Clotilde Randriamampita, Atef Asnacios, and Claire Hivroz. Different tcr-induced t lymphocyte responses are potentiated by stiffness with variable sensitivity. *eLife*, 6, 2017.

[86] Dillard P. Impact of ligand presentation on biophysics of t-lymphocyte adhesion. *PhD thesis, Aix-Marseille*, Dec 2014.

[87] J. Gallagher D. Pasqui M. Wood A. Curtis, B. Casey and C. Wilkinson. Substratum nanotopography and the adhesion of biological cells. are symmetry or regularity of nanotopography important?. *Biophys Chem*, 94:275–283, Dec 2001.

[88] R. Glass J. Blummel W. Eck M. Kantlehner H. Kessler M. Arnold, E. A. Cavalcanti-Adam and J. P. Spatz. Activation of integrin function by nanopatterned adhesive interfaces. *ChemPhysCem*, 5:383–388, Mar 2004.

[89] Dalby M.J., Gadegaard N., Tare R., Andar A., Riehle M.O., Herzyk P., Wilkinson C.D., and Oreffo R.O. The control of human mesenchymal cell differentiation using nanoscale symmetry and disorder. *Nature Materials*, 6:997–1003, 2007.

[90] Chen C.S., Mrksich M., Huang S., Whitesides G.M., and Ingber D.E. Geometric control of cell life and death. *Science*, 276:1425–1428, 1997.

[91] Marco Arnold, Vera C. Jakubick, Theobald Lohmüller, Patrick Heil, Jacques Blümmel, Elisabetta A. Cavalcanti-Adam, Mónica López-García, Paul Walther, Horst Kessler, Benjamin Geiger, and Joachim P. Spatz. Geometric control of cell life and death. *Science*, 276:1425–1428, 2008.

[92] Katalin Czöndör, Mikael Garcia, Amélie Argento, Audrey Constals, Christelle Breillat, Béatrice Tessier, and Olivier Thoumine. Micropatterned substrates coated with neuronal adhesion molecules for high-content study of synapse formation. *Nature communications*, 4:2252, 2013.

[93] Trichet L., Le Digabel J., Hawkins R.J., Vedula S.R., Gupta M., Ribrault C., Hersen P., Voituriez R., and Ladoux B. Evidence of a large-scale mechanosensing mechanism for cellular adaptation to substrate stiffness. *Proceedings of the National Academy of Sciences of the United States of America*, 109:6933–6938, 2012.

[94] Thery M. Micropatterning as a tool to decipher cell morphogenesis and functions. *J Cell Sci*, 123:4201–13, 2010.

[95] M. Moller R. Glass and J. P. Spatz. Block copolymer micelle nanolithography. *Nanotechnology*, 14:1153–1160, Sep 2003.

[96] M. Lopez-Garcia H. Kessler U. Schwarz C. Selhuber-Unkel, T. Erdmann and J. Spatz. Cell adhesion strength is controlled by intermolecular spacing of adhesion receptors. *Biophys J*, 98:543–551, Feb 2010.

[97] Doh J. and Irvine D.J. Immunological synapse arrays: Patterned protein surfaces that modulate immunological synapse structure formation in t cells. *Proceedings of the National Academy of Sciences of the United States of America*, 103:5700–5705, 2006.

[98] Shen K., Thomas V.K., Dustin M.L., and Kam L.C. Micropatterning of costimulatory ligands enhances cd4+ t cell function. *Proceedings of the National Academy of Sciences of the United States of America*, 105:7791–7796, 2008.

[99] J. Deeg, M. Axmann, J. Matic, A. Liapis, D. Depoil, J. Afrose, S. Curado, Dustin M.L., and J. P. Spatz. T cell activation is determined by the number of presented antigens. *Nano Letters*, 13:5090–5097, 2013.

[100] Matic J., Degg J., Scheffold A., Goldstein I., and Spatz J.P. Fine tuning and efficient t cell activation with stimulatory acd3 nanoarrays. *Nano Letters*, 13:5090–5097, 2013.

[101] Delcassian D., Depoil D., Rudnicka D., Liu M., Davis D.M., Dustin M.L., and Dunlop I.E. Nanoscale ligand spacing influences receptor triggering in t cells and nk cells. *Nano Letters*, 13:5608–5614, 2013.

[102] Pi F., Dillard P., Limozin L., Charrier A., and Sengupta K. Nanometric protein-patch arrays on glass and polydimethylsiloxane for cell adhesion studies. *Nano Letters*, 13:3372–3378, June 2013.

[103] Pierre Dillard, Fuwei Pi, Annemarie C Lellouch, Laurent Limozin, and Kheya Sengupta. Nano-clustering of ligands on surrogate antigen presenting cells modulates t cell membrane adhesion and organization. *Integrative Biology*, 8(3):287–301, 2016.

[104] B. Huang J. J. Moon and D. J. Irvine. Engineering nano-and microparticles to tune immunity. *Advanced mat*, 24:3724–3746, 2012.

[105] H. M. Grandin D. Falconnet, G. Csucs and M. Textor. Surface engineering approaches to micropattern surfaces for cell-based assays. *Biomaterials*, 27:3044–3063, Jun 2006.

[106] A. S. Biris T. Wang E. Dervishi A. Biswas, I. S. Bayer and F. Faupel. Advances in top-down and bottom-up surface nanofabrication: Techniques, applications and future prospects. *Adv Colloid Interface Sci.*, 170:2–27, Jan 2012.

[107] May lam. Independently controlling protein dot size and spacing in particle lithography. *httpscommons.wikimedia.orgwindex.phpcurid=56811443*, 28:9656–9663, Jun 2012.

[108] Ankur; Singh Deepak; Kant Rishi; Bhattacharya Shantanu Patel, Vinay Kumar; Gupta. Surface functionalization to mitigate fouling of biodevices: A critical review. *Reviews of Adhesion and Adhesives*, 3:444–478, Dec 2015.

[109] A. Kumar and G. M. Whitesides. Features of gold having micrometer to centimeter dimensions can be formed through a combination of stamping with an elastomeric stamp and an alkanethiol "ink" followed by chemical etching. *Appl. Phys. Lett*, 63:2002–2004, 1993.

[110] O. Kaspar V. Tokarova L. Filipponi, P. Livingston and D. V. Nicolau. Protein patterning by microcontact printing using pyramidal pdms stamps. *Biomed Microdevices.*, 18:1–7, Feb 2016.

[111] S. A. Ruiz and C. S. Chen. Microcontact printing: a tool to pattern. *Soft Matter*, 3:335–373, 2007.

[112] A. Bietsch E. Delamarche M. Geissler D. Juncker H. Kind J.-P. Renault H. Rothuizen H. Schmid-et al. B. Michel, A. Bernard. Printing meets lithography: soft approaches to high-resolution patterning. *IBM Journal of Research and Development*, 45:697–719, Sep 2001.

[113] P. R. Krauss S. Y. Chou and P. J. Renstrom. Nanoimprint lithography. *Journal of Vacuum Science and Technology*, 14:4129–4133, 1996.

[114] D. Sutherland L. Filipponi and I. N. Center. Nanoyou teachers training kit in nanotechnologies. *European Commision Document*, 2010.

[115] Pei-I Wang Zhuqiu Y Ya Ou Rajat Ghoshal Ramkrishna Ghoshal Toh-Ming Lu a Dexian Ye. Uv nanoimprint lithography of sub-100 nm nanostructures using a novel uv curable epoxy siloxane polymer. *Microelectron Eng*, 9:2411–2115, Nov 2010.

[116] Spatz J.P. and Geiger B. Nanolithographic control of the spatial organization of cellular adhesion receptors at the single-molecule level. *Nano Letters*, 11:1306–1312, 2011.

[117] J. P. Spatz. Nano-and micropatterning by organic inorganic templating of hierarchical self-assembled structures. *Angew Chem Int Ed Engl.*, 41:3359–3362, Sep 2002.

[118] E. Bock T. Lohmueller and J. P. Synthesis of quasi-hexagonal ordered arrays of metallic nanoparticles with tuneable particle size. *Adv Materials.*, 20:2297–2302, May 2008.

[119] P. Colson, C. Henrist, and R. Cloots. Nanosphere lithography: a powerful method for the controlled manufacturing of nanomaterials. *Journal of Nanomaterials*, 2013.

[120] D.-G. Choi S. Kim S.-M. Yang, S. G. Jang and H. K. Yu. Nanomachining by colloidal lithography. *Small.*, 2:458–475, Apr 2006.

[121] E. S. Sanchez M. B. Johnson Z. R. Taylor, J. C. Keay and D. W. Schmidtke. Independently controlling protein dot size and spacing in particle lithography. *Langmuir*, 28:9656–9663, Jun 2012.

[122] *http://en.rigaku-mechatronics.com/case/sputtering-systems.html.*

[123] Xia B., Xiao S.J., Guo D.J., Wang J., Chao J., Liu H.B., Chen Y.Q., Tang Y.C., and Liu J.N. Biofunctionalisation of porous silicon (ps) surfaces by using homobifunctional cross-linkers. *Journal of Material Chemistry*, 16:570–578, Dec 2006.

[124] Susanne F Fenz, Rudolf Merkel, and Kheya Sengupta. Diffusion and intermembrane distance: case study of avidin and e-cadherin mediated adhesion. *Langmuir*, 25(2):1074–1085, 2008.

[125] Belegrinous S., Dorn J., Kreiter M., Kita-Tokarczyk K., Sinner E.K., and Meier W. Biomimetic supported membranes from amphiphilic block copolymers. *Soft Matters*, 6:179–186, 2010.

[126] Butt H.J., Graf K., and Kappl M. *Physics and chemistry of interfaces*, 2:16, 2006.

[127] Holmberg K. *Handbook of Applied Surface and Colloid Chemistry*, 2:219, 2002.

[128] Lin W.C., Yu C.H., Triffo S, and Groves J.T. Supported membrane formation, characterization, functionalization, and patternig for application in biological science and technology. *Current Protocols in Chemical Biology*, 2:235–269, Dec 2010.

[129] Gonnenwein S. Generic and specific cell adhesion: Investigation of a model system by micro-interferometry. *PhD thesis, Technischen Universitat Munchen*, Feb 2003.

[130] Ulrich Schneider, Hans-Ulrich Schwenk, , and Georg Bornkamm. Characterization of ebv-genome negative "null" and "t" cell lines derived from children with acute lymphoblastic leukemia and leukemic transformed non-hodgkin lymphoma. *International Journal of Cancer*, 19:621–626, 1977.

[131] Jones S. Peng P.D. Yang S. Hsu C. Cohen C.J. Zhao Y. Abad J. Zheng Z. Rosenberg S.A. and Morgan R.A. Lentiviral vector design for optimal t cell receptor gene expression in the transduction of peripheral blood lymphocytes and tumor-infiltrating lymphocytes. *Human gene therapy*, 20:630–640, June 2009.

[132] A. Brodovitch, P. Bongrand, and A. Pierres. T lymphocytes sense antigens within seconds and make a decision within one minute. *The Journal of Immunology*, 191:2064–2071, 2013.

[133] Principles of fluorescence. *http://www.blizard.qmul.ac.uk/flow-cytometry/ what-is-flow-cytometry/principles-of-fluorescence.html.*

[134] Jose M Moran-Mirabal. Advanced-microscopy techniques for the characterization of cellulose structure and cellulose-cellulase interactions. In *Cellulose-Fundamental Aspects*. InTech, 2013.

[135] Stephen T. Ross, Stanley Schwartz, Thomas J. Fellers, and Michael W. Davidson. http://www.microscopyu.com/articles/fluorescence/tirf/tirfintro.html. 1999.

[136] Laurent Limozin and Kheya Sengupta. Quantitative reflection interference contrast microscopy (ricm) in soft matter and cell adhesion. *Chem. Phys. Chem.*, 10:2752–2768, 2009.

[137] Alameddine R. Nanostructuration bio-chimique de substrats mous pour l'etude de l'adhesion et de la mecanique cellulaire. *PhD thesis, Aix-Marseille*, Dec 2016.

[138] A.S. Curtis. The mechanism of adhesionof cells to glass. *Journal of Cell Biology*, 20:199–215, 1964.

[139] A Zilker, H Engelhardt, and E Sackmann. Dynamic reflection interference contrast (ric-) microscopy: a new method to study surface excitations of cells and to measure membrane bending elastic moduli. *Journal De Physique*, 48(12):2139–2151, 1987.

[140] Frise E Kaynig V Longair M Pietzsch T Preibisch S Rueden C Saalfeld S Schmid B-Tinevez JY White DJ Hartenstein V Eliceiri K Tomancak P Cardona A. Schindelin J, Arganda-Carreras I. Fiji: an open-source platform for biological-image analysis. *Nat Methods*, 9:676–82, 2012.

[141] Christian Dietrich, Rudolf Merkel, and Robert Tampe. Diffusion measurement of fluorescence labeled amphiphilic molecules with a standard fluorescence microscope. *Biophysical Journal*, 72:1701–1710, 1997.

[142] Pierre Dillard, Rajat Varma, Kheya Sengupta, and Laurent Limozin. Ligand-mediated friction determines morphodynamics of spreading t cells. *Biophysical journal*, 107(11):2629–2638, 2014.

[143] Fuwei Pi, Pierre Dillard, Ranime Alameddine, Emmanuelle Benard, Astrid Wahl, Igor Ozerov, Anne Charrier, Laurent Limozin, and Kheya Sengupta. Size-tunable organic nanodot arrays: A versatile platform for manipulating and imaging cells. *Nano letters*, 15(8):5178–5184, 2015.

[144] E. Cretel, D. Touchard, P. Bongrand, and A. Pierres. A new method for rapid detection of t lymphocyte decision to proliferate after encountering activating surfaces. *Journal of Immunologogical Methods*, 364:33–39, 2011.

[145] T. J. Crites, K. Padhan, J. Muller, M. Krogsgaard, P. R. Gudla, S. J. Lockett, , and R. Varma. Tcr microclusters pre-exist and contain molecules necessary for tcr signal transduction. *Journal of Immunology*, 193:56–67, 2014.

[146] T. Yokosuka, K. Sakata-Sogawa, W. Kobayashi, M. Hiroshima, A. Hashimoto-Tane, M. Tokunaga, Dustin M.L., and T Saito. Newly generated t cell receptor microclusters initiate and sustain t cell activation by recruitment of zap70 and slp-76. *Nature Immunology*, 6:1253–1262, 2005.

[147] J. A. Hammer and J. K. Burkhardt. Controversy and consensus regarding myosin ii function at the immunological synapse. *Current Opinion in Immunology*, 25:300–306, 2013.

[148] S. C. Bunnell, D. I. Hong, J. R. Kardon, T. Yamazaki, C. J. McGlade, V. A. Barr, and L. E. Samelson. T cell receptor ligation induces the formation of dynamically regulated signaling assemblies. *The Journal of cell biology*, 158:1263–1275, 2002.

[149] Jinsung Hong, Sricharan Murugesan, Eric Betzig, and John A Hammer. Contractile actomyosin arcs promote the activation of primary mouse t cells in a ligand-dependent manner. *PloS one*, 12(8):e0183174, 2017.

[150] X. S. Wu T. Crites Yi, J. and J. A. Hammer. Actin retrograde flow and actomyosin ii arc contraction drive receptor cluster dynamics at the immunological synapse in jurkat t cells. *Molecular biology of the cell*, 25:834–852, Mar 2012.

[151] Sricharan Murugesan, Jinsung Hong, Jason Yi, Dong Li, Jordan R Beach, Lin Shao, John Meinhardt, Grey Madison, Xufeng Wu, Eric Betzig, et al. Formin-generated actomyosin arcs propel t cell receptor microcluster movement at the immune synapse. *J Cell Biol*, 215(3):383–399, 2016.

[152] Peter Beemiller and Matthew F Krummel. Mediation of t-cell activation by actin meshworks. *Cold Spring Harbor perspectives in biology*, 2(9):a002444, 2010.

[153] Niña C Hartman, Jeffrey A Nye, and Jay T Groves. Cluster size regulates protein sorting in the immunological synapse. *Proceedings of the National Academy of Sciences*, 106(31):12729–12734, 2009.

[154] Kaushik Choudhuri, David Wiseman, Marion H Brown, Keith Gould, and P Anton van der Merwe. T-cell receptor triggering is critically dependent on the dimensions of its peptide-mhc ligand. *Nature*, 436(7050):578–582, 2005.

[155] Kumari S Liapis A Dustin ML Sheetz MP Kam LC Iskratsch T Tabdanov E, Gondarenko S. Micropatterning of tcr and lfa-1 ligands reveals complementary effects on cytoskeleton mechanics in t cells. *Integr Biol*, 7:1272–1284, 2015.

[156] K. T. Bashour, A. Gondarenko, H. Chen, K. Shen, X. Liu, M. Huse, J. C. Hone, and L. C. Kam. Cd28 and cd3 have complementary roles in t-cell traction forces. *Proceedings of the National Academy of Sciences of the United States of America*, 111:2241–2246, 2014.

[157] Ozerov I Charrier A Sengupta K Benard E, Pi F. Ligand nano-cluster arrays in a supported lipid bilayer. *J Vis Exp*, 122, Apr 2017.

[158] C Cabanas M P Stewart and N Hogg. T cell adhesion to intercellular adhesion molecule-1 (icam-1) is controlled by cell spreading and the activation of integrin lfa-1. *J.Immunol*, 156:1810–1817, Mar 1996.

[159] Sakata-Sogawa K Takamatsu M Hashimoto-Tane A Dustin ML Tokunaga M Saito T. Yokosuka T, Kobayashi W. Spatiotemporal regulation of t cell costimulation by tcr-cd28 microclusters and protein kinase c theta translocation. *Immunity*, 29:589–601, Oct 2008.

[160] Tristl M Haase I Fischer M-Sackmann E. Sengupta K, Limozin L. Coupling artificial actin cortices to biofunctionalized lipid monolayers. *Langmuir*, 22:5776–5785, 2006.

[161] Thermofisher, cd3 monoclonal antibody ucht1.

[162] Harold P.Erickson Timothy A.Springer. Donald E.Staunton, Michael L.Dustin. The arrangement of the immunoglobulin-like domains of icam-1 and the binding sites for lfa-1 and rhinovirus. *CellPress*, 61:243–254, 1990.

[163] Qingrong Yan Rotem Rubinstein Chenyang Zhan Vladimir Vigdorovich Udupi A. Ramagopal Jeffrey Bonanno Stanley G. Nathenson Kausik Chattopadhyay, Eszter Lazar-Molnar and Steven C. Almo. Sequence, structure, function, immunity: structural genomics of costimulation. *Immuno Rev*, 229:356–386, 2010.

[164] Dustin ML and Cooper JA. The immunological synapse and the actin cytoskeleton: molecular hardware for t cell signaling. *Nat Immunol*, 1:23–9, 2000.